Coordination of cAMP compartmentalisation in cardiac myocytes by G protein-coupled receptors



Alexander Demby

Christ Church

University of Oxford

A thesis submitted for the degree of

Doctor of Philosophy

Trinity 2026

Abstract

Spatial compartmentalisation of 3',5'-cyclic adenosine monophosphate (cAMP) signalling is essential for achieving specificity downstream of G protein coupled receptors (GPCRs). Local cAMP signals activate distinct subsets of protein kinase A (PKA) targets, enabling a single second messenger to regulate diverse physiological processes initiated by many GPCRs. cAMP compartmentalisation is critically important in cardiac myocytes, facilitating adrenergic regulation of contractility and relaxation, making the heart an ideal model for studying this signalling. While the roles of phosphodiesterases and A-kinase anchoring proteins (AKAPs) in shaping cAMP compartmentalisation are well established, the contribution of GPCRs to the specification of spatial cAMP signalling remains incompletely understood. A more complete understanding of how GPCRs shape compartmentalised signalling may facilitate discovery of novel drugs with fewer off-target effects. The aim of this thesis was to determine how receptor identity, ligand identity, and G protein coupling influence the spatial organisation of cAMP signalling in cardiac myocytes.

Fluorescence resonance energy transfer (FRET)-based cAMP and PKA reporters were used to measure signalling within distinct subcellular compartments in live neonatal rat ventricular myocytes. Targeted sensors were used to observe cAMP at the sarcoplasmic reticulum (SR), myofilament, AKAP79-associated plasma membrane nanodomain, and at the plasma membrane more broadly. PKA activity reporters and complementary biochemical approaches were used to assess PKA-dependent phosphorylation downstream.

Selective activation of β1-adrenergic receptors (β_1ARs) and β2-adrenergic receptors (β_2ARs) generated distinct spatial patterns of cAMP signalling. β_1AR stimulation elevated cAMP at the plasma membrane, SR, and myofilament but not at the AKAP79 nanodomain, whereas β_2AR signalling was restricted to the AKAP79 nanodomain. This difference could not be explained by β_2AR coupling to Gαi proteins, indicating that receptor identity itself contributes to the specification of spatial patterns of intracellular signalling.

Ligand identity was also found to influence cAMP compartmentalisation. The β-blocker carvedilol acted as a partial agonist, producing a modest β_2AR-dependent increase in cAMP. However, unlike the full agonists isoproterenol and noradrenaline, carvedilol generated cAMP signals at AKAP79 and the myofilament but not at the SR, demonstrating that different ligands acting at the same receptor can generate distinct spatial patterns of cAMP signalling.

Finally, activation of the Gi-coupled M_2 muscarinic acetylcholine receptor selectively opposed cAMP generation in the cytosol, at the plasma membrane, SR, and myofilament but not within the AKAP79 nanodomain. This provides evidence that Gi-mediated inhibition, like Gs-mediated cAMP generation, is spatially compartmentalised.

Together, these findings demonstrate that GPCRs do not merely initiate cAMP signalling but actively determine where within the cell it occurs. Receptor identity, ligand-dependent effects, and the balance between Gs- and Gi-mediated signalling each contribute to the spatial organisation of cAMP signalling. This work extends current concepts of GPCR signalling by demonstrating that biased signalling can include a spatial dimension and highlights GPCR-dependent specification of cAMP compartmentalisation as an important mechanism for achieving signalling specificity. These insights may inform the development of therapeutics with improved specificity and fewer off-target effects by enabling more precise targeting of GPCR signalling pathways.

Declaration

I declare that this thesis is my own work, except when stated otherwise. The contents of this work are original and have not been submitted for consideration for another degree or qualification.

Acknowledgements

I would like to thank the people without whom completing this project and producing this thesis would not have been possible.

Firstly, my supervisor Professor Manuela Zaccolo for guiding me through every step of the project. Her unwavering support has allowed me to grow as a person and as a scientist. I thank her for having confidence in me, allowing me to join her group for my DPhil despite having no previous research experience, and for encouraging me to make the most of all opportunities over the last four years, including publishing and presenting at multiple international research conferences. I could not have asked for a better mentor.

I am also indebted to members of the Zaccolo group past and present. In particular, I would like to thank Andreas, Anna, Emily, Ester, Inky, Jakub, Jianshu, Milda, Rahul, and Yvette who are not only colleagues, but also friends. You have made the Zaccolo group such a friendly and supportive place, and it has been a pleasure to work alongside you. Special thanks must go to Andreas and Inky for allowing me to constantly pester them with questions, to Anna, Milda, Emily, and Ester for always having time to chat and for being sources of support when experiments went wrong, and to Rahul for buying me endless cups of tea and coffee and looking after me both inside and outside of the lab. Outside of the Zaccolo group, I must also thank Professor Cristina Molina for her scientific and personal advice, her encouragement, and her continual positivity.

Many people have been influential in my scientific journey, leading me to the eventual decision to undertake a DPhil. I am grateful to my high school science teachers – especially Dr Sam Crawshaw – who fuelled my love for biology and helped me to believe that Oxford was not an unrealistic goal and that doing science is where I am meant to be. I owe thanks also to all of my undergraduate tutors, but in particular to Professor Robert Wilkins in whose tutorials I discovered my passion for physiology. Finally, I would like to thank Professor Colin Akerman and the

members of the Akerman group – especially Alexios and Matt – for welcoming me into their lab as an undergraduate student and giving me my first taste of research.

Without my undergraduate tutor and graduate college advisor Dr Michael Kohl, not only would I not have completed my DPhil, I likely wouldn't be here at all. I thank him for his never-ending support over the past seven years, his invaluable advice dispensed over cups of tea and coffee, pints of beer, and glasses of wine, for being a listening ear, and for always fighting my corner.

The last four years would have been far more difficult without the support of many people. Unfortunately, I cannot name all of them, but particular thanks must go to my friends from Manchester – Harry, Joe, Jonny, Josh, Louis, Noah, Rob and Sam. Although I haven't seen them as often as I'd like, our yearly trips have given me a much-needed break. Thank you also to Miri for always being at the end of the phone and for offering me somewhere to stay whenever I needed it. I am especially grateful to the people in Oxford, both past and present, who have made the last few years so much more enjoyable – especially Ama, Dec, Dillon, Dylan, Gianni, Hanya, Ingrid, Iris-Mae, Sanskriti, Tom C, Tom P. Special thanks must also go to Bozhen for his care, support, and encouragement, and for sharing the first part of my DPhil journey with me.

This project would not have been possible without the extraordinary generosity of Michael Moritz, Harriet Heyman, and Crankstart. Thank you not only for funding my research and education, but also for your advice, your kindness and hospitality when I came to stay with you in San Francisco, and your faith in me.

Finally, I would like to thank my family. To my parents, my brother Matthew, and my sister Freya: thank you for your love, understanding, and support; and, of course to the dogs, Freddie and Oscar, for being an unwavering source of stress relief.

Most of all, I am grateful to my parents, Elly and Neil. When I became ill as a first-year undergraduate seven years ago, I did not think it possible that I would complete my undergraduate degree. It is thanks to them that I am now completing my doctorate.

Contents

List of figures xv

List of tables xix

List of abbreviations xxi

1 Introduction 1

1.1 G protein coupled receptors 1

1.1.1 Canonical GPCR signalling 1

1.1.2 The Gα subunit 3

1.1.3 The Gβγ heterodimer 8

1.1.4 Signal termination and receptor desensitisation 11

1.1.5 β-arrestin-dependent signalling 13

1.1.6 Signalling from intracellular membranes 15

1.2 The cAMP signalling pathway 18

1.2.1 Canonical cAMP signalling 18

1.2.2 Spatiotemporal compartmentalisation of cAMP signalling 22

1.2.3 Phosphodiesterases and compartmentalisation 24

1.2.4 AKAP-organised signalling complexes 27

1.2.5 cAMP nanodomain signalling in cardiac myocytes 28

1.3 Thesis aims 33

2 Methods 37

2.1 Materials 37

2.1.1 Reagents 37

2.1.2 Genetic constructs 38

2.2 Experimental methods 38

2.2.1 HEK293T cell culture 38

2.2.2 Primary rat ventricular cardiac myocyte isolation and culture 39

2.2.3 Transfection and infection 41

2.2.4 Fluorescence resonance energy transfer (FRET) 41

2.2.5 Western blotting 51

2.2.6 Data and statistical analysis 53

3 Compartment specific cAMP signalling by β-adrenergic receptors 55

3.1 Introduction 55

3.1.1 β-adrenergic receptor isoforms 55

3.1.2 Structural differences between βAR isoforms underlie divergent signalling 57

3.1.3 Adrenergic signalling in the cardiac myocyte 58

3.1.4 Aims 62

3.2 Methods 63

3.2.1 FRET imaging 63

3.3 Results 64

3.3.1 Differential regulation of cAMP at β-adrenergic targets 64

3.3.2 Contribution of β-adrenergic receptor subtypes to the cAMP response in cardiac myocytes 66

3.3.3 Spatial compartmentalisation of cAMP signals generated by β_1ARs and β_2ARs 69

3.3.4 β-adrenergic cAMP signalling at the plasma membrane 71

3.3.5 The role of Gαi in cAMP compartmentalisation by β_2ARs 73

3.4 Discussion 74

3.4.1 β_1ARs regulate cytoplasmic targets whilst β_2ARs selectively regulate the AKAP79 nanodomain 74

3.4.2 Contribution of plasma membrane organisation to βAR cAMP compartmentalisation 76

3.4.3 β_2AR-Gi signalling may have a cAMP-independent component 78

3.5 Conclusions 81

4 Diversification of cAMP signalling driven by different ligands acting at the β-adrenergic receptor 83

4.1 Introduction 83

4.1.1 Biased signalling by GPCRs 83

4.1.2 β-blockers 85

4.1.3 Carvedilol 88

4.1.4 Aims 91

4.2 Methods 91

4.2.1 FRET imaging 91

4.2.2 Western blotting 92

4.3 Results 92

4.3.1 Carvedilol opposes isoproterenol-mediated stimulation of βARs 92

4.3.2 Carvedilol has a partial agonist effect at β_2ARs in cardiac myocytes 94

4.3.3 Carvedilol elicits a unique pattern of cAMP signalling 95

4.3.4 The absence of cAMP generation at the sarcoplasmic reticulum cannot be explained by diffusion limitation 97

4.3.5 Carvedilol elevates cAMP in a dose-dependent manner 100

4.3.6 Assessment of PKA target phosphorylation following βAR stimulation 101

4.4 Discussion 105

4.4.1 Current debate on the pharmacology of carvedilol 105

4.4.2 The role of β_1AR versus β_2AR 110

4.4.3 The role of intracellular receptors 112

4.4.4 Mechanistic basis of ligand-dependent spatial cAMP signalling 114

4.5 Conclusions 115

5 Integration of adrenergic and cholinergic signalling 117

5.1 Introduction 117

5.1.1 Gi protein coupled receptors 117

5.1.2 GAPs and RGS proteins 118

5.1.3 Muscarinic receptors 120

5.1.4 Cholinergic signalling in the cardiac myocyte 121

5.1.5 Aims 123

5.2 Methods 124

5.2.1 FRET imaging 124

5.3 Results 124

5.3.1 Validation of FRET reporters for measuring responses to Gi protein coupled receptor activation 124

5.3.2 Cholinergic stimulation does not oppose adrenergic stimulation at AKAP79 128

5.3.3 Cholinergic regulation of cAMP signalling differs between plasma membrane compartments 130

5.3.4 Cholinergic stimulation does not influence cAMP generation at AKAP79 132

5.3.5 Compartmentalisation of cholinergic cAMP signalling is mirrored by PKA activity 133

5.4 Discussion 136

5.4.1 Regulation of the L-type calcium channel $Ca_V1.2$ in cardiac myocytes 136

5.4.2 cAMP-independent cholinergic signalling 140

5.4.3 Spatial compartmentalisation of GiPCR signalling 145

5.5 Conclusions 149

6 Discussion and conclusions 151

6.1 Discussion 151

6.2 Limitations 158

6.3 Conclusions 162

Appendix 165

A Generation and characterisation of GalT-CUTie 165

B Calculation of predicted βAR occupancy during subtype-selective blockade 167

C β-adrenergic ligands drive distinct spatial patterns of signalling 171

D Carbachol does not detectably reduce basal cytosolic cAMP 172

Bibliography 173

List of Figures

1.1	Canonical GPCR signalling versus a modern perspective	18
1.2	cAMP signalling is compartmentalised in discrete subcellular pools	25
1.3	Different Gs-coupled GPCRs drive distinct patterns of cAMP signalling in cardiac myocytes	30
2.1	FRET-based sensors enable detection of cAMP and PKA activity in live cells	44
2.2	Localisation of CUTie sensors to specific subcellular nanodomains in cardiac myocytes	45
2.3	In cell calibration of FRET-based cAMP reporters	47
2.4	Preliminary tests of βAR subtype-selective antagonists	50
3.1	Receptor activation induces outward movement of TM6 and insertion of the Gαs α5 helix into the receptor cytoplasmic cavity	56
3.2	Sympathetic stimulation leads to positive inotropy and lusitropy	59
3.3	CUTie sensors enable measurement of subcellular compartmentalisation of cAMP signalling	66
3.4	Cytosolic adrenergic cAMP generation is driven predominantly by β_1ARs in NRVMs	67
3.5	β_1ARs and β_2ARs drive distinct spatial patterns of cAMP signalling in cardiac myocytes	70
3.6	Spatial compartmentalisation of βAR-dependent cAMP signalling is independent of Gi	72

3.7	Comparison of βAR subtype-specific cAMP signalling across subcellular compartments	74
4.1	Carvedilol opposes adrenergic cAMP generation	93
4.2	Carvedilol acts as a partial agonist at β2ARs in NRVMs	95
4.3	β-Adrenergic ligands drive distinct spatial patterns of cAMP signalling	96
4.4	The absence of cAMP signalling at the SR is not due to diffusion limitation	98
4.5	Carvedilol drives a dose-dependent increase in cAMP	100
4.6	βAR-driven phospholamban phosphorylation	101
4.7	βAR-driven CREB phosphorylation	102
4.8	βAR-driven troponin I phosphorylation	104
5.1	FRET-based reporters enable detection of Gi-dependent cholinergic signalling	125
5.2	Cholinergic opposition of β-adrenergic cAMP signalling is spatially compartmentalised	129
5.3	Cholinergic stimulation produces a strong Gi-dependent suppression of cAMP at the plasma membrane	131
5.4	Cholinergic stimulation opposes forskolin-stimulated cytosolic cAMP generation	132
5.5	Cholinergic inhibition of cAMP signalling is compartmentalised and excluded from the AKAP79 nanodomain	134
5.6	Compartmentalisation of cholinergic cAMP signalling is mirrored at the level of PKA activity	136
5.7	Potential mechanisms underlying cholinergic regulation of $Ca_V1.2$	144

S1	Generation and characterisation of GalT-CUTie	165
S2	β-adrenergic ligands drive distinct spatial patterns of cAMP signalling	171
S3	Carbachol does not detectably reduce basal cytosolic cAMP	172

List of Tables

2.1	Plasmids and adeno-associated viral vectors	38
2.2	Fluorescent sensors	48
2.3	Antibodies	52
4.1	Summary of previous experiments on the pharmacology of carvedilol	106

List of abbreviations

7TM	Seven-transmembrane
AC	Adenylyl cyclase
AKAP	A-kinase anchoring protein
AKAR	A-kinase activity reporter
ATP	Adenosine triphosphate
bPAC	photo-activatable adenylyl cyclase
BRET	Bioluminescence resonance energy transfer
C	PKA catalytic subunit
CaM	Calmodulin
CaMK	Calmodulin kinase
cAMP	3',5'-cyclic adenosine monophosphate
Carv	carvedilol
CaT	Calcium transient
$Ca_V1.2$	L-type calcium channel
CCh	Carbamylcholine chloride (carbachol)
CDI	Calcium-dependent inhibition
CFTR	cystic fibrosis transmembrane conductance regulator
cGMP	3',5'-cyclic guanosine monophosphate
CGP	CGP-20712A
CHO	Chinese hamster ovary cells
CICR	Calcium-induced calcium release
CNG	Cyclic nucleotide gated channel
CREB	cAMP response element binding protein
CTX	Cholera toxin

CUTie cAMP universal tag for imaging experiments

DAG diacylglycerol

ECD Extracellular domain

EPAC exchange protein directly activated by cAMP

ER endoplasmic reticulum

ERK Extracellular signal-related kinase

FRET fluorescence resonance energy transfer

Fsk Forskolin

GAP GTPase-activating protein

GDP Guanosine diphosphate

GEF Guanine nucleotide exchange factor

GiPCR Gi-coupled GPCR

GIRK G protein-gated inwardly rectifying potassium channel

GPCR G protein coupled receptor

GRK GPCR kinase

GsPCR Gs-coupled GPCR

GTP Guanosine triphosphate

HCN hyperpolarisation-activated, cyclic nucleotide-gated channel

HEK Human embryonic kidney cells

HF Heart failure

HFpEF Heart failure with preserved ejection fraction

HFrEF Heart failure with reduced ejection fraction

IBMX 3-isobutyl-1-methylxanthine

IC50 Inhibitory concentration 50%

$i_{Ca,L}$ L-type calcium current

ICL Intracellular loop

i_f	Funny current
$i_{K,ACh}$	Acetylcholine-activated potassium current
IP_3	Inositol 1,4,5-trisphosphate
ISA	Intrinsic sympathomimetic activity
Iso	Isoproterenol
K_m	Michaelis-Menten constant
LV	Left ventricle
M_2R	Type 2 muscarinic acetylcholine receptor
mAChR	muscarinic acetylcholine receptor
MAPK	Mitogen activated protein kinase
Met	Metoprolol
MyBPC	Myosin binding protein C
NE	Norepinephrine/noradrenaline
NO	Nitric oxide
NOS	Nitric oxide synthase
NRVM	Neonatal rat ventricular myocyte
OCT	Organic cation transporter
PDE	Phosphodiesterase
PGE_1	Prostaglandin E_1
PH	Pleckstrin homology domain
PIP2	phosphatidylinositol 4,5-bisphosphate
PKA	Protein kinase A
PKC	Protein kinase C
PKD	Protein kinase D
PKG	Protein kinase G
PLB	Phospholamban

PLC	Phospholipase C
POPDC	Popeye domain-containing protein
PP1	Protein phosphatase 1
PP2A	Protein phosphatase 2A
PP2B	Protein phosphatase 2B (calcineurin)
PTHR	Parathyroid hormone receptor
PTX	Pertussis toxin
R	PKA regulatory subunit
RAIN	Receptor associated independent nanodomain
RGS	Regulators of G protein signalling
RyR	Ryanodine receptor
sAC	Soluble adenylyl cyclase
SERCA	sarcoplasmic/endoplasmic reticulum calcium ATPase
sGC	Soluble guanylyl cyclase
SR	Sarcoplasmic reticulum
TPNI	Troponin I
TSHR	Thyroid stimulating hormone receptor
Veh	Vehicle control
αAR	α-adrenergic receptor
β-arr	β-arrestin
βAR	β-adrenergic receptor
μOR	μ-opioid receptor

1 Introduction

1.1. G protein coupled receptors

1.1.1. Canonical GPCR signalling

G protein coupled receptors (GPCRs) are the largest family of cell surface receptors in humans, comprising more than 800 genes[1,2] and constituting more than two-thirds of all human receptors[3]. Characterised by a signature seven-transmembrane (7TM) helix architecture, GPCRs mediate an extensive range of physiological processes in response to diverse stimuli. These range from chemical ligands such as hormones, neurotransmitters, lipids, odorants, and tastants to physical stimuli, including light, and mechanical stress[4]. GPCRs are essential for sensing the external environment through vision, olfaction, and taste, and for monitoring the internal milieu to coordinate intercellular communication. The importance of these receptors is underscored by the award of the 2012 Nobel Prize in Chemistry to Robert Lefkowitz and Brian Kobilka for studies of GPCRs. Given their broad physiological roles, GPCR dysfunction contributes to the pathophysiology of numerous diseases[5]. Consequently, GPCRs are the most common targets of FDA-approved drugs with GPCR-targeted therapeutics accounting for approximately 36%

of all approved drugs and constituting the focus of multiple drug discovery programmes in the pharmaceutical industry[6].

The GPCR superfamily is commonly subdivided into four major classes. Class A, or "rhodopsin-like" receptors, is the largest, comprising over 700 members, including approximately 400 olfactory receptors[7], as well as receptors for light (rhodopsin), amines, peptides, proteins, lipids, nucleotides, and certain steroid hormones[8]. Class B GPCRs are divided into the secretin (Class B1) and adhesion (Class B2) families, both characterised by extended extracellular N-terminal domains (ECDs)[8]. In secretin receptors, this domain mediates binding of large peptide hormones[9], such as vasoactive intestinal peptide, parathyroid hormone, glucagon, and glucagon-like peptide. In contrast, adhesion GPCRs contain complex ECDs with multiple adhesive motifs and undergo autoproteolytic cleavage, enabling their specialised roles in cell-cell and cell-matrix interactions[10].

Class C receptors, which include the metabotropic glutamate receptors, $GABA_B$ receptors, calcium-sensing receptors, certain pheromone receptors, and taste receptors[11], also possess large ECDs and function as obligate dimers[12]. Finally, Class F comprises the Frizzled and Smoothened receptors. Frizzled receptors bind Wnt, whilst Smoothened mediates Hedgehog pathway signalling. Both are distinguished by a cysteine rich N-terminal domain, a structurally distinct 7TM core lacking canonical Class A-C motifs, and utilise unique signalling mechanisms to regulate developmental processes[13]. This thesis focuses on Class A GPCRs.

The canonical model of GPCR signalling describes a linear cascade initiated by receptor activation. GPCRs are named for their ability to couple to heterotrimeric

guanine nucleotide-binding proteins (G proteins), which bind guanine nucleotides and utilise the energy derived from GTP hydrolysis to drive downstream signalling[14]. Heterotrimeric G proteins are composed of Gα, Gβ, and Gγ subunits, with Gβ and Gγ forming an obligate heterodimer. At rest, the Gα subunit is GDP-bound.

Ligand binding to the extracellular face of the receptor stabilises an active receptor conformation[15], promoting engagement of a heterotrimeric G protein at the intracellular surface[16]. The activated receptor functions as a guanine nucleotide exchange factor (GEF), catalyzing the release of GDP from Gα[17]. Because cytosolic GTP concentrations exceed those of GDP, this results in the exchange of GDP for GTP[18]. GTP loading induces conformational rearrangement of Gα, reducing its affinity for both the receptor and the Gβγ heterodimer, resulting in their dissociation[17].

Both Gα-GTP and the free Gβγ can then regulate distinct downstream effectors. Signal termination occurs through the intrinsic GTPase activity of Gα, which hydrolyses GTP to GDP, restoring the inactive heterodimer and completing the G protein cycle.

1.1.2. The Gα subunit

Historically, GPCRs have been classified according to the Gα subunit to which they predominantly couple. In humans, 16 Gα isoforms are grouped into four major families – Gαs, Gαi/o, Gαq/11, and Gα12/13 – each associated with distinct downstream signalling pathways.

The Gαs family comprises Gαs[19] and the closely related Gαolf, predominantly expressed in olfactory sensory neurons[20], which both stimulate adenylyl cyclases (ACs), a family of enzymes that catalyse the conversion of ATP to 3',5'-cyclic adenosine monophosphate (cAMP), a diffusible second messenger discussed extensively in **Section 1.2**. In contrast, the Gαi/o family inhibit AC activity, thereby reducing intracellular cAMP levels[21]. This family consists of seven proteins – Gαi1, Gαi2, Gαi3, Gαo, Gαz, Gαt1, Gαt2, and Gαgus – which differ in tissue distribution and signalling properties. Gαi1-3 are ubiquitously expressed with overlapping but distinct expression patterns[22], whereas Gαo is highly enriched in the nervous system[23]. Gαz, displays a more restricted distribution with expression reported in the brain, adrenal medulla, platelets, retina, and pancreatic β-cells[24,25].

The three remaining members of the Gαi/o family are specialised sensory G proteins. The visual transducins, Gαt1 and Gαt2, are expressed in rod and cone photoreceptors respectively[26]. Upon activation by their cognate GPCRs – rhodopsins in rods, and cone opsins in cones – Gαt1/2 stimulate phosphodiesterase (PDE) 6, which hydrolyses the second messenger 3',5'-cyclic guanosine monophosphate (cGMP) and initiates the phototransduction cascade[27]. The final Gαi/o family member Gαgus, forms part of the heterotrimeric gustducin complex and shares high sequence homology with the α-transducins[28]. Gαgus is expressed in taste receptor cells and certain enteroendocrine cells, where it mediates signal transduction downstream of sweet, bitter, and umami taste receptors[29,30]. Like the transducins, Gagus can stimulate PDE activity[31]. Although not their predominant signalling output, both the α-transducins[32] and α-

gustducin[30] retain the capacity to inhibit AC, consistent with their classification within the Gαi/o family.

Gαi1-3, Gαo, Gαt1/2, and Gαgus are all sensitive to pertussis toxin (PTX), which catalyses their ADP-ribosylation, preventing receptor coupling. In contrast, Gαz lacks the critical cysteine residue required for PTX modification and is therefore the only Gαi/o family protein that is PTX-insensitive[33]. Although all Gαi/o family proteins can reduce intracellular cAMP generation through AC inhibition and liberate Gβγ to regulate downstream effectors, they exhibit differences in nucleotide binding kinetics[34] and effector selectivity[35,36].

The Gαq/11 family comprises Gαq, Gα11, Gα14, and Gα15/16 (mouse/human orthologues, respectively), which share phospholipase C-β (PLC-β) as a common downstream effector. Upon activation, PLC-β catalyses the hydrolysis of phosphatidylinositol 4,5-bisphosphate (PIP_2) at the glycerol-phosphate bond, generating two key second messengers: diacylglycerol (DAG) and inositol 1,4,5-trisphosphate (IP_3)[37].

DAG remains membrane-associated and binds to conserved C1 domains within its effectors, stimulating the activity of enzymes including protein kinase C (PKC) and protein kinase D (PKD)[38]. DAG can also be further metabolised to produce the signalling lipid phosphatidic acid[39]. In contrast, IP_3, diffuses through the cytosol and binds to IP_3 receptors on the endoplasmic reticulum (ER), which function as ligand-gated Ca^{2+} channels. This triggers Ca^{2+} release from the ER lumen into the cytoplasm, and the resulting elevation in intracellular Ca^{2+} drives multiple downstream signalling events[40].

As with other G protein families, members of the Gαq/11 family exhibit differences in tissue distribution, receptor coupling selectivity, and downstream binding partners. Gαq and Gα11 are ubiquitously expressed at both mRNA and protein levels, whereas Gα14 and Gα15/16 display more restricted expression patterns[41]. Gα14 has been detected in spleen, lung, kidney, pancreas, liver, testis, and bone marrow stromal cells[42–44], while Gα15/16 are almost exclusively found in cells of haematopoietic origin[42].

Inositol signalling can be driven by direct activation of PLC-β by Gαq/11 family proteins or indirectly through Gβγ subunits released by Gi/o-coupled receptors. Consequently, GPCRs that stimulate inositol phosphate production and intracellular Ca^{2+} mobilisation in a PTX-insensitive manner are generally considered to be Gαq/11-coupled. Gαq and Gα11 preferentially engage receptors classically defined as Gq-coupled according to this definition. By contrast, Gα15/16 – and to a lesser extent Gα14 – display more promiscuous GPCR coupling, enabling interaction with receptors typically associated with Gs or Gi signalling[41]. Although all Gαq/11 family members activate PLC-β, they differ in their interactions with additional downstream effectors, including GRK2/3 and specific Rho guanine nucleotide exchange factors (RhoGEFs), demonstrating isoform-specific signalling properties.

Gα12 and Gα13 constitute the Gα12/13 family and were identified later than the other Gα subunits[45]. Consequently, their signalling mechanisms remain comparatively less well-characterised, in part due to the absence of a readily measurable second messenger and technical challenges associated with directly

monitoring their activity[46]. Gα12/13 proteins signal primarily through direct interaction with RGS homology (RH) domain-containing guanine nucleotide exchange factors (GEFs) (RH-RhoGEFs), including p115-RhoGEF, LARG, and PDZ-RhoGEF[47]. Activation of these RhoGEFs promotes GDP-GTP exchange on small Rho-family GTPases, most notably RhoA. RhoA regulates a range of cellular processes including actin cytoskeletal dynamics, transcriptional programs, and cell growth[48]. GPCR-dependent activation of RhoA is therefore commonly interpreted as evidence of Gα12/13 coupling. However, a unique feature of Gα12/13-coupled receptors is that they invariably couple to at least one other Gα family – in the majority of cases Gαq/11[46]. Despite increasing recognition of their roles in cytoskeletal regulation and mechanotransduction, many aspects of Gα12/13 signalling remain incompletely understood.

The choice of which of the 16 Gα subunits a receptor couples to constitutes a primary determinant of signalling output and physiological effect. Historically, GPCRs were considered to couple to a single Gα family, and receptors have traditionally been classified accordingly as Gαs-, Gαi/o- or Gαq/11-coupled[49]. This framework, in which signalling by this enormous receptor superfamily converges on a limited number of canonical signal transduction pathways, has raised a central question in GPCR biology: how is signalling specificity achieved?

One component of the answer is that the notion of highly selective one-to-one G protein coupling is likely an oversimplification. Advances in quantitative signalling approaches have revealed that most GPCRs are capable of engaging multiple G protein families[50,51]. Indeed, several receptors, including the cholecystokinin CCK1

receptor, endothelin ET_A receptor, histamine H_1 receptor, and orexin OX_2 receptor, have been reported to activate G proteins from all four families[51].

1.1.3. The Gβγ heterodimer

Historically, studies of GPCR signalling focused predominantly on the Gα subunit. However, the Gβγ heterodimer is an essential mediator of GPCR signalling and provides an additional layer of downstream diversification. High-resolution structures of both heterotrimeric Gαβγ complexes[52] and isolated Gβγ dimers[53], have revealed a conserved Gβ architecture comprising a seven-bladed β-propeller. The N-terminus of Gβ forms a coiled-coil interaction with Gγ, underpinning the stability of the obligate Gβγ dimer. Within the heterotrimer, Gα engages Gβγ at two independent contacts involving its N-terminal α-helix and switch II region. Structural comparisons indicate that the Gβγ heterodimer shows very little conformational rearrangement on dissociation from Gα[52,53]. Thus, in contrast to Gα – whose nucleotide-dependent conformational change enables effector engagement – Gβγ signalling competence appears to arise primarily from a relief of steric occlusion by Gα rather than from structural rearrangement.

Following receptor activation, the Gβγ dimer can signal independently of Gα by engaging an ever-expanding list of downstream effectors. The first such effector to be identified was the G protein-gated inwardly rectifying potassium (GIRK) channel, whose activation downstream of type 2 muscarinic acetylcholine receptors (M_2R) in atrial myocytes provided early evidence that Gβγ directly gates ion channels independently of second messenger signalling[54–56]. Since this initial discovery, the list of effectors for Gβγ has grown. These include both activation[57,58] and inhibition[57–

[60] of specific AC isoforms, activation of PLC-β[61–63], and PI3K-γ[64], recruitment and activation of GPCR kinases (GRK2 and GRK3)[65], and modulation of N-type[66] and P/Q-type[67] Ca^{2+} channels. No single consensus sequence is shared among these effectors, and structural studies suggest that multiple surfaces of the Gβγ dimer contribute to effector recognition[68]. The mechanisms of regulation broadly depend on effector localisation. In the case of cytosolic effectors such as PLC-β or GRK2/3, interaction with membrane-anchored Gβγ promotes their recruitment to the plasma membrane where their substrates reside[65]. In contrast, for those effectors which are themselves transmembrane proteins such as AC isoforms or GIRK channels, regulation occurs via direct allosteric modulation[69].

Humans express five Gβ and twelve Gγ subunits, theoretically permitting up to 60 distinct Gβγ dimer combinations[70]. However, in contrast to the more readily apparent functional distinctions among Gα families, the physiological significance of this combinatorial Gβγ diversity remains incompletely understood. Emerging evidence suggests that specific Gβγ pairings contribute to functional selectivity in GPCR signalling, with certain combinations displaying preferential coupling to particular receptors and downstream effectors[71–73].

For many years, it was widely thought that Gβγ signalling arose exclusively from Gαi/o-containing heterotrimers, whereas signalling from Gαs- and Gαq/11-derived Gβγ was considered negligible. This view was largely based on repeated observations that only GPCRs coupled to PTX-sensitive Gα subunits robustly activated classical Gβγ effectors, whereas receptors signalling through PTX-insensitive Gα proteins failed to do so[63]. Several hypotheses were proposed to

explain this apparent specificity. Increasing evidence has since challenged the canonical model of complete heterotrimer dissociation following receptor activation. Instead, accumulating data suggest that GPCR activation may induce conformational rearrangement within a Gαβγ complex without necessarily requiring full subunit separation.

Imaging experiments using fluorescence resonance energy transfer (FRET)- or bioluminescence resonance energy transfer (BRET)-based assays (see **Section 2.2.4**) to monitor proximity between Gα and Gβγ subunits frequently failed to detect the decrease in resonance energy transfer that would be predicted under a model of complete heterotrimer dissociation[74–76]. These findings suggest that receptor activation may not necessarily result in full physical separation of Gα and Gβγ. Notably, heterotrimers containing Gαo or Gαi have been shown to generate greater amounts of free Gβγ and to do so more rapidly than those containing other Gα subunits[77,78]. Therefore, differential dissociation of G protein heterotrimers depending on Gα subtype could underlie the Gαi/o specificity of Gβγ signalling. Notably, it has more recently been demonstrated that, under certain conditions, heterotrimers containing Gαs can also initiate Gβγ-mediated signalling[79,80], although Gαi/o-containing heterotrimers are still generally considered the predominant source of functionally significant Gβγ activity.

The capacity of GPCRs to signal through multiple Gα and Gβγ configurations provides a substantial degree of signalling flexibility, adding extra layers of diversification to the canonical linear cascade. This diversity arises not only from

signal initiation, but also from the processes that terminate, modify, and redirect GPCR signalling.

1.1.4. Signal termination and receptor desensitisation

Like other signal transduction systems, GPCR signalling must be tightly regulated to ensure appropriate temporal control. The canonical mechanism of GPCR signal termination involves receptor phosphorylation by GPCR kinases (GRK), recruitment of arrestins, and subsequent receptor internalisation[81]. The first GRK was identified through experiments demonstrating that desensitisation of the β_2-adrenergic receptor (β_2AR) required phosphorylation by a cAMP-independent kinase[82–85]. This kinase, initially termed β_2AR kinase 1 and now known as GRK2, selectively phosphorylates the agonist-bound β_2AR and was shown to be necessary, but not sufficient, for receptor desensitisation[86]. Arrestins, the second essential component of this process, were identified around the same time in photoreceptors as part of the molecular machinery responsible for terminating rhodopsin signalling[87].

The GRK and arrestin families comprise seven and four members, respectively. Based on sequence homology, GRKs are grouped into three subfamilies. GRK1 and GRK7 form the visual GRKs and phosphorylate rhodopsin[88] and cone opsins[89]. The five non-visual GRKs – GRK2[90], GRK3[91], GRK4[92], GRK5[93], and GRK6[94] – are expressed more broadly throughout the body. Distinct mechanisms underlie their membrane targeting. GRK1 and GRK7 are membrane anchored via C-terminal prenylation. In contrast, GRK2 and GRK3 are recruited to the plasma membrane following receptor activation through interaction of their pleckstrin homology (PH) domains with

Gβγ[95,96]. GRK4, GRK5, and GRK6 lack both a PH domain and prenylation motifs and instead associate with membranes through C-terminal lipid binding modifications and electrostatic interactions[97].

Similarly, the arrestin family comprises four members. Arrestin-1[98] (rod arrestin) and arrestin-4[99] (cone arrestin) function in visual photoreceptors, whereas arrestin-2[100] and arrestin-3[101] – more commonly referred to as β-arrestin 1 and β-arrestin 2 (β-arr1/2), respectively – regulate the majority of non-visual GPCRs[102,103].

Arrestins preferentially bind to GPCRs that are both active and phosphorylated by GRKs[104]. Canonical homologous desensitisation occurs through direct competition between β-arr and G proteins which both engage the receptor core[105–110]. High-affinity binding of β-arr to the phosphorylated receptor sterically prevents further engagement of G proteins and thereby attenuates G protein-mediated signalling. Beyond this steric hinderance, β-arr promotes receptor internalisation by functioning as adaptor proteins, directly interacting with clathrin[111] and the AP-2 complex[112]. Recruitment of this endocytic machinery facilitates receptor internalisation into endosomes, where receptors are either dephosphorylated and recycled to the cell surface or targeted for degradation[113].

This canonical view of arrestins as terminators of G protein signalling has evolved to recognise them as multifunctional regulators of GPCR activity and, in some contexts, independent signal transducers.

1.1.5. β-arrestin-dependent signalling

The expanded view of arrestin function emerged from observations that, in addition to recruiting endocytic machinery, β-arr can scaffold interactions between GPCRs and intracellular kinases, including Src[114] and ERK1/2[115]. Proteomics analyses have since identified over one hundred non-receptor binding partners for β-arr, many of which participate in signal transduction pathways[116].

Arrestin-mediated signalling was initially described as "G protein-independent". However, this terminology is somewhat misleading, as certain arrestin-ergic signalling events require functional G proteins[117]. It is therefore increasingly recognised that β-arr can facilitate both G protein-dependent and G protein-independent signalling processes, further expanding the diversification of GPCR signalling outputs.

Structural studies have revealed two principal modes by which β-arr can engage an active GPCR. In the "tail" conformation, β-arr interacts primarily with the phosphorylated C-terminal tail of the receptor. In contrast, the "core" conformation involves additional engagement of the receptor's transmembrane cavity through insertion of the β-arr finger-loop region. These distinct binding modes are associated with different functional outcomes. β-arr mutants lacking the finger-loop region – and therefore unable to adopt the core conformation – retain the ability to mediate receptor internalisation and β-arr-dependent signalling but do not desensitise G protein signalling[118]. The tail conformation also permits the formation of higher-order "megaplexes" comprising a single GPCR, β-arr, and a G protein[119,120].

The configuration in which β-arr engages a receptor is influenced by the phosphorylation pattern of the GPCR C-terminal tail, a concept referred to as the "phosphorylation barcode". Most GPCRs contain multiple serine and threonine residues within their intracellular C-termini that can be phosphorylated by GRKs. The specific combination of phosphorylated residues depends on which GRK isoform(s) are recruited to the receptor[121–123]. Distinct phosphorylation patterns can stabilise different β-arr conformations, thereby biasing downstream functional outcomes such as desensitisation, internalisation, or signalling[124].

The propensity of a GPCR to engage G protein-dependent versus β-arr-dependent signalling can depend on the identity of the activating ligand[125,126]. The capacity of different ligands acting at the same receptor to promote distinct downstream signalling profiles is termed "biased signalling" or "functional selectivity". This phenomenon arises from the ability of individual ligands to stabilise distinct active conformational states of a receptor[15,127–129], thereby favouring engagement of a particular signalling pathway.

The therapeutic exploitation of biased ligands has attracted considerable interest, particularly in the context of opioid receptors. The μ-opioid receptor (μOR) is a class A GPCR activated by endogenous enkephalin peptides involved in pain neuromodulation and is the molecular target of several widely prescribed analgesic drugs[6]. However, currently available μOR agonists are associated with significant adverse effect profiles, including respiratory depression and addictive potential. It has been proposed that differential receptor phosphorylation and internalisation contribute to these side effects, as certain opiates (e.g. morphine) induce

considerably less μOR phosphorylation and endocytosis, whereas others (e.g. fentanyl and methadone) promote considerably more receptor internalisation relative to the endogenous ligands[130,131]. Experimental studies suggested that β-arr2-mediated μOR internalisation contributes to the development of opioid tolerance[132], and that genetic deletion of β-arr2 enhances morphine-induced analgesia[133]. These findings motivated the development of G protein-biased μOR agonists, such as oliceridine (or TRV130), which demonstrated analgesic efficacy with a modestly improved adverse effect profile compared with morphine in clinical trials[134,135].

Thus, β-arr recruitment does not simply terminate G protein signalling but instead introduces additional layers of signalling diversification. Moreover, receptor internalisation, once considered solely a mechanism of desensitisation, is now recognised to traffic activated receptors to intracellular compartments where they can sustain and reshape signalling outputs.

1.1.6. Signalling from intracellular membranes

In the canonical model of homologous desensitisation, activated GPCRs undergo clathrin-mediated endocytosis and are delivered to early endosomes, where they are either dephosphorylated and recycled back to the plasma membrane or targeted for lysosomal degradation[136]. However, two studies published contemporaneously demonstrated persistent cAMP signalling by the Gs-coupled thyroid stimulating hormone receptor[137] (TSHR) and parathyroid hormone receptor[138] (PTHR) following receptor internalisation. These findings challenged the prevailing view of GPCRs as exclusively cell-surface receptors and the subsequent

decade and a half has seen a paradigm shift to a model in which GPCRs signal from a multitude of endomembrane compartments[139].

The development of fluorescently labelled single-chain antibodies ("nanobodies") that selectively recognise active receptor and G protein conformations has enabled direct visualisation of GPCR and G protein activation in living cells. Using these tools, active β_2AR-Gs complexes have been detected on endosomes[140] and active β_1AR-Gs complexes have been observed at the Golgi membrane[141].

Moreover, it is now evident that GPCR signalling from intracellular membranes is not restricted to receptors internalised from the plasma membrane. A subset of GPCRs is constitutively localised to a variety of intracellular compartments, where they can initiate signalling independently of surface receptor pools. Signalling has been reported from early endosomes[140,142], the Golgi[141,143–145], mitochondria[146,147], the nuclear membrane[148,149], the endoplasmic/sarcoplasmic reticulum[150,151], lysosomes[152,153], and even lipid droplets[154].

The existence of intracellular GPCR signalling raises important mechanistic questions, foremost among them how ligands access receptors located beyond the plasma membrane. Many endogenous GPCR ligands are membrane-impermeant, posing a challenge for activation of intracellular receptor pools. For receptors that signal from endosomes following internalisation, ligands are often co-endocytosed with their receptors[139]. In contrast, receptors resident at intracellular compartments, rely on ligand transport mechanisms for activation. For example, epinephrine and norepinephrine can access intracellular βARs via the organic cation transporter (OCT3)[141,151]. Consequently, the cellular response to a given ligand may depend on

the ligand's membrane permeability and transporter availability, which will determine which receptor pools are activated.

The demonstration of persistent signalling from internalised receptors, together with signalling initiated by GPCRs resident at intracellular sites, has led to the emergence of the concepts of "spatial encoding" or "location-biased signalling". These models recognise that the subcellular site of signal initiation constitutes an additional layer of signalling diversification[139,155–157]. Consequently, the functional outcome of GPCR activation depends not only on which signalling pathways are engaged, but also on the intracellular location from which those signals originate.

Collectively, these advances have transformed the view of GPCR signalling from a simple linear cascade initiated at the plasma membrane into a highly dynamic and multidimensional network **(Fig 1.1)**. Receptors are no longer regarded as binary on-off switches but as integrative signalling platforms capable of coordinating complex cellular responses. Signalling outcomes are shaped not only by receptor identity and G protein coupling, but also by ligand-specific conformations, arrestin engagement, and the spatial origin of signal initiation. This layered regulation enables remarkable signalling flexibility but also necessitates precise control of downstream second messenger systems.

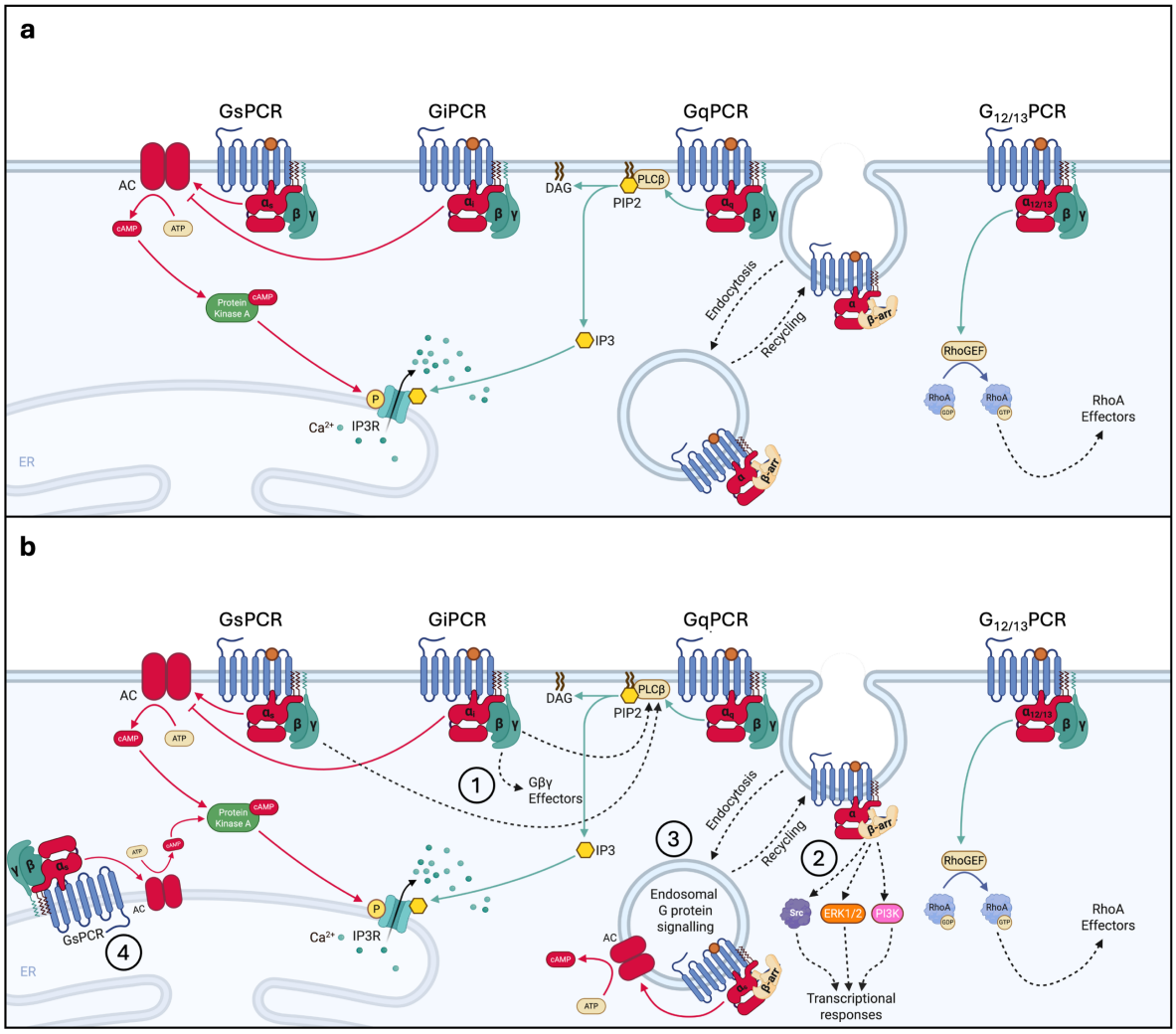


Fig 1.1 Canonical GPCR signalling versus a modern perspective. (a) Canonical linear GPCR signalling cascades in which signalling output is determined by Gα subunit coupling. **(b)** GPCRs are now understood to coordinate multidimensional signalling networks involving: **(1)** signalling mediated by the Gβγ heterodimer; **(2)** β-arrestin-dependent signalling; **(3)** signalling from endosomes following receptor internalisation; and **(4)** signalling from receptors resident on intracellular membranes. Created using BioRender.com.

1.2. The cAMP signalling pathway

1.2.1. Canonical cAMP signalling

3',5'-cyclic adenosine monophosphate (cAMP) was the first intracellular signalling molecule identified to function as a "second messenger"[158]. This concept emerged

from Earl Sutherland's studies of adrenergic regulation of liver metabolism, in which he demonstrated that adrenaline did not directly stimulate glycogen phosphorylase but instead did so via the formation of a diffusible intracellular messenger[159]. The identification of this messenger as cAMP[160] provided the first evidence that hormones drive intracellular responses through second messengers and earned Sutherland the Nobel Prize in Physiology or Medicine in 1971. Since its discovery, cAMP signalling has been widely regarded a prototypical example of intracellular signal transduction. cAMP is generated by the cyclisation of ATP by adenylyl cyclases (ACs), a family of ATP-pyrophosphate lyases comprising nine transmembrane AC isoforms (AC1-9) and one soluble isoform (sAC).

Transmembrane AC isoforms are regulated by heterotrimeric G proteins, with all isoforms stimulated by GTP-bound Gαs family members, while only a subset is inhibited by Gαi/o proteins[21]. Gαi1-3 and Gαz inhibit AC1, AC5, and AC6, whereas Gαo inhibits only AC1[57,161,162]. AC activity is further modulated by free Gβγ, which can either stimulate (AC2, AC4, AC5, AC6, AC7) or inhibit (AC1) cAMP production, as well as by PKC- and PKA-dependent phosphorylation, and by intracellular Ca^{2+} – either directly or by Ca^{2+}-binding proteins such as calmodulin[21]. In contrast to transmembrane ACs, the soluble isoform sAC is activated by bicarbonate and is regulated independently of G proteins[163].

In the canonical model, following its synthesis by ACs, cAMP is assumed to freely diffuse throughout the cytosol, where it can interact with downstream effectors. To date, four major classes of cAMP effector proteins have been identified: exchange

proteins directly activated by cAMP (EPACs), cyclic nucleotide gated (CNG) channels, Popeye domain-containing (POPDC) proteins, and protein kinase A (PKA).

EPAC1 and EPAC2 function as guanine nucleotide exchange factors (GEFs) for the small GTPases Rap1 and Rap2, which regulate diverse cellular processes, including proliferation, adhesion, cytoskeletal dynamics, and exocytosis[164]. Binding of cAMP relieves autoinhibition of EPAC proteins, enabling activation of Rap1/2[165].

CNG channels are non-selective cation channels whose open probability is increased upon binding of cyclic nucleotides such as cAMP or cGMP[166,167]. A well-characterised example is the HCN4 (hyperpolarisation-activated, cyclic nucleotide-gated) channel which contributes to spontaneous depolarisation in cardiac sino-atrial node cells[168].

The most recently identified cAMP effectors are the POPDC proteins, a family of transmembrane proteins containing a cytoplasmic C-terminal Popeye domain[169]. Although their precise biochemical functions remain incompletely defined, mutagenesis studies suggest a role in the regulation of membrane trafficking[170].

The most extensively studied cAMP effector is the cAMP-dependent protein kinase, PKA. In its inactive state, PKA exists as a heterotetramer composed of two catalytic (C) subunits, bound non-covalently to a regulatory (R) subunit dimer[171]. Each R subunit contains two cooperative cAMP binding sites, and binding of four cAMP molecules – two per R subunit – induces dissociation of the complex into an R subunit dimer and two free C subunits. The now catalytically active C subunits phosphorylate serine and threonine residues on target proteins.

The PKA family exhibits considerable heterogeneity, with four R subunit isoforms (RIα, RIβ, RIIα, RIIβ) and four C subunit isoforms (Cα, Cβ, Cγ, PRKX)[172]. Distinct combinations of these subunits display tissue-specific expression patterns and differ in their affinity for cAMP, resulting in variable activation thresholds[173].

Termination of cAMP signalling is mediated by phosphodiesterases (PDEs), which hydrolyse cyclic nucleotides. The PDE superfamily comprises 11 gene families (PDE1-PDE11), of which PDE4, PDE7, and PDE8 are cAMP-selective, PDE5, PDE6, and PDE9 are cGMP-selective, and PDE1, PDE2, PDE3, PDE10, and PDE11 exhibit dual specificity[174].

Each PDE family includes up to four distinct genes, which, in combination with extensive alternative splicing, and multiple transcriptional start sites gives rise to an enormous number of PDE isoforms[175]. These isoforms differ in their tissue-specific expression, kinetic properties (e.g. Km and V_{max}), subcellular localisation, and regulatory mechanisms[174].

Furthermore, the downstream effects of cAMP signalling mediated by PKA are determined not only by the rate of substrate phosphorylation, but also by the opposing activity of phosphoprotein phosphatases (PPPs)[176]. PPPs are generally multimeric enzymes composed of a catalytic subunit associated with multiple regulatory subunits that dictate subcellular localisation, substrate specificity, and modes of regulation[177]. PKA substrates are predominantly dephosphorylated by three phosphatases: protein phosphatase 1 (PP1), PP2A, and the Ca^{2+}-dependent PP2B, also known as calcineurin[176,177].

However, this canonical view of cAMP as a freely diffusible second messenger acting on globally distributed targets via a linear cascade cannot adequately explain how specificity is achieved in cellular signalling.

1.2.2. Spatiotemporal compartmentalisation of cAMP signalling

More than 200 non-sensory GPCRs couple to Gs or Gi/o family proteins, thereby regulating adenylyl cyclase (AC) activity and cAMP production[178]. However, different Gαs-coupled GPCRs can elicit distinct cellular responses, even when intracellular cAMP levels and global PKA activity are comparable. This phenomenon was demonstrated in a seminal series of experiments by Mayer, Brunton, and Hayes, who showed that in perfused rat hearts, stimulation of βARs with isoproterenol and E-type prostaglandin receptors with PGE_1 produced comparable increases in cAMP. Despite this, only isoproterenol stimulation led to phosphorylation of the canonical cardiac PKA substrates and an increase in contractility[179–181]. These observations raised a fundamental question – how can different Gs-coupled GPCRs (GsPCR) elicit specific downstream responses despite driving seemingly identical signal transduction cascades?

Contemporaneous studies provided further evidence challenging the classical view of cAMP signalling. Species-specific differences were observed between rat and guinea pig hearts, which predominantly express type I PKA (containing RI subunits) and type II PKA (containing RII subunits), respectively[182,183]. These studies demonstrated that PKA RI is largely cytosolic whereas PKA RII is associated with particulate cellular fractions. Subsequent experiments showed that whilst isoproterenol stimulation increased the activity of both soluble and particulate PKA,

PGE_1 elevated only soluble PKA activity[184]. In addition, single-cell patch-clamp electrophysiology experiments revealed that isoproterenol increased in L-type Ca^{2+} current ($i_{Ca,L}$) locally at the site of application, but not at more distant regions within the same cell[185]. This spatial restriction was dependent on PDE activity. Taken together, these observations indicate that the canonical linear cAMP-PKA cascade is too simplistic and that spatial specificity plays a role in encoding receptor-specific responses.

The development of genetically encoded FRET-based cAMP reporters allowed spatial compartmentalisation of cAMP signalling to be directly visualised in living cells for the first time[186,187]. These imaging experiments revealed that cAMP does not increase uniformly throughout the cell following activation of Gs-coupled GPCRs but instead forms spatially restricted gradients. On the basis of these observations, a model of spatiotemporal compartmentalisation of cAMP signalling has emerged[188,189]. In this model distinct subcellular regions experience different amplitudes and kinetics of cAMP elevation, forming localised signalling domains. In some subcellular locations, cAMP will be elevated whereas in others, it will not. Consequently, receptor-specific cellular responses can be achieved through the generation of distinct spatial and temporal patterns of cAMP.

The establishment of tightly compartmentalised cAMP signalling requires both spatial organisation of signalling components and restriction of cAMP diffusion. These are achieved through two key mechanisms: the assembly of local signalling complexes by A-kinase anchoring proteins (AKAPs), and the localised degradation of cAMP by PDEs **(Fig 1.2)**.

1.2.3. Phosphodiesterases and compartmentalisation

Early studies established a critical role for PDEs in the compartmentalisation of cAMP signalling[185,187,190,191]. The extensive diversity of the PDE superfamily, comprising numerous isoforms with distinct subcellular localisation and regulatory properties, enables these enzymes to shape local cAMP nanodomains. Differential rates of cAMP degradation generate spatially heterogeneous cAMP signals, restricting access to specific downstream effectors[192–194].

The development of targeted FRET-base cAMP reporters (discussed in more detail in **Section 2.2.4**), which incorporate targeting domains to enable measurement of cAMP within defined subcellular regions, has provided direct evidence for the role of PDEs in maintaining compartmentalisation. Using these approaches, the CUTie (cAMP Universal Tag for imaging experiments) reporters developed by our group, targeted to key adrenergic PKA substrates in cardiac myocytes, revealed distinct magnitude and kinetics of cAMP signalling at the sarcoplasmic reticulum (SR), myofilament, and AKAP79-associated plasma membrane domains following adrenergic stimulation[195]. Notably, these spatial differences were abolished upon inhibition of PDE activity with pan-PDE inhibitor IBMX.

Further insight into the nanoscale organisation of cAMP signalling has been obtained using ‘nanorulers’, in which spacers of defined length are conjugated to FRET reporters. These studies demonstrated that cAMP nanodomains can be confined to regions as small as 10 nm[196]. Direct conjugation of FRET reporters to PDEs has shown that these enzymes generate local zones of low cAMP concentration[197], the size of which depends on the PDE isoform[198]. Nanoruler-based

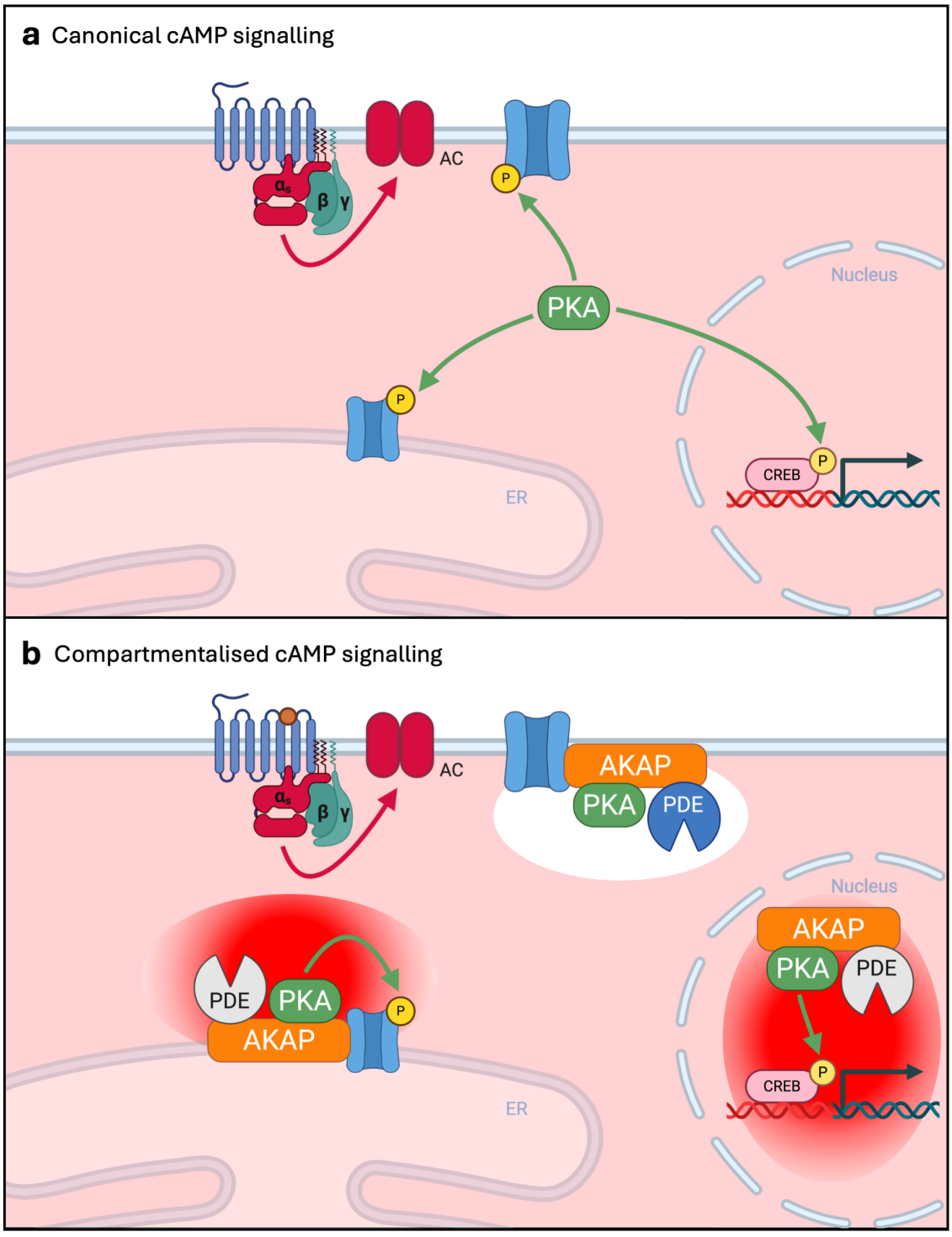


Fig 1.2 cAMP is compartmentalised in discrete subcellular pools. (a) Canonical model of cAMP signalling in which cAMP (pink) diffuses freely through the cell, activating soluble protein kinase A (PKA) which diffuses and phosphorylates downstream targets. **(b)** Modern model of compartmentalised signalling in which PKA is anchored by A-kinase anchoring proteins (AKAPs) close to phosphorylation targets. AKAPs also scaffold phosphodiesterases (PDEs) that degrade cAMP. At any one time, some PDEs are more active (blue) and some less active (grey). Areas of high

PDE activity create cAMP sinks in which PKA does not get activated and thus phosphorylation is reduced. In areas of lower PDE activity, cAMP will be higher (dark red), resulting in increased PKA activity and more downstream phosphorylation. Created using BioRender.com.

measurements revealed that PDE4A1 (high-affinity, low V_{max}) depletes cAMP within a 10 nm radius, whereas PDE2A3 (lower-affinity, higher V_{max}) generates a cAMP-deficient region more than 30 nm in radius, highlighting how PDE isoform-specific properties define the size and shape of cAMP nanodomains.

Several models have been proposed to explain how PDEs maintain tight compartmentalisation of cAMP signalling. The barrier hypothesis posits that PDEs act as barriers to cAMP diffusion, confining cAMP proximal to sites of production. Some functional evidence supports this model. For example, βAR-mediated regulation of $i_{Ca,L}$ is restricted to nearby $Ca_V1.2$ channels and only influences more distant channels following PDE inhibition[185]. Similar spatial restriction has been observed in the regulation of the Cl^- channel CFTR (cystic fibrosis transmembrane conductance regulator) by adenosine A_{2B} receptors[199].

Further support for this hypothesis comes from FRET-based nanoruler experiments, which demonstrate that at very low agonist concentrations, GPCR activation generates highly localised cAMP pools confined to regions within tens of nanometres of the receptor[196]. These 'receptor associated independent nanodomains' (RAINs) are not influenced by cAMP generated by other GPCRs and are abolished upon PDE inhibition.

However, this model is insufficient to fully account for other experimental observations. It does not explain, for example, how cAMP effectors located deep

within the cell, distant from plasma membrane-localised ACs, are regulated. Moreover, a quantitative inconsistency arises; given the rapid diffusion of cAMP (~ 40 μm^2 s^{-1} in cell), reported K_m and V_{max} values for PDEs are insufficient to maintain cAMP concentrations below the activation threshold of PKA under conditions of increased AC activity[200].

An alternative, and now more widely accepted, hypothesis proposes that PDEs act as localised cAMP sinks rather than barriers[189,201,202]. In this model, PDEs gate access to cAMP effectors by generating local regions of low cAMP concentration, thereby 'protecting' cAMP effectors in their vicinity from activation. Spatial variation in PDE activity creates heterogeneous cAMP landscapes, enabling the generation of distinct downstream signalling responses.

The formation of these local cAMP nanodomains requires not only enzymatic control of cAMP degradation but also precise spatial control of signalling components. This is achieved through the assembly of multi-protein signaling complexes, predominantly mediated by A-kinase anchoring proteins (AKAPs).

1.2.4. AKAP-organised signalling complexes

PKA is a highly promiscuous enzyme with the capacity to phosphorylate hundreds of target proteins[203]. To achieve signalling specificity, it is therefore essential to restrict phosphorylation to defined subsets of substrates. This is accomplished through spatial targeting of PKA in close proximity to its substrates, such that localised elevations in cAMP selectively activate specific PKA molecules already at

the site of the desired phosphorylation target. A-kinase anchoring proteins (AKAPs) mediate this targeting and are defined by their ability to bind the R subunit of PKA[204].

To date, more than 60 AKAPs have been identified in the human genome[204]. All share a conserved 14-18 residue amphipathic helix that binds to the dimerization-docking (D/D) domain at the N-terminus of the PKA R subunit[205,206]. Additional structural motifs within AKAPs determine their subcellular localisation and mediate interactions with other signalling proteins, thereby co-localising these components with PKA[207].

In addition to PKA, AKAPs scaffold a wide range of signalling molecules, including GPCRs[208], ACs[209,210], PDEs[211,212], phosphatases[213–215], ion channels[216,217], and other kinases such as protein kinase C (PKC)[218], and protein kinase D (PKD)[219]. Through these interactions, AKAPs organise multi-protein signalling complexes referred to as 'signalosomes', at defined subcellular locations. This spatial organisation enables local cAMP signalling events to produce distinct downstream responses.

1.2.5. cAMP nanodomain signalling in cardiac myocytes

The principles of cAMP compartmentalisation are particularly well-illustrated in cardiac myocytes **(Fig 1.3)**, where precise spatial and temporal control of signalling is essential for the regulation of excitation-contraction coupling[220,221]. Autonomic regulation of cardiac function is mediated predominantly through GPCR-dependent cAMP signalling pathways.

Sympathetic stimulation of the heart occurs via β-adrenergic receptors (βARs) which signal primarily through the Gαs-AC-cAMP-PKA pathway[222]. Activation of

βARs by the endogenous catecholamines noradrenaline and adrenaline increases contractility (inotropy), heart rate (chronotropy) and the rate of relaxation (lusitropy)[223]. In contrast, parasympathetic stimulation exerts opposing effects via acetylcholine (ACh) acting on M_2 muscarinic receptors (M_2Rs)[224]. These receptors couple to Gαi/o proteins, inhibiting AC activity and reducing cAMP production[225]. The presence of robust physiological readouts of cAMP signalling, namely contractility, heart rate, and Ca^{2+} handling, has made cardiac myocytes an ideal model system for investigating the spatial organisation of cAMP signalling.

Key cAMP-regulated targets in cardiac myocytes include the L-type Ca^{2+} channel ($Ca_V1.2$), the ryanodine receptor (RyR2), phospholamban (PLB), and myofilament proteins such as troponin I (TPNI) and myosin binding protein C (MyBPC)[223]. $Ca_V1.2$ is indirectly regulated by cAMP through PKA-dependent phosphorylation of the RGK family small GTPase Rad[226]. Rad tonically inhibits $Ca_V1.2$ via association with the $Ca_V\beta$ subunit, and its phosphorylation by PKA promotes dissociation from the channel, relieving this inhibition.

cAMP also regulates Ca^{2+} handling at the SR. Phosphorylation of PLB, relieves its inhibition of the sarcoplasmic/endoplasmic reticulum Ca^{2+} ATPase (SERCA2A), enhancing Ca^{2+} reuptake into the SR and increasing the magnitude of cytosolic Ca^{2+} transients[227]. PKA has also been reported to phosphorylate the SR Ca^{2+} release channel RyR2, with some evidence suggesting modulation of channel open probability[228,229], although the role PKA-dependent phosphorylation of RyR2 in physiological regulation of excitation-contraction coupling remains debated[223].

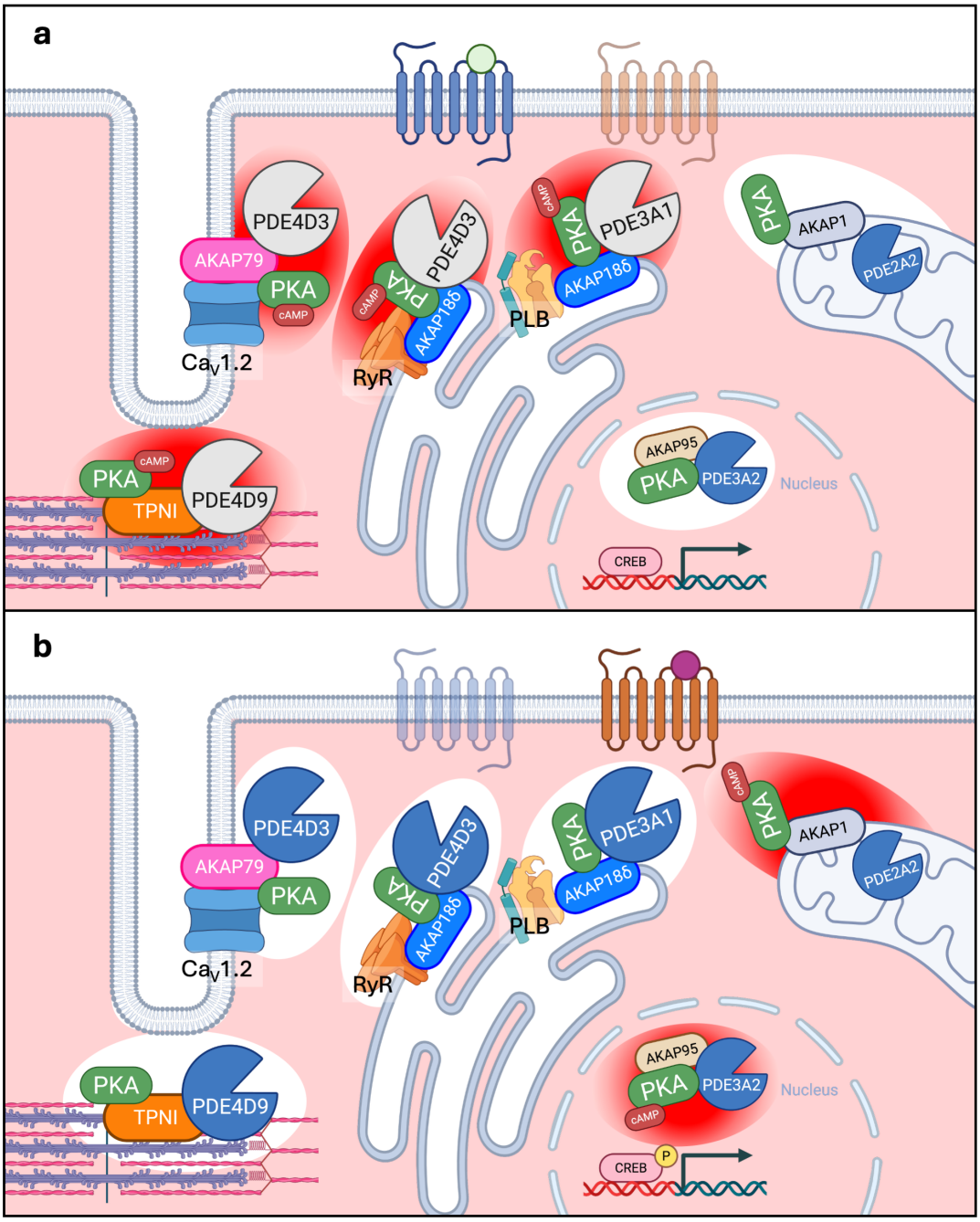


Fig 1.3. Different Gs-coupled GPCRs drive distinct patterns of cAMP signalling in cardiac myocytes. Representative schematic of cardiac myocyte showing activation of one GPCR (blue) **(a)** drives cAMP generation at the L-type Ca^{2+} channel ($Ca_V1.2$), ryanodine receptor (RyR2), phospholamban/SERCA2A complex (PLB), and troponin I at the myofilament (TPNI) whilst activation of a different GPCR (orange) **(b)** results in cAMP generation in the nucleus and at the mitochondrion, thus resulting in distinct spatial patterns of PKA substrate phosphorylation and downstream functional responses. Red shading represents locally elevated cAMP. Created using BioRender.com.

At the myofilament, PKA-dependent phosphorylation of TPNI reduces the affinity of troponin C for Ca^{2+}[230], while phosphorylation of MyBPC enhances cross-bridge formation[231]. Collectively, these effects enable adrenergic stimulation to increase contractility through enhanced Ca^{2+} entry via $Ca_V1.2$ and augmented cross-bridge cycling, while also accelerating relaxation primarily through elevated SR Ca^{2+} reuptake, as well as via reduced myofilament Ca^{2+} sensitivity. In contrast, cholinergic stimulation opposes these processes by suppressing cAMP production and limiting PKA-dependent phosphorylation of these targets.

Targeted FRET-based reporters for cAMP and PKA activity have been used extensively to characterise cAMP nanodomains in cardiac myocytes, revealing independently regulated signalling domains at key functional sites including the plasmalemma, SR, and myofilament[195,232–236].

At the plasmalemma, AKAP79/150 organises a subsarcolemmal signalosome that scaffolds PKA and the Ca^{2+}-dependent phosphatase calcineurin at $Ca_V1.2$[216,237–240]. Anchoring of PKA by AKAP79 is required for β-adrenergic regulation of $i_{Ca,L}$ [216,237]. In rodent myocytes, cAMP degradation within this nanodomain is mediated predominantly by PDE4B and PDE4D[241]. PDE1C has also been implicated in this compartment, as its inhibition enhances $Ca_V1.2$ conductance following βAR stimulation in guinea pig myocytes[242].

At the SR, AKAP18δ assembles a multi-protein signalling complex that includes PKA, PDE3A1, PDE4D, SERCA2A, PLB, calmodulin (CaM) and CaM kinase (CaMK)IIδ[243,244]. Within this nanodomain, both PDE3A and PDE4D contribute to cAMP degradation[245,246]. In addition to its role in regulating the SERCA2A/PLB

complex, AKAP18δ has also been reported to localise to the RyR2 where it anchors CaMKIIδ[244,247].

At the myofilament, cAMP nanodomains may be highly restricted to such a degree that individual proteins such as TPNI and MyBPC, are regulated by distinct localised cAMP pools[201,248]. Troponin T functions as an AKAP, anchoring PKA within the troponin complex[249], while cAMP levels within this compartment are regulated by PDE4D[248].

Much of the work characterising these signalling complexes has used targeted FRET-based reporters. However, this requires prior knowledge of their composition and localisation in order to direct sensors to specific compartments. To overcome this limitation, significant progress has been made by our group in mapping cAMP nanodomains in cardiac myocytes by combining PDE-family specific phosphoproteomic analysis with PDE-isoform specific interactomics[250]. This strategy enables identification of both the subcellular localisation of individual PDE isoforms, and the PKA-phosphorylation targets they regulate[251].

Collectively, these studies have demonstrated how distinct AKAP-PKA-PDE signalling complexes generate highly localised cAMP nanodomains that control specific components of excitation contraction coupling, as well as broader aspects of cardiac physiology.

1.3. Thesis aims

Compartmentalisation of cAMP signalling into discrete nanodomains is now well established[188,189,202]. Significant progress has been made in defining the roles of key components of the cAMP signalling pathway – including ACs, PDEs and AKAP-organised multi-protein complexes – in generating these localised signals. This framework provides a mechanistic basis for how GPCRs can elicit specific cellular responses despite engaging shared signalling pathways.

However, the higher-level organisation of compartmentalisation remains a mystery. In particular, how cells coordinate the appropriate spatial pattern of cAMP signalling in response to the activation of a specific Gs-coupled GPCR, in order to generate the desired physiological output, is still not understood.

Most studies addressing this question have focused on downstream components of the signalling pathway, particularly the organisation of signalosomes and the role of PDEs[174,188,189,202]. In contrast, comparatively less attention has been paid to the initiation of signalling at the level of GPCR activation. Since their identification, GPCRs have come to be understood not as binary on-off switches but as integrative signalling platforms that operate within complex multidimensional signalling networks rather than simple linear cascades[4,156,252–254].

Increasing attention has been given to features of GPCR signalling such as coupling to multiple Gα families, signalling by the Gβγ heterodimer, and β-arrestin-dependent signalling. Furthermore, considerable attention has focused on the ability of GPCRs to generate signals from intracellular compartments such as endosomes and the Golgi. However, comparatively few studies have directly

examined how GPCR signalling shapes local cAMP dynamics within discrete subcellular nanodomains.

This thesis aims to address this gap by investigating how GPCR signalling contributes to the generation of spatially defined cAMP signals.

To achieve this, the research has been focused into three specific aims centred on neonatal rat ventricular myocytes (NRVMs) as a model system:

Aim 1:

Rationale: Ventricular myocytes express both β_1-adrenergic receptors (β_1ARs) and β_2-adrenergic receptors (β_2ARs) which are primarily Gs-coupled GPCRs, although β_2ARs can additionally couple to Gi/o family proteins. Activation of β_1ARs and β_2ARs is known to elicit distinct functional outcomes in cardiac myocytes.

Within aim 1, the specific objectives are:

(a) To systematically compare cAMP signalling at multiple key subcellular adrenergic targets following selective activation of β_1AR versus β_2AR.

(b) To determine the contribution of β_2AR-Gi coupling to the compartmentalisation of its cAMP signal.

Aim 2:

Rationale: Biased signalling – the ability of different ligands acting at the same receptor to elicit distinct downstream signalling responses – has been studied predominantly in the context of G protein- versus β-arrestin-

mediated signalling. However, it remains unclear whether different ligands acting at the same GPCR can generate distinct spatial patterns of cAMP signalling. To address this, the β-blocker carvedilol – a clinically relevant drug with reported bias and partial agonist properties at βARs – was selected as a tool.

Within aim 2 the specific objectives are:

(a) To assess whether carvedilol acts as a partial agonist at βARs in ventricular myocytes.

(b) To compare the spatial patterns of cAMP signalling generated by carvedilol, the full βAR agonists isoproterenol and noradrenaline, and the neutral beta-blocker metoprolol.

Aim 3:

Rationale: Although it is well established that stimulation of cAMP generation by Gαs-coupled GPCRs is spatially compartmentalised, it remains unclear whether inhibition of cAMP production by Gαi/o-coupled GPCRs is similarly compartmentalised. The prototypical Gαi-coupled receptor in cardiac myocytes is the M_2 muscarinic acetylcholine receptor (M_2R), which mediates parasympathetic regulation of cardiac function.

Within aim 3 the specific objective is:

(a) To determine whether M_2R activation produces a homogeneous or a spatially compartmentalised reduction in cAMP generation in ventricular myocytes.

Together, these aims seek to define how GPCR isoform diversity, ligand identity, and G protein coupling contribute to the spatial organisation of cAMP signalling in ventricular myocytes and its translation into physiological responses.

2
Methods

2.1. Materials

2.1.1. Reagents

Carbamylcholine chloride (carbachol), forskolin, 3-isobutyl-1-methylxanthine (IBMX), isoproterenol, and norepinephrine were from Sigma-Aldrich; and bucindolol, carvedilol, CGP-20712A, ICI 118,551, metoprolol (succinate), and pertussis toxin, were from Cayman Chemical.

Collagenase A, PhosSTOP phosphatase inhibitor cocktail, and Complete EDTA-free protease inhibitor cocktail were from Roche; pancreatin (porcine) and RIPA buffer were from Sigma-Aldrich; laminin (mouse) was from Gibco; and DMEM (high glucose, and high glucose, HEPES), F-12, horse serum, L-glutamine, MEM199, newborn calf serum, PBS, and penicillin/streptomycin (1000 U/mL) were from Invitrogen. SNAP-Surface 594 was from New England Biolabs. Transfection reagents were Transfectin from BioRad and Polyplus jetPRIME from Sartorius.

2.1.2. Genetic constructs

Table 2.1 Plasmids and adeno-associated viral vectors

Name	Description	Reference
Epac-S^{h187}	Untargeted FRET-based cAMP reporter	Klarenbeek *et al.* (2015)[255]
MP-Epac-S^{h187}	FRET-based cAMP reporter targeted via N-terminal domain of Lyn kinase that is post-translationally myristoylated and palmitoylated	Unpublished*
CUTie	Untargeted FRET-based cAMP reporter	Surdo *et al.* (2017)[195]
AKAP18δ-CUTie	FRET-based cAMP reporter targeted via AKAP18δ to the PLB/SERCA2A complex at the sarcoplasmic reticulum	
AKAP79-CUTie	FRET-based cAMP reporter targeted via AKAP79 to the βAR/LTCC complex at the plasmalemma	
TPNI-CUTie	FRET-based cAMP reporter targeted via TPNI to the myofilament	
AKAR4	Untargeted FRET-based PKA activity reporter	Depry *et al.* (2010)[256]
AKAP79-AKAR4	FRET-based PKA activity reporter targeted via AKAP79 to the βAR/LTCC complex at the plasmalemma	Unpublished**

Adeno-associated viral vectors carrying these constructs were generated by Vector BioLabs (Malvern, PA, USA).

* Generated in our lab based on Epac-S^{h187}

** Generated in our lab based on AKAR4

2.2. Experimental Methods

2.2.1. HEK293T cell culture

HEK293T cells were cultured in Dulbecco's modified eagle medium (DMEM) supplemented with 10% v/v fetal bovine serum (FBS), 1% v/v penicillin-streptomycin, and 1% v/v L-glutamine, and kept in a humidified incubator at 37ºC with 5% CO_2.

2.2.2. Primary rat ventricular cardiac myocyte isolation and culture

All animal procedures conform to the guidelines from Directive 2010/63/EU on the protection of animals used for scientific purposes. Neonatal rat ventricular myocytes (NRVM) were isolated from 2 – 3-days-old Sprague-Dawley pups (Charles River) as described before[250]. Briefly, neonatal rats were sacrificed by cervical dislocation and exsanguination followed by decapitation with sterile scissors. The sternum was opened, and hearts were extracted and transferred immediately into ice-cold ADS buffer (1.2 mM NaCl, 0.05 mM KCl, 0.18 HEPES, 0.008 mM NaH2PO4, 0.06 mM glucose, 0.004 mM MgSO4). The great vessels and atria were removed, and the remaining ventricles were washed in fresh ice-cold ADS buffer. Ventricles were transferred to a 60mm dish with ice-cold ADS and minced with scissors. The pieces were transferred into 5 ml of digestion buffer (0.45 mg/mL collagenase A, 1.25 mg/mL pancreatin in ADS buffer) and incubated at 37ºC under continuous agitation with a magnetic stirrer for 5 min. After discarding the supernatant, the tissue underwent four serial digestions. During each, the tissue was first incubated at 37ºC under continuous agitation in 9 mL digestion buffer for 20 min. Following the digestion, the supernatant was collected, added to 1 mL newborn calf serum (NCS), and centrifuged at 1250 rpm for 5 min. The pellet was resuspended in 2 mL NCS and incubated at 37ºC. The remaining tissue was used in the subsequent digestion step. After four digestions, the NCS cell suspensions were pooled and centrifuged at 1250 rpm for 5 min. The pellet was resuspended in 20 mL M1 medium (Dulbecco's Modified Eagle's Medium (DMEM) (with 25 mM Hepes) supplemented with 17.5% medium 199 (M199), 10% v/v horse serum (HS), 5% v/v newborn calf serum (NCS), 200 mM L-glutamine, 100 U/mL penicillin, and 100 µg/mL streptomycin). This

suspension was pre-plated on two 100 mm dishes and incubated at 37ºC in a humidified incubator with 5% CO_2. During pre-plating, non-cardiac myocytes adhered, whilst the cardiac myocytes remained non-adherent. After 2 hours, the cardiac myocyte-containing medium was collected from the dishes and centrifuged at 1250 rpm for 5 min. The supernatant was discarded, and the pellet resuspended in 1 mL M1 medium per heart.

For viral transduction and/or plasmid transfection, 200 µL of the cardiac myocyte suspension was seeded on 24 mm laminin-coated glass coverslips in 6-well plates for a cell density of 20 – 60,000 cells per well. After incubation for two hours, wells were topped up with 2 mL M1 medium and incubated overnight in a humidified incubator at 37ºC with 5% CO_2. After 18 hours, the cells were washed with ADS buffer and the medium was replaced with M2 medium (DMEM (with 25 mM Hepes) supplemented with 17% v/v M199, 5% v/v HS, 0.5% v/v NCS, 200 mM L-glutamine, 100 U/mL penicillin, and 100 µg/mL streptomycin). The cells were kept for at least 2 hours in a humidified incubator at 37ºC with 5% CO_2 before transduction or transfection.

For western blotting, the cardiac myocyte suspension was seeded in laminin-coated 60mm dishes for a cell density of 150-450, 000. After incubation overnight in a humidified incubator at 37ºC with 5% CO_2, the cells were washed with ADS buffer, and the medium was replaced with M2 medium. Cells were seeded on day 0 following isolation then treated and harvested on day 3.

2.2.3. Transfection and infection

HEK293T cells were seeded onto 24mm glass coverslips on day 0, transfected using Polyplus jetPRIME transfection reagent according to the manufacturer's instructions on day 1, and imaged on day 2.

For imaging experiments, Neonatal rat ventricular myocytes (NRVMs) were seeded onto 24mm glass coverslips on day 0, transfected/infected on day 1, and imaged on day 2 or day 3. NRVM were transfected using Transfectin reagent according to the manufacturer's instructions. For all transfected primary myocytes, imaging was performed 48h following transfection. For adeno-associated viral vector infection, 200 µL M2 medium was collected from each well and mixed with the relevant adenoviral vector for a multiplicity of infection (MoI) of 10-100 before being added back to the cells. For infection with TPNI-CUTie, the virus-containing medium was removed and replaced with fresh M2 medium 2h following infection. For all FRET reporters transduced with adenoviral vectors, imaging was performed 24h following infection, except from AKAP79-CUTie and AKAP79-AKAR4 for which imaging was performed 48h following infection.

2.2.4. Fluorescence Resonance Energy Transfer (FRET)

FRET-based reporters for cAMP and PKA activity

Fluorescence resonance energy transfer (FRET) is a physico-chemical phenomenon in which an excited donor fluorophore transfers energy to a fluorescent acceptor, provided there is overlap between the donor and acceptor's excitation/emission spectra and the donor and acceptor are sufficiently close to each other (typically

<10 nm). The FRET efficiency is inversely proportional to the sixth power of the distance between donor and acceptor making FRET extremely sensitive to small changes in their proximity.

FRET-based biosensors have been used extensively to characterise G protein coupled receptor (GPCR) and second messenger signalling[253]. The fluorescent reporters used in this work are listed in **Table 2.2**. All FRET-based reporters used in this thesis rely on a cyan fluorescent protein (CFP) donor and yellow fluorescent protein (YFP) acceptor. FRET-based cAMP reporters are composed of a donor and an acceptor fluorophore sandwiching a cyclic nucleotide binding domain (CNBD) which binds cAMP. On cAMP binding, the CNBD undergoes a conformational change, changing the distance between the fluorophores and therefore FRET efficiency **(Fig 2.1a-d)**. These reporters can be described as either gain of FRET (GoF) or loss of FRET (LoF) depending on whether the conformational change brings the fluorophores closer together (GoF) **(Fig 2.1a)** or further apart (LoF) **(Fig 2.1b)**.

In order to study cAMP compartmentalisation, it must be possible to compare the CFP/YFP emission from different subcellular locations. However, the nanodomains into which cAMP signalling is organised are very small – in the order of tens of nanometers[196] – whilst the limit of resolution for a standard light microscope is around 200 nm. This makes it impossible to distinguish different subcellular cAMP pools. To circumvent this issue, one approach is to conjugate the FRET reporter to a targeting domain, thus placing the reporter inside the cAMP nanodomain and ensuring that for each cell, a specific subcellular location be observed directly.

The first targeted FRET sensors (ICUE1) used the CAAX-box sequence to localise the sensor to the plasma membrane, a nuclear localisation sequence to retain the sensor in the nucleus, or a section of cytochrome-C oxidase to localise the sensor to the mitochondrion[232]. These sensors were used for the first time to compare the differential dynamics of cAMP responses at different subcellular locations, demonstrating that the cAMP response is fastest at the plasma membrane, followed by the cytosol and mitochondria, and slowest within the nucleus. Although useful, these sensors face one major limitation in being able to compare signalling through the cell. Because the targeting domain is conjugated directly to one of the fluorophores **(Fig 2.1e)**, the size and geometry of each different targeting domain will result in different steric hindrance, affecting the spectral properties of the fluorophore and thus the fluorescent properties of the sensor[195].

The suite of FRET reporters used throughout this work – cAMP Universal Tag for imaging experiments (CUTie) – was designed specifically to avoid this problem[195]. Unlike all other cAMP FRET reporters, the fluorophores are not fused to the N- and C-termini of the CNBD. Rather, the ECFP donor is bound to the C-terminus and the EYFP donor is incorporated into an external loop region of the CNBD, leaving the N-terminus free for the conjugation of a targeting domain **(Fig 2.1f)**. The higher structural similarity between these sensors means that their dynamic range and kinetics are more similar[195]. This means that comparison between sensors can be more reliably interpreted as being a result of their subcellular location rather than differences between the sensors themselves.

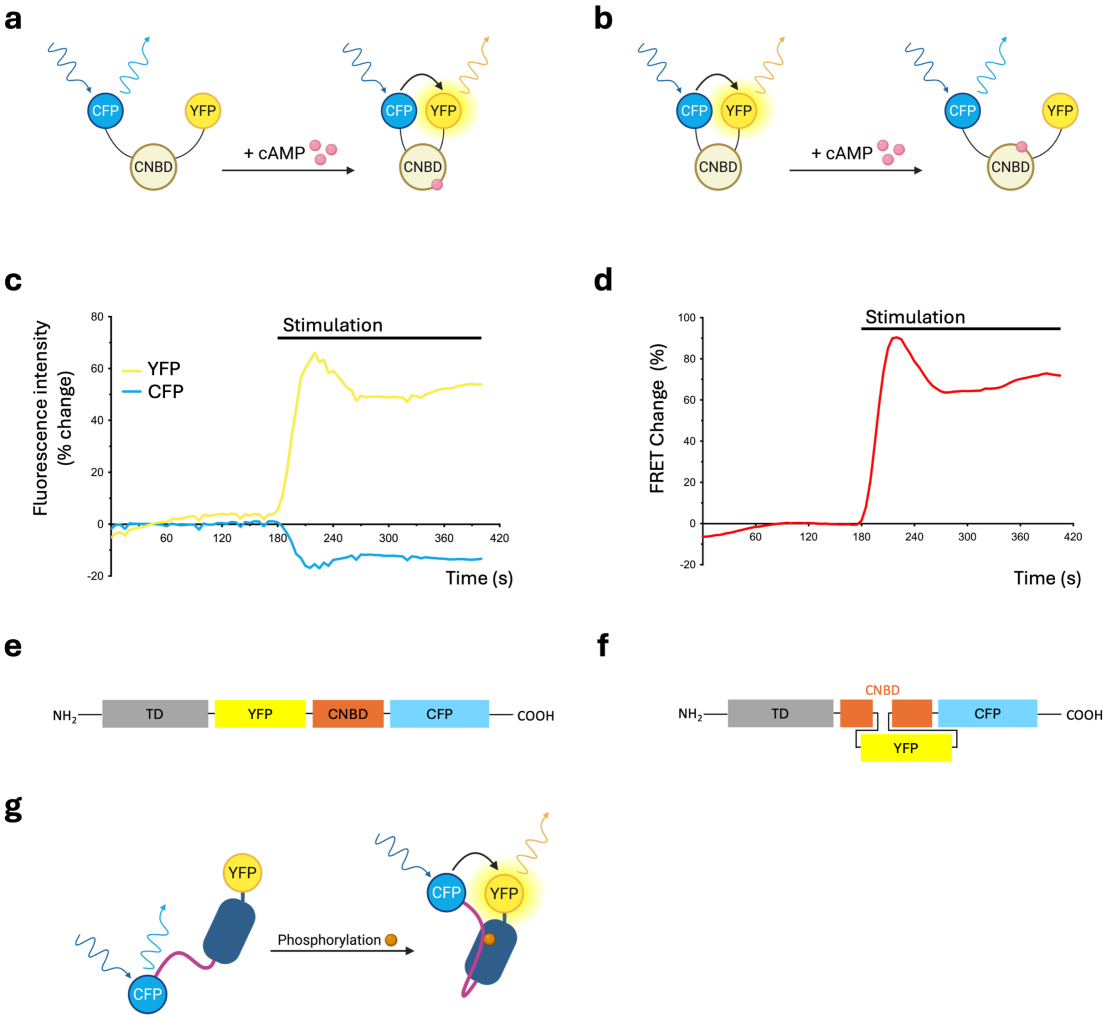


Fig 2.1 FRET-based sensors enable detection of cAMP and PKA activity in live cells. Schematic representations of generic gain of FRET **(a)** and loss of FRET **(b)** cAMP reporters. Representative curves showing change in YFP and CFP fluorescence intensity **(c)** and FRET change **(d)** in neonatal rat ventricular myocytes in response to bath application with β-adrenergic receptor agonist isoproterenol (1 nM). Fluorescence intensity and FRET change is shown as % change from initial value (F0) with F0 calculated as the average of the first six frames. Schematic representations of the structure of targeted FRET-based cAMP reporters **(e)** and CUTie **(f)**. **(g)** Cartoon representation of PKA activity reporter AKAR4. Created using BioRender.com.

Interpretation of experiments using targeted reporters depends critically on accurate localisation of the reporter to the intended compartment. The localisation of the CUTie sensors has been extensively validated previously in adult rat ventricular myocytes (ARVMs)[195]. The CUTie reporters used throughout this work –

TPNI-CUTie, AKAP18δ-CUTie and AKAP79-CUTie – target the troponin complex at the myofilament, the sarcoplasmic reticulum (SR), and a plasma membrane nanodomain, respectively. Their localisation was validated using both immunofluorescence microscopy **(Fig 2.2a)** and co-immunoprecipitation **(Fig 2.2b)**.

Localisation of TPNI-CUTie was verified by confocal imaging following co-staining for α-actinin. As expected, TPNI-CUTie showed a striated pattern alternating with the α-actinin-rich Z-discs, consistent with localisation to the myofilament **(Fig 2.2a)**. In addition, following immunoprecipitation of the sensor and its interacting proteins, cardiac Troponin T (cTPNT) was detected, further confirming localisation to the troponin complex **(Fig 2.2b)**.

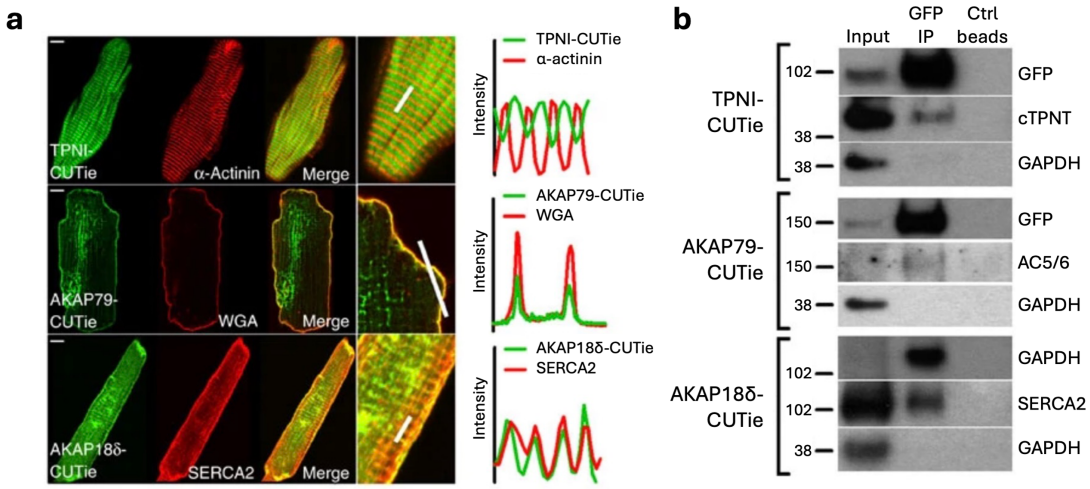


Fig 2.2 Localisation of CUTie sensors to specific subcellular nanodomains in cardiac myocytes. **(a)** Confocal images of adult rat ventricular myocytes (ARVMs) expressing TPNI-CUTie, AKAP79-CUTie or AKAP18δ-CUTie showing the localization of the sensor relative to the localization of α-actinin, wheat germ agglutinin (WGA) and SERCA2, respectively. Scale bar: 10 µm. A merge of two images and a magnified detail for each cell are also shown. On the right, the fluorescence intensity profiles for the indicated targeted sensors (green) and the reference signal (red) are shown. Intensities were calculated along the line indicated in the zoomed-in images. **(b)** Western blotting analysis of proteins in complex with targeted CUTie. ARVMs were infected with adenovirus carrying TPNI-CUTie, AKAP18δ-CUTie or AKAP79-CUTie. Targeted CUTie chimeras and their interacting

proteins were pulled down using GFP beads. Membranes were probed with the antibodies indicated on the right of each panel. **Reproduced from Surdo *et al. Nat. Commun.* (2017)[195].**

Confocal imaging demonstrated co-localisation of AKAP18δ-CUTie with the sarcoplasmic/endoplasmic reticulum Ca^{2+} ATPase (SERCA2) **(Fig 2.2a)**, whilst SERCA2 was also detected following immunoprecipitation **(Fig 2.2b)**, consistent with localisation to the SR. Similarly, AKAP79-CUTie co-localised with the plasma membrane marker wheat germ agglutinin (WGA) **(Fig 2.2a)**, and co-immunoprecipitation demonstrated interaction with adenylyl cyclases 5 and 6 (AC5/6) **(Fig 2.2b)**, confirming plasma membrane localisation. Together, these findings demonstrate that each CUTie reporter is targeted to its intended signalling compartment, allowing compartment-specific cAMP measurements to be interpreted with confidence.

In addition to CUTie, which uses the CNBD from PKA-RIIβ, this work makes use of an Epac-based sensor[255] – Epac-S^{h187}. Several Epac-based cAMP sensors have been developed[232,255,257], and their latest iterations are the sensors with the largest dynamic range, making them ideal for experiments where detection of small differences in cAMP concentration is necessary.

The concentration dependence of the FRET response of both CUTie and Epac-S^{h187} has previously been characterised *in cell* by other members of my group by intracellular microperfusion of known concentrations of cAMP**.** Both reporters respond to cAMP over a similar concentration range[200] **(Fig 2.3a)**, with reported EC50 values of approximately 7.4 μM for both cytosolic CUTie and Epac-S^{h187}. Thus,

despite their different designs and opposite directions of FRET change, the two reporters exhibit similar cAMP sensitivity.

The effect of the addition of a targeting domain on the cAMP sensitivity of the CUTie sensors has also been characterised previously[195] **(Fig 2.3b)**. AKAP18δ-CUTie, TPNI-CUTie, and AKAP79-CUTie exhibit similar concentration-dependent responses to cAMP, with substantial overlap between their concentration-response curves and similar reported EC50 values of 7.1 µM, 7.2 µM, and 7.12 µM respectively. This indicates that conjugation of the different targeting domains does not substantially alter the reporters' cAMP sensitivity.

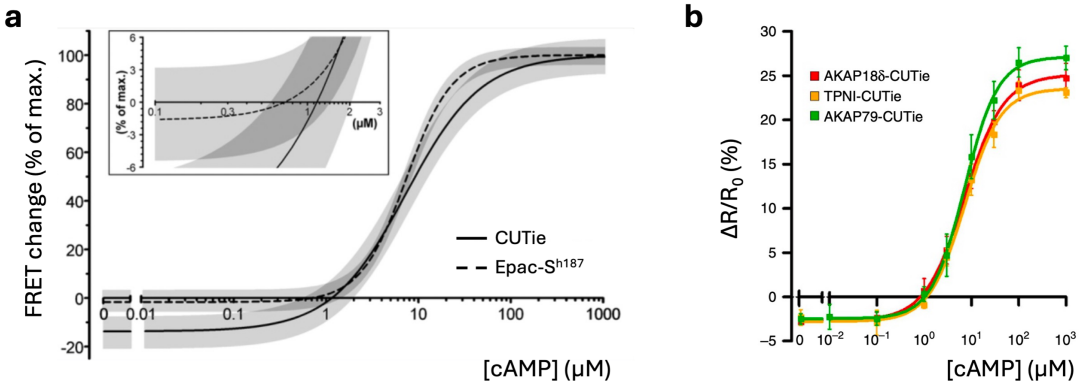


Fig 2.3 In cell calibration of FRET-based cAMP reporters. cAMP-FRET concentration-response curves generated by microinfusion of known cAMP concentrations in CHO cells stably expressing **(a)** the cytosolic cAMP FRET reporters CUTie or Epac-S^{h187}, with FRET change expressed as percentage of maximal response, or **(b)** AKAP18δ-CUTie, TPNI-CUTie, or AKAP79-CUTie, with FRET change expressed as ΔR/R0. **(a)** Reproduced from Koschinski and Zaccolo Sci Rep. (2017)[200]. **(b)** Reproduced from Surdo et al. Nat. Commun. (2017)[195].

Table 2.2 Fluorescent sensors

Name	Type	Gain or loss of FRET	Fluorophores	Localisation	Reference
CUTie*	cAMP	Gain	ECFP/EYFP FRET pair	cytosolic	Surdo *et al.* (2017)[195]
AKAP18δ-CUTie*	cAMP	Gain	ECFP/EYFP FRET pair	PLB/SERCA2A (SR)	
AKAP79-CUTie*	cAMP	Gain	ECFP/EYFP FRET pair	βAR/LTCC (membrane)	
TPNI-CUTie*	cAMP	Gain	ECFP/EYFP FRET pair	myofilament	
Epac-S^{h187}	cAMP	Loss	Turqiose2/circularly permuted (cp)Venus FRET pair	cytosolic	Klarenbeek *et al.* (2015)[255]
MP-Epac-S^{h187}*	cAMP	Loss	Turqiose2/circularly permuted (cp)Venus FRET pair	Cholsterol rich regions of the plasma membrane	Unpublished*
AKAR4	PKA activity	Gain	Cerulean/cpVenus FRET pair	cytosolic	Depry *et al.* (2010)[256]
AKAP79-AKAR4*	PKA activity	Gain	Cerulean/cpVenus FRET pair	βAR/LTCC (membrane)	Unpublished*

* Generated in our lab

Finally, in addition to FRET sensors for cAMP, FRET-based PKA activity reporters are used in this work. A-kinase activity reporters (AKAR) are four-part chimeric proteins, consisting of a CFP FRET donor, a phosphoamino acid binding domain, a PKA-specific phosphorylatable sequence, and a YFP FRET acceptor[258]. Upon phosphorylation of the PKA-specific sequence by PKA, the phosphorylated sequence binds to the phosphoamino acid binding domain resulting in conformational rearrangement of the whole molecule, a reduction in the distance between the fluorophores, and a gain of FRET **(Fig 2.1g)**. Similarly to the cAMP

sensors, targeted versions of AKAR have been developed, allowing comparison of PKA activity at different subcellular locations. The latest version of AKAR (AKAR4) has a much-improved dynamic range owing to its incorporation of brighter fluorophores – a cerulean FRET donor and a circularly permuted Venus as its acceptor[256]. When interpreting results from experiments with AKAR4, there is one extra variable that must be considered. Unlike some earlier versions of AKAR, in addition to phosphorylation by PKA, AKAR4 can be dephosphorylated by phosphatases and so the signal reflects the balance between PKA activity and phosphatase activity. This can be useful when probing the role of phosphatases in a particular signalling cascade.

FRET imaging

Cells were imaged at room temperature in a modified Ringer's solution (125 mM NaCl, 5 mM KCl, 1 mM Na3PO4, 1 mM MgSO4, 20 mM HEPES, 5.5 mM glucose, 1 mM CaCl2, pH 7.4) after 10 min pre-incubation at room temperature. Images were acquired using an inverted microscope (Olympus IX71) using a PlanApoN, 40X, NA 1.42 oil immersion objective (Olympus, UK) and equipped with a CoolSNAP HQ2 CCD camera (Photometrics) and a DV2 beam-splitter (MAG Biosystems, Photometrics). Image acquisition and processing used Metafluor 7.1 (Meta Imaging Series, Molecular Devices) (RRID:SCR_014294). FRET change was measured as change in background-subtracted 480 nm/545 nm fluorescence emission intensity ratio on excitation at 430 nm expressed as R/R0, where R is the ratio at time t and R0 is the average ratio of the first 8 frames. Drugs were added as indicated. FRET time courses were normalised to R0 to allow comparison of different FRET curves.

Quantification was performed by normalising to the maximum FRET change elicited by sensor saturation (achieved by application of 25 µM forskolin and 100 µM IBMX). FRET change is often expressed as percentage of this maximum response. Analysis was performed using Microsoft Excel (RRID:SCR_016137) and GraphPad Prism version 10.4.1 (RRID:SCR_002798).

Optimisation of βAR antagonist concentrations

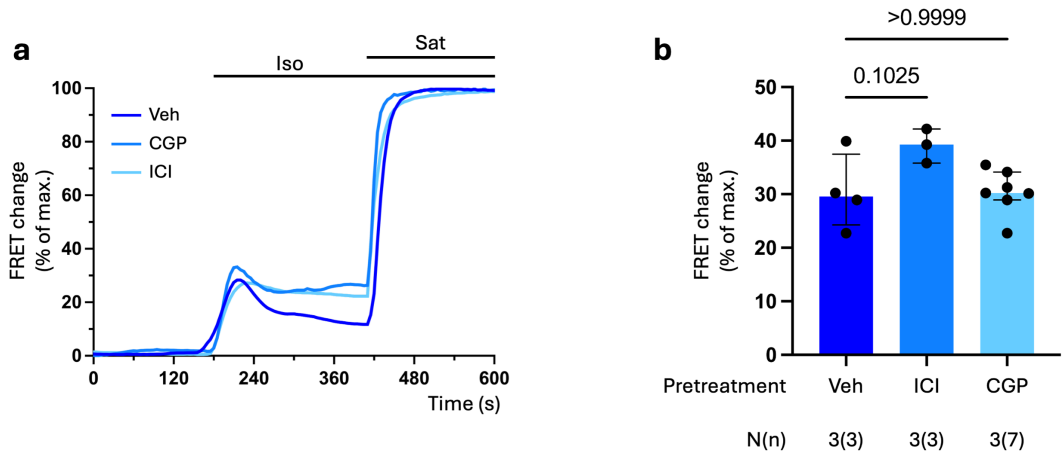


Fig 2.4 Preliminary tests of βAR subtype-selective antagonists. Representative kinetics **(a)** and summary **(b)** of FRET change in NRVMs expressing Epac-S^{h187} cAMP FRET reporter in response to bath application of 1 nM isoproterenol (Iso). Cells were pretreated with either β_1AR-selective antagonist CGP-20712A (CGP), β_2AR-selective antagonist ICI-118,551 (ICI), or an equivalent volume of vehicle (Veh, 0.1% DMSO) for at least 16 hours preceding imaging. FRET change is shown normalised to the maximum response elicited by a saturating stimulus (Sat) (25 µM forskolin + 100 µM IBMX). Error bars represent median +/- IQR. Sample size given as N(n) where N = biological replicates (cell isolations); n = individual cells.

The β_2AR-selective antagonist ICI 118,551 (ICI) and β_1AR-selective antagonist CGP-20712A (CGP) were used to isolate β_1AR- and β_2AR-dependent cAMP responses respectively. Concentrations of 50 nM ICI and 100 nM CGP, consistent with concentrations used previously for βAR-subtype selective blockade[259,260], were

initially tested in NRVMs. However, under our experimental conditions, these concentrations did not reliably inhibit the response to 1 nM isoproterenol (Iso) **(Fig 2.4)**. Therefore, the antagonist concentrations were increased to 200 nM ICI and 200 nM CGP for subsequent experiments to ensure robust functional blockade of the intended βAR subtype.

2.2.5. Western blotting

Western blotting experiments were performed as described before[250] . Neonatal rat ventricular myocytes (NRVM) were treated and/or infected as indicated and lysed with ice-cold RIPA buffer supplemented with PhosStop phosphatase inhibitor cocktail and Complete EDTA-free protease inhibitor cocktail.

For Western blotting, total protein concentration was determined using the Pierce BCA protein assay kit (Thermo Fisher Scientific) and samples were prepared using NuPAGE LDS sample and reducing buffers (Thermo Fisher Scientific) and boiled at 96ºC for 6 min. 10 to 30 µg protein per sample was resolved on either 16% tricine (Mw < 20 kDa) or 4 to 12% Bis-Tris polyacrylamide gels (Mw > 20 kDa) and transferred to nitrocellulose membranes using the Mini Blot Module (Thermo Fisher Scientific). Membranes were blocked in 5% wbv milk (Millipore) or phosphoblocker (Cell Biolabs) in TBST for 1 hr at room temperature. Incubation with primary antibodies **(Table 2.3)** was performed at 4ºC overnight with gentle agitation. Incubation with horseradish peroxidase-conjugated secondary antibodies was performed for 1 hr at room temperature. Immunoreactive bands were visualised using either SuperSignal West Pico Plus, SuperSignal West Dura, or SuperSignal West Atto (Thermo Fisher

Scientific) ECL substrates and detected using a ChemiDoc XRS+ imaging system (Bio-Rad). Membranes were stripped of bound antibodies by incubation with stripping buffer (Thermo Fisher Scientific) for 45 min at room temperature with gentle agitation. Blots were then re-probed with other antibodies as indicated. Quantification of band intensity was performed using Image Lab Software (Bio-Rad) (version 6.1.0 build 7) (RRID:SCR_014210). The extent of protein phosphorylation was calculated as the ratio of the adjusted (background-subtracted) volume of the band corresponding to the phosphorylated protein to the adjusted volume of the band corresponding to the total protein.

Table 2.3 Antibodies

Type	**Target**	**Species**	**Details**	**Dilution**
Primary	Phospholamban (phospho S16)	Rabbit	Badrilla A010-12AP	1:2500
Primary	Phospholamban	Mouse	Badrilla A010-14	1:4000
Primary	Cardiac troponin I (phospho S22 + S23)	Rabbit	Abcam ab190697	1:1000
Primary	Cardiac troponin I	Mouse	Abcam ab10231	1:1500
Primary	CREB (phospho S133)	Rabbit	Abcam ab32096	1:1000
Primary	CREB	Mouse	Cell signalling 9104S	1:1000
Primary	GAPDH	Mouse	Proteintech 60004-1	1:2000
Type	**Target**	**Species**	**Details**	**Dilution**
Secondary (HRP-linked)	Anti-rabbit	Goat	Cell Signalling 7074S	1:2000
Secondary (HRP-linked)	Anti-mouse	Horse	Cell Signalling 7076S	1:2000

2.2.6. Data and statistical analysis

Sample size (n) is specified in figure legends. All data presented were obtained from at least three separate NRVM isolations to ensure reproducibility and mitigate batch effects. The number (N) of NRVM isolations used for the experiments are also indicated in the figure legends. Each data point represents an observation from an individual cell. Observations from different cells were considered independent, supported by pilot experiments where identical stimuli elicited distinct responses in adjacent cells on the same coverslip. Data are presented as mean ± standard deviation (SD) for normal datasets and median with interquartile range (IQR) for non-normally distributed datasets. Normality was assessed using the Shapiro-Wilk test for small samples ($n<50$) and data were considered normally distributed if the p-value was greater than 0.05. If data were normally distributed and variances equal, a t-test or a one-way analysis of variance (ANOVA) was conducted with a Bonferroni correction for multiple comparisons. For non-normal datasets, the Wilcoxon rank-sum test or Kruskal-Wallis test was used with Dunn's correction for multiple comparrisons. Significance level was taken as $p \leqslant 0.05$. p-values are presented in figures. Statistical tests were performed using GraphPad Prism version 10.4.1 (RRID:SCR_002798).

3

Compartment-specific cAMP signalling by β-adrenergic receptors

3.1. Introduction

3.1.1. β-adrenergic receptor isoforms

The adrenergic receptor family comprises three receptor classes – α_1, α_2, and β – each of which is further divided into three subtypes, giving a total of nine members (α_{1A}, α_{1B}, α_{1D}, α_{2A}, α_{2B}, α_{2C}, β_1, β_2, β_3)[261,262]. Together these receptors represent one of the best characterised families of class A GPCRs. Adrenergic receptors exhibit diverse tissue expression and participate in a wide range of essential physiological processes including regulation of hepatic[262] and adipocyte[263] metabolism, and control of vascular[264] and bronchial tone[265], neurotransmission[266,267], and modulation of cardiac function[268]. The receptor classes also differ in their G protein coupling preferences. The α_1-adrenergic receptors (α_1ARs) predominantly couple to Gq/11 and signal via activation of phospholipase C[269,270], whereas the α_2ARs couple predominantly to Gi[271] and the βARs couple primarily to Gs[222], respectively inhibiting and stimulating cAMP synthesis by adenylyl cyclases.

The βARs are prototypical GPCRs and much of our understanding of GPCR signalling originated from studies of this receptor family[4,252]. In particular, the β_2AR

was the first GPCR for a diffusible ligand whose structure was solved[272] (with the first GPCR structure being rhodopsin[273]) and has since served as a central model for GPCR activation, G protein coupling, and arrestin-mediated signalling[4,105,252,274]. Both the β_1AR and β_2AR have been solved in inactive conformations stabilised by binding of the antagonist cyanopindolol (β_1AR)[275] and the inverse agonist carazolol (β_2AR)[272] respectively. In addition, agonist-bound structures have been determined for both β_1AR[276] and β_2AR[274] as well as structures of ternary complexes composed of agonist, receptor, and Gs[105,277]. The structural landscape of the β_2AR has been particularly extensively characterised and these structures provided the first direct visualisation of the now canonical outward movement of the sixth transmembrane helix (TM6) during receptor activation[272,274] and insertion of the C-terminus of the Gαs α5-helix deep into the cytoplasmic cavity of the receptor during G protein coupling[105] **(Fig 3.1)**.

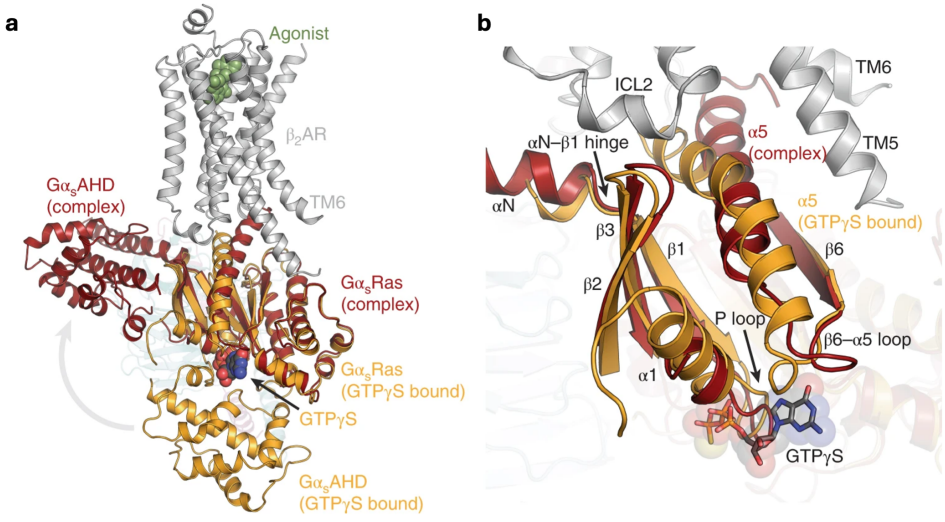


Fig 3.1 Receptor activation induces outward movement of TM6 and insertion of the Gαs α5 helix into the receptor cytoplasmic cavity. (a) Structural comparison of nucleotide-free Gαs (red) coupled to β2AR (gray, PDB 3SN6) and GTPγS-bound Gαs (orange, PDB 1AZT). GTPγS is shown as

spheres. Receptor coupling of Gs induces an outward movement of the α-helical domain of Gαs (GαsAHD) relative to its position in the GTPγS-bound state. Gβ (cyan) and Gγ (magenta) have been made transparent for clarity. **(b)** The α5 helix undergoes a rotational translation into an intracellular cavity of the receptor that is formed by outward movement of transmembrane helices TM5 and TM6 upon receptor activation. Displacement of α5 leads to perturbation of the β6–α5 loop and the hydrophobic core interaction between α5, β2 and β3 and α1, which results in a rearrangement of the β6–α5 loop and destabilization of α1, which are important for the binding of the purine ring and the phosphates of the nucleotide, respectively. Interaction between the intracellular loop 2 (ICL2) of the receptor and the αN–β1 hinge region of Gαs may also lead to conformational changes in β1 and the adjacent P loop that forms part of the phosphate-binding site in the GTPγS-bound Gαs structure. **Reproduced from Hilger *et al*. *Nat Struct Mol Bio* (2018)[278].**

3.1.2. Structural differences between βAR isoforms underlie divergent signalling

Despite sharing a highly conserved overall architecture, structural studies have revealed key differences between the β_1AR and β_2AR isoforms. The orthosteric ligand-binding pocket displays subtle distinctions, including variations in residues at the extracellular faces of TM5, TM6, and TM7 which confer differences in ligand-binding affinity[279]. This is further highlighted by naturally occurring polymorphisms in the β_2AR that increase its structural similarity to the β_1AR and are associated with reduced basal and agonist-stimulated receptor activity[279]. Additional differences in ligand sensitivity arise from divergence in the amino acid sequences of the extracellular vestibule, which forms the access pathway to the orthosteric binding pocket[280]. These differences in the ligand-binding pathway also underlie the approximately tenfold selectivity of norepinephrine for β_1AR over β_2AR[281].

Two additional key functional differences between β_1AR and β_2AR are in G protein coupling selectivity and β-arrestin recruitment. Although both β_1AR and β_2AR are considered canonical G_s-coupled GPCRs, functional studies have demonstrated

that β_2AR is also capable of coupling to G_i[282]. Structural analyses suggest that the intracellular face of the β_2AR – particularly the second intracellular loop (ICL2) – exhibits greater conformational flexibility than that of β_1AR, accommodating the α5-helix of Gαi in addition to Gαs[105,277]. Furthermore, β_2AR recruits β-arrestin more strongly and stably than β_1AR[283]. This difference is attributed, at least in part, to more efficient phosphorylation of β_2AR by GPCR kinases (GRKs)[284], whereas β_1AR exhibits weaker arrestin engagement due to structural constraints, including a proline-rich ICL3[285] and truncated C-terminal tail[286].

3.1.3. Adrenergic signalling in the cardiac myocyte

Sympathetic drive to the heart, mediated by noradrenaline released from sympathetic nerve terminals and circulating catecholamines activate cardiac βARs, increasing contractility (positive inotropy) and heart rate (chronotropy) and accelerating relaxation (lusitropy)[223]. The principal pathways through which β-adrenergic signalling regulates ventricular excitation-contraction coupling are summarised in **Fig 3.2**. Positive inotropy is achieved through PKA-dependent phosphorylation of multiple targets, including the small GTPase Rad, which regulates the L-type Ca^{2+} channel ($Ca_V1.2$)[226], and the ryanodine receptor (RyR2)[229]. Increased Ca^{2+} entry through $Ca_V1.2$ and enhanced SR Ca^{2+} release augment cytosolic Ca^{2+} transients (CaT) and thus contractile force. The lusitropic effect is mediated primarily through phosphorylation of phospholamban[227], a regulator of the sarcoplasmic/endoplasmic reticulum Ca^{2+} ATPase (SERCA2A), as well as phosphorylation of the contractile protein troponin I (TPNI)[230] which accelerate Ca^{2+} reuptake and reduce myofilament Ca^{2+} sensitivity, respectively.

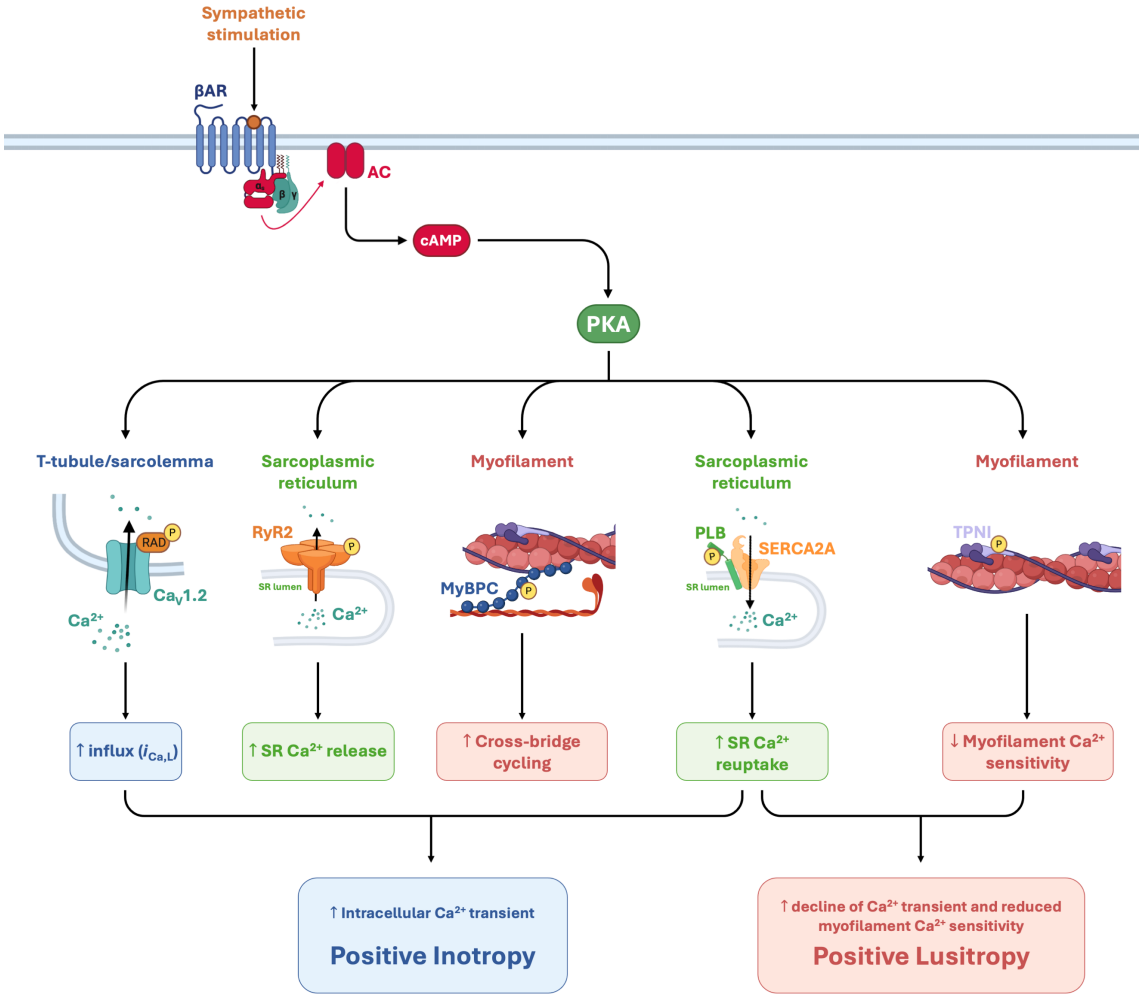


Fig 3.2 Sympathetic stimulation leads to positive inotropy and lusitropy. β-adrenergic receptors (βARs) are activated by noradrenaline released from sympathetic nerve terminals and circulating catecholamines. This results in stimulation of adenylyl cyclase (AC) by Gαs, raising intracellular cAMP and activating protein kinase A (PKA). PKA phosphorylates several targets involved in excitation-contraction coupling, including: Rad, relieving inhibition of the L-type Ca^{2+} channel ($Ca_V1.2$) and increasing Ca^{2+} influx; the ryanodine receptor (RyR2), which may increase its open probability and enhance Ca^{2+} release from the sarcoplasmic reticulum (SR); myosin-binding protein C (MyBPC), increasing cross-bridge cycling; phospholamban (PLB), relieving its inhibition of SERCA2A and increasing SR Ca^{2+} reuptake; and troponin I (TPNI), reducing myofilament Ca^{2+} sensitivity. Together, these effects increase cardiac force of contraction (positive inotropy) and accelerate relaxation (positive lusitropy).

β_1ARs are the predominant subtype in healthy ventricular myocardium, accounting for approximately 70-80% of total cardiac βARs, with β_2ARs comprising most of the remainder and β_3ARs expressed at much lower levels[287]. Beyond differences in abundance, the receptor subtypes also exhibit distinct subcellular localisation. In healthy ventricular myocytes, β_2ARs are preferentially localised to the T-tubular network, whereas β_1ARs are distributed more broadly across the sarcolemma, including both T-tubules and crest regions[288,289].

The canonical cardiac adrenergic effects of positive inotropy, chronotropy, and lusitropy are mediated predominantly by β_1AR activation rather than β_2AR stimulation[287,290]. Although this reflects, in part, the greater abundance of β_1ARs, it also arises from subtype-specific differences in signalling. Beyond their differential effects on contractile performance, β_1AR and the β_2AR drive distinct phenotypic outcomes. Chronic β_1AR stimulation promotes cardiomyocyte apoptosis, whereas β_2AR activation exerts anti-apoptotic effects[291,292]. The protective actions of β_2ARs are thought to rely on its ability to couple to Gi, in addition to Gs, as they are abolished by pertussis toxin which irreversibly ADP-ribosylates Gαi[291,292]. Consistent with these divergent signalling pathways, cardiac-specific overexpression of β_1AR induces maladaptive hypertrophy and ventricular dysfunction[293,294], whereas β_2AR overexpression results in a comparatively mild remodeling phenotype[295–297].

Subtype-specific differences are also evident at the level of cAMP/PKA signalling and downstream phosphorylation. β_1AR enhances SR Ca^{2+} handling through PKA-dependent phosphorylation of phospholamban (PLB), resulting in increased CaT amplitude, whereas β_2AR activation does not significantly modulate these

parameters in healthy ventricular myocytes[298–300]. Notably, both receptor subtypes elevate cytosolic cAMP[298,301]; however, the differing functional consequences arise due to subtype-specific compartmentalisation of cAMP signalling.

The first evidence for this came from experiments in which local stimulation of either β_1AR or β_2AR using a patch pipette in cardiac myocytes expressing a cytosolic FRET-based cAMP reporter demonstrated that β_1AR stimulation generated a cAMP signal that propagated throughout the cell, whereas β_2AR activation produced a spatially restricted increase in cAMP, confined to the site of activation[259]. This differential compartmentalisation is mirrored by PKA-dependent phosphorylation; β_1AR activation, but not β_2AR stimulation, results in phosphorylation of cytoplasmic PKA-substrates including PLB, troponin I (TPNI), and myosin binding protein C (MyBPC)[298,300].

Most studies characterising downstream differences between β_1AR and β_2AR signalling have focused on global readouts such as substrate phosphorylation, cytosolic cAMP, L-type Ca^{2+} current ($i_{Ca,L}$), or CaT amplitude. However, relatively few have directly examined local cAMP signalling[236,259,302]. Previous work using targeted FRET-based reporters has largely focused on SR-associated nanodomains and has confirmed biochemical findings, demonstrating that β_1AR, but not β_2AR, stimulation elevates cAMP at PLB[236] and RyR2[302].

The organisation of β-adrenergic signalling is remodelled in heart failure. Selective downregulation of β_1AR expression, results in an altered β_1AR:β_2AR ratio from approximately 80:20 in healthy ventricular myocytes to approximately 60:40 in the failing heart[287]. Consequently, the relative contribution of β_2AR to adrenergic

responses is increased[287]. The spatial organisation of βAR signalling is also remodelled in heart failure. Loss and disruption of the T-tubular network alters the subcellular distribution of β_2ARs, with redistribution towards crest regions of the sarcolemma, accompanied by loss of the tight spatial restriction of β_2AR-dependent cAMP signalling[288,289]. Thus, heart failure is associated with changes in both the relative abundance and compartmentalisation of βAR subtype signalling.

Despite this extensive characterisation of β_1AR and β_2AR -dependent signalling, several key questions remain unresolved. While functional differences between receptor subtypes have been attributed to differential compartmentalisation of cAMP signalling, this model is largely based on indirect or global readouts, and relatively few studies have directly measured local cAMP dynamics across multiple subcellular targets within the same experimental framework. As a result, it remains unclear how subtype-specific receptor activation translates into spatial patterns of cAMP signalling, and whether the current model of "global β_1AR signalling versus local β_2AR signalling" captures the complete picture.

Furthermore, the mechanisms by which this spatial restriction of β_2AR-dependent cAMP signalling is achieved remain incompletely understood. In particular, the extent to which the ability of the β_2AR to couple to Gαi contributes to distinguishing its cAMP signalling from that of the β_1AR is unclear.

3.1.4. Aims

While the distinct functional outcomes of β_1AR and β_2AR stimulation in ventricular myocytes have been attributed, in part, to differences in compartmentalisation of

cAMP signalling, a systematic comparison of cAMP generation at multiple key subcellular adrenergic targets following selective activation of β_1AR versus β_2AR has not previously been undertaken.

The aims of the experiments presented in this chapter are:

(a) To systematically compare cAMP signalling at multiple key subcellular adrenergic targets following selective activation of β_1AR versus β_2AR.

(b) To assess the impact of β_2AR-Gi coupling on the cAMP signal generated in distinct subcellular compartments.

3.2. Methods

3.2.1. FRET imaging

FRET experiments were performed as described in **Section 2.2.4**. Pre-treatment with CGP-20712A (CGP) or ICI-118,551 (ICI) was performed 16 hours preceding imaging by removing the M2 medium from the NRVMs and replacing it with fresh M2 medium including ICI, CGP, or equivalent volume (2 µL per well) of 0.1% DMSO vehicle as a control. Pertussis toxin (PTX) pretreatment was performed according to the same protocol. For PTX, an equivalent volume (4 µL per well) of Ringer's buffer was used as a control. ICI, CGP, PTX, and DMSO were also added to the buffer used for washing the cells and for imaging.

The antagonist concentrations used were selected based on the optimisation experiments outlined in Section 2.2.4. Although the higher concentrations ensured

a robust blockade of the intended receptor subtype, increasing antagonist concentration may also increase blockade of the non-target βAR subtype. Assuming a KD of 2 μM for Iso at both β_1AR and β_2AR, in the presence of 200 nM ICI, approximately 60% of the unblocked Iso occupancy of the β_1AR would be predicted to remain, while in the presence of 200 nM CGP, approximately 80% of the unblocked Iso occupancy of β_2AR is predicted to remain **(Appendix B)**. Thus, the concentrations used represent a conservative approach in which robust blockade of the intended receptor subtype was prioritized over minimizing potential blockade of the non-target subtype. The effectiveness of these concentrations in functionally isolating β_1AR- and β_2AR-dependent responses was subsequently assessed experimentally **(Section 3.3.2)**.

3.3. Results

3.3.1. Differential regulation of cAMP at β-adrenergic targets

The cAMP Universal Tag for imaging experiments (CUTie) comprise a suite of targeted FRET-based cAMP reporters used throughout this work. The unique structure of these sensors (described in more detail in **Section 2.2.4**) ensures that their photophysical properties are unaffected by the addition of diverse targeting domains. As a result, differences in FRET change detected by these reporters can be reliably interpreted as differences in local cAMP signalling, rather than arising from differences in sensor behaviour[195,253]. Previous work from our group using these sensors demonstrated differential regulation of both the magnitude and kinetics of cAMP signalling across subcellular adrenergic targets[195]. To ensure comparability

between the results presented here and those obtained previously, these experiments were first repeated to verify that the published findings could be reproduced.

In neonatal rat ventricular myocytes (NRVMs) individually expressing CUTie sensors targeted via AKAP18δ to the sarcoplasmic reticulum (SR), via AKAP79 to a sub-sarcolemmal nanodomain, or via troponin I (TPNI) to the myofilament **(Fig 3.3a)**, FRET changes were recorded in response to application of non-selective β-adrenergic receptor (βAR) agonist isoproterenol (Iso) (1 nM).

Consistent with data previously published by our laboratory, the cAMP responses detected by AKAP18δ-CUTie (mean FRET change = 27 ± 7% of maximal response) and AKAP79-CUTie (29 ± 13%) were not significantly different, but were significantly larger than signals detected by TPNI-CUTie (18 ± 7%) **(Fig 3.3b-d)**. In addition to differences in magnitude, the kinetics of the FRET response also differed, with the cAMP response detected by AKAP18δ-CUTie and AKAP79-CUTie occurring faster than that detected by TPNI-CUTie **(Fig 3.3c)**.

Another notable difference previously observed between these cAMP nanodomains is that the FRET responses at AKAP18δ and AKAP79 are sustained, whereas the response at TPNI is transient, peaking approximately one minute after Iso application before plateauing at a lower magnitude[195,248]. This pattern was also recapitulated here **(Fig 3.3b-c)**.

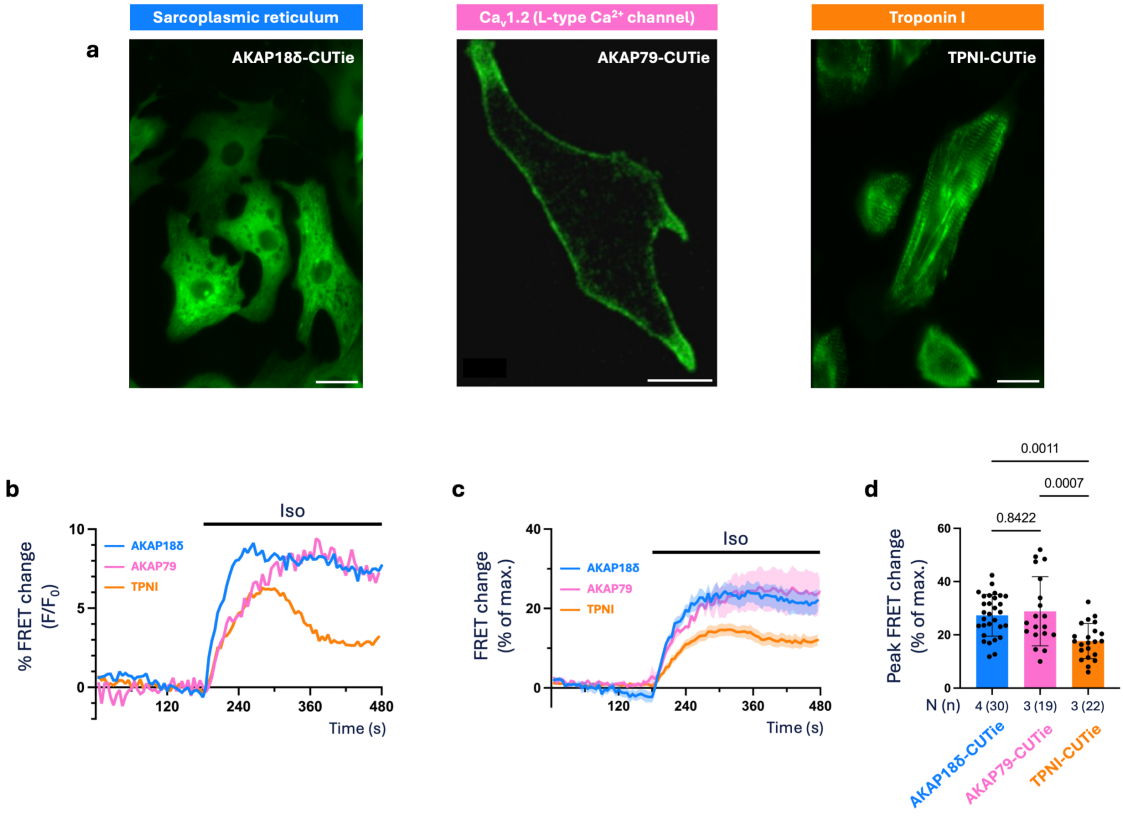


Fig 3.3 CUTie sensors enable measurement of subcellular compartmentalisation of cAMP signalling. (a) Representative images of NRVMs individually expressing AKAP18δ-CUTie, AKAP79-CUTie, and TPNI-CUTie targeted FRET-based cAMP reporters. Scale bar = 20 µm. Kinetics **(b-c)** and summary **(d)** of FRET change in NRVMs individually expressing AKAP18δ-CUTie, AKAP79-CUTie, or TPNI-CUTie in response to bath application of 1 nM isoproterenol (Iso). **(b)** Representative curves. FRET change is shown as % change from initial value (F0) with F0 calculated as the average of the first six frames. **(c)** Average curves; FRET change is shown normalised to the maximum response elicited by a saturating stimulus (Sat; 25 µM forskolin + 100 µM IBMX). Line represents mean, shading represents SD. **(d)** Points represent maximum FRET change elicited by stimulus normalised to the maximum response elicited by a saturating stimulus. Error bars represent mean +/- SD. Sample size given as N (n) where N = biological replicates (cell isolations); n = individual cells. The same sample is used in **(c)** and **(d)** with one representative trace selected from this sample for **(b)**.

3.3.2. Contribution of β-adrenergic receptor subtypes to the cAMP response in cardiac myocytes

NRVMs express both β_1-adrenergic receptors (β_1ARs) and β_2-adrenergic receptors (β_2ARs)[301] with very low levels of β_3 -adrenergic receptor (β_3AR) expression[303]. To

assess the relative contribution of the β_1AR and β_2AR to cAMP signalling at these adrenergic targets, first, a protocol for isoform-specific stimulation was validated. βAR subtype-selective agonists generally display lower specificity than subtype-selective antagonists[304,305], reflecting the high conservation of the orthosteric agonist binding pocket between β_1AR and β_2AR[279]. Accordingly, a widely used strategy[259,260,301,306,307] is to combine the non-specific βAR agonist Iso with the highly selective β_1AR and β_2AR antagonists CGP-20712A (CGP) and ICI-118,551 (ICI) respectively.

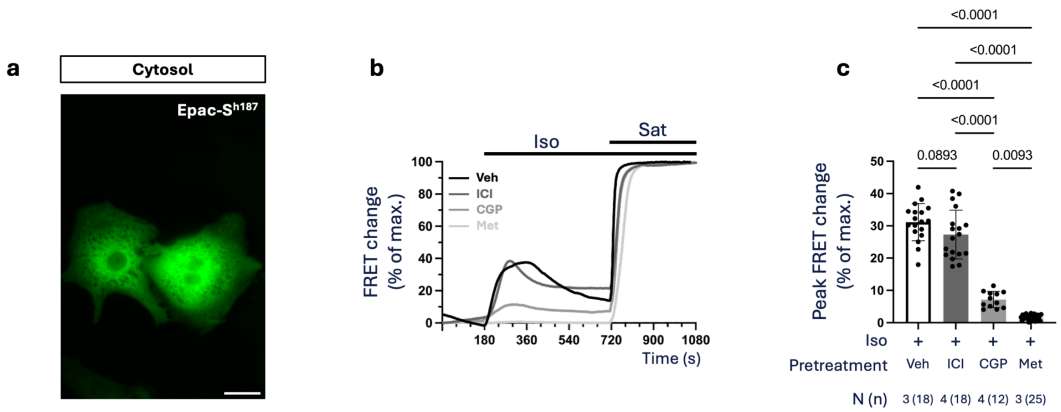


Fig 3.4 Cytosolic adrenergic cAMP generation is driven predominantly by β_1ARs in NRVMs. (a) Representative image of NRVMs expressing Epac-S^{h187} cytosolic FRET-based cAMP reporter. Scale bar = 20 µm. Representative kinetics **(b)** and summary **(c)** of FRET change in NRVM expressing Epac-S^{h187} cAMP FRET reporter in response to bath application of 1 nM isoproterenol (Iso). Cells were pretreated with either β_2AR-selective antagonist ICI-118,551 (ICI, 200 nM), β_1AR-selective antagonist CGP-20712A (CGP, 200 nM), non-selective βAR antagonist metoprolol (Met, 10 µM), or an equivalent volume of vehicle (Veh, 0.1% DMSO) for at least 16 hours preceding imaging. Data represent maximum FRET change elicited by stimulus normalised to the maximum response elicited by a saturating stimulus (Sat) (25 µM forskolin + 100 µM IBMX). Error bars represent mean +/- SD. Sample size given as N (n) where N = biological replicates (cell isolations); n = individual cells.

Non-specific βAR-blockade is achieved with metoprolol. Although metoprolol exhibits β_1-selectivity at clinically relevant concentrations (pK_D β_1AR=7.26±0.07; β_2AR=6.89±0.09)[305], at the higher concentration used here (10 μM), this selectivity is effectively lost, resulting in functional inhibition of both β_1ARs and β_2ARs. This approach enables confirmation that the observed cAMP responses are mediated specifically by βARs. Metoprolol was chosen over a non-selective antagonist due to its well-characterised pharmacology and minimal reported off-target effects at the concentrations used.

To establish the utility of this approach in our system, the effects of βAR subtype-selective blockade on cytosolic cAMP generation were first examined. In NRVMs expressing the Epac-S^{h187} cytosolic FRET-based cAMP reporter[255], responses to Iso (1 nM) were compared in cells pretreated with CGP (200 nM), ICI (200 nM), metoprolol (10 μM) for non-selective βAR blockade, or an equivalent volume of vehicle (0.1% DMSO) **(Fig 3.4)**.

In vehicle-treated control cells, Iso application elicited a mean FRET change of 31 ± 6% of maximal response. Blockade of β_1AR with CGP significantly attenuated the FRET response (7 ± 3%), whereas β_2AR blockade with ICI did not significantly reduce the FRET response (27 ± 8%). Pretreatment with metoprolol abolished the FRET response to Iso (2 ± 1%). These data indicate that β_1AR activation is the predominant contributor to adrenergic cytosolic cAMP generation in NRVMs, with a smaller contribution from β_2AR signalling.

3.3.3. Spatial compartmentalisation of cAMP signals generated by β_1ARs and β_2ARs

We then sought to determine the contribution of the βAR subtypes to compartment-specific cAMP signalling. In NRVMs expressing SR-targeted reporter AKAP18δ-CUTie, blockade of β_2AR significantly attenuated the Iso-stimulated FRET response from 29 ± 6. % to 18 ± 7%, whereas β_1AR blockade abolished the Iso-stimulated FRET response (3 ± 4%) **(Fig 3.5a-c)**. Similarly, in cells expressing the myofilament-targeted reporter TPNI-CUTie, the Iso-stimulated FRET response (18 ± 7%) was abolished by β_1AR blockade (4 ± 3%) , while β_2AR blockade had no significant effect (18 ± 9%) **(Fig 3.5d-f)**.

By contrast, in cells expressing AKAP79-CUTie, which reports cAMP within a sub-sarcolemmal nanodomain, the Iso-stimulated FRET response (24 ± 8%) was abolished by β_2AR blockade (3 ± 5%) but unaffected by β_1AR blockade (23 ± 17%) **(Fig 3.5g-i)**. Together, these data demonstrate that β_1AR signalling is the primary contributor to adrenergic cAMP generation at deeper intracellular targets such as the SR and myofilament, whereas cAMP generation within the AKAP79 nanodomain, close to the plasmalemma, is driven predominantly by β_2AR. These findings indicate that adrenergic cAMP generation within the AKAP79 nanodomain is exclusively by β_2AR, in contrast to intracellular compartments where β_1AR predominates.

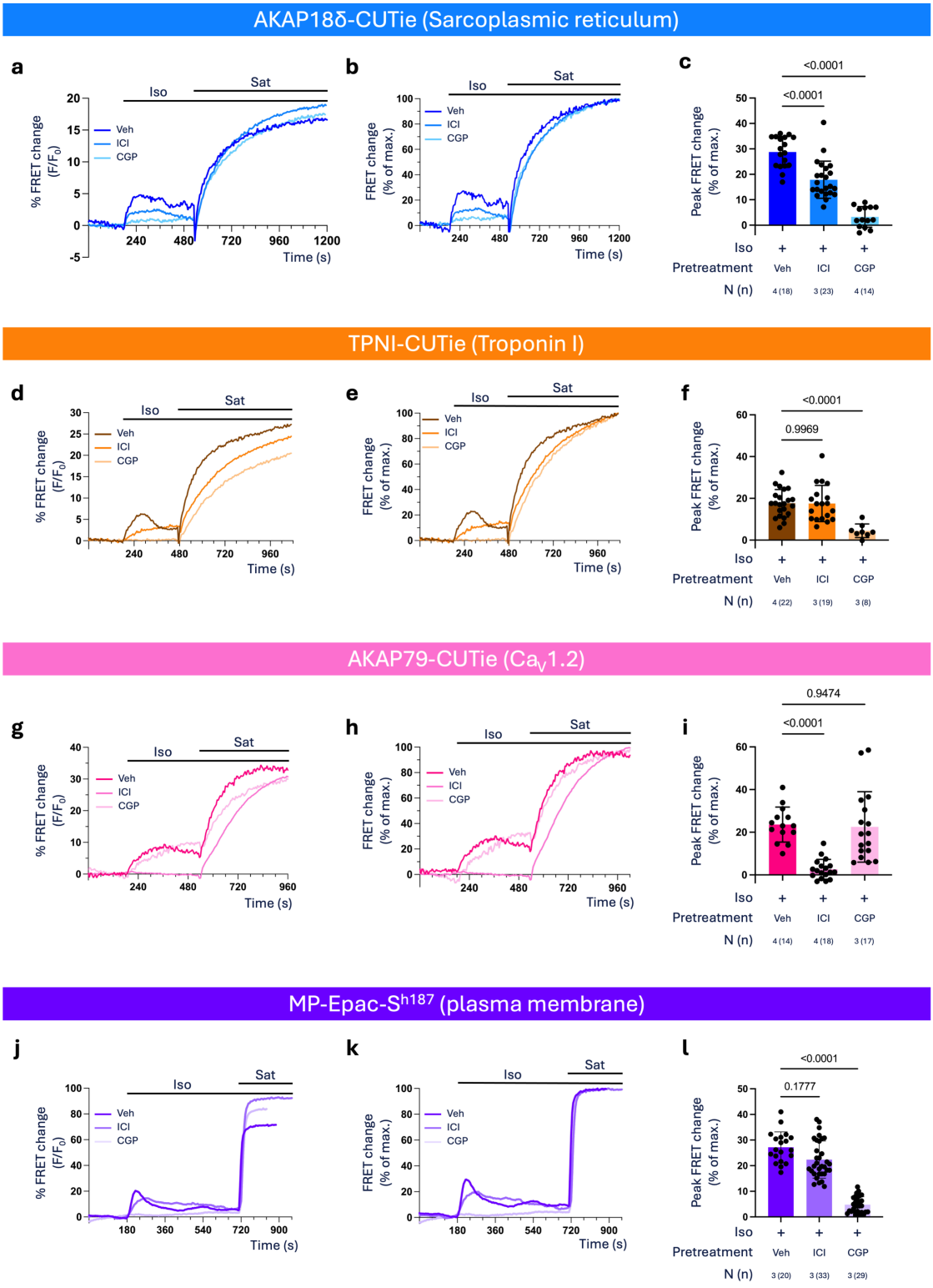


Fig 3.5 β_1ARs and β_2ARs drive distinct spatial patterns of cAMP signalling in cardiac myocytes. Representative summary **(a-b), (d-e), (g-h), (j-k)** and kinetics **(c), (f), (i) & (l)** of FRET changes in NRVMs individually expressing AKAP18δ-CUTie **(a-c)**; TPNI-CUTie **(d-f)**; AKAP79-CUTie **(g-i)**; or MP-Epac-S^{h187} **(j-l)** cAMP FRET reporters in response to bath application of 1 nM isoproterenol (Iso). Cells

were pretreated with either β_2AR-selective antagonist ICI-118,551 (ICI, 200 nM), β_1AR-selective antagonist CGP-20712A (CGP, 200 nM), or an equivalent volume of vehicle (Veh, 0.1% DMSO) for at least 16 hours preceding imaging. **(a), (d), (g) & (j)** FRET change is shown as % change from initial value (F0) with F0 calculated as the average of the first six frames. **(b), (e), (h) & (k)** FRET change is shown normalised to the maximum response elicited by a saturating stimulus (Sat) (25 μM forskolin + 100 μM IBMX). **(c), (f), (i) & (l)** Points represent maximum FRET change elicited by stimulus normalised to the maximum response elicited by a saturating stimulus. Error bars represent mean +/- SD. Sample size given as N (n) where N = biological replicates (cell isolations); n = individual cells.

3.3.4. β-adrenergic cAMP signalling at the plasma membrane

The prevailing model of subtype-specific β-adrenergic cAMP signalling proposes that β_1AR activation generates a cAMP signal that propagates throughout the cell whereas β_2AR-dependent cAMP signalling remains confined to the vicinity of the plasma membrane[259]. Our data refine this model by showing that β_1AR-dependent cAMP is excluded from the AKAP79-associated nanodomain. In addition, the question remains of whether β_2AR-driven cAMP elevation is distributed broadly across the plasma membrane or instead restricted to discrete nanodomains such as that associated with AKAP79.

To address this, βAR subtype-selective cAMP responses was compared in NRVMs expressing the plasma membrane-targeted FRET-based cAMP reporter MP-Epac-S^{h187} **(Fig 3.5j-l)**. This sensor was generated by fusion of the N-terminal targeting sequence of Lyn kinase to the N-terminus of the cytosolic Epac-S^{h187} reporter. This targeting sequence undergoes post-translational myristoylation and palmitoylation, resulting in localisation of the reporter to cholesterol-rich domains throughout the plasma membrane.

Non-selective βAR activation with Iso elicited a FRET response of 27 ± 6% of maximal response. In the presence of the β_2AR antagonist ICI, the FRET response (22 ± 7%) was not significantly different from Iso alone. In contrast, β_1AR blockade with CGP resulted in a significantly reduced FRET response (5 ± 3%), indicating that adrenergic cAMP generation at the plasma membrane is predominantly mediated by β_1ARs.

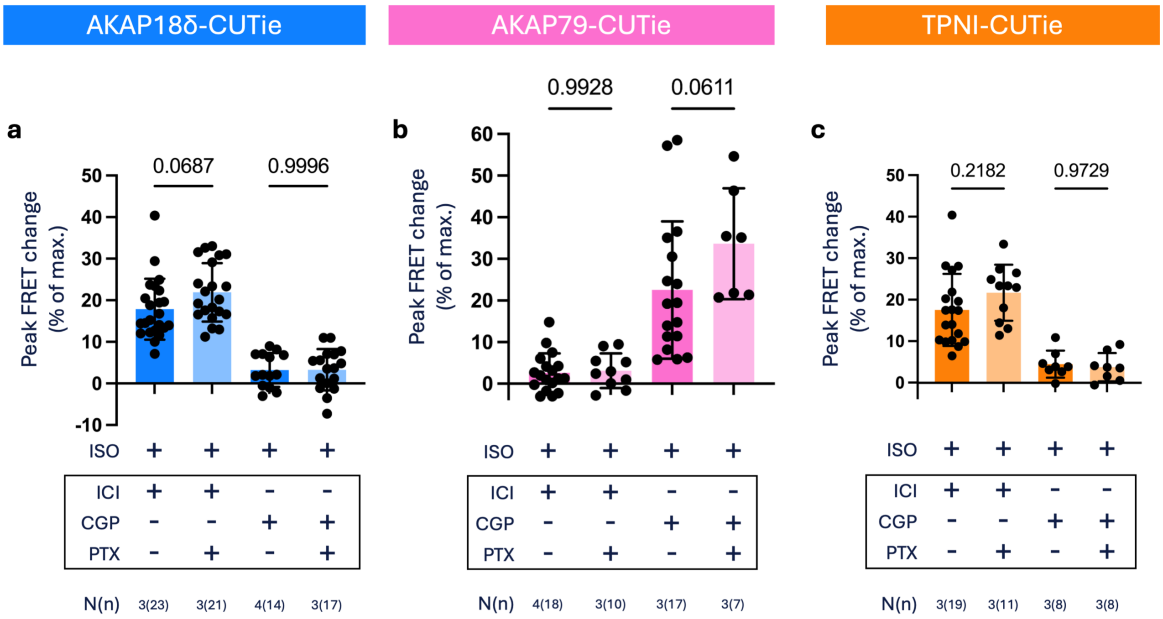


Fig 3.6 Spatial compartmentalisation of βAR-dependent cAMP signalling is independent of Gi. Summary of FRET change in NRVM individually expressing **(a)** AKAP18δ-CUTie, **(b)** AKAP79-CUTie, or **(c)** TPNI-CUTie in response to bath application of 1 nM Isoproterenol (Iso). Cells were pretreated with either β_2AR-selective antagonist ICI-118,551 (ICI, 200 nM) or β_1AR-selective antagonist CGP-20712A (CGP, 200 nM) and with either 200 ngmL^{-1} pertussis toxin (PTX) or the same volume of Ringer's buffer for at least 16 hours preceding imaging. FRET change is shown normalised to the maximum response elicited by a saturating stimulus (Sat) (25 μM forskolin + 100 μM IBMX). Error bars represent mean +/- SD. Sample size given as N (n) where N = biological replicates (cell isolations); n = individual cells.

3.3.5. The role of Gαi in cAMP compartmentalisation by β_2ARs

One of the key distinctions between the β_1AR and β_2AR is the ability of the β_2AR to couple not only to Gs, but also to Gi under certain conditions[282]. Given that Gi activation can oppose Gs-driven adenylyl cyclase activation, we hypothesised that the spatially restricted cAMP signal generated by the β_2AR might depend on its coupling to Gi. To test this, cells were pretreated with pertussis toxin (PTX), which inhibits receptor-mediated Gi activation through ADP-ribosylation of Gαi. The effectiveness of PTX treatment (200 $ngmL^{-1}$ for at least 16hrs) in inhibiting Gi-dependent signalling in NRVMs was independent confirmed using M2 muscarinic receptor activation as a positive control, as described in **Section 5.3.1 (Fig 5.1)**.

FRET responses were measured following stimulation of either β_1ARs or β_2ARs in cells expressing AKAP18δ-CUTie, AKAP79-CUTie, or TPNI-CUTie **(Fig 3.6)**. Surprisingly, the FRET changes measured in PTX-treated cells were not significantly different from controls treated with the same ligands but in the absence of PTX. These findings indicate that the exclusion of β_2AR-derived cAMP from the SR and myofilament compartments and sub-plasmalemma regions outside the AKAP79 domain is not mediated by Gi-dependent signalling.

To facilitate comparison of βAR subtype-specific cAMP signalling across the different subcellular compartments examined, the data presented above are summarised by receptor stimulation condition in **Fig 3.7**. This highlights that β_1AR activation drives cAMP signalling across multiple compartments examined, including at the plasma membrane overall, SR, and myofilament, whilst β_2AR-

dependent signalling generates a robust cAMP signal at the AKAP79-associated nanodomain.

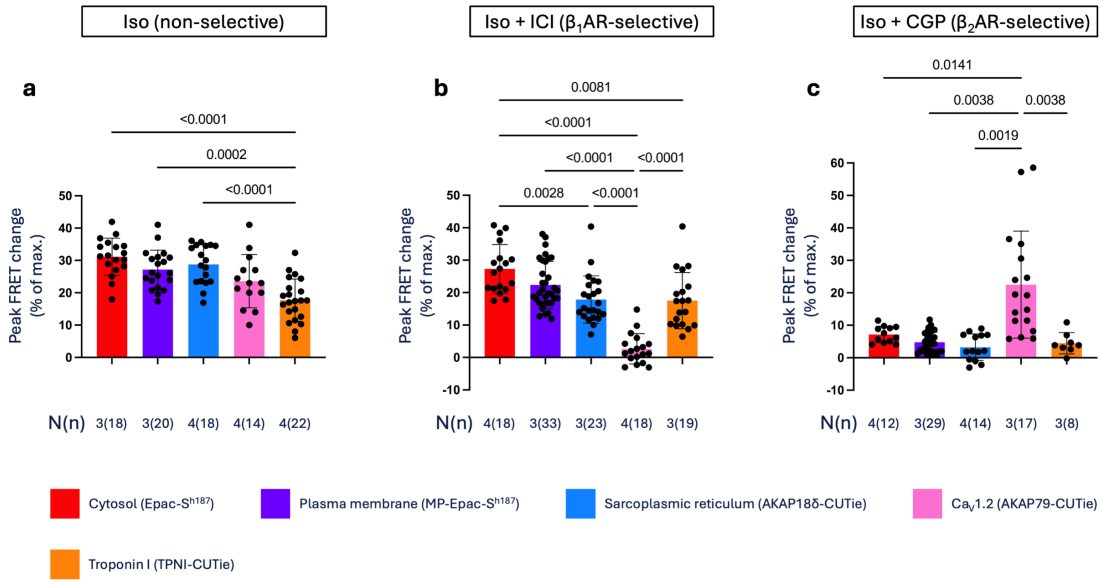


Fig 3.7 Comparison of βAR subtype-specific cAMP signalling across subcellular compartments. Summary of FRET changes in NRVMs individually expressing Epac-S^{h187}, MP-Epac-S^{h187}, AKAP18δ-CUTie, AKAP79-CUTie, or TPNI-CUTie cAMP FRET reporters in response to bath application of 1 nM isoproterenol (Iso). Cells were pretreated with either β_2AR-selective antagonist ICI-118,551 (ICI, 200 nM), β_1AR-selective antagonist CGP-20712A (CGP, 200 nM), or an equivalent volume of vehicle (Veh, 0.1% DMSO) for at least 16 hours preceding imaging. Peak FRET change is shown normalised to the maximum response elicited by a saturating stimulus (Sat) (25 μM forskolin + 100 μM IBMX). Error bars represent mean +/- SD. Sample size given as N (n) where N = biological replicates (cell isolations); n = individual cells. Data presented here are the same data as presented in **Figs. 3.3 & 3.4.**

3.4. Discussion

3.4.1. β_1ARs regulate cytoplasmic targets whilst β_2ARs selectively regulate the AKAP79 nanodomain

The canonical sympathetic effects of noradrenergic stimulation of the heart – namely positive inotropy, chronotropy, and lusitropy – are primarily mediated by

β_1ARs, whilst signalling by β_2ARs produces a comparatively smaller inotropic effect and little or no detectable lusitropic effect[282,308]. Most previous studies examining βAR subtype-selective signalling have focused on downstream functional outputs, including phosphorylation of PKA substrates and electrophysiological or contractile parameters such as L-type Ca^{2+} current ($i_{Ca,L}$), Ca^{2+} transients (CaT), and sarcomere shortening.

Biochemical studies have demonstrated that β_1AR-selective activation drives phosphorylation of key sarcoplasmic reticulum (SR) and myofilament targets, including phospholamban (PLB)[298,309,310], troponin I, and myosin binding protein C (MyBPC)[300,311], whereas β_2AR-selective stimulation produces little or no detectable phosphorylation of these substrates. These molecular findings are consistent with functional observations showing that adrenergic regulation of CaT magnitude and decay kinetics follows β_1AR activation but not β_2AR stimulation[298,299,312]. In contrast, β_2AR-selective activation has been shown to modulate $Ca_V1.2$, increasing both the peak amplitude and duration of $i_{Ca,L}$[299,309,310,312,313]. Although β_1AR activation has also been reported to enhance $i_{Ca,L}$[298–300,312–314], most studies compared β_2AR-selective stimulation with non-subtype-selective βAR activation, making it difficult to isolate effects attributable specifically to β_1AR signalling.

Our data obtained using targeted FRET-based CUTie sensors not only corroborate previous studies but also uncover previously unappreciated spatial specificity in βAR dependent cAMP signalling, thereby refining the current model.

Based on previous FRET imaging studies[259] and the functional data discussed above, the prevailing model proposes that β_2AR-derived cAMP is tightly compartmentalised,

allowing β_2ARs to regulate only plasma membrane targets, whereas β_1AR-derived cAMP can diffuse more freely, enabling regulation of targets throughout the cell[308].

Our results challenge the current view of β_1AR-cAMP as diffuse and β_2AR-cAMP as broadly membrane-restricted. Specifically, we demonstrate that β_2AR-driven cAMP is not broadly distributed across the plasma membrane but instead is confined to discrete nanodomains, specifically the domain associated with AKAP79. Furthermore, we show that β_1AR-dependent cAMP is not simply a global signal but engages distinct subcellular compartments differentially, driving cAMP generation cytoplasmic targets such as the SR and myofilament, but not at AKAP79 (see **Section 5.4.1** for detailed discussion of AKAP79 localisation and $Ca_V1.2$ regulation), whereas its signal is robust at membrane regions outside the AKAP79 domain. Collectively, these findings indicate that the classic global-versus-local paradigm is incomplete, and that both β_1ARs and β_2ARs generate spatially restricted cAMP signals that engage distinct subcellular compartments.

3.4.2. Contribution of plasma membrane organisation to βAR cAMP compartmentalisation

These findings raise the question of how cardiac myocytes coordinate these differently compartmentalised cAMP signals. One potential contributing factor is spatial organisation within the sarcolemma. Ventricular cardiac myocytes possess a highly structured plasma membrane architecture characterised by an extensive network of invaginations called transverse tubules (T-tubules) which extend the cell surface membrane deep within the cell and position $Ca_V1.2$ in close proximity to the RyR2 on the SR, facilitating Ca^{2+}-induced Ca^{2+} release (CICR)[223,315]. A study

combining live-cell FRET-based cAMP imaging with scanning ion conductance microscopy to achieve highly localised βAR stimulation demonstrated that β_2AR-cAMP signalling is exclusively localised to T-tubules whereas β_1ARs are distributed across both crests and T-tubules[288]. This differential localisation could provide a structural framework that may underlie the selective engagement of distinct cAMP nanodomains by βAR subtypes.

However, neonatal rat ventricular myocytes (NRVMs), which were used for our experiments, differ structurally from adult ventricular myocytes in that they lack a mature T-tubular network[308]. Instead, NRVMs exhibit a higher density of smaller plasma membrane invaginations called caveolae that are thought to contribute to T-tubule development, sharing some of their functional characteristics[316]. Biochemical studies have demonstrated that β_2ARs and Gαi are enriched within caveolar fractions, whereas β_1ARs, Gαs, and AC 5/6 are distributed between caveolae and non-caveolar membrane fractions[317]. The findings described in this chapter suggest that, despite the absence of T-tubules, NRVMs retain membrane microdomain organisation capable of supporting βAR subtype-specific spatial signalling, indicating that factors other than membrane organisation may be responsible for this differential signalling.

AKAP79 has been shown to anchor ACs, PKA, and the Ca^{2+}-dependent phosphatase calcineurin within caveolin-3-associated complexes[238] and at T-tubules[318] in ventricular myocytes. Close spatial proximity between β_2AR and the AKAP79 nanodomain at these membrane sites could therefore facilitate local cAMP generation within this scaffold, even in the context of only a modest increase in bulk

cytosolic cAMP. Consistent with this, AKAP79 has been reported to co-immunoprecipitate with β_2AR[319,320].

However, this receptor-AKAP association alone does not fully account for the pronounced spatial restriction of β_2AR-derived cAMP compared with β_1AR signalling. Furthermore, it remains unclear why β_1AR stimulation fails to generate cAMP within the AKAP79 nondomain, given evidence that β_1AR is also present within T-tubular and caveolar membrane fractions and has also been reported to co-immunoprecipitate with AKAP79[321]. Notably, our data demonstrate that even within the plasma membrane, cAMP signalling is non-uniform; measurements using MP-Epac-S^{h187} reveal functional heterogeneity across the membrane. These observations suggest that additional mechanisms beyond simple receptor-nanodomain proximity must contribute to subtype-specific cAMP compartmentalisation.

3.4.3. β_2AR-Gi signalling may have a cAMP-independent component

An obvious mechanistic candidate for differential cAMP nanodomain engagement is the ability of the β_2AR to couple not only to Gs but also, under certain conditions, to Gi, whereas the β_1AR is generally considered to only signal via Gs[282]. Given that Gi activation can oppose Gs-mediated stimulation of adenylyl cyclase (AC), differential Gi engagement has been proposed as a mechanism underlying the distinct downstream effects of β_1AR and β_2AR activation. Indeed, inhibition of Gi-receptor coupling with pertussis toxin (PTX), results in β_2AR-dependent phosphorylation of phospholamban and enhances the positive inotropic and lusitropic effects in response to β_2AR stimulation[309]. Although cAMP was not

measured directly in these studies, the findings have been widely interpreted as indicating that Gi recruitment is responsible for the tight compartmentalisation of β_2AR-derived cAMP.

However, our findings do not support a role of Gi in the observed cAMP compartmentalisation. In PTX-treated cardiac myocytes, β_2AR-selective activation remained unable to generate detectable cAMP at the SR and myofilament, indicating that the exclusion of β_2AR-derived cAMP from these compartments persists despite inhibition of Gi signalling. When considered alongside previous reports demonstrating enhanced phosphorylation and augmented functional responses following PTX treatment, these data suggest a more complex regulatory framework. Specifically, our results indicate that the tight compartmentalisation of β_2AR-derived cAMP is not solely dependent on Gi coupling. Instead, the increased PLB phosphorylation observed after PTX treatment may reflect Gi-dependent mechanisms that are independent of cAMP.

Although the canonical view of Gi signalling centres on AC inhibition and consequent reduction of cAMP generation, Gi-mediated signalling is more accurately described as multimodal. In addition to direct inhibition of AC by the Gαi subunit, signalling downstream of Gi coupled receptors (GiPCRs) also involves the Gβγ heterodimer[68]. As discussed in greater detail in **Sections 1.2.3 and 5.1.1**, GiPCR activation results in the release of the free Gβγ heterodimer which independently drives downstream signalling events through interaction with a variety of effectors, including specific AC isoforms[57–60], phospholipase C (PLC)-β[61–

[63], phosphoinositide 3 kinase (PI3K)-γ[64], mitogen activated protein kinases (MAPKs/ERKs)[322], and GPCR kinases (GRK) 2 and 3[65].

Much of our understanding of Gβγ-dependent signalling derives from studies of GPCRs that predominantly couple to Gi, such as the type 2 muscarinic acetylcholine receptor (M_2R). Nevertheless, there is experimental evidence supporting β_2AR-mediated Giβγ signalling, including activation of PI3K[323,324], and ERK1/2[325,326]. PI3K represents a plausible candidate for mediating β_2AR-Giβγ-dependent regulation of cytosolic phosphorylation. Inhibition of PI3K in cardiac myocytes has been shown to increase PLB phosphorylation and augment isoproterenol-stimulated positive inotropic and lusitropic responses[327,328]. Consistent with this, β_2AR-selective activation has been reported to stimulate PI3K activity, with cardiac myocytes treated with β_2AR-selective agonist formoterol exhibiting increased PI3K activity whereas those treated with β_1AR-selective agonist dobutamine did not[324].

Several mechanisms could explain how β_2AR-driven PI3K activity might limit PLB phosphorylation. One possibility is that PI3K stimulates phosphodiesterase (PDE) activity at the SR, thereby enhancing local cAMP degradation and restricting accumulation of cAMP within the PLB nanodomain. Supporting this hypothesis, PDE4 inhibitor rolipram increases PLB phosphorylation in wild-type myocytes but not in PI3K-deficient cells[328], suggesting that PI3K activity may influence PDE-dependent regulation of PLB.

However, the evidence for a PI3K-PDE-cAMP axis is not unequivocal. Although PI3K inhibition has been reported to elevate cytosolic cAMP[329,330], treatment with the PI3K

inhibitor LY294002 did not alter β_2AR driven cAMP generation[327]. It should be noted that these studies quantified bulk cAMP in whole-cell lysates, which may not accurately reflect local cAMP dynamics at the SR. Nevertheless, if PI3K-mediated stimulation of PDE4 at the SR were responsible for suppressing PLB phosphorylation, one would predict elevated basal PLB phosphorylation in PI3K knockout myocytes, which has not been observed[328]. Furthermore, under a model in which β_2AR stimulation promotes Gi$\beta\gamma$-dependent activation of PDE4 at the SR, PTX treatment would be expected to permit β_2AR-driven cAMP accumulation within this compartment. This was not detected in our experiments.

Given that phosphorylation status reflects a balance between kinase activity and phosphatase-mediated dephosphorylation, an alternative mechanism more consistent with our data is that β_2AR stimulation enhances phosphatase activity at cytosolic PKA substrates, thereby limiting their phosphorylation independently of local cAMP concentration.

3.5. Conclusions

The main findings of the work described in this chapter are:

Consistent with previous reports, we confirmed that:

- β_1AR and β_2AR drive distinct cAMP signals in cardiac myocytes.

The original findings of the work described in this chapter are:

- β_1AR activation results in detectable cAMP generation at the plasma membrane and at intracellular targets, including the sarcoplasmic reticulum

(SR) and myofilament, but not within the AKAP79-associated plasma membrane nanodomain.

- β_2AR activation selectively generates cAMP within the AKAP79 nanodomain but not more broadly at the plasma membrane or at the SR or myofilament.

- The absence of β_2AR-derived cAMP generation at the SR and myofilament does not rely on Gi coupling.

Collectively, these findings refine the classical view that β_1AR signalling is diffuse whereas β_2AR signalling is confined to the plasma membrane. Instead, our data support a model in which both receptor subtypes generate spatially restricted cAMP signals but engage distinct subcellular nanodomains.

4

Diversification of cAMP signalling driven by different ligands acting at the β-adrenergic receptor

4.1. Introduction

4.1.1. Biased signalling by GPCRs

Classically, all signalling output resulting from the activation of a GPCR was attributed to G proteins. Relatively newer, is a model in which GPCRs are able to couple other downstream effectors and drive completely distinct signalling. The first of these effectors to be identified – and also best characterised – are the beta-arrestins (β-arr).

The arrestins were first identified in photoreceptors as part of the cellular machinery responsible for switching off rhodopsin[87]. Around the same time, desensitisation of the beta 2 adrenergic receptor (β_2AR) was shown to require phosphorylation by a cAMP-independent kinase[82–84]. The purified kinase – originally referred to as β_2AR kinase (β_2ARK1) – was shown to phosphorylate the agonist-bound form of the receptor[85]. Phosphorylation by β_2ARK1 – now referred to as G protein coupled receptor kinase 2 (GRK2) – was shown to be necessary but not sufficient for receptor desensitisation. This also required an analogue of visual arrestin[86].

Now, seven GRKs and four arrestins have been identified. These include two visual GRKs – GRK1[88] and GRK7[89] – which phosphorylate rhodopsin and cone opsins respectively, and five non-visual GRKs – GRK2[90], GRK3[91], GRK4[92], GRK5[93], and GRK6[94] which are expressed throughout the rest of the body. Similarly, there are two visual arrestins, arrestin 1[98] (the rod arrestin) and arrestin 4[99] (the cone arrestin), and two non-visual arrestins, arrestin 2[100] and arrestin 3[101]. Arrestins 2 and 3 are more commonly referred to as β-arrestin 1 and β-arrestin 2 respectively. Along with the identification of this full complement of GRKs and arrestins, evidence that desensitisation of receptors other than the β_2AR rely on a similar cascade[102,103] led to the paradigm of GPCR desensitisation by GRK-mediated phosphorylation followed by recruitment of β-arr and receptor internalisation[81].

Unexpectedly, in addition to this role in terminating G protein-dependent signalling, arrestins have been shown to act as adaptor proteins, platforming the interaction between GPCRs and kinases including Src[114] and ERK1/2[115]. This led to the idea that GPCRs can drive bimodal signal transduction either via the canonical G protein-dependent signalling or via β-arrestin-dependent signalling. It is worth noting that β-arrestin-ergic signalling is sometimes referred to as G protein-independent signalling and although arrestin-mediated GPCR endocytosis is G protein-independent, β-arr signalling requires functional G proteins in addition to β-arr[117].

'Biased signalling' also termed 'functional selectivity' refers to the observation that the propensity of a GPCR to drive G protein-dependent versus β-arrestin-dependent signalling depends on which ligand has activated that receptor[125,126]. Arrestin-biased ligands are those which on binding to a GPCR, do not result in G protein recruitment

or activation but do lead to arrestin recruitment and subsequent downstream signalling. The ability of different ligands acting at the same receptor to drive distinct signalling outputs has since been attributed to the fact that rather than having one single active state, different ligands can stabilise different active conformations of the same receptor[15,127–129].

As with other aspects of GPCR signalling, including receptor activation and G protein coupling, β-adrenergic receptors (βARs) have served as key model systems for studying arrestin-dependent signalling and functional selectivity[252], and have consequently become important targets for therapeutic modulation.

4.1.2. β-blockers

βARs are among the most extensively targeted GPCRs[6], with competitive antagonists at βARs – commonly referred to as β-blockers – representing one of the most widely prescribed drug classes in the UK[331]. β-blockers are used for a range of cardiovascular indications, including hypertension, angina, myocardial infarction, arrhythmias, and heart failure[332].

A wide variety of β-blockers are in clinical use, differing in their pharmacodynamic properties, including selectivity for β_1ARs versus β_2ARs, partial agonist activity, off-target effects, and lipid solubility which in turn determines CNS access[333,334].

Based on some of these properties, β-blockers are commonly classified into three generations. First generation β-blockers are non-selective, exhibiting similar affinity for β_1ARs and β_2ARs. This class includes propranolol – the first β-blocker to be developed – which is often considered the prototypical first-generation agent[335]. The

rational development of propranolol by James Black transformed the treatment of cardiovascular disease and was recognised by the award of the 1988 Nobel Prize in Physiology or Medicine. Other non-selective β-blockers include nadolol, pindolol, timolol, and sotolol[333,334]. Due to their lack of receptor selectivity, these agents are associated with adverse effects, including bronchoconstriction arising from blockade of β_2ARs in airway smooth muscle.

To address this limitation, β_1-selective agents were developed, constituting the second generation of β-blockers. The first such agent, practolol, was subsequently withdrawn from the market due to toxic off-target effects; however, several cardioselective β-blockers remain in widespread clinical use, including atenolol, bisoprolol, and metoprolol[333].

Third generation β-blockers, in addition to βAR antagonism, possess vasodilatory properties that reduce total peripheral resistance and, consequently, afterload. This helps preserve haemodynamic function despite reduced cardiac contractility. These agents achieve vasodilation through distinct mechanisms. For example, carvedilol and labetalol also antagonise α_1ARs in vascular smooth muscle[336,337], whereas nebivolol promotes nitric oxide production[338]. Despite their shared vasodilatory effects, third generation β-blockers differ in receptor selectivity, with carvedilol and labetalol being non-selective[305] and nebivolol displaying β_1-selectivity[339].

Another distinguishing property of some β-blockers is their so-called “intrinsic sympathomimetic activity” (ISA), which refers to their activity as partial agonists at one or more βAR subtypes. As a result, these agents can both attenuate the effects

of high-efficacy full agonists, such as endogenous catecholamines, and simultaneously provide low-level βAR stimulation[340]. Early studies measuring contractile force in isolated cardiac muscle preparations treated with a range of β-blockers were used to classify ISA[341–343]. Initially, this property was thought to confer clinical benefit, as it was hypothesised to reduce undesirable bradycardia – an adverse effect of β-blocker therapy – and that β_2AR stimulation might help maintain bronchodilation[340].

In fact, β-blockers with ISA appear to be less effective in the treatment of heart failure. Six β-blockers have been evaluated in clinical trials for this indication. Bisoprolol[344], carvedilol[345], metoprolol[346], and nebivolol[347] have all been shown to reduce all-cause mortality compared with placebo. In contrast, bucindolol had no significant effect on mortality[348], whereas xamoterol was associated with an increase in mortality[349]. Notably, of these six agents, bucindolol and xamoterol are the only two that have consistently demonstrated ISA[341–343,350] and neither are currently approved for clinical use.

These differences in clinical efficacy can be understood in the context of heart failure pathophysiology. Chronic heart failure is characterised by impaired cardiac function, in which the heart is unable to maintain adequate cardiac output, or can only do so at elevated filling pressures. This may arise from systolic dysfunction (heart failure with reduced ejection fraction, HFrEF), in which contractility is reduced, or diastolic dysfunction (heart failure with preserved ejection fraction, HFpEF), in which ventricular filling is impaired.

In HFrEF, reduced contractility might intuitively suggest a role for positive inotropic agents, such as βAR agonists. However, in the context of a compensatory increase in sympathetic drive, chronic adrenergic stimulation is detrimental to the failing heart, promoting maladaptive cardiac remodelling, arrhythmia, and increased mortality[293,294,351,352]. Consequently, β-blockers are used to counteract sustained sympathetic drive[353]. This provides a mechanistic basis for the poorer clinical outcome observed with β-blockers exhibiting ISA.

These differences in clinical efficacy indicate that β-blockers do not seem to behave as a homogeneous class, suggesting that their distinct pharmacological properties, beyond simple βAR antagonism, influence clinical outcomes. Notably, although controversial, the only head-to-head trial of β-blockers in heart failure showed carvedilol reduced all-cause mortality to a greater extent than metoprolol[354], raising the possibility that certain β-blockers possess unique signalling properties that contribute to their clinical efficacy.

4.1.3. Carvedilol

Initial mechanistic explanations for the clinical superiority of carvedilol focused on properties beyond βAR antagonism, including antioxidant, anti-inflammatory, antiapoptotic, and antidysrhythmic effects, as well as its activity as an α_1AR antagonist[337,355–357]. However, a study from the Lefkowitz group proposed an alternative mechanism, suggesting that carvedilol acts as a β-arrestin (β-arr) biased ligand at β_2ARs[358] .

In HEK293 cells overexpressing β_2ARs, carvedilol promotes GRK-mediated phosphorylation of the receptor as well as recruitment of β-arr-GFP[358]. Furthermore, while several β-blockers were shown to induce ERK1/2 phosphorylation, carvedilol was unique in retaining this effect in cells expressing mutant β_2ARs that are unable to couple to G proteins but remain able to recruit β-arr. Carvedilol-induced ERK1/2 phosphorylation was abolished following siRNA-mediated knockdown of β-arr2. Together, these findings established a model in which, carvedilol acts as an inverse agonist at the Gs-AC-cAMP pathway and an agonist for β-arr-dependent ERK signalling[268].

Despite its widespread acceptance, this model is supported by surprisingly limited experimental evidence for carvedilol's action as a β-arr-biased ligand. In fact, the broader literature paints a complex, and in some cases contradictory, picture of carvedilol's pharmacology.

In more recent studies carvedilol-driven β-arr-dependent signalling could not be reproduced. Using a "zero functional G" HEK293 knockout cell line which lacks any functional G proteins, the Kostenis group did not observe ERK1/2 activation following carvedilol treatment[359]. Instead, their data indicated that carvedilol stimulates ERK1/2 phosphorylation via the β_2AR-Gs-AC-cAMP pathway, suggesting that carvedilol does in fact possess ISA. In their experiments, carvedilol did not promote β-arr recruitment. ERK1/2 activation persisted in the absence of β-arr expression, suggesting that arrestins are not required for carvedilol-induced ERK phosphorylation.

These findings have been subject to considerable debate, particularly regarding their consistency with established clinical pharmacology[360,361]. One point of contention relates to intrinsic sympathomimetic activity (ISA). As discussed previously, carvedilol is not typically classified as a β-blocker with ISA[342,343,362]. However, if carvedilol were to elevate cytosolic cAMP, as observed by the Kostenis group, it would be expected to exhibit ISA. But this is difficult to reconcile with clinical data, as β-blockers possessing ISA have consistently demonstrated poorer outcomes in HFrEF trials[348,349] compared with non-ISA agents[344,346,347], whereas carvedilol not only has been shown to improve clinical outcomes[345] but, in a head-to-head comparison, to perform even better than the non-ISA β-blocker metoprolol[354].

Critics have also pointed out that the study by the Kostenis group was performed in a heterologous HEK293 system overexpressing β_2ARs and used a relatively high concentration of carvedilol (10 μM)[360], raising the possibility that the observed signalling reflects non-physiological receptor activation rather than a property of carvedilol under endogenous conditions. Consequently, it remains unclear whether carvedilol can elevate cAMP in native cardiac myocytes expressing physiological levels of βARs.

Although signalling downstream of the β_2AR in response to carvedilol has been extensively studied, its effects on cAMP compartmentalisation have not been investigated.

4.1.4. Aims

Biased signalling has been predominantly studied in the context of G protein- versus β-arr-mediated pathways. However, it remains unknown whether different ligands acting at the same GPCR can generate distinct spatial patterns of cAMP signalling. Given the conflicting reports regarding its effects on cAMP signalling, carvedilol was selected as a model ligand to address this question.

The aims of the experiments presented in this chapter are:

(a) To assess whether carvedilol acts as a partial agonist at βARs in cardiac myocytes and to establish whether these effects are mediated by β_1ARs or β_2ARs.

(b) To compare the spatial patterns of cAMP signalling generated by carvedilol, the full βAR agonists isoproterenol and noradrenaline, and the neutral beta-blocker metoprolol.

4.2. Methods

4.2.1. FRET Imaging

FRET experiments were performed as described in **Section 2.2.4.** Pre-treatment with ICI or CGP was performed 16 hours preceding imaging by removing the M2 medium from the NRVMs and replacing it with fresh M2 medium with the appropriate concentration of ICI or CGP (or equivalent volume of vehicle).

4.2.2. Western blotting

Western blotting was performed as described in **Section 2.2.5.** Membranes were probed first with phosphoantibodies for pPLB, pTPNI, or pCREB, stripped and re-probed for total PLB, TPNI, or CREB, stripped again, and probed for GAPDH. For detection of pPLB/PLB, a 16% tricine gel was used due to its low molecular weight, whereas for detection of the relatively higher molecular weight pTPNI/TPNI and pCREB/CREB, a 4-12% gradient gel was used.

4.3. Results

4.3.1. Carvedilol opposes isoproterenol-mediated stimulation of βARs

To validate the experimental system, the ability of carvedilol to antagonise βAR-mediated cAMP generation was assessed in primary neonatal rat ventricular myocytes (NRVMs) expressing endogenous βARs and the cytosolic FRET-based cAMP reporter Epac-S^{h187}. Cells were stimulated with the βAR agonist isoproterenol (Iso; 1 nM), followed by either carvedilol (Carv; 10 μM) **(Fig 4.1b,d)** or vehicle control (Veh; 1% DMSO) **(Fig 4.1a,c)**.

Stimulation with Iso, elicited a characteristic transient increase in cytosolic cAMP (**Fig 4.1a**). This response reflects rapid activation of adenylyl cyclase (AC) following βAR stimulation, resulting in a sharp rise in cAMP, followed by a partial decline as phosphodiesterase (PDE) activity increases. A plateau is subsequently reached as cAMP production and degradation equilibrate.

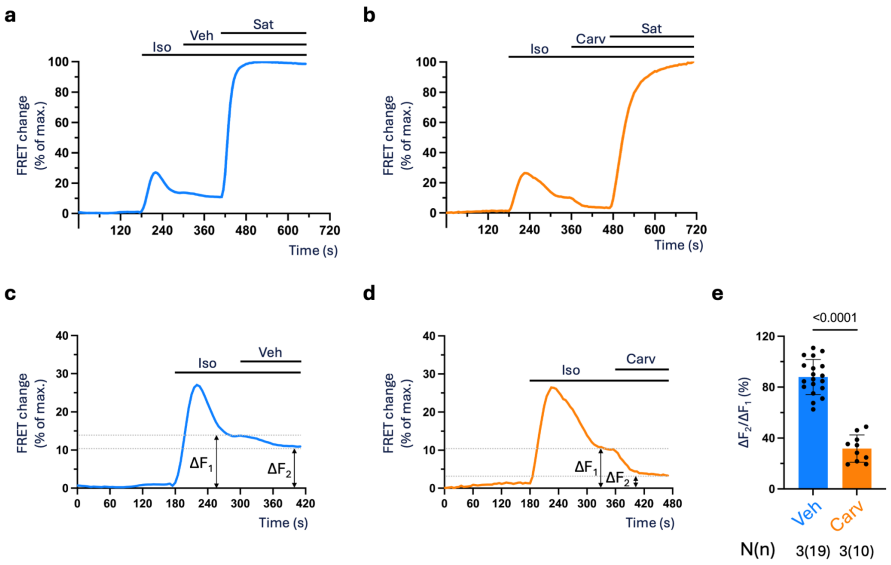


Fig 4.1 Carvedilol opposes adrenergic cAMP generation. Representative kinetics of FRET changes from neonatal rat ventricular myocytes (NRVMs) expressing Epac-S^{h187} cAMP FRET reporter in response to bath application of 1 nM isoproterenol (Iso) followed by either 10 μM carvedilol (carv) **(b)** or an equivalent volume of 1% DMSO (veh) **(a)**. **(c)** Zoomed in **(a)**; **(d)** zoomed in **(b)** with labelled ΔF_1 and ΔF_2. **(e)** Summary of ΔF_1 /ΔF_2 (expressed as %). Error bars represent mean +/- SD. Sample size given as N (n) where N = biological replicates (cell isolations); n = individual cells.

To quantify the effects of carvedilol on Iso-stimulated cAMP generation, changes in the plateau phase of the response following the addition of carvedilol were analysed **(Fig 4.1 c-e)**. As the magnitude of the initial cAMP response to Iso varied between cells, FRET changes following carvedilol or vehicle addition could not be directly compared. Instead, responses were normalised by expressing the change following carvedilol or vehicle treatment (ΔF_2) as a percentage of the cAMP level immediately prior to addition (ΔF_1). Application of carvedilol significantly reduced Iso-stimulated cAMP compared with vehicle control **(Fig 4.1e)** consistent with its role as a β-blocker.

4.3.2. Carvedilol has a partial agonist effect at β_2ARs in cardiac myocytes

To determine whether carvedilol exhibits agonist activity, the effect of carvedilol alone on resting cytosolic cAMP levels was measured using the Epac-S^{h187} cytosolic cAMP FRET reporter. This sensor was selected to take advantage of its large dynamic range, enabling detection of small changes in cAMP concentration[255] .

Carvedilol elicited a mean FRET change corresponding to 11% of the maximum response induced by a saturating stimulus (25 μM forskolin (Fsk) and 100 μM IBMX) **(Fig 4.2 a-c)**. In comparison, the full βAR agonists isoproterenol (Iso) and norepinephrine (NE) produced responses of 31% and 34% of maximum, respectively. The β-blocker metoprolol elicited a negligible response (1% of max.).

Metoprolol was selected as a comparator as like carvedilol, it is in widespread clinical use but, unlike carvedilol, has never been reported to exhibit partial agonist or intrinsic sympathomimetic activity[342,343,350]. Together, these data demonstrate that carvedilol induces a measurable increase in cAMP in cardiac myocytes, albeit to a lesser extent than full agonists, consistent with partial agonist activity.

To determine the relative contributions of β_1AR and β_2AR to carvedilol-induced cAMP generation, cells were pretreated with either the β_1AR-selective antagonist CGP 20712A (CGP), the β_2AR-selective antagonist ICI 118,551 (ICI), or vehicle control (1% DMSO) **(Fig 4.2 d-f)** as described in **Chapter 3**. Blockade of β_2ARs with ICI significantly attenuated the FRET response to carvedilol, whereas β_1AR blockade with CGP had no significant effect. These findings indicate that the cAMP-elevating effect of carvedilol is mediated predominantly by β_2ARs, consistent with previous reports[359].

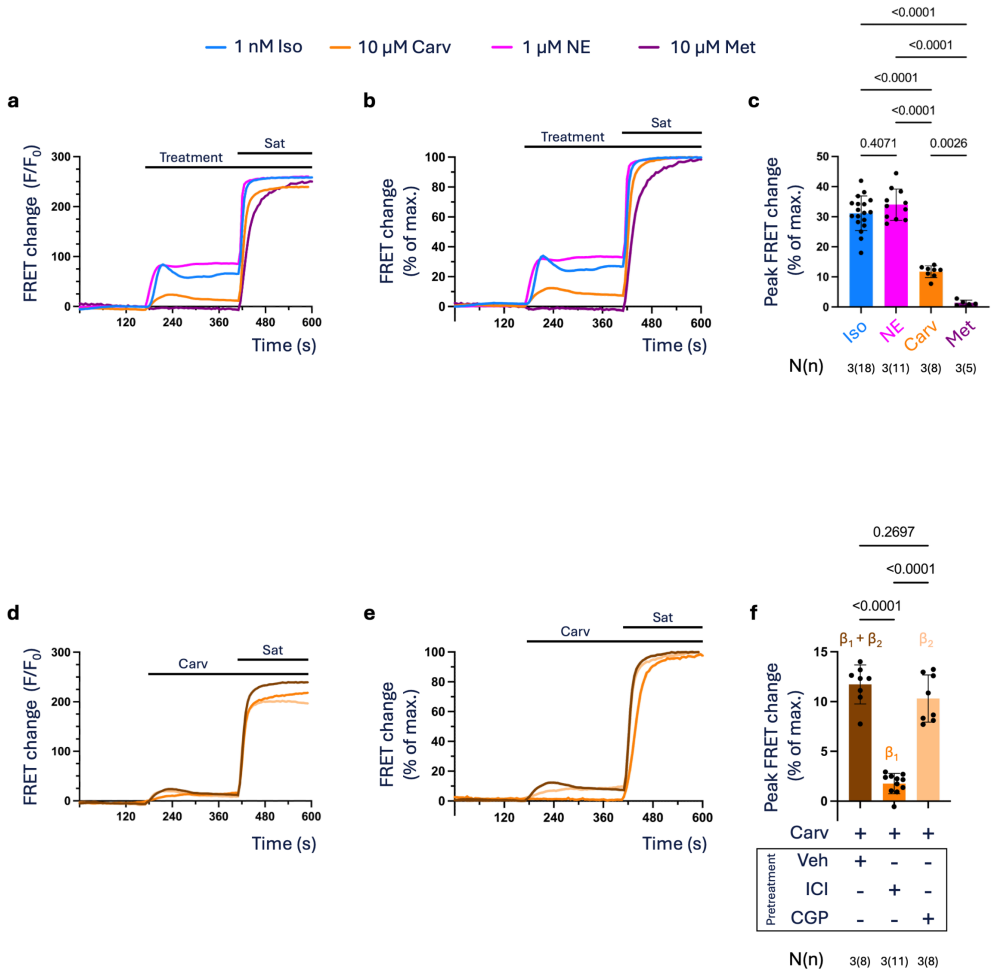


Fig 4.2 Carvedilol acts as a partial agonist at β_2ARs in NRVMs. Representative kinetics **(a)** and **(b)** and summary **(c)** of FRET change in NRVM expressing Epac-S^{h187} cAMP FRET reporter in response to bath application of either 1 nM isoproterenol (Iso), 1 μM norepinephrine (NE), 10 μM carvedilol (Carv), or 10 μM metoprolol (Met). Representative kinetics **(d)** and **(e)** and summary **(f)** of FRET change in NRVM expressing Epac-S^{h187} in response to bath application of 10 μM carv. Cells have been pre-treated with either β_1AR antagonist CGP 20712 A (200 nM), β_2AR antagonist ICI-118,551 (200 nM) or 0.01% DMSO (Veh) for at least 16 hours preceding imaging. Data represent FRET change as either % change from initial value (F/F_0) **(a)** and **(d)** or as % of maximum response elicited by a saturating stimulus (25 μM forskolin + 100 μM IBMX) **(b)**, **(c)**, **(e)** and **(f)**. Error bars represent mean +/- SD. Sample size given as N (n) where N = biological replicates (cell isolations); n = individual cells.

4.3.3. Carvedilol elicits a unique pattern of cAMP signalling

Following the observation that carvedilol elevates cytosolic cAMP, the subcellular localisation of this signalling was investigated. To address this, the CUTie suite of

targeted cAMP FRET reporters was used. Prior to examining compartmentalised signalling, the untargeted cytosolic CUTie sensor (hereafter “CUTie”) was used to confirm that carvedilol-induced cAMP changes could be reliably detected with CUTie despite its lower dynamic range[195] compared with Epac-S^{h187}.

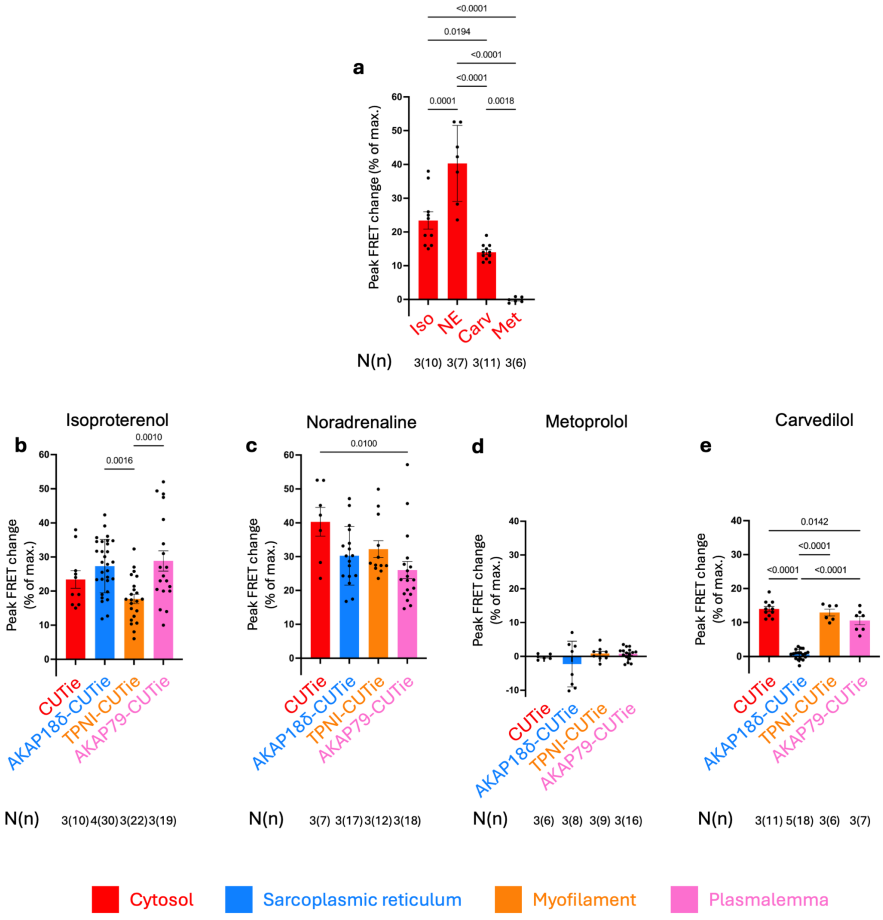


Fig 4.3 β-Adrenergic ligands drive distinct spatial patterns of cAMP signalling. (a) Summary of FRET change in NRVM expressing CUTie cAMP FRET reporter in response to bath application of 1 nM isoproterenol (Iso), 1 μM noradrenaline (NE), 10 μM metoprolol (met), and 10 μM carvedilol (Carv). Summary of FRET change in NRVM individually expressing CUTie, AKAP18δ-CUTie, TPNI-CUTie, or AKAP79-CUTie cAMP FRET reporters in response to bath application of either **(b)** 1 nM Iso, **(c)** 1 μM NE, **(d)** 10 μM met, or **(e)** 10 μM carv. Points represent maximum FRET change elicited by stimulus normalised to the maximum response elicited by a saturating stimulus (25 μM forskolin + 100 μM IBMX). Error bars represent mean +/- SD. Sample size given as N (n) where N = biological replicates (cell isolations); n = individual cells. Only P values <0.05 are shown.

In cells expressing CUTie, carvedilol elicited a mean FRET change corresponding to 14% of max., whereas Iso and NE produced larger responses and metoprolol elicited a negligible response **(Fig 4.3a)**. These results are consistent with those obtained using Epac-S^{h187} and confirm that the dynamic range of CUTie is sufficient to detect carvedilol-induced cAMP signalling.

Three targeted sensors were used to monitor cAMP nanodomains associated with β-adrenergic-regulated PKA phosphorylation targets: AKAP18δ-CUTie localised to the phospholambam/SERCA2A (PLB/SERCA2A) complex at the sarcoplasmic reticulum (SR), AKAP79-CUTie localised to a plasma membrane nanodomain close to the L-type Ca^{2+} channel ($Ca_V1.2$), and TPNI-CUTie localised to the troponin complex at the myofilament. As expected, full agonists Iso and NE elicited robust FRET responses at all three locations **(Fig 4.3b-c)**, whereas the antagonist metoprolol produced no significant response at any site **(Fig 4.3d)**.

In contrast, carvedilol, elicited a FRET response in cells expressing AKAP79-CUTie and TPNI-CUTie, but not AKAP18δ-CUTie **(Fig 4.3e)**. These data indicate that carvedilol, generates a spatially restricted pattern of cAMP signalling, with elevations at the plasma membrane and myofilament, but not at the SR.

4.3.4. The absence of cAMP generation at the sarcoplasmic reticulum cannot be explained by diffusion limitation

One potential explanation for the absence of cAMP elevation at the SR is diffusion limitation. cAMP is generated close to activated βARs and its spread throughout the cell is constrained by PDE activity generating local cAMP sinks. Consequently,

different cAMP nanodomains may require different levels of cAMP production before a measurable signal is detected. As 1 nM Iso elicits a substantially greater cytosolic cAMP response than 10 μM Carvedilol, it is possible that 1 nM Iso generates sufficient cAMP to overcome these constraints and reach the AKAP18δ-associated nanodomain at the SR, whereas 10 μM carvedilol does not. Under this model, cAMP elevation may still be detected in other nanodomains which may be more readily accessible from the site of cAMP generation or less constrained by local cAMP degradation.

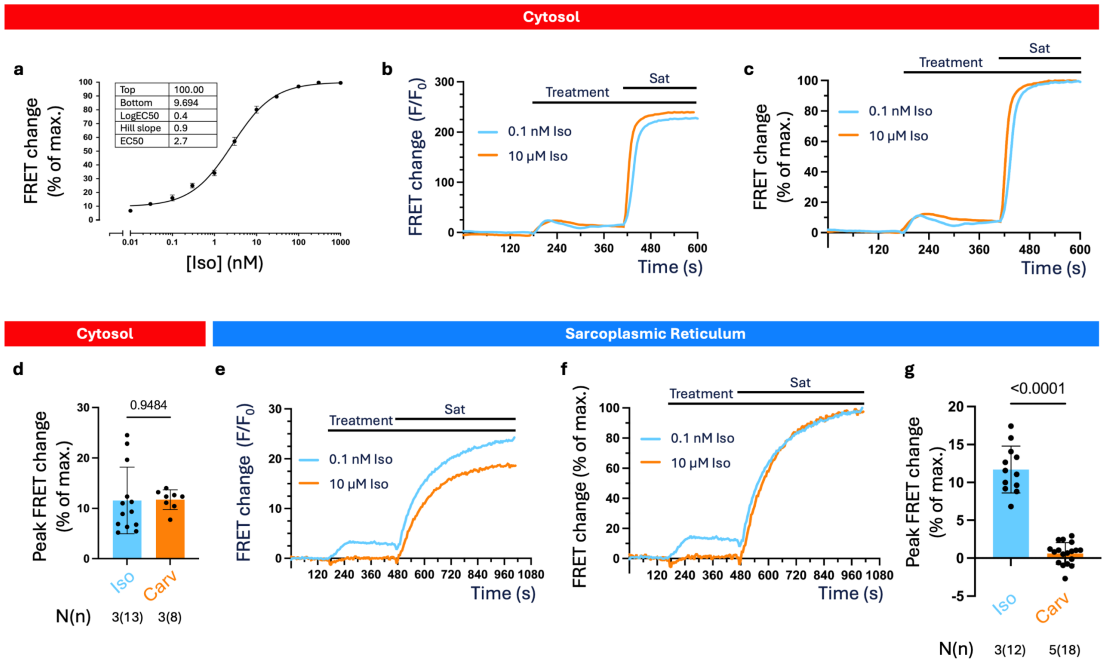


Fig 4.4 The absence of cAMP signalling at the SR is not due to diffusion limitation. (a) Dose-response curve of FRET change (as % of max. response) in NRVMs expressing Epac-S^{h187} cAMP FRET reporter in response to bath application of varying doses of isoproterenol (Iso). Representative kinetics **(b)** and **(c)** and summary **(d)** of FRET change in NRVMs expressing Epac-S^{h187} in response to bath application of either 0.1 nM Iso or 10 μM carvedilol (Carv). Representative kinetics **(e)** and **(f)** and summary **(g)** of FRET change in NRVM expressing sarcoplasmic reticulum-targeted AKAP18δ-CUTie in response to bath application of either Iso or Carv. Data represent FRET change as either % change from initial value (F/F_0) **(b)** and **(e)** or as % of maximum response elicited by a saturating

stimulus (25 μM forskolin + 100 μM IBMX) **(c)**, **(d)**, **(f)** and **(g)**. Error bars represent mean +/- SD. Sample size given as N (n) where N = biological replicates (cell isolations); n = individual cells.

To test this hypothesis, an Iso concentration that elicits a global cAMP elevation comparable to that induced by 10 μM carvedilol was required. To this end, a dose-response curve was generated **(Fig 4.4a),** plotting peak FRET changes (normalised to maximum) following Iso application in myocytes expressing the Epac-S^{h187} cAMP reporter.

The mean normalised FRET change measured in response to application of 10 μM carvedilol (11% of max.) was not significantly different from that elicited by 0.1 nM Iso (11% of max.) **(Fig 4.4b-d)**. Thus, 0.1 nM Iso was used as a functionally equivalent concentration to 10 μM carvedilol in terms of global cAMP elevation.

In cells expressing AKAP18δ-CUTie, 0.1 nM Iso evoked a FRET response comparable to that observed at the same Iso concentration with the cytosolic sensor (11.7 % of max.) **(Fig 4.4e-g)**. Diffusion limitation can therefore be excluded as an explanation for the absence of a response to carvedilol, as 0.1 nM Iso generated cAMP at the SR despite producing a similar global increase in cytosolic cAMP. These findings suggest that differences in downstream signalling following βAR activation by Iso versus carvedilol determine whether cAMP reaches the SR.

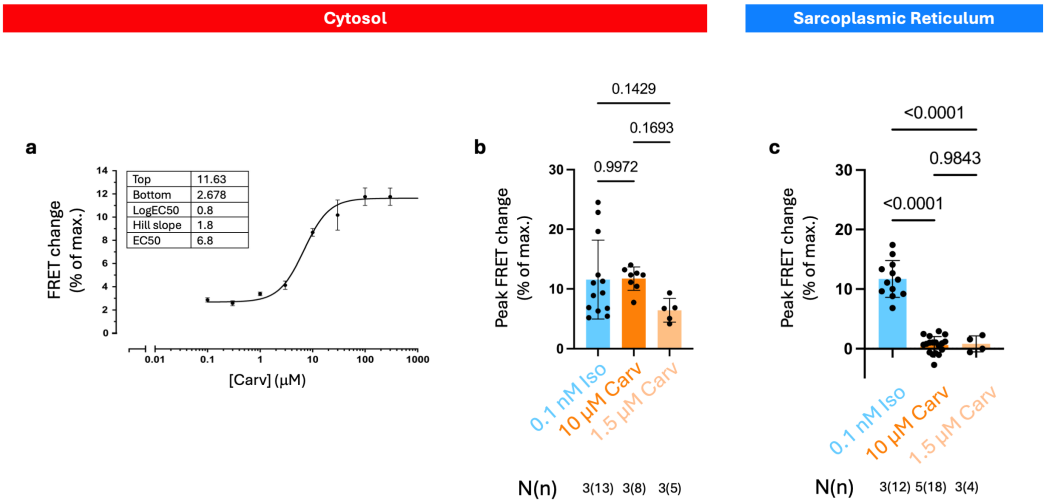


Fig 4.5 Carvedilol drives a dose-dependent increase in cAMP. (a) Dose-response curve of FRET change (as % of max. response) in NRVMs individually expressing Epac-S^{h187} cAMP FRET reporter in response to bath application of varying doses of carvedilol (Carv). Summary of peak FRET change in NRVMs expressing Epac-S^{h187} **(b)** or AKAP18δ-CUTie **(c)** in response to bath application of either 0.1 nM isoproterenol (Iso), 10 μM carvedilol (Carv) or 1.5 μM carv. FRET change presented as maximum FRET change elicited by stimulus normalised to the maximum response elicited by a saturating stimulus (25 μM forskolin + 100 μM IBMX). Error bars represent mean +/- SD. Sample size given as N (n) where N = biological replicates (cell isolations); n = individual cells.

4.3.5. Carvedilol elevates cAMP in a dose-dependent manner

Initially, a concentration of 10 μM carvedilol was selected to replicate previously reported observations of its partial agonist activity[359]. However, the use of this concentration has been criticised as being too high[360], with the suggestion that at more clinically relevant concentrations, carvedilol may not elicit G protein-dependent signalling. Notably, the original studies describing carvedilol as a β-arrestin biased ligand were also conducted using similarly high concentrations[358].

To determine whether the cAMP-elevating effect of carvedilol is dependent on concentration, a dose-response curve was generated in NRVMs expressing the Epac-S^{h187} cAMP FRET reporter **(Fig 4.5a)**. Peak FRET changes (normalised to

maximum) were measured following application of increasing concentrations of carvedilol. Carvedilol elicited a dose-dependent increase in cAMP, with measurable responses observed even at lower doses, indicating that its cAMP-generating activity is not restricted to higher doses.

To establish whether the spatial pattern of cAMP signalling elicited by carvedilol is dependent on concentration, these experiments were repeated using a lower, more clinically relevant concentration (1.5 µM)[363]. At this concentration, a FRET response can still be measured in NRVMs expressing a cytosolic FRET reporter **(Fig 4.5b)**. However, no significant response was detected in cells expressing AKAP18δ-CUTie **(Fig 4.5c)**.

4.3.6. Assessment of PKA target phosphorylation following βAR stimulation

As a partial agonist, carvedilol elicits a relatively modest increase in cAMP compared with the full βAR agonists isoproterenol and norepinephrine. This raises the question of whether this cAMP signal is sufficient to drive downstream physiological responses. To address this, the effect of carvedilol on phosphorylation of PKA targets was assessed.

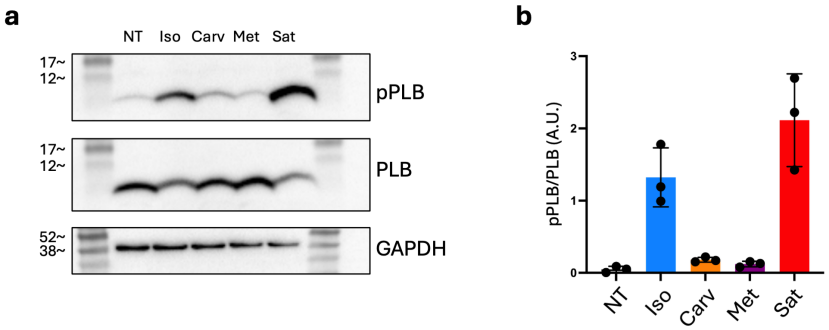


Fig 4.6 βAR-driven phospholamban phosphorylation. (a) Representative Western blot showing phosphorylated phospholamban (pPLB), total phospholamban (PLB), and GAPDH in whole cell lysates obtained from NRVMs treated for 10 minutes with either vehicle control (NT), 1 nM isoproterenol (Iso), 10 μM carvedilol (Carv), 10 μM metoprolol (met), or a combination of 25 μM forskolin and 100 μM IBMX (Sat). **(b)** Densitometric quantification. Error bars represent mean +/- SD.

First, phosphorylation of phospholamban (PLB) was investigated. Whole-cell lysates from NRVMs treated for 10 minutes with Iso (1 nM), carvedilol (10 μM), metoprolol (10 μM), vehicle control (NT, DMSO), or a saturating stimulus consisting of 25 μM forskolin and 100 μM IBMX prior to cell lysis were analysed by Western blotting. Phosphorylated phospholamban (pPLB) and total phospholamban (PLB) were quantified and the pPLB/PLB ratio calculated. Consistent with the cAMP responses detected using AKAP18δ-CUTie at the SR, Iso and Sat increased PLB phosphorylation whereas carvedilol and metoprolol had no detectable effect **(Fig 4.6)**. These findings suggest that the absence of a carvedilol-induced cAMP signal at the SR is reflected in downstream PKA activity in this compartment.

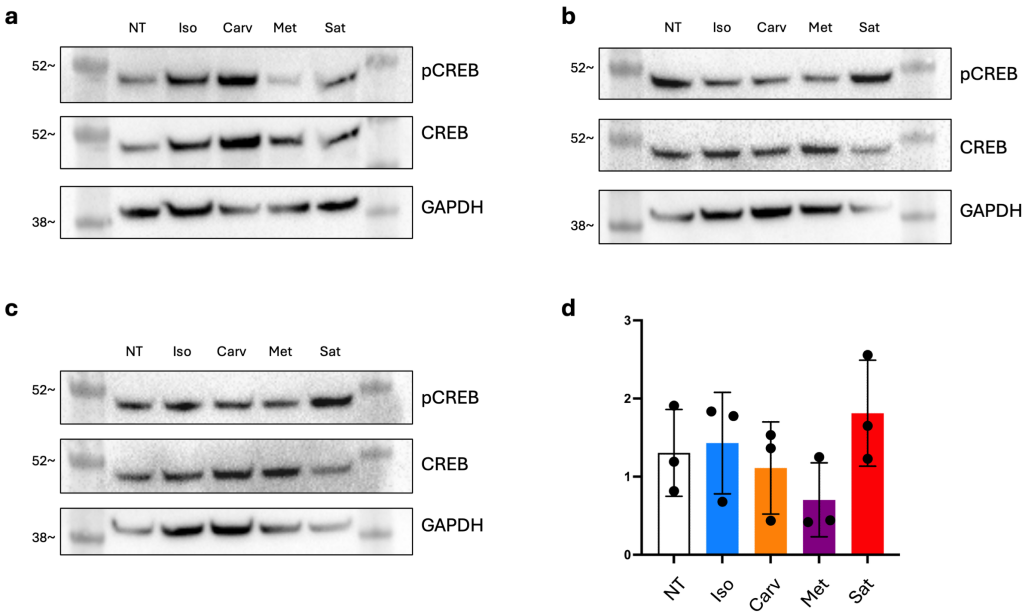


Fig 4.7 βAR-driven CREB phosphorylation. (a-c) Western blots showing phosphorylated CREB (pCREB), total CREB (CREB), and GAPDH in whole cell lysates obtained from NRVMs treated for 10 minutes with either vehicle control (NT), 1 nM isoproterenol (Iso), 10 μM carvedilol (Carv), 10 μM metoprolol (met), or a combination of 25 μM forskolin and 100 μM IBMX (Sat). **(d)** Densitometric quantification. Error bars represent mean +/- SD.

We next examined additional PKA targets for which FRET experiments suggested that carvedilol may increase phosphorylation. CREB was selected as a downstream target expected to reflect cytosolic cAMP elevation and PKA activation. However, substantial variability between blots made interpretation challenging. Overall, these preliminary experiments suggest that Sat produced a modest increase in CREB phosphorylation, whereas Iso and Carv produced little change in pCREB, and metoprolol reduced CREB phosphorylation **(Fig 4.7)**. Several factors may contribute to the limited response observed. Technical factors, including antibody sensitivity, may have reduced the ability to detect changes in CREB phosphorylation. In addition, CREB phosphorylation is not determined solely by cytosolic PKA activity. As a nuclear transcription factor, CREB requires cAMP/PKA access to the nucleus and may not accurately reflect cytosolic cAMP levels. Furthermore, the Ser133 phosphosite can phosphorylated by kinases other than PKA[364]. Future experiments should therefore assess an alternative cytosolic PKA target that exhibits a more robust phosphorylation response to Sat which would facilitate interpretation of the other treatment conditions.

Finally, carvedilol was also found in our FRET experiments to raise cAMP at troponin I (TPNI). Sat produced a small increase in TPNI phosphorylation, while only a weak band was observed in Iso-treated cells **(Fig 4.8)**. Given the limited signal observed

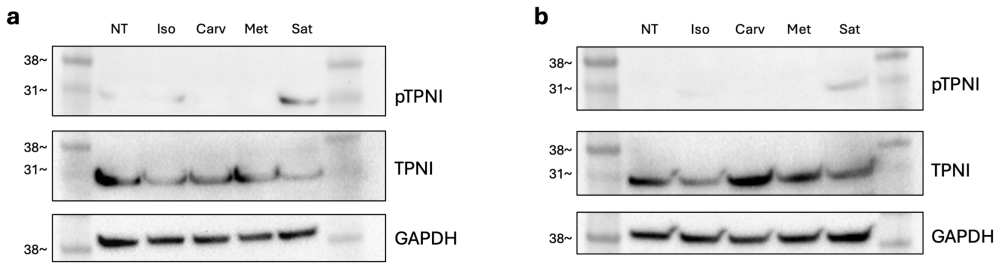


Fig 4.8 βAR-driven troponin I phosphorylation. (a-b) Western blots showing phosphorylated troponin I (pTPNI), total troponin I (TPNI), and GAPDH in whole cell lysates obtained from NRVMs treated for 10 minutes with either vehicle control (NT), 1 nM isoproterenol (Iso), 10 μM carvedilol (Carv), 10 μM metoprolol (met), or a combination of 25 μM forskolin and 100 μM IBMX (Sat).

even with Iso stimulation, it is not possible to determine reliably whether carvedilol or metoprolol alter TPNI phosphorylation under these experimental conditions. Potential approaches to improve detection would be incubation with the treatments for longer than 10 mins or immunoprecipitation of TPNI prior to probing for phosphorylated TPNI.

Overall, PLB phosphorylation closely reflected the compartment-specific cAMP signalling observed using AKAP18δ-CUTie at the SR. In contrast, experiments examining additional downstream targets were inconclusive and require further optimisation and repetition. In addition to assessing alternative PKA targets and using immunoprecipitation to improve detection sensitivity, future experiments can employ fluorescent reporters for PKA activity. Although these experiments were not completed within the timeframe of this project, the FRET-based PKA reporter AKAR4 is used in **Chapter 5** and would provide sensitive means of investigating whether the localised cAMP signals elicited by carvedilol are sufficient to drive compartment-specific PKA activation.

4.4. Discussion

4.4.1. Current debate on the pharmacology of carvedilol

Following the findings of the Lefkowitz group described earlier – namely that carvedilol promotes GRK-mediated phosphorylation of, and β-arrestin recruitment to, β_2ARs – carvedilol has been widely classified as an arrestin-biased ligand. However, multiple studies have demonstrated that carvedilol exhibits guanine-nucleotide modulatable binding at βARs in cardiac myocytes[342,365,366], indicating that carvedilol-bound receptors are capable of engaging G proteins. This is supported by proximity ligation and fluorescence-based assays showing Gαs recruitment to β_2ARs following carvedilol treatment in HEK293 cells[359,367]. In contrast, the signalling observed in the original study by the Lefkowitz group, persisted in cells expressing mutant β_2ARs unable to recruit G proteins[358].

Furthermore, studies of downstream signalling have reported contradictory effects of carvedilol on cAMP production, with increases[359,367,368,370–373], decrease[358], or no detectable change[341,366,369,373]. Among studies reporting elevated cAMP, there is further inconsistency regarding receptor subtype involvement with this effect attributed to exclusively β_1ARs[373], exclusively β_2ARs[359,367], or both[368,371,372]. In contrast, studies assessing adenylyl cyclase activity rather than cAMP levels directly have reported no effect of carvedilol[343,366]. A summary of the relevant literature can be found in **Table 4.1**.

Table 4.1 Summary of previous experiments on the pharmacology of carvedilol

Reference	Cell/tissue type	Carvedilol effect on cAMP	Carvedilol effect on chronotropy	Carvedilol effect on inotropy
Bristow *et al.* (1992)[365]	Human LV tissue from HF patients	n/a	n/a	No effect
Böhm *et al.* (1998)[366]	Isolated myocardial membranes from adult HF rats	No effect on AC activity	Negative	n/a
Willette *et al.* (1999)[341]	Neonatal rat ventricular myocytes	No effect	No effect	n/a
Lattion *et al.* (1999)[368]	HEK293 overexpressing β1AR or β2AR	Increased	n/a	n/a
Maack *et al.* (2000)[342]	Human LV papillary muscle strips	n/a	n/a	negative
Maack *et al.* (2001)[350]	Human ventricular and atrial myocytes	n/a	n/a	Opposes Iso-stimulated inotropy (but not as much as other beta-blockers)
Brixius *et al.* (2001)[343]	Human LV tissue	No effect on AC activity	n/a	Negative (but not as strong as metoprolol)
Andreka *et al.* (2002)[369]	Myocardial strips from adult rats and human	No effect	n/a	n/a
Yao *et al.* (2002)[370]	Adult Guinea pig ventricular myocytes	Increased	n/a	n/a
Baker *et al.* (2003)[371]	CHO overexpressing β1AR	Increased	n/a	n/a
Baker *et al.* (2003)[372]	CHO overexpressing β2AR	Increased	n/a	n/a
Galandrin & Bouvier (2006)[373]	HEK293S overexpressing β1AR	Increased	n/a	n/a
	HEK293S overexpressing β2AR	No effect	n/a	n/a

Reference	Cell/tissue type	Carvedilol effect on cAMP	Carvedilol effect on chronotropy	Carvedilol effect on inotropy
Wisler *et al*. (2007)[358]	HEK293 overexpressing β2AR	Decreased (Opposed IBMX-stimulated cAMP elevation)	n/a	n/a
Shen *et al*. (2019)[367]	HEK293 overexpressing β2AR	Increased in proximity to β2AR	n/a	n/a
Benkel *et al*. (2022)[359]	HEK293 overexpressing β2AR	Increased	n/a	n/a
	Adult mouse ventricular myocytes	Increased (close to plasmalemma)	Increased	n/a

n/a means parameter was not assessed in that publication

In myocardial tissue preparations across a range of species, carvedilol has been reported to exert positive[359] or negative[366] chronotropic effects or to have no effect on heart rate[341]. In contrast, carvedilol has been consistently shown to produce negative inotropic effects[343,350], although to a lesser extent than other β-blockers such as metoprolol.

Finally, studies examining alternative signalling outputs have consistently shown that carvedilol increases ERK1/2 phosphorylation. However, in some cases this has been attributed to β-arr-dependent signalling independent of G proteins[358] while others have demonstrated G protein-dependent, β-arr-independent ERK1/2 activation[359,367,373].

A wide range of experimental systems have been used to investigate carvedilol's pharmacology, including heterologous cell lines (e.g. HEK, CHO, and COS-7) and primary myocytes or myocardial tissue from rats, mice, guinea pigs, and humans **(Table 4)**. However, differences in cell types alone cannot account for the observed

discrepancies, as conflicting results have been reported even within the same system (e.g. Ref[368] and Ref[358], both in HEK293 cells). Notably, in all studies in which cAMP generation was measured in cardiac myocytes, carvedilol has consistently been reported to elevate cAMP.

Interpretation of these findings is further complicated by methodological differences, including the use of overexpression systems for βARs and/or other downstream signalling components, including G proteins and arrestins, which may alter signalling behaviour, as well as experiments conducted in isolated membrane preparations rather than intact cells.

Although the experiments presented here were not designed to elucidate the mechanism of action of carvedilol, but rather to investigate ligand-dependent effects on compartmentalised cAMP signalling by βARs, it is nonetheless informative to consider these findings in the context of the studies discussed above.

In our experiments, carvedilol acted as a partial agonist, stimulating cAMP generation. While this is consistent with several previous reports, other studies have found no effect of carvedilol on cAMP levels. One possible explanation for this discrepancy is the sensitivity of the assays used. The relatively small cAMP elevation we observed may fall below the detection threshold of the systems used previously. This interpretation is supported by studies in which negligible changes in cAMP were associated with larger increases in CRE-mediated luciferase transcription, reflecting the amplification of the downstream signal[371,372].

In many previous studies measuring cAMP, assays were performed in whole cell lysates using radioligand binding, often over extended time courses and in the presence of phosphodiesterase inhibition with IBMX and, in some cases, forskolin to enhance Gαs-AC coupling. These conditions may alter the dynamics of cAMP signalling and obscure subtle changes. In contrast, our experiments were conducted in live cells under more physiological conditions, with endogenous receptor expression. Notably, an increase in cAMP in response to carvedilol was also observed in the only two previous studies using FRET-based cAMP reporters in primary cells[359,367].

The spatial pattern of cAMP signalling observed in our experiments is consistent with previous reports showing that cAMP generation occurs in close proximity to the receptor [367] or at the plasma membrane[359], corresponding to the localisation of the AKAP79-CUTie sensor. In line with this, carvedilol has been shown to stimulate a PKA-dependent increase in the conductance of $Ca_V1.2$ (L-type calcium channels) in hippocampal neurons[367], which is regulated by this local cAMP pool.

However, the observation that carvedilol stimulates cAMP generation at the $Ca_V1.2$ seems at odds with its reported negative inotropic effects[342,343,350]. In these functional studies, other β-blockers such as metoprolol produced greater negative inotropy than carvedilol, consistent with the absence of partial agonist activity we observed for metoprolol.

Carvedilol's negative inotropic effects are also consistent with its lack of cAMP elevation at, and phosphorylation of, phospholamban, which would be expected to reduce SR Ca^{2+} loading and the amplitude of the Ca^{2+} transient.

One can speculate on how these observed actions of carvedilol could be clinically beneficial in heart failure (HF). Excessive β-adrenergic blockade may be detrimental in acute or marginally compensated HF where some degree of sympathetic drive is required to maintain cardiac output[374–376]. However, β-blockers possessing intrinsic sympathomimetic activity, such as bucindolol and xamoterol, have performed poorly in clinical trials and are not licenced for clinical use[348,349]. This apparent contradiction may be reconciled by the relatively weak partial agonist activity of carvedilol compared with other β-blockers exhibiting ISA.

Additionally, the spatial pattern of cAMP signalling may confer further advantages. SERCA2A is a major consumer of ATP in cardiac myocytes[377,378] and reduced SERCA2A activity, and therefore ATP consumption, may be beneficial in the energetically compromised failing heart. Furthermore, the carvedilol-induced cAMP elevation at the myofilament, may contribute to a beneficial lusitropic effect.

The question therefore arises as to how carvedilol generates this distinct spatial pattern of cAMP signalling.

4.4.2. The role of β_1AR versus β_2AR

Previous studies reporting carvedilol-induced cAMP generation have been inconsistent in attributing this effect to either β_1ARs or β_2ARs, although the majority of evidence supports a predominant role for β_2ARs. Carvedilol is typically described as a non-selective β-blocker; however, it has been reported to exhibit higher affinity for β_2ARs (pK_D 9.40±0.08) compared with β_1ARs (8.75±0.09)[305] . Notably, carvedilol binds both βAR subtypes with greater affinity than metoprolol (pK_D β_1AR=7.26±0.07;

β_2AR=6.89±0.09) which is generally classified as β_1-selective. This selectivity would not be maintained at the concentration used in our experiments (10 μM), and thus both carvedilol and metoprolol would be expected to engage to both βAR subtypes with full occupancy.

One possible explanation for the distinct patterns of cAMP signalling observed with Iso and NE, compared with carvedilol, is that carvedilol's partial agonist activity is mediated primarily by β_2ARs, whereas Iso and NE activate both βAR subtypes.

However, as shown in **Chapter 3**, selective activation of β_2ARs resulted in cAMP generation restricted to the AKAP79-CUTie nanodomain. Here we have shown that although carvedilol-induced cAMP signalling is mediated predominantly by β_2ARs **(Fig 4.2d-f)**, cAMP elevation is also observed at the troponin complex within the myofilament **(Fig 4.3e)**. Notably, a small cytosolic cAMP signal persists during β_2AR blockade (**Fig 4.2f)**, suggesting a minor contribution from β1ARs. This may account for the cAMP elevation observed at TPNI; however, it does not explain the absence of cAMP signalling at the SR.

Several mechanisms may account for the unique spatial pattern of cAMP signalling elicited by carvedilol at β_2ARs. Given the established role of phosphodiesterases (PDEs) in shaping local cAMP gradients[174,188], one possibility is that enhanced PDE activity at the SR limits cAMP accumulation following carvedilol stimulation but not following Iso or NE stimulation. Alternatively, these ligands may preferentially activate distinct populations of β_2ARs. These possibilities are considered in more detail below.

4.4.3. The role of intracellular receptors

As outlined in **Section 1.2.4**, βAR signalling is not only initiated from the plasma membrane but can also originate from intracellular sites, although the functional role of these receptor pools remains incompletely understood. Both β_1ARs and β_2ARs have been shown to signal from endomembrane sites. β_1ARs have been identified at the SR[151] and Golgi apparatus[141,143–145], while the presence of active β_2ARs has been demonstrated on early endosomes[140,379].

One possible explanation for the distinct patterns of cAMP signalling observed with different βAR ligands is that these ligands preferentially activate receptors located in different subcellular compartments. Of particular relevance to our findings is evidence for the role of Golgi-resident β_1ARs in regulating PLB phosphorylation in cardiac myocytes. In HeLa cells, a population of β_1ARs have been shown to reside at the Golgi under basal conditions, rather than being internalised from the plasma membrane upon activation[141]. Furthermore, blockade of this Golgi-localised receptor pool reduces cytosolic cAMP generation in response to the β_1AR agonist dobutamine, indicating that these receptors contribute to global cAMP elevation.

Using optogenetic approaches to selectively generate cAMP at the trans-Golgi, together with a combination of membrane-permeant and -impermeant ligands to target distinct receptor populations, the roles of plasma membrane and intracellular βARs have begun to be delineated[145]. cAMP production at the Golgi was sufficient to increase phosphorylation of PLB, but not of TPNI or the ryanodine receptor (RyR2), whereas selective activation of plasma membrane β_1ARs produced the opposite pattern of phosphorylation.

These findings have been interpreted to indicate that activation of Golgi-localised βARs is both necessary and sufficient to drive phosphorylation of PLB. If so, this suggests that the absence of cAMP signalling at the SR in response to carvedilol may reflect a failure to activate this Golgi-localised receptor pool.

Two important limitations of these studies should be considered. First, the optogenetic approach employs a Golgi-targeted photo-activatable adenylyl cyclase (bPAC), which is non-physiological and isolates cAMP production from other signalling outputs of βAR activation. Second, although experiments using membrane-impermeant antagonists support a requirement for intracellular βAR activation in driving PLB phosphorylation, they do not definitively localise these receptors to the Golgi. Further investigation could make use of CUTie sensors targeted to the Golgi and other intracellular compartments from which adrenergic signalling has been reported. A Golgi-targeted CUTie sensor (GalT-CUTie) has been generated and characterised **(Fig S1)**, providing a platform for future studies.

Access of ligands to intracellular receptors depends either on their co-internalisation with receptors from the plasma membrane or on their ability to cross the cell membrane independently[139]. For receptors resident at intracellular sites, the latter mechanism is required. Endogenous βAR agonists, epinephrine and norepinephrine, are not membrane-permeant and instead enter cells via the organic cation transporter OCT3, enabling activation of βARs at internal sites[141,151].

In contrast, carvedilol, is lipophilic and is predicted to partition into lipid membranes[380]. However, there is no direct experimental evidence of carvedilol's intracellular accumulation, and its ability to access internal βARs therefore remains

uncertain. Interestingly, carvedilol has been shown to inhibit OCT1 and OCT2 in HEK293 cells[381], and given the overlapping substrate and inhibitor profiles within the OCT family, it is plausible that carvedilol may also inhibit OCT3, restricting its access to intracellular βARs.

Overall, based on its physicochemical properties, carvedilol is likely to be membrane-permeant and therefore capable of accessing intracellular βARs. It is therefore unlikely that a failure to activate Golgi-localised βARs accounts for the absence of cAMP generation at the SR. Furthermore, the majority of carvedilol-induced cAMP signalling appears to be mediated by β_2ARs which, unlike β_1ARs, have not been identified at the SR or Golgi compartments. However, this does not exclude a role for local cAMP generation by βAR at other intracellular sites. Further studies will be required to explore this possibility.

4.4.4 Mechanistic basis of ligand-dependent spatial cAMP signalling

There are several remaining potential mechanisms that may underlie the distinct spatial pattern of cAMP signalling elicited by carvedilol. Our experiments rule out diffusion limitation as an explanation for the absence of cAMP generation at the SR. As discussed above, this phenomenon cannot be explained solely by differences between β_1AR and β_2AR signalling. Although further investigation is required to clarify the role of intracellular receptors, it is unlikely that this alone accounts for the observed signalling pattern.

These findings raise the possibility that a single plasma membrane GPCR may generate distinct spatial patterns of cAMP signalling in a ligand-dependent manner.

It is well established that different ligands stabilise distinct active conformations of the same receptor[15,127–129], leading to differential recruitment of downstream signalling partners and functional selectivity of signalling output. Such ligand-dependent differences in signalling complex assembly could, in turn, alter local PDE activity, thereby shaping the spatial distribution of cAMP. Possible mechanisms underlying ligand-dependent spatial signalling are considered further in **Chapter 6**.

4.5. Conclusions

Consistent with previous reports, we confirmed that:

- Carvedilol acts as a partial agonist at β_2ARs
- Carvedilol elicits a global cAMP elevation in cardiac myocytes

The original findings of the work described in this chapter are:

- Carvedilol elevates cAMP in cardiac myocytes under conditions of endogenous receptor expression and at physiologically relevant concentrations
- Carvedilol elicits a distinct spatial pattern of cAMP signalling compared with isoproterenol or noradrenaline
- The absence of carvedilol-induced cAMP signalling at the SR is reflected in reduced phosphorylation of the SR-localised PKA target phospholamban

Together, these findings indicate that GPCRs can generate ligand-dependent spatial patterns of cAMP signalling, extending the concept of functional selectivity beyond pathway selection to include spatial compartmentalisation.

5

Integration of adrenergic and cholinergic signalling

5.1. Introduction

5.1.1. Gi protein coupled receptors

So far, the focus of this project has been on the influence of Gs-coupled receptors on cAMP signalling. The other G protein family which directly regulates cAMP signalling is Gi. The Gi family consists of Gαi1, Gαi2, Gαi3, Gαo, and Gαz. Canonical GiPCR signalling relies on inhibition of cAMP synthesis by adenylyl cyclases (ACs) by the Gα subunit. Nine membrane-spanning AC isoforms are expressed in humans and whilst all are stimulated by Gαs-GTP, only a subset is inhibited by Gαi family proteins[21]. Gαi (1, 2, 3), Gαo, and Gαz can all inhibit AC1, especially in its calmodulin-stimulated state[161] , whilst AC5 and AC6 – the predominant AC isoforms in cardiac myocytes – are inhibited by Gαi (1, 2, 3) and Gαz[57,161,162]. Although the majority of signal transduction by Gαi family proteins has canonically been attributed to inhibition of adenylyl cyclase, GiPCR signalling is more complex.

In addition to the inhibitory effect on cAMP generation, another major mediator of GiPCR signalling is the Gβγ heterodimer[68]. Following nucleotide exchange by Gαi, the α subunit becomes functionally uncoupled, releasing free Gβγ that can interact

with a variety of downstream effectors. One of the best characterised Gβγ effectors is the G protein-gated inwardly rectifying potassium channel (GIRK) to which Gβγ binds and increases open probability[54–56]. Other actions of Gβγ include activating[57,58] or inhibiting[57–60] ACs (depending on isoform), activating phospholipase C (PLC)-β[61–63] and phosphoinositide 3 kinase (PI3K) γ[64], recruiting and activating GPCR kinases (GRK) 2 and 3[65], and regulating N type[66] and P/Q type[67] calcium channels.

Almost all of these actions of Gβγ are inhibited by pertussis toxin (PTX) which selectively ADP-ribosylates Gαi-family proteins, preventing them from interacting with a receptor[68]. For this reason, it has generally been accepted that most, if not all, signalling by Gβγ is mediated by free Gβγ derived from Gi family-containing heterotrimers and not Gs or Gq. This is likely an oversimplification as there is some recent evidence that Gs-containing heterotrimers can also release free Gβγ which drives downstream signalling[79,80]. Despite this, it is clear that Gi-coupled GPCRs remain the predominant source of free Gβγ[77] and that signalling by free Gβγ heterodimers constitutes a key component of GiPCR signalling.

5.1.2. GAPs and RGS proteins

Another feature that distinguishes Gαi family proteins from Gαs is their greater reliance on GTPase-activating proteins (GAPs) – particularly RGS (Regulators of G protein Signalling) family proteins. The rate of G protein signalling, and consequently the spread of these signals, depends on the amount of time the G proteins spend in their active state which is dictated by the rates of G protein activation and deactivation[382]. The transition from Gα-GDP to Gα-GTP, which results in activation, is facilitated by guanine nucleotide exchange factors (GEFs), with the primary GEF

for heterotrimeric G proteins being ligand-bound GPCRs[17]. Deactivation is determined by the rate of GTP hydrolysis but the intrinsic GTPase activity of Gα is relatively slow, occurring on the timescale of seconds to minutes[383]. Although such slow intrinsic GTP hydrolysis is compatible with the relatively slow kinetics of AC deactivation in Gαs-mediated signalling[384,385], this is too slow to be responsible for the short activation lifetimes observed for Gi- and Gq-family proteins[383].

The role of GAPs is to accelerate GTP hydrolysis by the Gα subunit, allowing reassociation with Gβγ[386–388]. The largest family of GAPs are the RGS proteins, constituting more than 20 members[383]. RGS proteins do not function as GAPs for Gαs- and Gα12/13-family proteins; a small number interact with and regulate Gαq-family proteins, while the majority RGS show highest catalytic efficiency for Gαi-family proteins[389]. RGS proteins are grouped into four subfamilies – RZ, R4, R7, R12 – based on sequence similarity within their RGS domain and the presence of other domains[390].

In addition to their GAP activity, RGS proteins are increasingly recognised as important mediators of cell signalling, particularly by Gi coupled receptors[391]. Some of the first evidence of this was their role in the regulation of the GIRK channel. Due to their GAP activity, overexpression of RGS proteins accelerates the inactivation of the GIRK channel following cholinergic activation but, unexpectedly, the activation of the GIRK current is also accelerated[392,393]. RGS expression changes signalling kinetics without affecting current amplitude, suggesting rather than acting simply as inhibitors of G protein signalling, RGS proteins play a more complex role in G protein signalling. RGS overexpression has a similar effect on another Gβγ-

regulated ion channel – the N-type Ca^{2+} channel – which is inhibited by free Gβγ binding[394,395]. Furthermore, RGS6 expression is critically important for cholinergic regulation of the GIRK current, as RGS6 knockout mice display exaggerated bradycardic responses to cholinergic stimulation and increased heart rate variability[396,397].

This, and other evidence, indicates a role beyond GAP-activity for RGS proteins in signal transduction. Several roles have been proposed, including RGS proteins acting as scaffolds assembling related signalling components, acting as integrators of multiple signalling pathways – both G protein-dependent and G protein-independent – and regulating trafficking of signalling components[391]. What is increasingly clear is that RGS family proteins play a currently underappreciated role in G protein signalling and this contribution is particularly important to consider when examining signalling by GiPCRs.

5.1.3. Muscarinic receptors

Along with adrenergic receptors, muscarinic acetylcholine receptors (mAChRs) represent one of the most extensively pharmacologically targeted class A GPCR families[6]. There are five mAChR subtypes, designated M_1R to M_5R. The oddly numbered receptors, M_1R, M_3R, and M_5R signal primarily through stimulation of PLC-β and mobilisation of intracellular Ca^{2+} by coupling to Gαq whilst the M_2R and M_4R inhibit adenylyl cyclase via Gαi-family proteins[225,398,399]. The receptor subtypes also differ in their tissue expression pattern and can be found in pre- and postsynaptic peripheral (M_1R and M_2R) and central neurons (M_1R, M_2R, and M_4R)[400],

smooth muscle (M_3R and M_2R)[401,402], exocrine glands (mainly M_3R)[403,404], and cardiac muscle (mainly M_2R)[224,405].

Despite differing in their tissue expression and G protein coupling specificity, the structure of the mAChR subtypes is highly conserved. To date, the crystal structures of four muscarinic receptors (M_1R – M_4R) have been solved in inactive conformations[406–408]. In particular, the orthosteric binding site shows the highest degree of structural homology, underlying a long-standing difficulty in developing mAChR subtype-specific orthosteric ligands[408]. The presence of a large extracellular vestibule which is more heterogeneous between subtypes has made the development of subtype-selective allosteric modulators for mAChRs possible[409]. Additionally, structures of M_1R and M_2R have been solved in complex with Gα11 and GαoA respectively, demonstrating broad similarity between active conformations despite a preference for different G protein partners[410].

5.1.4. Cholinergic signalling in the cardiac myocyte

The M_2R is the predominant mAChR isoform in cardiac muscle and is the paradigmatic mediator of vagal parasympathetic drive to the heart, triggering the negative inotropic and chronotropic effects of acetylcholine[224]. Whilst it is a common misconception that M_2R expression is restricted to nodal cells and atrial myocytes, the ventricular myocardium also exhibits M_2R expression and is under significant parasympathetic influence[411–413]. Autonomic drive to the heart is a classic example of physiological antagonism, with sympathetic and parasympathetic limbs exerting opposing effects on rate and force of cardiac contraction as well as pace making and atrioventricular node conduction[414]. The effects of these two branches

of the autonomic nervous system as the ‘accelerator’ and ‘brake’ on cardiac function have historically been ascribed to adrenergic signalling via β-adrenergic receptors (βAR) and cholinergic signalling via M_2R respectively. It is worth noting, however, the importance of other neurotransmitters in autonomic signalling[415].

As discussed in more detail in **Chapter 3**, the positive chronotropic and inotropic action of βAR activation is mediated by stimulation of adenylyl cyclase (AC) activity by Gαs, elevating cAMP, and leading to phosphorylation of adrenergic targets. M_2R activation drives two modes of signalling, both mediated by the receptor’s Gi protein coupling – one directly and the other indirectly. Firstly, primarily in the sinoatrial node, atrioventricular node, and atrial cells, the free Gβγ heterodimer directly interacts with the G protein-gated inwardly rectifying potassium (GIRK) channel, increasing conductance and hyperpolarising the plasma membrane, reducing excitability[416,417]. Historically, the remaining effects of M_2R activation on cardiac function have been attributed to reduced cAMP synthesis due to Gαi-mediated inhibition of AC activity[418,419], opposing adrenergic-stimulation of HCN and phosphorylation of PKA targets. Whilst GIRK channel activation is the dominant pathway responsible for tonic vagal tone, opposition to adrenergic stimulation is predominantly thought to be mediated by inhibition of cAMP synthesis[420].

However, there is a significant volume of evidence that this model may not tell the whole story. Firstly, in many studies, the sympatholytic effects of cholinergic stimulation do not correlate with a reduction in cAMP[421–425]. Furthermore, even when cAMP is elevated by phosphodiesterase inhibition with IBMX[426], Gαs activation with cholera toxin[427], or superfusion of the cAMP analogue 8-Br cAMP[428], cholinergic

stimulation still has a negative inotropic effect despite being unable to reduce cAMP under these conditions. This indicates that reducing cAMP is not a necessary component of M_2R's negative inotropic signalling. Not only do cholinergic effects on contraction appear not to correlate with cAMP, reduced phosphorylation of PKA targets by cholinergic stimulation can also occur without any reduction in cytosolic cAMP and even without reducing PKA activity[424,428]. Together, these data point to a cAMP/PKA-dependent, but indirect, pathway or a cAMP/PKA-independent pathway by which M_2R activation can oppose adrenergic stimulation. Several such mechanisms have been proposed and are discussed later.

This dissociation between cholinergic influence on cAMP and on contractility could reflect compartmentalisation of the cAMP response downstream of M_2R activation. There is some evidence for this, such as the observation that inhibition of L-type calcium current by ACh occurs only when the ACh is added to the same cellular region as a βAR agonist and not when added distantly[429]. This suggests a degree of spatial restriction to effects exerted by M_2R activation, but this is one of the few previous investigations directly probing spatial aspects of M_2R signalling. At the time, the authors interpreted these results as indicating that the inhibitory effect of M_2R occurs upstream of AC, based on the apparent inability of the signal to diffuse and act at distal sites. However, these experiments were conducted before the concept of spatiotemporal compartmentalised cAMP signalling had been introduced.

5.1.5. Aims

As has already been discussed extensively elsewhere, the stimulation of cAMP generation by Gs-coupled GPCRs is spatially compartmentalised. Whether the

effect of Gi-coupled GPCRs activation on cAMP levels also shows compartmentalisation has not been previously examined.

The aim of the experiments presented in this chapter is to determine whether M_2R activation produces a homogenous or a spatially compartmentalised reduction in the cAMP signal in cardiac myocytes.

5.2. Methods

5.2.1. FRET imaging

FRET experiments were performed as described in **Section 2.2.4**. Isoproterenol (Iso) and carbachol (CCh) were added simultaneously as indicated. Pre-treatment with pertussis toxin (PTX) was performed 16 hours preceding imaging by removing the M2 medium from the NRVMs and replacing it with fresh M2 medium including 200 $ngmL^{-1}$ PTX or equivalent volume (4 µL per well) of vehicle (Veh; Ringer's buffer). PTX or Veh were also added to the buffer used for washing the cells and for imaging. FRET experiments using AKAR4 and targeted variants of this sensor were performed identically to those using FRET-based cAMP reporters.

5.3. Results

5.3.1. Validation of FRET reporters for measuring responses to Gi protein coupled receptor activation

All of the experiments described so far using FRET-based reporters for cAMP have used them to measure cAMP generation in response to ligands acting at Gs-coupled

GPCRs (GsPCRs). Therefore, the first step was to confirm that the inhibition of cAMP synthesis upon activation of a GiPCR could be detected using these reporters.

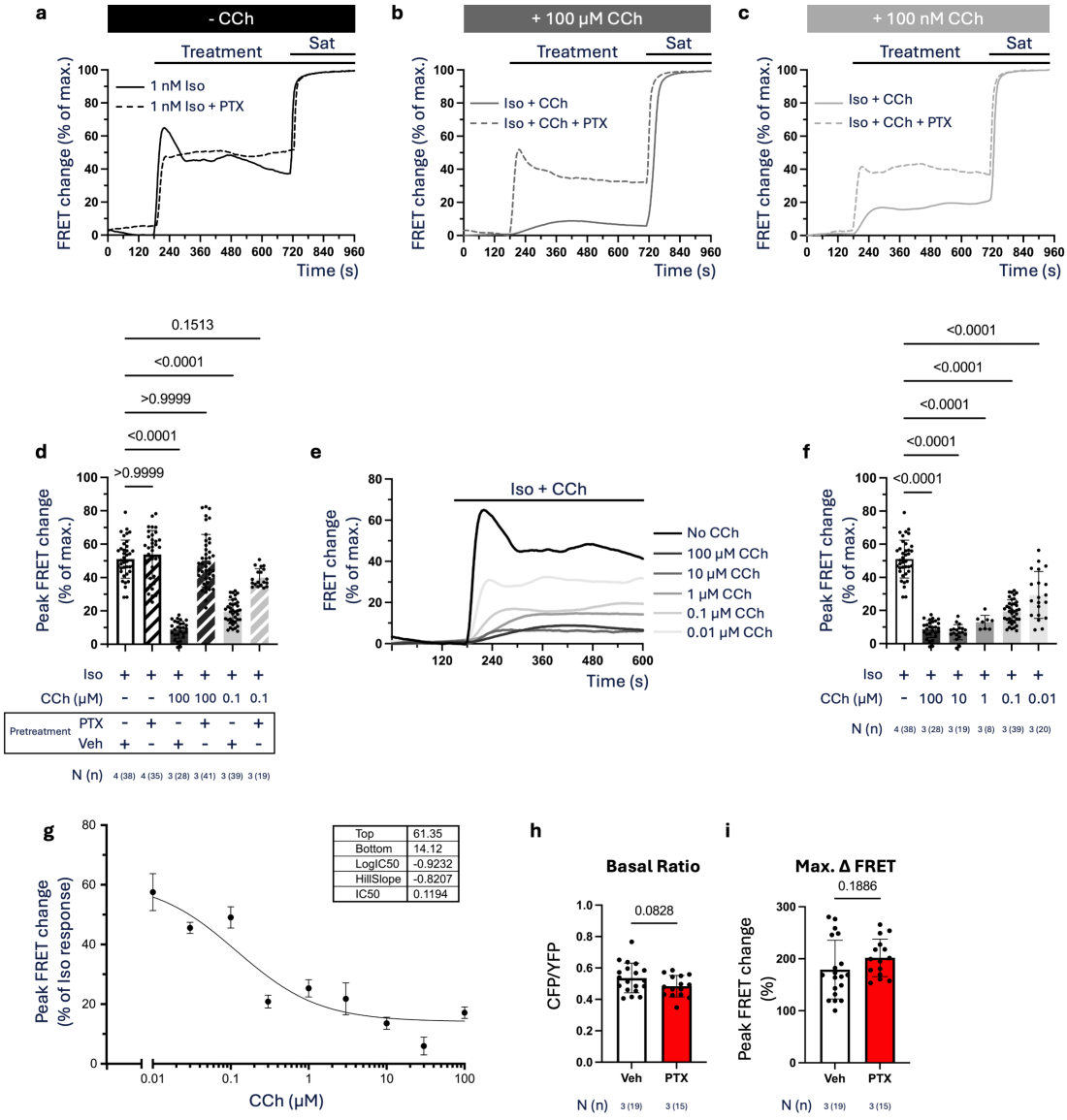


Fig 5.1 FRET-based reporters enable detection of Gi-dependent cholinergic signalling. Representative kinetics **(a-c)** and summary **(d)** of normalised FRET changes in NRVMs expressing Epac-S^{h187} cAMP FRET reporter in response to bath application of either 1 nM isoproterenol (Iso) only **(a)**, or 1 nM Iso and 100 µM carbachol (CCh) added simultaneously **(b)**, or 1 nM Iso and 100 nM CCh added simultaneously **(c)**. Cells were pretreated with either 200 ngmL^{-1} pertussis toxin (PTX) or the same volume of Ringer's buffer (Veh) for at least 16 hours preceding imaging. Representative kinetics **(e)** and summary **(f)** of normalised FRET changes in NRVMs expressing Epac-S^{h187} in response to bath application of either 1 nM Iso only or 1 nM Iso and varying doses of CCh added simultaneously. **(a-f)**

FRET change presented normalised to the maximum response elicited by a saturating stimulus (Sat) (25 μM forskolin + 100 μM IBMX). **(g)** Dose-response curve of FRET changes in NRVMs expressing Epac-S^{h187} in response to simultaneous bath application of 1 nM Iso and varying doses of CCh. Data are expressed as % of mean peak response to 1 nM Iso alone. Basal FRET ratio **(h)** and maximum FRET change **(i)** in NRVMs expressing Epac-S^{h187}. Basal FRET ratio is the average ratio (CFP emission intensity/YFP emission intensity) from the first six frames before the addition of any drugs. Maximum FRET change was quantified as the mean percentage change from baseline measured over the final six frames following stimulation with a saturating stimulus (25 μM forskolin + 100 μM IBMX). Cells were pretreated with either 200 $ngmL^{-1}$ pertussis toxin (PTX) or the same volume of Ringer's buffer (Veh) for at least 16 hours preceding imaging. Error bars represent mean +/- SD. Sample size given as N (n) where N = biological replicates (cell isolations); n = individual cells.

In preliminary experiments, the effect of M_2R activation on basal cytosolic cAMP was assessed by application of 100 μM carbachol (CCh) alone. CCh did not produce a detectable reduction in cAMP compared with vehicle-treated controls **(Fig S3)**. In fact, in ventricular tissue, cholinergic inotropic effects are difficult to observe in the absence of concomitant adrenergic activation[430,431]. The relationship between muscarinic and adrenergic signalling has been termed 'accentuated antagonism' referring to the observation that the functional effects of muscarinic agonists are enhanced in the presence of catecholamines. This is consistent with previous observations that constitutive AC activity and basal cAMP levels are low in ventricular myocytes in the absence of βAR stimulation[432–434]. Therefore, to observe an effect on cAMP generation, cells were treated simultaneously with Iso to activate βARs and CCh to activate muscarinic acetylcholine receptors (mAChRs). Iso and CCh were applied simultaneously rather than sequentially because the kinetics of the Iso-induced cAMP response varies between cells, making it difficult to ensure that subsequent CCh application occurred at a comparable point in the Iso response across experiments.

Initially, a large dose (100 μM) of CCh was used to establish if any effect could be observed. In neonatal rat ventricular myocytes (NRVMs) expressing Epac-S^{h187} FRET-based cytosolic cAMP reporter, Iso treatment alone resulted in an average FRET change of 51.0% of max. whilst addition of CCh significantly reduced the FRET change to 8.7% **(Fig 5.1a-b, d)**. Given CCh is a non-specific muscarinic agonist and can also activate the other mAChR isoforms, to ensure that this observed effect was mediated by Gi-coupled muscarinic receptors (M_2R), the experiment was repeated in the presence of Gi inhibition with pertussis toxin (PTX) **(Fig 5.1a-b, d)**. PTX had no effect on basal FRET ratio **(Fig 5.1h)**, maximum FRET change **(Fig 5.1i)**, or Iso-stimulated cAMP generation **(Fig 5.1a,d)** but abolished the effect of 100 μM CCh on Iso-stimulated cAMP generation **(Fig 5.1b)** with an average FRET change of 50.2% – similar to Iso treatment alone **(Fig 5.1d)**. This confirms that the FRET-based cAMP reporters can be used to observe Gi-dependent reduction of Iso-stimulated cAMP by CCh.

To determine an appropriate dose of CCh to use for subsequent experiments, the effects of several doses were compared **(Fig 5.1e-f)**. NRVM expressing Epac-S^{h187} were treated simultaneously with 1 nM Iso and either 100 μM, 10 μM, 100 nM, or 10 nM CCh. At all doses tested, CCh treatment significantly attenuated the FRET change compared with treatment with 1 nM Iso alone. A dose-response curve was generated, with values normalised to the FRET response elicited by 1 nM iso alone **(Fig 5.1g)**. The IC_{50} calculated from the fitted curve (0.119 μM) is consistent with previously published values[435] and in line with doses used previously to elicit

negative inotropic responses[56,436,437]. Therefore, 100 nM CCh was selected as a more appropriate dose.

5.3.2. Cholinergic stimulation does not oppose adrenergic stimulation at AKAP79

After validating that Gi-mediated inhibition of cAMP synthesis by M_2Rs can be observed using FRET-based reporters, we asked whether this inhibition is spatially homogeneous or compartmentalised. To address this, the same protocol of simultaneous treatment with Iso and CCh was applied to cells individually expressing the targeted FRET-based cAMP reporters AKAP18δ-CUTie, AKAP79-CUTie, and TPNI-CUTie, localised to the sarcoplasmic reticulum (SR), AKAP79 nanodomain at the plasma membrane, and troponin I at the myofilament, respectively.

Application of 100 nM CCh significantly attenuated the Iso-stimulated FRET response by AKAP18δ-CUTie **(Fig 5.2a-c)** or TPNI-CUTie **(Fig 5.2g-i)** but had no effect on the signal detected by AKAP79-CUTie **(Fig 5.2d-f)**. These data indicate that cholinergic stimulation opposes cAMP generation at the SR and at the myofilament but not in the AKAP79 nanodomain at the plasmalemma.

This effect persisted even at substantially higher concentrations of CCh. Treatment with 100 μM CCh had no effect on Iso-stimulated FRET change in cells expressing AKAP79-CUTie **(Fig 5.2d-f)**, while abolishing Iso-stimulated FRET change in cells expressing AKAP18δ-CUTie **(Fig 5.2a-c)** or TPNI-CUTie **(Fig 5.2g-i)**. Thus, even maximal cholinergic stimulation does not oppose adrenergic-stimulated cAMP generation at AKAP79.

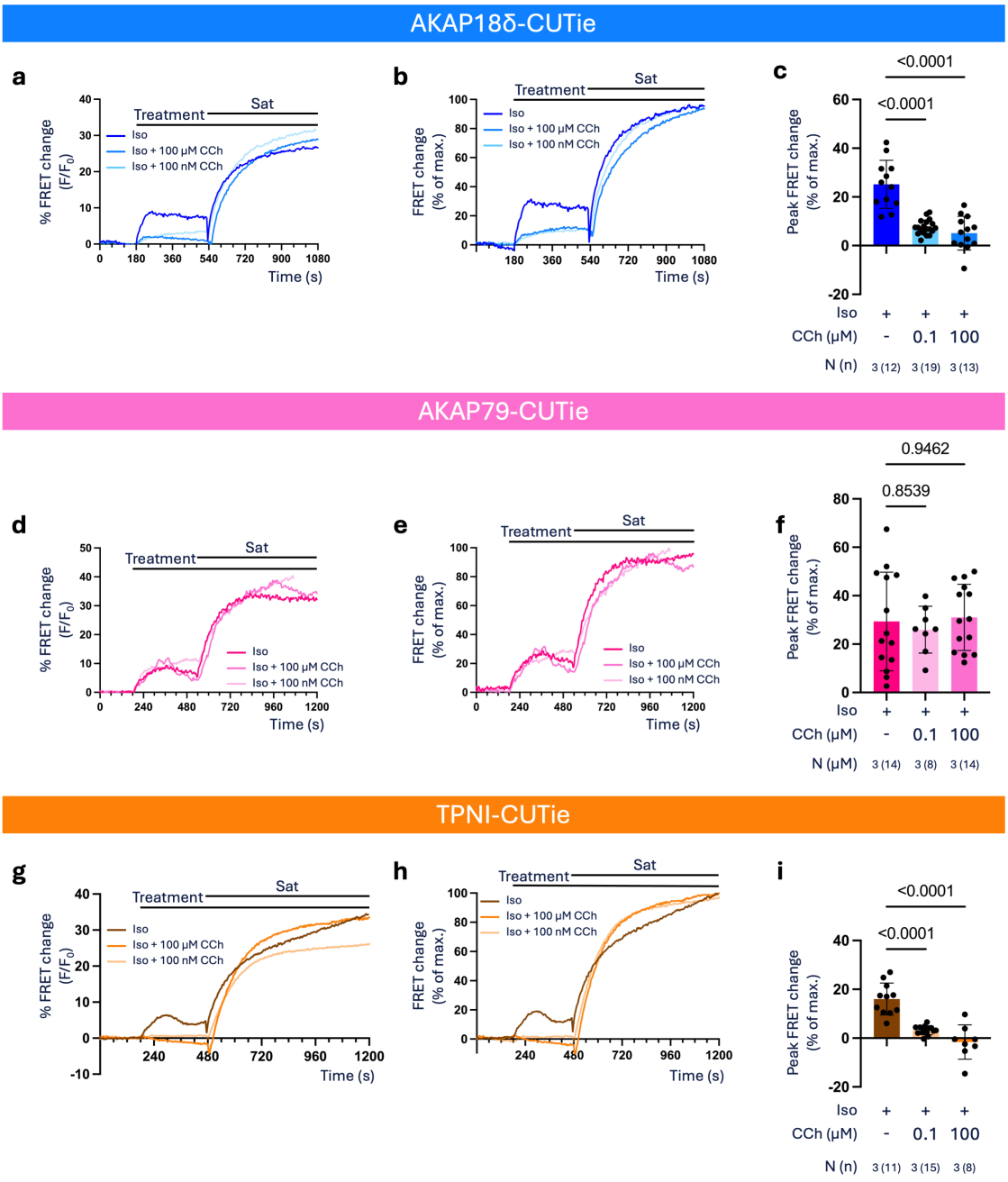


Fig 5.2 Cholinergic opposition of β-adrenergic cAMP signalling is spatially compartmentalised. Representative kinetics **(a-b), (d-e), (g-h)** and summary **(c), (f) & (i)** of FRET changes in NRVMs individually expressing AKAP18δ-CUTie **(a-c)**; AKAP79-CUTie **(d-f)**; or TPNI-CUTie **(g-i)** cAMP FRET reporters in response to bath application of either 1 nM isoproterenol (Iso) only or 1 nM Iso and carbachol (CCh; 100 µM or 100 nM) added simultaneously. **(a), (d) & (g)** FRET change is shown as % change from initial value (F0) with F0 calculated as the average of the first six frames. **(b), (e) & (h)** FRET change is shown normalised to the maximum response elicited by a saturating stimulus (Sat) (25 µM forskolin + 100 µM IBMX). **(c), (f) & (i)** Points represent peak FRET change elicited by a stimulus

normalised to the maximum response elicited by a saturating stimulus. Error bars represent mean +/- SD. Sample size given as N (n) where N = biological replicates (cell isolations); n = individual cells.

5.3.3. Cholinergic regulation of cAMP signalling differs between plasma membrane compartments

Given the localisation of AKAP79 to discrete plasma membrane nanodomains, this raised the question of whether cholinergic modulation of adrenergic cAMP signalling is excluded specifically from this nanodomain or more broadly across the plasma membrane. To address this, the effects of Iso alone or in combination with CCh were assessed in cells expressing the plasma membrane-targeted FRET-based cAMP reporter MP-Epac-S^{h187}, a post-translationally myristoylated and palmitoylated variant of Epac-S^{h187}.

Application of Iso resulted in a mean FRET response of 27.16% of maximal response, whereas simultaneous application of Iso and 100 nM CCh produced a FRET response in the opposite direction, reflecting a reduction in cAMP levels (-50.5% of max.) **(Fig 5.3a-b)**. Notably, the maximum response elicited by a saturating stimulus (25 µM Fsk and 100 µM IBMX) was reduced on average in cells treated with Iso and CCh compared with Iso alone **(Fig 5.3c)** which could exaggerate differences following normalisation. To account for this, FRET changes were also expressed as a % of the initial value and remained significantly different between conditions **(Fig 5.3d)**, confirming that this effect is not an artefact of normalisation. The response seen following co-application of Iso and CCh indicates a reduction in cAMP levels below basal. This effect was abolished by pre-treatment with PTX, confirming that it is mediated by Gi-dependent signalling.

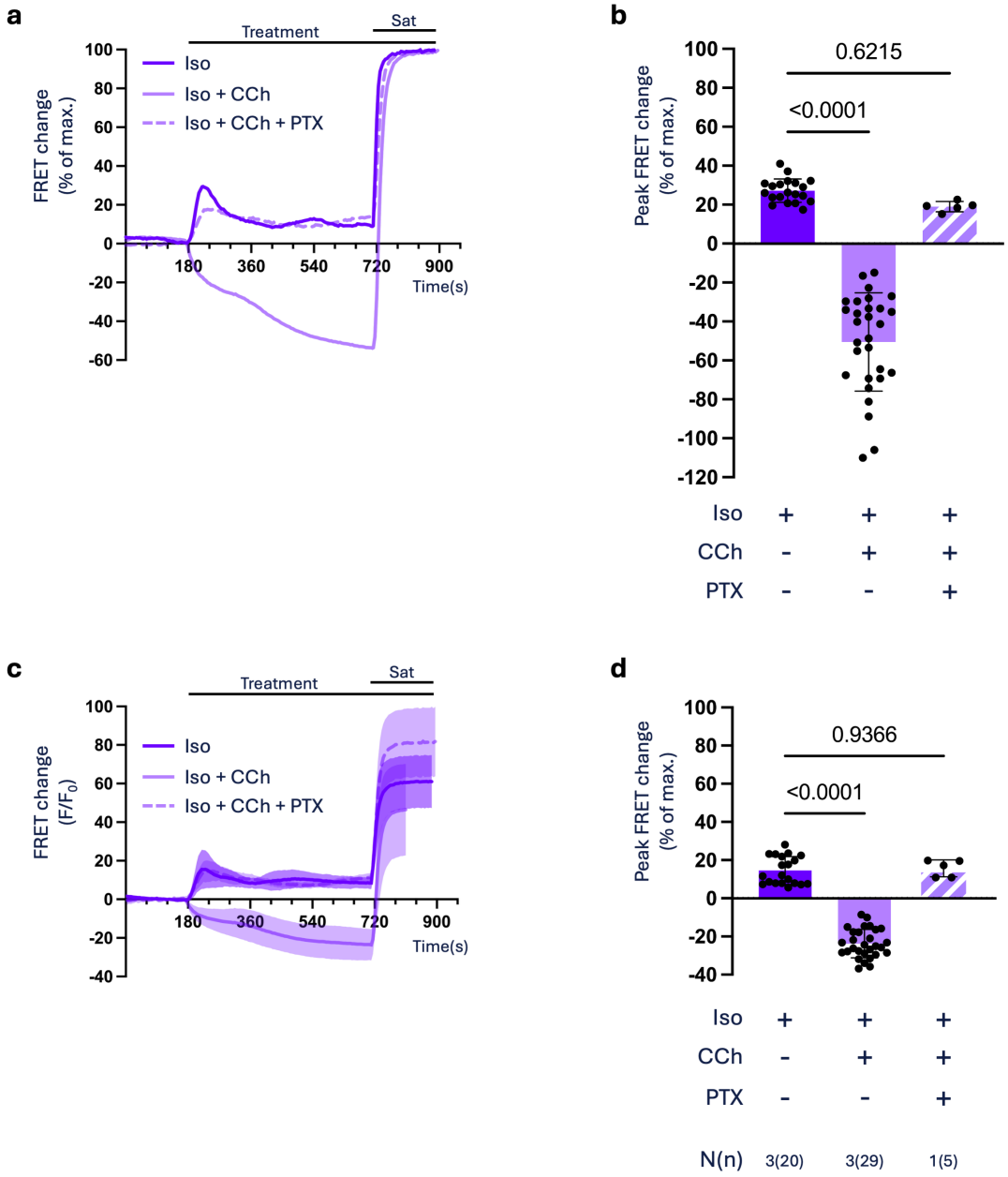


Fig 5.3 Cholinergic stimulation produces a strong Gi-dependent suppression of cAMP at the plasma membrane. Representative kinetics **(a)**, mean kinetics **(c)**, and summary **(b) & (d)** of FRET changes in NRVMs expressing MP-Epac-S^{h187} plasma membrane-targeted cAMP FRET reporter in response to bath application of either 1 nM isoproterenol (Iso) only or 1 nM Iso and 100 nM carbachol (CCh) added simultaneously. **(a-b)** FRET change is shown normalised to the maximum response elicited by a saturating stimulus (Sat) (25 µM forskolin + 100 µM IBMX). **(c-d)** FRET change is shown as % change from initial value (F0) with F0 calculated as the average of the first six frames. **(c)** Shows mean FRET change from all n cells. Line and shading represent mean +/- SD. Cells were pretreated with either 200 ngmL^{-1} pertussis toxin (PTX) or the same volume of Ringer's buffer (Veh) for at least 16

hours preceding imaging. Error bars represent mean +/- SD. Sample size given as N (n) where N = biological replicates (cell isolations); n = individual cells.

These findings demonstrate that cholinergic inhibition of cAMP signalling is not uniform across the plasma membrane, but instead exhibits marked spatial heterogeneity, with strong Gi-dependent suppression of cAMP at the membrane overall, in contrast to the AKAP79 nanodomain.

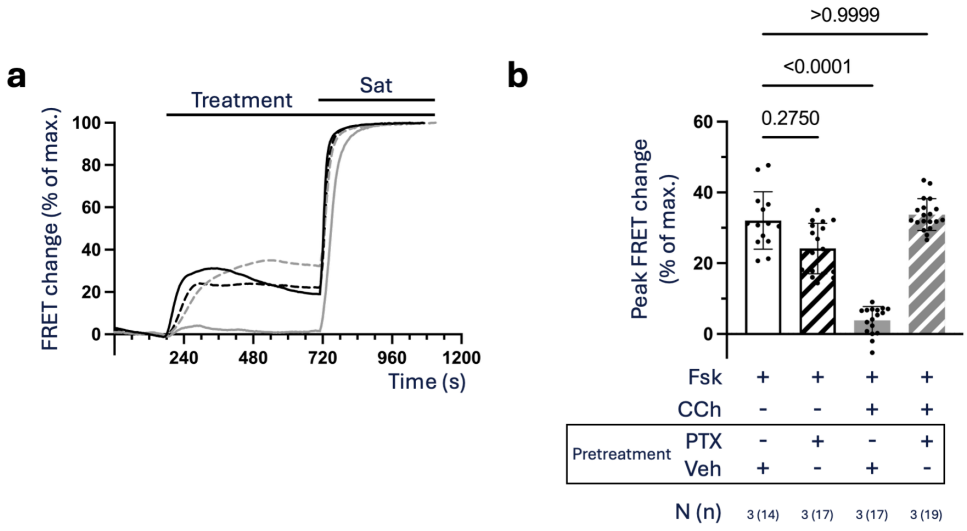


Fig 5.4 Cholinergic stimulation opposes forskolin-stimulated cytosolic cAMP generation. Representative kinetics **(a)** and summary **(b)** of FRET changes in NRVMs expressing Epac-S^{h187} cAMP FRET reporter in response to bath application of either 1 µM forskolin (Fsk) only or 1 µM Fsk and 100 µM carbachol (CCh) added simultaneously. Cells were pre-treated with either 200 ngmL-1 pertussis toxin (PTX) or the same volume of Ringer's buffer (Veh) for at least 16 hours preceding imaging. **(b)** Data represents peak FRET change elicited by a stimulus normalised to the maximum response elicited by a saturating stimulus (Sat) (25 µM forskolin + 100 µM IBMX). Error bars represent mean +/- SD. Sample size given as N (n) where N = biological replicates (cell isolations); n = individual cells.

5.3.4. Cholinergic stimulation does not influence cAMP generation at AKAP79

Two higher-level explanations could account for the observed lack of cholinergic effect at AKAP79. This could reflect a βAR-dependent mechanism that protects cAMP signalling within the AKAP79 nanodomain from cholinergic influence.

Alternatively, it could be explained by an inability of M_2R-driven Gαi signalling to access or effectively regulate this signalling compartment. These possibilities can be distinguished by testing whether this lack of cholinergic inhibition persists when cAMP generation is independent of βAR activation.

Therefore, the same experimental protocol was repeated, but with cAMP generation driven by direct cyclase activation using forskolin (Fsk) rather than βAR stimulation. As an initial validation, the ability of cholinergic stimulation to oppose Fsk-stimulated cAMP generation was confirmed using a cytosolic reporter. In NRVMs expressing the cytosolic sensor Epac-S^{h187}, application of 100 μM CCh significantly reduced the FRET response to 1 μM Fsk **(Fig 5.4a-b)**. PTX pre-treatment abolished this effect, confirming Gi-dependence, but had no effect on Fsk-stimulated cAMP generation alone.

Using targeted cAMP reporters, application of 100 μM CCh significantly attenuated the FRET response to Fsk in NRVMs expressing AKAP18δ-CUTie **(Fig 5.5a-c)** or TPNI-CUTie **(Fig 5.5g-i)** but had no effect in cells expressing AKAP79-CUTie **(Fig 5.5d-f)**. These data demonstrate that the cAMP elevation detected by AKAP79-CUTie is unaffected by cholinergic stimulation irrespective of the mechanism by which cAMP is generated. This suggests that shielding of the AKAP79 cAMP nanodomain from cholinergic influence does not rely on βAR activation.

5.3.5. Compartmentalisation of cholinergic cAMP signalling is mirrored by PKA activity

The lack of influence of cholinergic stimulation on cAMP at AKAP79 was unexpected. AKAP79 has been shown to anchor protein kinase A (PKA) at the L-type Ca^{2+} channel

($Ca_V1.2$) in cardiac myocytes[216,238,438] and cholinergic stimulation has a well-established inhibitory effect on L-type Ca^{2+} current[423,429,439]. We therefore asked whether, in addition to cAMP generation, PKA activity remains elevated in the AKAP79 nanodomain in the presence of cholinergic stimulation, as a way to further corroborate our findings. To address this question, the FRET-based PKA activity reporter, A-kinase anchoring reporter (AKAR4)[256], was used.

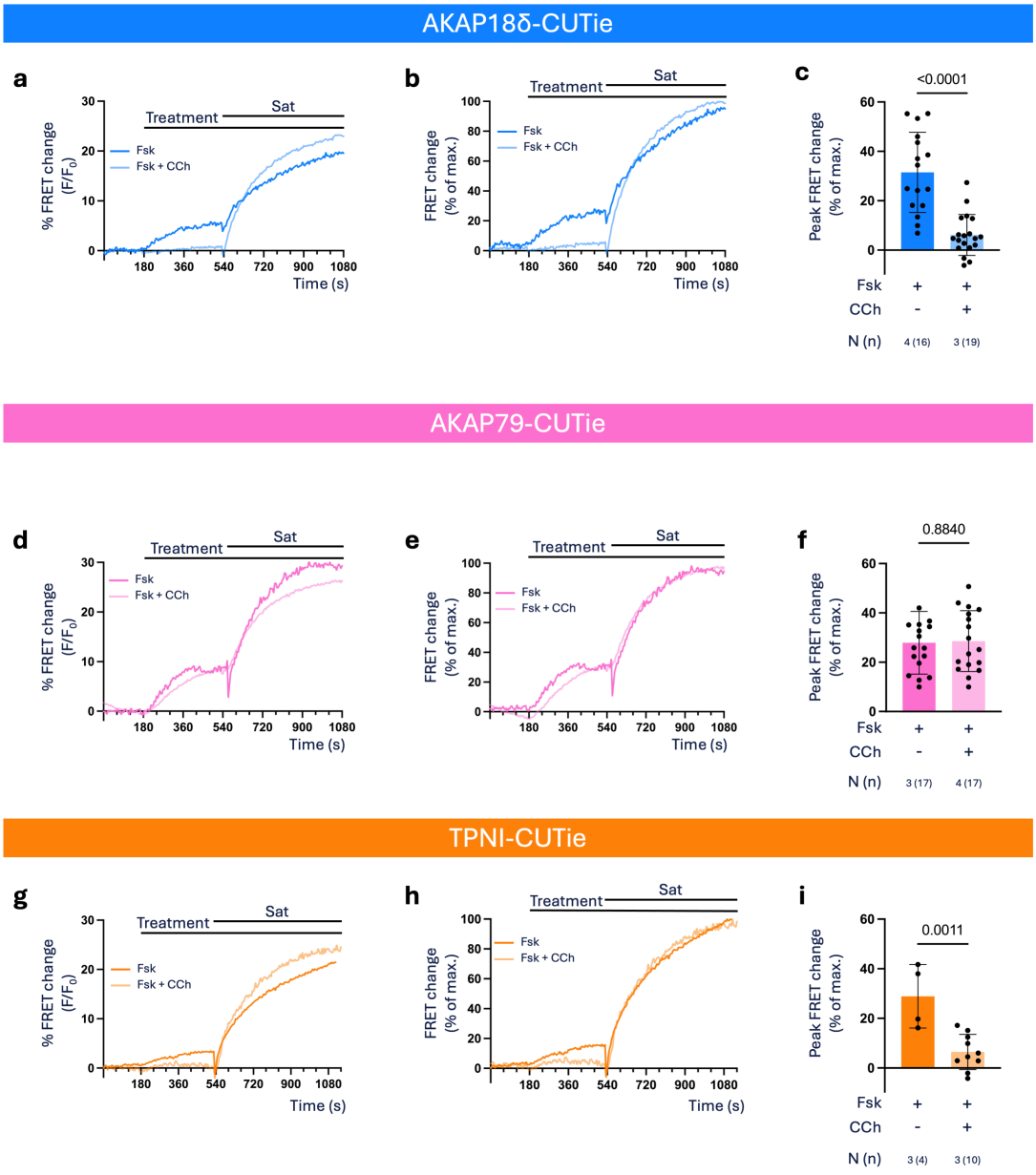


Fig 5.5 Cholinergic inhibition of cAMP signalling is compartmentalised and excluded from the AKAP79 nanodomain. Representative kinetics **(a-b), (d-e), (g-h)** and summary **(c), (f) & (i)** of FRET changes in NRVMs individually expressing AKAP18δ-CUTie **(a-c)**; AKAP79-CUTie **(d-f)**; or TPNI-CUTie **(g-i)** cAMP FRET reporters in response to bath application of either 1 μM forskolin (Fsk) only or 1 μM Fsk and 100 μM carbachol (CCh) added simultaneously. **(a), (d) & (g)** FRET change is shown as % change from initial value (F0) with F0 calculated as the average of the first six frames. **(b), (e) & (h)** FRET change is shown normalised to the maximum response elicited by a saturating stimulus (Sat) (25 μM forskolin + 100 μM IBMX). **(c), (f) & (i)** Points represent peak FRET change elicited by a stimulus normalised to the maximum response elicited by a saturating stimulus. Error bars represent mean +/- SD. Sample size given as N (n) where N = biological replicates (cell isolations); n = individual cells.

The effects of treatment with either 1 nM Iso alone or simultaneous treatment with 1 nM Iso and 100 nM CCh were measured in cells expressing either a cytosolic AKAR4 sensor (hereafter 'AKAR4') to assess global PKA activity or AKAP79-AKAR4 to monitor PKA activity within the AKAP79 nanodomain. In cells expressing AKAR4, Iso application produced a significant gain of FRET which was significantly attenuated by co-application of CCh **(Fig 5.6a-c)**. However, in cells expressing AKAP79-AKAR4, the Iso-stimulated FRET response was unchanged by simultaneous CCh application **(Fig 5.6d-f)**. Thus, the increase in PKA activity in the AKAP79 nanodomain following adrenergic stimulation is unaffected by cholinergic signalling. This mirrors the lack of cholinergic inhibition of cAMP generation observed at the same subcellular location.

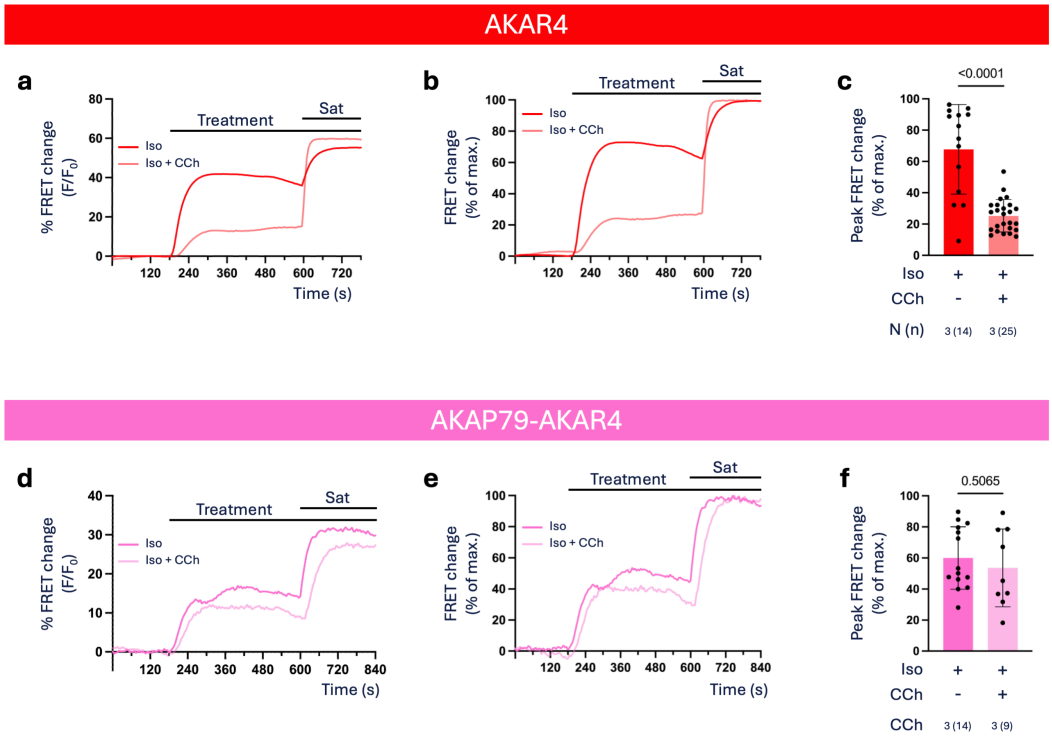


Fig 5.6 Compartmentalisation of cholinergic cAMP signalling is mirrored at the level of PKA activity. Representative kinetics **(a-b), (d-e)** and summary **(c) & (f)** of FRET changes in NRVMs individually expressing AKAR4 **(a-c);** or AKAP79-AKAR4 **(d-f)** FRET-based PKA activity reporters in response to bath application of either 1 nM isoproterenol (Iso) only or 1 nM Iso and 100 nM carbachol (CCh) added simultaneously. **(a) & (d)** FRET change is shown as % change from initial value (F0) with F0 calculated as the average of the first six frames. **(b) & (e)** FRET change is shown normalised to the maximum response elicited by a saturating stimulus (Sat) (25 µM forskolin + 100 µM IBMX). **(c) & (f)** Points represent peak FRET change elicited by a stimulus normalised to the maximum response elicited by a saturating stimulus. Error bars represent mean +/- SD. Sample size given as N (n) where N = biological replicates (cell isolations); n = individual cells.

5.4. Discussion

5.4.1. Regulation of the L-type calcium channel $Ca_V1.2$ in cardiac myocytes

L-type voltage-gated Ca^{2+} channels are the primary source of Ca^{2+} entry in cardiac myocytes with the $Ca_V1.2$ isoform ubiquitously expressed in all cardiac chambers and pacemaker cells and representing the predominant isoform in ventricular

myocytes[440,441]. The L-type calcium current ($i_{Ca,L}$) provides Ca^{2+} that activates the ryanodine receptor (RyR2), triggering Ca^{2+} release from the sarcoplasmic reticulum (SR), in a process termed calcium-induced calcium-release[223]. Modulation of $i_{Ca,L}$ is therefore a key contributor to adrenergic-stimulated positive inotropy and chronotropy. The classical textbook description of βAR regulation of $i_{Ca,L}$ involves βAR-driven activation of AC via Gαs, leading to cAMP generation, PKA activation, and phosphorylation of $Ca_V1.2$, increasing the channel's open probability[442]. Channel activity is negatively regulated by Ca^{2+}-dependent inhibition (CDI) mediated by Ca^{2+}/calmodulin and the Ca^{2+}-dependent phosphatase calcineurin[239]. AKAP79/150 scaffolds both PKA and calcineurin at $Ca_V1.2$, establishing a sub-sarcolemmal signalosome that tightly regulates $i_{Ca,L}$[216,237–240,443] and anchoring of PKA by AKAP79 at $Ca_V1.2$ is required for β-adrenergic regulation of $i_{Ca,L}$[216,238]. This cAMP/PKA nanodomain is therefore the signalling compartment which is thought to be reported using the AKAP79-targeted CUTie and AKAR4 FRET reporters[195].

Despite being the textbook description, it became clear some time ago that the βAR-Gαs-AC-cAMP-PKA pathway leading to phosphorylation of $Ca_V1.2$ and increased channel conductance was incomplete (Reviewed in Ref.[442]). One of the most striking examples supporting this was the observation that knock-in mice carrying phospho-null mutations at the canonical PKA consensus site of $Ca_V1.2$ retained adrenergic regulation of $i_{Ca,L}$[444,445], demonstrating that $Ca_V1.2$ phosphorylation at these sites is not required for adrenergic regulation. This, together with other evidence, suggested the presence of an additional component within this signalling pathway. More recently, Rad was identified as a critical component of this

regulation[226]. Rad is an RGK family small GTPase and a PKA phosphorylation substrate that tonically inhibits $Ca_V1.2$ via interaction with the $Ca_V\beta$ subunit; following PKA-dependent phosphorylation, Rad dissociates from the channel complex, relieving this inhibition. Our experiments are entirely consistent with this updated model, showing that βAR activation with Iso raises cAMP **(Fig 5.2d-f)** and increases PKA activity **(Fig 5.6d-f)** at AKAP79, in close proximity to $Ca_V1.2$.

The mechanism underlying cholinergic regulation of $Ca_V1.2$ has proved even more elusive. The traditional view has been that cholinergic signalling opposes the adrenergic regulatory pathway, with Gαi-mediated inhibition of AC reducing cAMP generation and thereby decreasing PKA activity and $i_{Ca,L}$[420]. It is likely that elucidating the mechanisms of muscarinic signalling has been particularly challenging because M_2R signals through multiple pathways[225], including one that is cAMP-dependent, and at least one cAMP-independent pathway.

There is substantial evidence that M_2R activation inhibits adenylyl cyclase, reducing cAMP generation[418,421,426,446–448] and our data are consistent with this. We observed a reduction in cytosolic cAMP following cholinergic stimulation that was abolished by pertussis toxin (PTX) **(Fig 5.1a-f)**, demonstrating Gi-dependence. Additionally, we observed opposition to Iso-stimulated cAMP elevation at the SR and myofilament **(Fig 5.2)**, consistent with literature describing acetylcholine-mediated attenuation of Iso-stimulated phosphorylation of phospholamban (PLB) and troponin I (TPNI)[424]. However, in a number of other publications, cholinergic stimulation has been reported to have no effect on global cAMP[421–426,439,449]. Furthermore, in these experiments, despite not observing any reduction in cAMP, cholinergic stimulation

still produced a negative inotropic effect. Further evidence supporting a cAMP-independent component of M_2R-mediated negative inotropy comes from experiments in which cAMP was artificially elevated using IBMX[426], cholera toxin (CTX)[427], or 8-Br cAMP[428]; under these conditions in which cAMP would not be reduced by AC inhibition, cholinergic stimulation still exerted a negative inotropic effect. It is worth noting that earlier studies measured cAMP in whole-cell lysates using endpoint immunoassays, whereas our approach enables real-time measurement of cAMP dynamics in live cells with greater sensitivity and subcellular resolution. This methodological difference may explain why we observe a cholinergic reduction in cAMP which has not consistently been observed in previous studies.

Our results show that, unlike other subcellular locations, Iso-stimulated cAMP **(Fig 5.2)** and PKA activity **(Fig 5.6)** at AKAP79 are not attenuated by cholinergic stimulation. This protection is particularly striking given that cholinergic stimulation produces strong Gi-dependent suppression of cAMP at the plasma membrane more generally **(Fig 5.3)**, indicating that signalling within the AKAP79 nanodomain is insulated from broader membrane-associated Gi-activity. Given the well-established cholinergic opposition to the adrenergic-stimulated increase in $i_{Ca,L}$[423,439,450,451], this finding is surprising. These data, therefore, provide further support for the existence of a cAMP-independent component of M_2R signalling regulating $i_{Ca,L}$.

5.4.2. cAMP-independent cholinergic signalling

Before considering alternative signalling mechanisms, it is worth evaluating the possibility that the observed lack of cholinergic effect at AKAP79 reflects a limitation of the experimental model rather than a physiological feature of M_2R signalling. Specifically, one possibility is that AKAP79 is not associated with all $Ca_V1.2$ channels, but instead with a distinct subpopulation that is not subject to muscarinic regulation. In this scenario, the AKAP79-targeted sensor would report cAMP signalling within a compartment that is insensitive to M_2R activation, while cholinergic signalling could still modulate $i_{Ca,L}$ via the remainder of the channels which are not AKAP79-associated. Alternatively, overexpression of our AKAP79-targeted reporters may lead to mislocalisation, such that the cAMP signals reported do not accurately reflect those experienced by $Ca_V1.2$ channels.

However, several lines of evidence argue against these explanations. AKAP79/150 has been consistently shown to scaffold PKA at $Ca_V1.2$ and is required for β-adrenergic regulation of $i_{Ca,L}$[216,238,438]. Furthermore, our data presented in **Chapter 3** demonstrate that β_2AR, but not β_1AR, stimulation robustly increases cAMP within the AKAP79 nanodomain, indicating that this sensor reports a well-defined adrenergic signalling compartment. If the lack of cholinergic effect were due to mislocalisation of the reporter, a similar inconsistency might be expected for βAR-mediated signalling, which was not observed.

Although it remains possible that AKAP79-associated channels represent only a subpopulation of $Ca_V1.2$ that is differentially regulated, these considerations suggest that the absence of cholinergic modulation at this site more likely reflets a

genuine feature of M_2R signalling. This therefore raises the possibility that cholinergic regulation of $i_{Ca,L}$ involves mechanisms that are independent of local cAMP/PKA signalling.

If cholinergic modulation at AKAP79 is not mediated by cAMP/PKA, several alternative, cAMP-independent pathways downstream of M_2R could link M_2R activation to regulation of $Ca_V1.2$. One of the best-characterised M_2R-driven signalling pathways is mediated by free Gβγ, whose interaction with GIRK channels, stimulates $i_{k,ACh}$, representing the dominant pathway underlying parasympathetic effects in nodal and atrial cells, rather than inhibition of AC. The converse is true in ventricular myocytes, which exhibit little to no functional GIRK expression[452–455] and where parasympathetic signalling has traditionally been attributed to Gi-dependent inhibition of cAMP generation. However, our data in ventricular myocytes indicate an important role for cAMP-independent M_2R signalling in the ventricle and are consistent with previous studies demonstrating a dissociation between M_2R-mediated reduction in $i_{Ca,L}$ and inhibition of cAMP synthesis, alongside established roles for cAMP-dependent regulation of SR Ca^{2+} handling and myofilament Ca^{2+} sensitivity.

There are several possible cAMP-independent pathways by which M_2R could inhibit $Ca_V1.2$. Firstly, cholinergic opposition to βAR-stimulated $i_{Ca,L}$ may still be mediated by opposing PKA-dependent phosphorylation of Rad; however, rather than acting via reduced cAMP synthesis and PKA activity, M_2R activation could instead promote phosphatase activity, resulting in dephosphorylation of Rad. It has been reported in some publications that cholinergic stimulation promotes phosphatase activity[456], or

that phosphatase inhibition blocks cholinergic opposition to adrenergic stimulation[424,457]. However, acetylcholine (ACh) does not increase the rate of PKA-substrate dephosphorylation in cardiac myocytes[458]; although this study did not examine the rate of $Ca_V1.2$ or Rad phosphorylation so does not rule out a local increase in phosphatase activity in this nanodomain. Furthermore, phosphatase activation alone would not account for the ability of ACh to antagonise phosphorylation-independent responses such as adrenergic stimulation of the funny current (i_f), which is mediated directly by cAMP[167].

Our data also seem to be inconsistent with a phosphatase-driven mechanism. The fourth-generation AKAR reporter is a substrate for both PKA-mediated phosphorylation and phosphatase-mediated dephosphorylation such that the FRET response reflects the balance between PKA activity and phosphatase activity[256]. Even if PKA activity remained elevated in the AKAP79 nanodomain following cholinergic stimulation, an increase in phosphatase activity would be expected to reduce the AKAP79-AKAR4 FRET response; but no such effect was observed **(Fig 5.6d-f)**. Although, if the amount of protein phosphatase in this nanodomain is relatively low, its activation may not be able to outcompete the PKA-dependent phosphorylation of AKAR which is very efficient. Together, these findings further support the conclusion that M_2R activation engages multiple complementary signalling pathways, including at least one cAMP-independent mechanism.

Another possibility is that the Gβγ heterodimer mediates M_2R regulation of $Ca_V1.2$. Gβγ-mediated inhibition of $Ca_V2.1$ (P/Q-type Ca^{2+} channels) and $Ca_V2.2$ (N-type Ca^{2+} channels) is well documented[66,67,459]. However, similar Gβγ-mediated inhibition has

not been convincingly demonstrated for $Ca_V1.2$ and, unlike the Ca_V2 channels, $Ca_V1.2$ lacks a canonical Gβγ-binding domain[460–462]. It therefore seems unlikely that Gβγ directly interacts with $Ca_V1.2$; nevertheless, indirect regulation remains a possibility via canonical Gβγ effectors. For example, phospholipase C (PLC)β is activated by direct interaction with Gβγ[61–63], leading to cleavage of phosphatidylinositol 4,5-bisphosphate (PIP_2) and generation of inositol 1,4,5-triphosphate (IP_3) and diacylglycerol (DAG). DAG in turn activates protein kinase C (PKC)[40]. PKC has been reported to phosphorylate $Ca_V1.2$ and, in cardiac myocytes, reduce $I_{Ca,L}$[463]. It should be noted that this mechanism remains speculative; however, this and other means of indirect regulation by Gβγ represent plausible hypotheses that warrant experimental investigation.

Finally, cholinergic cGMP signalling has received considerable attention[420]. In some studies, ACh raised cGMP in cardiac myocytes[421,464], and exogenous application of cGMP antagonised βAR-stimulated elevation of $I_{Ca,L}$[465,466]. One proposed mechanism is increased cAMP degradation through cGMP-mediated stimulation of phosphodiesterase 2 (PDE2), as well as activation of protein kinase G (PKG)[420]; although this is not consistent with our data.

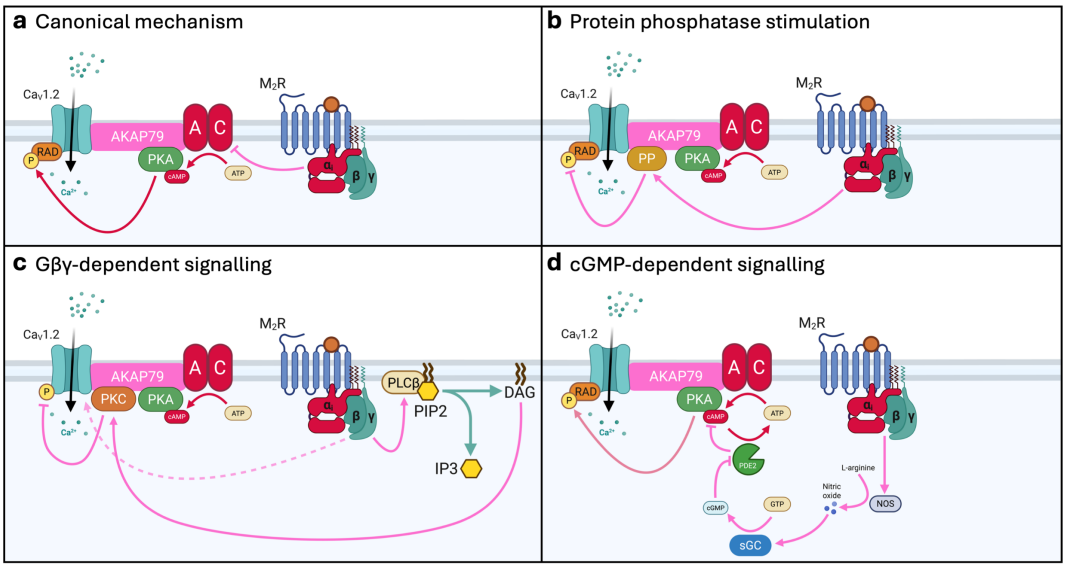


Fig 5.7 Potential mechanisms underlying cholinergic regulation of $Ca_V1.2$. (a) The canonical mechanism of M_2R mediated inhibition of $Ca_V1.2$ relies on Gαi-dependent inhibition of adenylyl cyclase (AC), reducing cAMP synthesis and protein kinase A (PKA) activity, resulting in reduced phosphorylation of RAD and $i_{Ca,L}$. **(b)** M_2R activation could reduce RAD phosphorylation through stimulation of protein phosphatases (PPs). **(c)** M_2R activation could reduce $i_{Ca,L}$ via Gβγ-dependent signalling, either through a direct interaction between Gβγ and $Ca_V1.2$ (dotted line) or through activation of phospholipase C (PLC)β. PLC-β cleaves phosphatidylinositol 4,5-bisphosphate (PIP_2), forming inositol 1,4,5-triphosphate (IP_3) and diacylglycerol (DAG). DAG activates protein kinase C (PKC) which can phosphorylate $Ca_V1.2$. **(d)** M_2R activation has been reported to activate nitric oxide synthase (NOS) which generates nitic oxide from L-arginine. No activates soluble guanylyl cyclase (sGC) which generates cGMP from GTP. cGMP stimulates phosphodiesterase (PDE)2 which degrades cAMP, reducing PKA-dependent RAD phosphorylation. Although this pathway ultimately acts through modulation of cAMP signalling, it represents a potential alternative to direct Gαi-mediated inhibition of AC; although it is inconsistent with our results. It should be noted that these models are speculative and could exist in parallel. Created using BioRender.com.

Cholinergic stimulation has also been reported to stimulate the activity of nitric oxide synthase (NOS)[467], which catalyses the generation of nitric oxide (NO) from L-arginine. NO, in turn, promotes soluble guanylyl cyclase (sGC) activity and the synthesis of cGMP. In addition, nitric oxide donors can mimic anti-adrenergic effects[468]. Neither of these observations, however, provides direct evidence that the muscarinic regulation of $Ca_V1.2$ is mediated by NO/cGMP. Furthermore,

interpretation of these findings is complicated by reports that NO donors can oxidise βAR agonists[469] and that NOS inhibitor L-NAME, used in some of these studies, can act as a mAChR antagonist[470].

In summary, it is clear that M_2R activation drives multiple distinct downstream signalling events, which have been proposed to include stimulation of phosphatase activity, both direct and indirect effects mediated by the free Gβγ heterodimer, and generation of cGMP **(Fig 5.7)**. Any or all of these mechanisms could contribute to the cAMP-independent regulation of $i_{Ca,L}$ by M_2R. Future work should aim to define the relative contributions of these pathways, as well as identify additional mechanisms that may be involved.

5.4.3. Spatial compartmentalisation of GiPCR signalling

Aside from how M_2R regulates $Ca_V1.2$, another salient question raised by our results is how, despite attenuating adrenergic-stimulated cAMP at other subcellular locations, cholinergic stimulation has no effect on cAMP generation at AKAP79. It is now well established that activation of Gαs-coupled GPCRs drives spatially compartmentalised cAMP signalling[188,195]. For the first time, we have investigated whether the inhibition of cAMP generation by a Gαi-coupled GPCR (GiPCR) also shows compartmentalisation, using the prototypical example of M_2R in cardiac myocytes. Our results demonstrate a spatially heterogeneous effect on the modulation of cAMP levels, in which cAMP levels are reduced in some subcellular locations but preserved in others.

Our data further demonstrate that this spatial heterogeneity extends within the plasma membrane, with strong Gi-dependent suppression of cAMP at the bulk membrane, in contrast to the AKAP79 nanodomain where no cholinergic inhibition was observed. Notably, the protection of the cAMP response at AKAP79 from cholinergic influence is not limited to opposition of adrenergic signalling, as direct activation of AC with forskolin, produced the same pattern. How this compartmentalisation of Gi-mediated cAMP inhibition is achieved remains to be determined.

In **Chapter 3** differences in cAMP generation stimulated by activation of β_1AR and β_2AR were discussed. Briefly, we showed that in NRVMs β_1AR stimulation evoked a cAMP response at the plasma membrane, SR, and myofilament but not at AKAP79, whereas β_2AR activation drove cAMP elevation at AKAP79 only. Taken together with the data presented in this chapter, these findings highlight the possibility that M_2R activation opposes β_1AR-driven cAMP but not β_2AR-driven cAMP.

One potential model to explain this would require, first, spatial segregation of β_1AR and β_2AR at the cell surface, and second, that β_1AR and M_2R exert influence over the same pool of ACs, whilst β_2AR-driven cAMP is generated by a distinct pool of ACs which is not subject to M_2R regulation. Differential membrane localisation of β_1ARs and β_2ARs is well-established in cardiac myocytes[220,288]. Whilst all AC isoforms can be stimulated by Gαs, not all isoforms are inhibited by Gαi[21], raising the possibility that cAMP synthesis at AKAP79 relies on a Gαi-insensitive isoform of AC. However, this model would require β_1AR and β_2AR to differentially couple to distinct AC isoforms, and there are currently no reports that this occurs. Alternatively, proximity

between M_2R and β_1AR could facilitate co-regulation of a shared pool of cyclases, while spatial separation between M_2R and β_2AR would dissociate their signals. However, immunogold labelling experiments reveal that M_2R clusters and β_1AR clusters do not co-localise[471], arguing against this proximity-based mechanism.

A role for Gαi-insensitive AC isoforms is therefore worth further consideration. The predominant AC isoforms expressed in ventricular myocytes are AC5 and AC6 which are both inhibited by Gαi. However, the Gαi-insensitive AC9 and AC4 have also been reported in cardiac tissue, albeit at lower levels[472]. If cAMP generation within the AKAP79 nanodomain were mediated by one of these Gαi-insensitive AC isoforms, this could account for its apparent resistance to M_2R-mediated inhibition.

However, several lines of evidence suggest this not to be the case. AKAP79 has been reported to co-immunoprecipitate with AC5 and AC6[473]. Furthermore, in wild-type cardiac myocytes, $Ca_V1.2$ channels localise to caveolin 3 (CAV3)-rich membrane regions, as do AKAP79 and AC6, whereas in AKAP79 knockout cells, co-localisation of AC6 and CAV3 is lost[238]. Together, these observations support the presence of Gαi-sensitive AC5/6 within the AKAP79 nanodomain, making it unlikely that selective coupling to Gαi-insensitive AC isoforms underlies the lack of cholinergic modulation at this site.

An alternative possibility is that cAMP within this nanodomain is generated by an AC isoform that is ordinarily Gαi-sensitive, but whose sensitivity to Gαi is locally modulated. For example, phosphorylation of AC5/6 by the serine/threonine kinase C-Raf has been reported to reduce Gαi-mediated inhibition of cAMP generation in HEK293 cells and neurons[474,475]. If a similar regulatory mechanism operates within

the AKAP79 compartment, local modulation of AC5/6 activity could diminish the inhibitory effect of Gαi, thereby limiting cholinergic suppression of cAMP. The presence of C-Raf, or other modulators of AC5/6 Gαi sensitivity within this signalosome, may therefore contribute to the lack of cholinergic effect observed at AKAP79.

Rather than reflecting differences in AC isoform identity or sensitivity within the AKAP79 nanodomain, the lack of cholinergic effect at this site could also be explained by limited access of active Gαi to this location. The classical view of freely diffusible second messengers is increasingly being supplemented by the concept of local signal generation[156,189]. As discussed in more detail elsewhere, cAMP signals can be generated locally by GsPCRs internalised from the cell surface or resident at intracellular locations. Consistent with this, we observe that cholinergic stimulation produces strong Gi-dependent suppression of cAMP at the bulk plasma membrane, while exerting weaker effects in the cytosol and at deeper subcellular targets. These observations suggest that cAMP levels within subcellular compartments are determined not only by diffusion from the plasma membrane, but also by localised regulation of adenylyl cyclase activity.

In addition to local signal generation by Gs, one could speculate that compartmentalisation of inhibition of cAMP synthesis by GiPCRs may similarly rely on Gαi internalisation and inhibition of AC in proximity to sites of PKA activity. It could, for example, be the case that Gαi has access to the AC generating cAMP at the SR and myofilament but is prevented from influencing AC activity at AKAP79. A

higher concentration of RGS proteins at this location would be sufficient to achieve this by accelerating Gαi deactivation.

Protection of the AKAP79 nanodomain from muscarinic regulation could potentially be multifactorial, arising from a combination of receptor localisation, G protein diffusion or trafficking, and additional signalling components. Targeted perturbation of these individual elements will help to define their respective contributions to the compartmentalisation of M_2R signalling.

5.5. Conclusions

Work in this chapter demonstrates that FRET reporters are appropriate tools to monitor the effects of M_2R activation on cAMP signalling.

Consistent with previous reports, we confirmed that:

- Cholinergic stimulation opposes cAMP generation in ventricular myocytes.
- This effect is dependent on Gαi-mediated inhibition of adenylyl cyclase.

The original findings of the work described in this chapter are:

- Cholinergic stimulation opposes cAMP generation at the plasma membrane, sarcoplasmic reticulum and myofilament but not at AKAP79.
- Cholinergic stimulation opposes β-adrenergic-stimulated PKA activity in the cytosol but not at AKAP79.
- Cholinergic stimulation produces a strong Gi-dependent suppression of cAMP at the bulk plasma membrane but not at AKAP79.

- Inhibition of cAMP synthesis by Gαi-coupled M_2Rs is spatially compartmentalised in rat ventricular myocytes.

Together these findings expand the model of spatial compartmentalisation of cAMP signalling to include not only cAMP generation by Gs-coupled GPCRs but also inhibition of cAMP signalling by Gi-coupled GPCRs.

6

Discussion and conclusions

6.1. Discussion

It is now widely accepted that cAMP signalling is spatially compartmentalised within cells. Upon activation of a Gαs-coupled GPCR, the downstream response is determined not only by the magnitude of cAMP generation, but also by the subcellular location of cAMP elevation[188,189]. A-kinase anchoring proteins (AKAPs) organise multi-protein signalling complexes that localise protein kinase A (PKA), and associated signalling components, to specific subcellular domains, such that local increases in cAMP selectively activate defined subsets of PKA targets[204,207,476]. Specificity is further maintained by phosphodiesterases (PDEs) which form cAMP sinks and prevent activation of inappropriate signalling complexes[174,202]. Variation of the spatial pattern of cAMP signalling enables selective engagement of the desired subset of PKA substrates, allowing cells to generate the appropriate physiological response to receptor activation.

While some of the mechanisms underlying cAMP compartmentalisation are well defined, it remains unclear how the appropriate spatial pattern of cAMP signalling is selected to generate desired downstream responses. The contribution of phosphodiesterases to this process has been extensively studied[174,185,190,191,195,250,477],

whereas the role of the GPCRs themselves in directing these patterns is less well understood.

In this thesis, we show that GPCR isoform diversity, ligand identity, and G protein coupling all contribute to determining the spatial patterning of cAMP signalling in cardiac myocytes.

In **Chapter 3** we show that stimulation of β_1-adrenergic receptors (β_1ARs) and β_2ARs drive distinct spatial patterns of cAMP signalling. Activation of β_1ARs elicited cAMP generation at the plasma membrane, sarcoplasmic reticulum (SR) and at troponin I (TPNI) within the myofilament, but not at AKAP79. In contrast, β_2AR stimulation produced cAMP only at AKAP79 with no detectable signal at the SR or TPNI or more broadly at the plasma membrane. The spatially restricted cAMP response to β_2AR activation was not attributable to its ability to couple to Gαi, indicating that receptor-specific mechanisms independent of G protein coupling underlie this spatial selectivity.

Previous studies have established a "global" vs "local" model of β-adrenergic signalling, in which β_1AR activation drives a widespread increase in cAMP associated with canonical cardiac adrenergic responses, whereas β_2AR stimulation generates more spatially restricted cAMP signals with distinct functional outcomes[259,298,300]. Two principal explanations have been put forward to account for this difference: diffusion limitation[259] and Gi-coupling[309,314].

The diffusion-based model suggests that the larger magnitude of cAMP produced following β_1AR activation allows it to spread more broadly than cAMP generated by

β_2AR stimulation[259]. However, our findings are not consistent with this explanation. β_1AR but not β_2AR stimulation elevated cAMP in proximity to the plasmalemma, whereas only β_2AR produced a signal within the AKAP79 nanodomain. This indicates that the observed differences cannot be explained solely by the magnitude of cAMP production and instead reflect distinct receptor isoform-specific mechanisms of compartmentalisation.

An alternative explanation is that β_2AR-specific coupling to Gαi restricts cAMP signalling. However, inhibition of Gαi did not alter the spatial pattern of cAMP observed for either receptor. Together, these findings demonstrate that GPCR identity itself encodes spatial information, independently of both signal magnitude and G protein coupling, highlighting receptor identity as a key determinant of spatial cAMP signalling.

Having established that GPCR identity encodes spatial information, an important question is whether this specificity can also arise from ligand identity at a single receptor. In **Chapter 4**, we confirmed a previous study[359], demonstrating that the β-blocker carvedilol is a partial agonist, driving cAMP generation predominantly via β_2ARs rather than β_1ARs.

While the full βAR agonists isoproterenol and noradrenaline elicited cAMP signals at the SR, TPNI, and AKAP79, and the neutral β-blocker metoprolol produced no detectable cAMP signal at any location, carvedilol generated a distinct spatial pattern of cAMP signalling. Specifically, carvedilol induced cAMP elevation at AKAP79 and TPNI, but not at the SR.

Taken together with the findings presented in **Chapter 3**, these results indicate that stimulation of β_2AR with isoproterenol or carvedilol drives distinct spatial patterns of cAMP signalling. This finding expands the concept of biased signalling, which has traditionally focused on ligand-directed selectivity between signalling pathways (e.g. G protein versus β-arrestin), suggesting that biased signalling extends beyond pathway selection to include specification of the spatial organisation of intracellular signalling.

In a parallel study conducted in our laboratory, preliminary experiments indicate that cAMP elevation following bucindolol treatment is detectable using AKAP18δ-CUTie and TPNI-CUTie, but not AKAP79-CUTie. This pattern is consistent with bucindolol acting predominantly as a partial agonist at β_1ARs rather than β_2ARs. Importantly, this spatial pattern of signalling differs from that observed with carvedilol, suggesting that β-blockers exhibiting partial agonist activity may not represent a homogenous class and that ligand-specific compartmentalisation of cAMP signalling could contribute to differences in their physiological and clinical effects.

Recent advances in fluorescent biosensors, including an approach based on biorthogonal labelling of GPCRs incorporating unnatural amino acids, have revealed a complex landscape of ligand-specific receptor conformations[15]. This demonstrates that different ligands stabilise distinct active states of the same receptor in living cells.

In this context, it is likely that isoproterenol and carvedilol stabilise distinct conformations of the β_2AR, enabling differential engagement of intracellular

signalling machinery, and resulting in distinct downstream cAMP signalling patterns. The specific molecular determinants of these interactions, however, remain to be determined.

One potential approach to address this would be to combine conformational biosensors, targeted FRET-based cAMP reporters, and proximity proteomics. Proximity labelling strategies have recently been used to identify dynamic interaction partners of GPCRs following activation, including studies of the β_2AR[478,479], μ-opioid receptor[480], angiotensin II type 1 receptor[479], and luteinizing hormone receptor[481]. These investigations have primarily focused on receptor trafficking and subcellular localisation, for example to compare ligands that differentially induce receptor internalisation[480].

However, this approach could be extended to compare the signalling partners recruited to a receptor following activation by ligands that generate distinct spatial patterns of signalling. In combination with the nanodomain-resolved cAMP measurements employed in this thesis, such strategies could provide mechanistic insight into how ligand-specific signalling complexes give rise to distinct spatial patterns of cAMP.

While these findings highlight how receptor identity and ligand identity contribute to spatial patterning of cAMP signalling, physiological signalling does not occur in isolation. cAMP generation driven by Gs-coupled GPCRs is balanced by the opposing influence of Gi-coupled receptors. In cardiac myocytes, cholinergic input via M_2Rs provides a physiological counterbalance to β-adrenergic signalling. This

raises the question of whether inhibitory signalling by Gi-coupled receptors is also spatially organised and selectively modulates specific cAMP nanodomains.

The findings summarised in **Chapter 5** show that M_2R stimulation selectively opposes cAMP generation in the cytosol, at the plasma membrane, the SR, and at TPNI, but not at AKAP79. This effect was observed both when cAMP production was driven by βAR activation, and when stimulated directly with forskolin. The absence of M_2R-mediated inhibition of cAMP at AKAP79 was mirrored in measurements of PKA activity.

These findings demonstrate for the first time that like Gs-driven cAMP generation, Gi-mediated inhibition is spatially compartmentalised. This provides further evidence that spatial patterning of cAMP signalling is governed by a complex regulatory network.

Notably, the lack of M_2R-mediated inhibition within the AKAP79 nanodomain suggests that the regulation of the L-type Ca^{2+} channel by adrenergic and cholinergic stimulation may not be mediated solely through cAMP/PKA signalling. More broadly, this indicates that the interplay between adrenergic and cholinergic pathways in cardiac myocytes is more complex than a simple opposition at the level of cAMP generation.

The contribution of Gβγ to these signalling patterns should be investigated directly in future experiments. Fluorescent biosensors capable of reporting Gβγ activation[482] could be used to compare the magnitude and kinetics of Gβγ signalling following βAR and M_2R activation. Targeted variants of such sensors could additionally

establish whether Gβγ activity is itself spatially restricted and whether this corresponds to the distinct patterns of cAMP signalling observed here. A complementary approach would be to repeat the targeted cAMP FRET experiments in the presence of gallein, which inhibits signalling through a subset of Gβγ-effector interactions. Unlike PTX, which prevents receptor-mediated activation of Gi/o and therefore inhibits signalling through both Gαi and Gi/o-derived Gβγ, this approach would allow the contribution of Gβγ-dependent signalling to be investigated more selectively. Together, these experiments could determine whether spatial regulation of Gβγ contributes to the receptor-dependent compartmentalisation of cAMP observed in our experiments.

Observations from both **Chapters 3** and **5** highlight the AKAP79-associated nanodomain as being regulated independently, not only from cytosolic compartments such as the SR and myofilament, but also from the broader plasma membrane. This emphasises the scale on which cAMP compartmentalisation takes place, with PKA targets in close proximity experiencing differing cAMP signals. This is consistent with reports that cAMP nanodomains can be as small as 10 nm in diameter[196] and that PKA targets in very close proximity, such as TPNI and myosin binding protein C within the myofilament, can be independently regulated by distinct cAMP pools[248]. More broadly, these findings support the concept that cellular structures such as the plasma membrane, SR, and myofilament do not constitute single signalling compartments, but instead comprise multiple independently regulated cAMP nanodomains with distinct regulatory mechanisms and downstream functional consequences.

Beyond their mechanistic significance, these findings may have implications for drug development. GPCR-directed therapeutics currently constitute around one third of all approved drugs[6] and their development is traditionally based on receptor selectivity, and more recently, on their propensity to promote biased signalling. The observation that different ligands acting at the same receptor can generate distinct spatial patterns of cAMP signalling raises the possibility that spatial signalling bias represents an additional layer of pharmacological selectivity. Drugs that produce similar overall levels of cAMP, or activate the same canonical signalling pathways, may nevertheless differ in their ability to engage specific cAMP nanodomains and downstream effectors. Targeting spatially compartmentalised signalling could provide opportunities to enhance therapeutic efficacy while reducing adverse effects arising from engagement of inappropriate cAMP nanodomains.

Taken together, these findings demonstrate that both Gs- and Gi-coupled GPCRs produce spatially compartmentalised cAMP signalling, and that the identity of both the receptor and the activating ligand contribute to specifying the resulting spatial pattern of cAMP. While these findings provide new insights into the contribution of GPCRs to cAMP compartmentalisation, several limitations of the current study should be considered.

6.2. Limitations

All experiments in this thesis were conducted using neonatal rat ventricular myocytes (NRVMs) as a model system. These cells are widely used in studies of cAMP compartmentalisation, facilitating comparison with previous work. However,

neonatal myocytes differ from adult cardiac myocytes in several important respects, including βAR expression, Ca^{2+} handling, and excitation-contraction coupling[301,483].

While these differences should be considered when interpreting the findings, they do not detract from the central conclusions of this work. In particular, the key questions addressed in this thesis – such as whether Gi-coupled receptors can generate spatially compartmentalised signalling – concern the existence of these mechanisms rather than their precise physiological context. As such, demonstration of these phenomena in NRVMs provides a valid proof-of-principle. Nevertheless, validation of these findings in adult cardiac myocytes will be important to establish their physiological relevance. To establish the clinical relevance of findings, particularly those relating to carvedilol, key observations will need to be validated in human ventricular myocytes.

The experimental conditions used for FRET imaging also differ from the physiological environment of ventricular myocytes in vivo. Cells were neither spontaneously beating nor electrically paced during imaging and therefore did not undergo beta-to-beat Ca^{2+} transients. Intracellular Ca^{2+} can influence cAMP signalling through regulation of both cAMP synthesis and degradation. Although the Ca^{2+}/calmodulin-stimulated AC isoforms AC1 and AC8 are not thought to be major contributors to cAMP generation in ventricular myocytes, the predominant ventricular isoforms AC5 and AC6 are inhibited by Ca^{2+}, while PDE1 activity is stimulated by Ca^{2+}/calmodulin. The absence of physiological Ca^{2+} cycling may therefore have influenced the magnitude, kinetics, or spatial organisation of the cAMP signals measured in this work.

Furthermore, FRET imaging was performed at room temperature rather than at 37ºC. Temperature can influence molecular diffusion as well as the kinetics of many of the enzymatic processes governing cAMP synthesis and degradation. Consequently, cAMP diffusion and the activities of ACs and PDEs may differ under the imaging conditions used here compared with physiological conditions. Nevertheless, as comparisons between experimental conditions were performed under the same imaging conditions, these limitations are more likely to influence the absolute characteristics of the measured cAMP responses rather than the relative differenced observed between experimental groups.

A further limitation of this work relates to the FRET-based sensors used. The CUTie sensors were selected due to their improved comparability across different subcellular locations relative to other targeted cAMP reporters[195]. However, cytosolic cAMP was typically measured using the Epac-S^{h187} sensor rather than CUTie, due to its greater sensitivity[255]. In **Chapters 3** and **5**, sub-sarcolemmal cAMP was also detected using Epac-S^{h187} due to technical challenges encountered with the equivalent CUTie sensor. As a result, the absolute magnitude of cAMP signals measured within nanodomains using CUTie sensors cannot be directly compared with cytosolic and sub-sarcolemmal measurements. Nevertheless, relative differences in cAMP responses between stimuli can still be reliably interpreted.

cAMP was measured at a defined set of subcellular locations which included the cytosol, SR, TPNI, the AKAP79-associated plasma membrane domain, and the plasma membrane more broadly. While this provides a representative overview of cAMP signalling at key functional sites in cardiac myocytes, other important

nanodomains were not examined. These include nuclear cAMP[250], mitochondrial nanodomains[484,485], and additional myofilament-associated sites including myosin-binding protein C[201,248]. Furthermore, additional plasma membrane associated nanodomains, aside from that associated with AKAP79, should be investigated to determine whether our results with AKAP79-CUTie represent a unique feature of this compartment.

Although clear differences were observed across the sites studied for all three aims, a more comprehensive understanding of how βAR isoform specificity, ligand-dependent effects, and balance between adrenergic and cholinergic signalling regulate cardiac function will require investigation of a broader range of cAMP nanodomains.

Finally, all experiments presented here rely on pharmacological manipulations of signalling pathways. Compounds were selected to maximise specificity; for example, selective activation of β_1ARs and β_2ARs was achieved using isoproterenol in combination with isoform-selective antagonists, rather than isoform-selective agonists, due to the greater specificity of the antagonists[304,305].

However, interpretation of results based solely on pharmacological approaches requires caution. Complementary strategies that directly manipulate specific elements of the signalling pathways, such as genetic approaches, could further clarify the roles of individual signalling components.

6.3. Conclusions

Although cAMP compartmentalisation is now well established, the higher-level organisation of this local signalling has remained unclear. While it is known that different Gs-coupled GPCRs generate distinct spatial patterns of cAMP signalling, leading to phosphorylation of specific subsets of PKA substrates, resulting in receptor-specific physiological responses, the mechanisms by which these patterns are selected are not well-characterised. The roles of phosphodiesterase isoform diversity and AKAP-anchored signalling complexes have been extensively studied, whereas the contribution of signal initiation by GPCRs has received comparatively less attention. This thesis aimed to address this gap.

The findings of this thesis demonstrate that GPCR signalling actively specifies these spatial patterns through a combination of receptor identity, ligand-dependent effects, and the balance between Gs- and Gi-mediated signalling.

Specifically, we demonstrate that βAR isoforms generate distinct spatial patterns of cAMP signalling that cannot be explained solely by differing G protein coupling selectivity. Furthermore, we show that cAMP compartmentalisation is not fixed for a given receptor, but can vary depending on the activating ligand, thereby extending the concept of biased signalling beyond pathway selection to include a spatial dimension. Finally, our findings indicate for the first time, that like Gs-mediated cAMP generation, Gi-mediated inhibition is also spatially compartmentalised.

Together, these findings demonstrate that GPCR signalling actively specifies the spatial pattern of cAMP generation within the cell. Receptor identity, ligand-dependent effects, and the balance between Gs- and Gi- mediated signalling all

contribute to this spatial organisation. These results advance our understanding of how signalling specificity is achieved within the cAMP pathway and highlight the selection of spatial signalling patterns as a key mechanism by which GPCRs regulate cellular physiology. In this way, GPCRs do not simply initiate cAMP signalling, but play a vital role in determining where within the cell it occurs.

A

Appendix

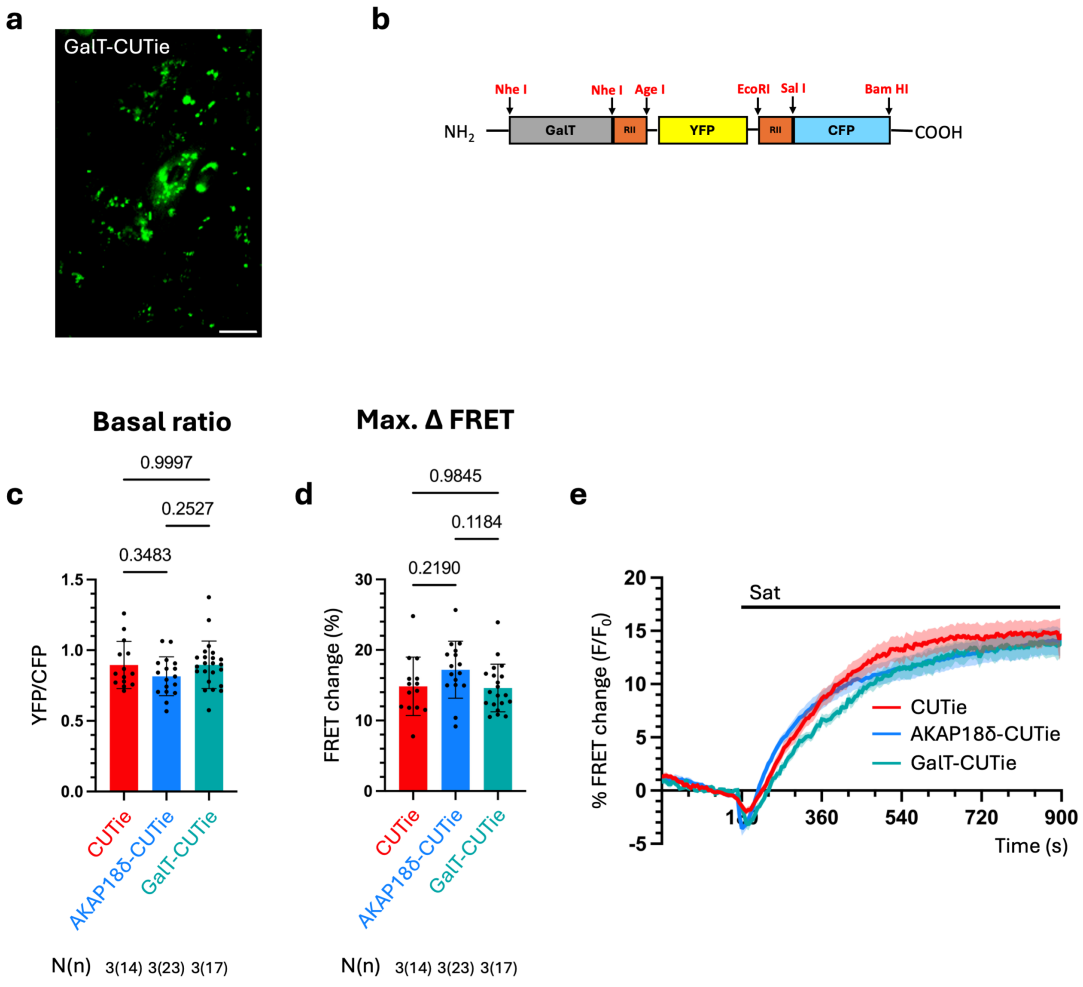


Fig S1 Generation and characterisation of GalT-CUTie. (a) Representative image of neonatal rat ventricular myocytes (NRVMs) expressing GalT-CUTie, a Golgi-targeted FRET-based cAMP reporter. **(b)** GalT-CUTie was generated using beta 1,4 Galactosyltransferase (GalT), a commonly used trans-Golgi marker, as a targeting domain. GalT was subcloned from pCMV-GalT-mCherry, a gift from Shinya Tsukiji (Addgene plasmid #214271) and inserted between the two NheI restriction sites in AKAP18δ-CUTie. Basal FRET ratio **(c)** and maximum FRET change **(d)** in HEK293T cells individually

expressing CUTie, AKAP18δ-CUTie, or GalT-CUTie. Basal FRET ratio is the average ratio (YFP emission intensity/CFP emission intensity) from the first six frames before the addition of any drugs. Maximum FRET change was quantified as the mean percentage change from baseline measured over the final six frames following stimulation with a saturating stimulus (Sat; 25 μM forskolin + 100 μM IBMX). Error bars represent mean +/- SD. **(e)** Average kinetics of FRET changes in HEK293T cells individually expressing CUTie, AKAP18δ-CUTie, or GalT-CUTie in response to a saturating stimulus. FRET change is shown as % change from initial value (F0) with F0 calculated as the average of the first six frames. Line and shading represent mean +/- SD. Sample size given as N(n) where N = biological replicates (different passages); n = individual cells.

B
Appendix

Calculation of predicted βAR occupancy during subtype-selective blockade

To assess the potential contribution of non-target βAR activation during subtype-selective blockade, receptor occupancy was estimated using a competitive binding model.

For a receptor in equilibrium with an agonist – in this case isoproterenol (Iso), the fractional receptor occupancy by Iso:

$$f_{Iso} = \frac{[Iso]}{[Iso] + K_D}$$

In the presence of a competitive antagonist, the apparent dissociation constant of Iso is increased according to:

$$K_{D,app} = K_D \left(1 + \frac{[B]}{K_i}\right)$$

Where $[B]$ is the antagonist concentration and K_i is its inhibitory dissociation constant at the receptor. Thus, Iso occupancy in the presence of antagonist is:

$$f_{Iso,block} = \frac{[Iso]}{[ISO] + K_D \left(1 + \frac{[B]}{K_i}\right)}$$

For our experiments, $[Iso]$ = 1 nM, $[B]$ = 200 nM, and an Iso K_D of 2 μM was assumed for both β_1AR and β_2AR. Antagonist affinities were taken as 3 nM at the intended receptor subtype, 300 nM for ICI-118,551 (ICI) at β_1AR, and 800 nM for CGP-20712A at β_2AR, consistent with published values[305].

ICI-118,551 blockade of β_2AR

For the receptor of interest, β_2AR, assuming K_i = 3 nM:

$$K_{D,app} = 2000\left(1 + \frac{200}{3}\right) = 135333 \text{ nM}$$

Therefore:

$$f_{Iso,block} = \frac{1}{1+ 135333} = 7.38 \text{ x } 10^{-6}$$

or approximately 0.00074% occupancy.

In the absence of antagonist:

$$f_{Iso} = \frac{1}{1+ 2000} = 4.998 \text{ x } 10^{-4}$$

or approximately 0.05% occupancy.

Thus, 200 nM ICI is predicted to reduce Iso occupancy of β_2AR to approximately:

$$\frac{0.00074}{0.05} \text{ x } 100 \approx 1.5\%$$

of the unblocked value, corresponding to 98.5% blockade.

Residual β_1AR occupancy during ICI blockade

For the non-target receptor, β_1AR, assuming K_i = 300 nM

$$K_{D,app} = 2000\left(1 + \frac{200}{300}\right) = 3333.3 \text{ nM}$$

Therefore:

$$f_{Iso,block} = \frac{1}{1+ 3333.3} = 2.999 \text{ x } 10^{-4}$$

or approximately 0.03% occupancy.

Relative to the unblocked occupancy:

$$\frac{0.03}{0.05} \text{ x } 100 \approx 60\%$$

So approximately 60% of the unblocked Iso occupancy of β_1AR is predicted to remain in the presence of 200 nM ICI.

CGP-20712A blockade of β_1AR

The equivalent calculation for CP at β_1AR, assuming K_i = 3 nM, predicts approximately 98.5% blockade of Iso occupancy at β_1AR.

Residual β_1AR occupancy during ICI blockade

For the non-target receptor, β_2AR, assuming K_i = 800 nM, the equivalent calculation gives approximately 80% of unblocked Iso occupancy.

Summary

Condition	Receptor	Predicted Iso occupancy without blocker	Predicted occupancy with 200 nM blocker	Fraction of unblocked occupancy remaining
ICI-118,551	β_2AR (target)	0.05%	0.00074%	~1.5%
ICI-118.551	β_1AR (non-target)	0.05%	0.03%	~60%
CGP-20712A	β_1A (target)	0.05%	0.00074%	~1.5%
CGP-20712A	β_2A (non-target)	0.05%	0.04%	~80%

These calculations indicate that the 200 nM antagonist concentrations are predicted to produce near-complete blockade of the target receptor subtype while allowing some residual Iso occupancy of the non-target subtype. The concentrations were therefore selected to prioritise robust functional blockade of the receptor of interest.

C
Appendix

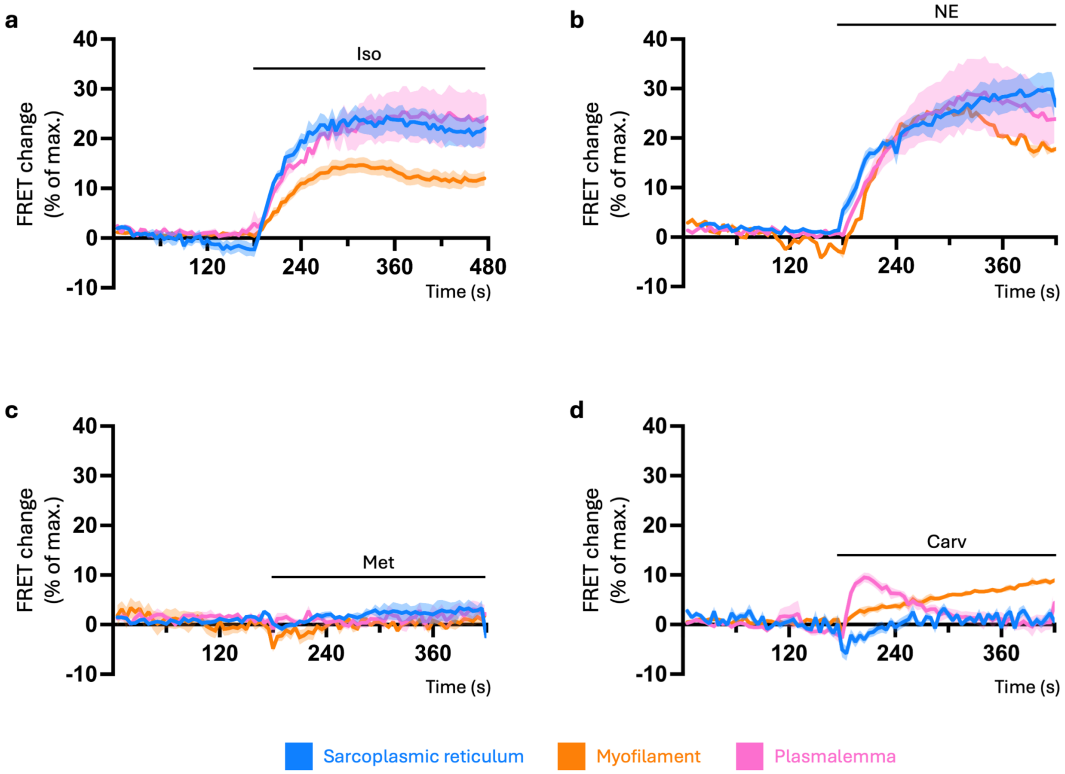


Fig S2 β-Adrenergic ligands drive distinct spatial patterns of cAMP signalling. Average kinetics of FRET changes in NRVMs individually expressing AKAP18δ-CUTie (blue), AKAP79-CUTie (pink), or TPNI-CUTie (orange) cAMP FRET reporters in response to bath application of either **(a)** 1 nM isoproterenol (Iso), **(b)** 1 μM norepinephrine (NE), **(C)** 10 μM metoprolol (Met), or **(d)** 10 μM carvedilol (carv). FRET change presented normalised to the maximum response elicited by a saturating stimulus (25 μM forskolin + 100 μM IBMX). Shading represents mean +/- SD.

D
Appendix

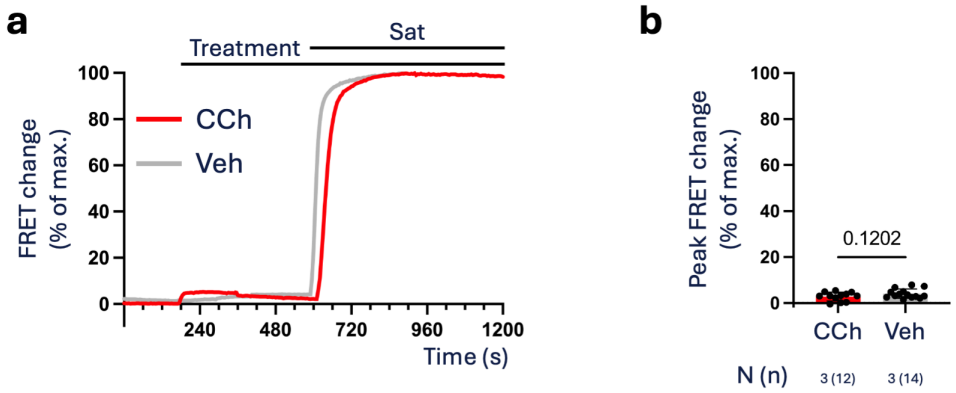


Fig S3 Carbachol does not detectably reduce basal cytosolic cAMP. Representative kinetics **(a)** and summary **(b)** of FRET changes in NRVMs expressing Epac-S^{h187} cAMP FRET reporter in response to bath application of either 100 µM carbachol (CCh) or an equivalent volume of vehicle (Ringer's buffer). **(b)** Data represents peak FRET change elicited by a stimulus normalised to the maximum response elicited by a saturating stimulus (Sat) (25 µM forskolin + 100 µM IBMX). Error bars represent mean +/- SD. Sample size given as N (n) where N = biological replicates (cell isolations); n = individual cells.

Bibliography

1. Consortium, I. H. G. S. *et al.* Initial sequencing and analysis of the human genome. *Nature* **409**, 860–921 (2001).

2. Venter, J. C., Smith, H. O. & Adams, M. D. The Sequence of the Human Genome. *Clin. Chem.* **61**, 1207–1208 (2015).

3. Fredriksson, R. & Schiöth, H. B. The Repertoire of G-Protein–Coupled Receptors in Fully Sequenced Genomes. *Mol. Pharmacol.* **67**, 1414–1425 (2005).

4. Pierce, K. L., Premont, R. T. & Lefkowitz, R. J. Seven-transmembrane receptors. *Nat. Rev. Mol. Cell Biol.* **3**, 639–650 (2002).

5. Heng, B. C., Aubel, D. & Fussenegger, M. An overview of the diverse roles of G-protein coupled receptors (GPCRs) in the pathophysiology of various human diseases. *Biotechnol. Adv.* **31**, 1676–1694 (2013).

6. Lorente, J. S. *et al.* GPCR drug discovery: new agents, targets and indications. *Nat. Rev. Drug Discov.* **24**, 458–479 (2025).

7. Spehr, M. & Munger, S. D. Olfactory receptors: G protein-coupled receptors and beyond. *J. Neurochem.* **109**, 1570–1583 (2009).

8. Yang, D. *et al.* G protein-coupled receptors: structure- and function-based drug discovery. *Signal Transduct. Target. Ther.* **6**, 7 (2021).

9. Liu, T., Naidoo, N. R., Agyemang, E. & Lamichhane, R. Insights into the structural dynamics of the secretin family (class B1) G protein-coupled receptors. *J. Biol. Chem.* **301**, 110466 (2025).

10. Seufert, F., Chung, Y. K., Hildebrand, P. W. & Langenhan, T. 7TM domain structures of adhesion GPCRs: what's new and what's missing? *Trends Biochem. Sci.* **48**, 726–739 (2023).

11. Niswender, C. M. & Conn, P. J. Metabotropic Glutamate Receptors: Physiology, Pharmacology, and Disease. *Annu. Rev. Pharmacol. Toxicol.* **50**, 295–322 (2010).

12. Pin, J. *et al.* Allosteric functioning of dimeric class C G-protein-coupled receptors. *FEBS J.* **272**, 2947–2955 (2005).

13. Schulte, G. & Ohlstein, E. International Union of Basic and Clinical Pharmacology CXV: The Class F of G Protein-Coupled Receptors. *Pharmacol. Rev.* **76**, 1009–1037 (2024).

14. Gilman, A. G. G Proteins: Transducers of Receptor-Generated Signals. *Annu. Rev. Biochem.* **56**, 615–649 (1987).

15. Thomas, R. *et al.* Ligand-specific activation trajectories dictate GPCR signalling in cells. *Nature* **650**, 1053–1062 (2026).

16. Calebiro, D., Koszegi, Z., Lanoiselée, Y., Miljus, T. & O'Brien, S. G protein-coupled receptor-G protein interactions: a single-molecule perspective. *Physiol. Rev.* **101**, 857–906 (2021).

17. Oldham, W. M. & Hamm, H. E. Heterotrimeric G protein activation by G-protein-coupled receptors. *Nat. Rev. Mol. Cell Biol.* **9**, 60–71 (2008).

18. Bos, J. L., Rehmann, H. & Wittinghofer, A. GEFs and GAPs: Critical Elements in the Control of Small G Proteins. *Cell* **129**, 865–877 (2007).

19. Levitzki, A. From Epinephrine to Cyclic AMP. *Science* **241**, 800–806 (1988).

20. Jones, D. T. & Reed, R. R. Golf: an Olfactory Neuron Specific-G Protein Involved in Odorant Signal Transduction. *Science* **244**, 790–795 (1989).

21. Sadana, R. & Dessauer, C. W. Physiological Roles for G Protein-Regulated Adenylyl Cyclase Isoforms: Insights from Knockout and Overexpression Studies. *Neurosignals* **17**, 5–22 (2009).

22. Leiss, V., Reisinger, E., Speidel, A., Beer-Hammer, S. & Nürnberg, B. Analyses of Gnai3-iresGFP reporter mice reveal unknown Gαi3 expression sites. *Sci. Rep.* **11**, 14271 (2021).

23. Iguchi, T. & Kasahara, K. Encyclopedia of Signaling Molecules. 1–9 (2017) doi:10.1007/978-1-4614-6438-9_101497-1.

24. FIELDS, T. A. & CASEY, P. J. Signalling functions and biochemical properties of pertussis toxin-resistant G-proteins. *Biochem. J.* **321**, 561–571 (1997).

25. Kimple, M. E. *et al.* A Role for Gz in Pancreatic Islet β-Cell Biology*. *J. Biol. Chem.* **280**, 31708–31713 (2005).

26. Deng, W.-T. *et al.* Functional interchangeability of rod and cone transducin α-subunits. *Proc. Natl. Acad. Sci.* **106**, 17681–17686 (2009).

27. Martemyanov, K. A. G protein signaling in the retina and beyond: the Cogan lecture. *Investig. Ophthalmol. Vis. Sci.* **55**, 8201–7 (2014).

28. McLaughlin, S. K., McKinnon, P. J. & Margolskee, R. F. Gustducin is a taste-cell-specific G protein closely related to the transducins. *Nature* **357**, 563–569 (1992).

29. Spielman, A. I. Gustducin and its Role in Taste. *J. Dent. Res.* **77**, 539–544 (1998).

30. Ozeck, M., Brust, P., Xu, H. & Servant, G. Receptors for bitter, sweet and umami taste couple to inhibitory G protein signaling pathways. *Eur. J. Pharmacol.* **489**, 139–149 (2004).

31. McLaughlin, S. K., McKinnon, P. J., Spickofsky, N., Danho, W. & Margolskee, R. F. Molecular cloning of G proteins and phosphodiesterases from rat taste cells. *Physiol. Behav.* **56**, 1157–1164 (1994).

32. Manning, D. R. & Gilman, A. G. The regulatory components of adenylate cyclase and transducin. A family of structurally homologous guanine nucleotide-binding proteins. *J. Biol. Chem.* **258**, 7059–7063 (1983).

33. Ho, M. K. & Wong, Y. H. Gz signaling: emerging divergence from Gi signaling. *Oncogene* **20**, 1615–1625 (2001).

34. Carty, D. J. *et al.* Distinct guanine nucleotide binding and release properties of the three Gi proteins. *J. Biol. Chem.* **265**, 6268–6273 (1990).

35. Chandan, N. R., Abraham, S., SenGupta, S., Parent, C. A. & Smrcka, A. V. A network of Gαi signaling partners is revealed by proximity labeling proteomics analysis and includes PDZ-RhoGEF. *Sci. Signal.* **15**, eabi9869 (2022).

36. Zhang, L., Zhang, L., Gao, S., Shi, X. & Zuo, L. Gαi3: a crucial biomarker and therapeutic target in bladder cancer. *NPJ Precis. Oncol.* **9**, 181 (2025).

37. Kadamur, G. & Ross, E. M. Mammalian Phospholipase C. *Annu. Rev. Physiol.* **75**, 127–154 (2013).

38. Katti, S. & Igumenova, T. I. Structural insights into C1-ligand interactions: Filling the gaps by in silico methods. *Adv. Biol. Regul.* **79**, 100784 (2021).

39. Zhou, H., Huo, Y., Yang, N. & Wei, T. Phosphatidic acid: from biophysical properties to diverse functions. *FEBS J.* **291**, 1870–1885 (2024).

40. Berridge, M. J. The Inositol Trisphosphate/Calcium Signaling Pathway in Health and Disease. *Physiol Rev* **96**, 1261–1296 (2016).

41. Hubbard, K. B. & Hepler, J. R. Cell signalling diversity of the Gqα family of heterotrimeric G proteins. *Cell. Signal.* **18**, 135–150 (2006).

42. Wilkie, T. M., Scherle, P. A., Strathmann, M. P., Slepak, V. Z. & Simon, M. I. Characterization of G-protein alpha subunits in the Gq class: expression in murine tissues and in stromal and hematopoietic cell lines. *Proc. Natl. Acad. Sci.* **88**, 10049–10053 (1991).

43. Nakamura, F. *et al.* Identification of two novel GTP-binding protein alpha-subunits that lack apparent ADP-ribosylation sites for pertussis toxin. *J. Biol. Chem.* **266**, 12676–12681 (1991).

44. Zigman, J. M., Westermark, G. T., LaMendola, J. & Steiner, D. F. Expression of cone transducin, Gz alpha, and other G-protein alpha-subunit messenger ribonucleic acids in pancreatic islets. *Endocrinology* **135**, 31–37 (1994).

45. Strathmann, M. P. & Simon, M. I. G alpha 12 and G alpha 13 subunits define a fourth class of G protein alpha subunits. *Proc. Natl. Acad. Sci.* **88**, 5582–5586 (1991).

46. Riobo, N. A. & Manning, D. R. Receptors coupled to heterotrimeric G proteins of the G12 family. *Trends Pharmacol. Sci.* **26**, 146–154 (2005).

47. Suzuki, N., Hajicek, N. & Kozasa, T. Regulation and Physiological Functions of G12/13-Mediated Signaling Pathways. *Neurosignals* **17**, 55–70 (2009).

48. Eckenstaler, R., Hauke, M. & Benndorf, R. A. A current overview of RhoA, RhoB, and RhoC functions in vascular biology and pathology. *Biochem. Pharmacol.* **206**, 115321 (2022).

49. Satagopam, V. P. *et al.* GPCRs, G-proteins, effectors and their interactions: human-gpDB, a database employing visualization tools and data integration techniques. *Database: J. Biol. Databases Curation* **2010**, baq019 (2010).

50. Masuho, I. *et al.* Rules and mechanisms governing G protein coupling selectivity of GPCRs. *Cell Rep.* **42**, 113173–113173 (2023).

51. Hauser, A. S. *et al.* Common coupling map advances GPCR-G protein selectivity. *eLife* **11**, e74107 (2022).

52. Wall, M. A. *et al.* The structure of the G protein heterotrimer Gi alpha 1 beta 1 gamma 2. *Cell* **83**, 1047–58 (1995).

53. Lambright, D. G. *et al.* The 2.0 Å crystal structure of a heterotrimeric G protein. *Nature* **379**, 311–319 (1996).

54. Logothetis, D. E., Kurachi, Y., Galper, J., Neer, E. J. & Clapham, D. E. The beta gamma subunits of GTP-binding proteins activate the muscarinic K+ channel in heart. *Nature* **325**, 321–6 (1987).

55. Krapivinsky, G., Krapivinsky, L., Wickman, K. & Clapham, D. E. Gβγ Binds Directly to the G Protein-gated K+ Channel, IKACh (*). *J. Biol. Chem.* **270**, 29059–29062 (1995).

56. Yamada, M. The Role of Muscarinic K+ Channels in the Negative Chronotropic Effect of a Muscarinic Agonist. *J. Pharmacol. Exp. Ther.* **300**, 681–687 (2002).

57. Taussig, R., Tang, W. J., Hepler, J. R. & Gilman, A. G. Distinct patterns of bidirectional regulation of mammalian adenylyl cyclases. *J. Biol. Chem.* **269**, 6093–6100 (1994).

58. Tang, W.-J. & Gilman, A. G. Type-Specific Regulation of Adenylyl Cyclase by G Protein βγ Subunits. *Science* **254**, 1500–1503 (1991).

59. Sunahara, R. K. & Taussig, R. Isoforms of Mammalian Adenylyl Cyclase: Multiplicities of Signaling. *Mol. Interv.* **2**, 168–184 (2002).

60. Diel, S., Klass, K., Wittig, B. & Kleuss, C. Gβγ Activation Site in Adenylyl Cyclase Type II ADENYLYL CYCLASE TYPE III IS INHIBITED BY Gβγ*. *J. Biol. Chem.* **281**, 288–294 (2006).

61. Camps, M. *et al.* Isozyme-selective stimulation of phospholipase C-β2 by G protein βγ-subunits. *Nature* **360**, 684–686 (1992).

62. Boyer, J. L., Waldo, G. L. & Harden, T. K. Beta gamma-subunit activation of G-protein-regulated phospholipase C. *J. Biol. Chem.* **267**, 25451–25456 (1992).

63. Smrcka, A. V. & Sternweis, P. C. Regulation of purified subtypes of phosphatidylinositol-specific phospholipase C beta by G protein alpha and beta gamma subunits. *J. Biol. Chem.* **268**, 9667–9674 (1993).

64. Stephens, L. *et al.* A novel phosphoinositide 3 kinase activity in myeloid-derived cells is activated by G protein βγ subunits. *Cell* **77**, 83–93 (1994).

65. Pitcher, J. A. *et al.* Role of βγ Subunits of G Proteins in Targeting the β-Adrenergic Receptor Kinase to Membrane-Bound Receptors. *Science* **257**, 1264–1267 (1992).

66. Ikeda, S. R. Voltage-dependent modulation of N-type calcium channels by G-protein beta gamma subunits. *Nature* **380**, 255–8 (1996).

67. Herlitze, S. *et al.* Modulation of Ca2+ channels βγ G-protein py subunits. *Nature* **380**, 258–262 (1996).

68. Smrcka, A. V. G protein βγ subunits: Central mediators of G protein-coupled receptor signaling. *Cell. Mol. Life Sci.* **65**, 2191–2214 (2008).

69. Jin, T. *et al.* The βγ Subunits of G Proteins Gate a K+ Channel by Pivoted Bending of a Transmembrane Segment. *Mol. Cell* **10**, 469–481 (2002).

70. Hurowitz, E. H. *et al.* Genomic Characterization of the Human Heterotrimeric G Protein , , and Subunit Genes. *DNA Res.* **7**, 111–120 (2000).

71. Tennakoon, M. *et al.* Subtype-dependent regulation of Gβγ signalling. *Cell. Signal.* **82**, 109947 (2021).

72. Masuho, I., Skamangas, N. K., Muntean, B. S. & Martemyanov, K. A. Diversity of the Gβγ complexes defines spatial and temporal bias of GPCR signaling. *Cell Syst.* **12**, 324-337.e5 (2021).

73. Khan, S. M. *et al.* The Expanding Roles of Gβγ Subunits in G Protein–Coupled Receptor Signaling and Drug Action. *Pharmacol. Rev.* **65**, 545–577 (2013).

74. Bünemann, M., Frank, M. & Lohse, M. J. Gi protein activation in intact cells involves subunit rearrangement rather than dissociation. *Proc. Natl. Acad. Sci.* **100**, 16077–16082 (2003).

75. Frank, M., Thümer, L., Lohse, M. J. & Bünemann, M. G Protein Activation without Subunit Dissociation Depends on a Gαi-specific Region*. *J. Biol. Chem.* **280**, 24584–24590 (2005).

76. Galés, C. *et al.* Probing the activation-promoted structural rearrangements in preassembled receptor–G protein complexes. *Nat. Struct. Mol. Biol.* **13**, 778–786 (2006).

77. Digby, G. J., Sethi, P. R. & Lambert, N. A. Differential dissociation of G protein heterotrimers. *J. Physiol.* **586**, 3325–3335 (2008).

78. Touhara, K. K. & MacKinnon, R. Molecular basis of signaling specificity between GIRK channels and GPCRs. *eLife* **7**, e42908 (2018).

79. Wellner-Kienitz, M.-C., Bender, K. & Pott, L. Overexpression of β1 and β2Adrenergic Receptors in Rat Atrial Myocytes DIFFERENTIAL COUPLING TO G PROTEIN-GATED INWARD RECTIFIER K+ CHANNELS VIA Gs AND Gi/o *. *J. Biol. Chem.* **276**, 37347–37354 (2001).

80. Brands, J. *et al.* A molecular mechanism to diversify Ca2+ signaling downstream of Gs protein-coupled receptors. *Nat. Commun.* **15**, 7684 (2024).

81. Gurevich, V. V. & Gurevich, E. V. GPCR Signaling Regulation: The Role of GRKs and Arrestins. *Front Pharmacol* **10**, 125 (2019).

82. Stadel, J. M. *et al.* Catecholamine-induced desensitization of turkey erythrocyte adenylate cyclase. Structural alterations in the beta-adrenergic receptor revealed by photoaffinity labeling. *J. Biol. Chem.* **257**, 9242–9245 (1982).

83. Stadel, J. M. *et al.* Catecholamine-induced desensitization of turkey erythrocyte adenylate cyclase is associated with phosphorylation of the beta-adrenergic receptor. *Proc. Natl. Acad. Sci.* **80**, 3173–3177 (1983).

84. Strasser, R. H., Sibley, D. R. & Lefkowitz, R. J. A novel catecholamine-activated adenosine cyclic 3',5'-phosphate independent pathway for beta-adrenergic receptor phosphorylation in wild-type and mutant S49 lymphoma cells: mechanism of homologous desensitization of adenylate cyclase. *Biochemistry* **25**, 1371–7 (1986).

85. Benovic, J. L., Strasser, R. H., Caron, M. G. & Lefkowitz, R. J. Beta-adrenergic receptor kinase: identification of a novel protein kinase that phosphorylates the agonist-occupied form of the receptor. *Proc. Natl. Acad. Sci.* **83**, 2797–2801 (1986).

86. Benovic, J. L. *et al.* Functional desensitization of the isolated beta-adrenergic receptor by the beta-adrenergic receptor kinase: potential role of an analog of the retinal protein arrestin (48-kDa protein). *Proc. Natl. Acad. Sci.* **84**, 8879–8882 (1987).

87. Pfister, C. *et al.* Retinal S Antigen Identified as the 48K Protein Regulating Light-Dependent Phosphodiesterase in Rods. *Science* **228**, 891–893 (1985).

88. Lorenz, W. *et al.* The receptor kinase family: primary structure of rhodopsin kinase reveals similarities to the beta-adrenergic receptor kinase. *Proc. Natl. Acad. Sci.* **88**, 8715–8719 (1991).

89. Weiss, E. R. *et al.* The cloning of GRK7, a candidate cone opsin kinase, from cone- and rod-dominant mammalian retinas. *Mol. Vis.* **4**, 27 (1998).

90. Benovic, J. L., DeBlasi, A., Stone, W. C., Caron, M. G. & Lefkowitz, R. J. β-Adrenergic Receptor Kinase: Primary Structure Delineates a Multigene Family. *Science* **246**, 235–240 (1989).

91. Boekhoff, I. *et al.* Olfactory desensitization requires membrane targeting of receptor kinase mediated by beta gamma-subunits of heterotrimeric G proteins. *J. Biol. Chem.* **269**, 37–40 (1994).

92. Premont, R. T. *et al.* Characterization of the G Protein-coupled Receptor Kinase GRK4 IDENTIFICATION OF FOUR SPLICE VARIANTS (∗). *J. Biol. Chem.* **271**, 6403–6410 (1996).

93. Kunapuli, P. & Benovic, J. L. Cloning and expression of GRK5: a member of the G protein-coupled receptor kinase family. *Proc. Natl. Acad. Sci.* **90**, 5588–5592 (1993).

94. Benovic, J. L. & Gomez, J. Molecular cloning and expression of GRK6. A new member of the G protein-coupled receptor kinase family. *J. Biol. Chem.* **268**, 19521–19527 (1993).

95. Koch, W. J., Inglese, J., Stone, W. C. & Lefkowitz, R. J. The binding site for the beta gamma subunits of heterotrimeric G proteins on the beta-adrenergic receptor kinase. *J. Biol. Chem.* **268**, 8256–8260 (1993).

96. Touhara, K., Inglese, J., Pitcher, J. A., Shaw, G. & Lefkowitz, R. J. Binding of G protein beta gamma-subunits to pleckstrin homology domains. *J. Biol. Chem.* **269**, 10217–10220 (1994).

97. Gurevich, E. V., Tesmer, J. J. G., Mushegian, A. & Gurevich, V. V. G protein-coupled receptor kinases: More than just kinases and not only for GPCRs. *Pharmacol. Ther.* **133**, 40–69 (2012).

98. Shinohara, T. *et al.* Primary and secondary structure of bovine retinal S antigen (48-kDa protein). *Proc. Natl. Acad. Sci.* **84**, 6975–6979 (1987).

99. Craft, C. M. & Whitmore, D. H. The arrestin superfamily: cone arrestins are a fourth family. *FEBS Lett.* **362**, 247–255 (1995).

100. Parruti, G. *et al.* Molecular analysis of human beta-arrestin-1: cloning, tissue distribution, and regulation of expression. Identification of two isoforms generated by alternative splicing. *J. Biol. Chem.* **268**, 9753–9761 (1993).

101. Attramadal, H. *et al.* Beta-arrestin2, a novel member of the arrestin/beta-arrestin gene family. *J. Biol. Chem.* **267**, 17882–17890 (1992).

102. Gurevich, V. V. *et al.* Arrestin interactions with G protein-coupled receptors. Direct binding studies of wild type and mutant arrestins with rhodopsin, beta 2-adrenergic, and m2 muscarinic cholinergic receptors. *J. Biol. Chem.* **270**, 720–31 (1995).

103. Lohse, M. J. *et al.* Receptor-specific desensitization with purified proteins. Kinase dependence and receptor specificity of beta-arrestin and arrestin in the beta 2-adrenergic receptor and rhodopsin systems. *J. Biol. Chem.* **267**, 8558–8564 (1992).

104. Krupnick, J. G. & Benovic, J. L. THE ROLE OF RECEPTOR KINASES AND ARRESTINS IN G PROTEIN–COUPLED RECEPTOR REGULATION. *Annu. Rev. Pharmacol. Toxicol.* **38**, 289–319 (1998).

105. Rasmussen, S. G. F. *et al.* Crystal structure of the β2 adrenergic receptor–Gs protein complex. *Nature* **477**, 549–555 (2011).

106. Kang, Y. *et al.* Crystal structure of rhodopsin bound to arrestin by femtosecond X-ray laser. *Nature* **523**, 561–567 (2015).

107. Carpenter, B., Nehmé, R., Warne, T., Leslie, A. G. W. & Tate, C. G. Structure of the adenosine A(2A) receptor bound to an engineered G protein. *Nature* **536**, 104–7 (2016).

108. Liang, Y.-L. *et al.* Phase-plate cryo-EM structure of a class B GPCR-G protein complex. *Nature* **546**, 118–123 (2017).

109. Zhang, Y. *et al.* Cryo-EM structure of the activated GLP-1 receptor in complex with a G protein. *Nature* **546**, 248–253 (2017).

110. Zhou, X. E. *et al.* Identification of Phosphorylation Codes for Arrestin Recruitment by G Protein-Coupled Receptors. *Cell* **170**, 457-469.e13 (2017).

111. Goodman, O. B. *et al.* β-Arrestin acts as a clathrin adaptor in endocytosis of the β2-adrenergic receptor. *Nature* **383**, 447–450 (1996).

112. Laporte, S. A. *et al.* The β2-adrenergic receptor/βarrestin complex recruits the clathrin adaptor AP-2 during endocytosis. *Proc. Natl. Acad. Sci.* **96**, 3712–3717 (1999).

113. Pierce, K. L. & Lefkowitz, R. J. Classical and new roles of β-arrestins in the regulation of G-PROTEIN-COUPLED receptors. *Nat. Rev. Neurosci.* **2**, 727–733 (2001).

114. Luttrell, L. M. *et al.* Beta-arrestin-dependent formation of beta2 adrenergic receptor-Src protein kinase complexes. *Sci. (N. York, NY)* **283**, 655–61 (1999).

115. DeFea, K. A. *et al.* β-Arrestin–Dependent Endocytosis of Proteinase-Activated Receptor 2 Is Required for Intracellular Targeting of Activated Erk1/2. *J. Cell Biol.* **148**, 1267–1282 (2000).

116. Xiao, K. *et al.* Functional specialization of β-arrestin interactions revealed by proteomic analysis. *Proc. Natl. Acad. Sci.* **104**, 12011–12016 (2007).

117. Grundmann, M. *et al.* Lack of beta-arrestin signaling in the absence of active G proteins. *Nat. Commun.* **9**, 341 (2018).

118. Cahill, T. J. *et al.* Distinct conformations of GPCR–β-arrestin complexes mediate desensitization, signaling, and endocytosis. *Proc. Natl. Acad. Sci.* **114**, 2562–2567 (2017).

119. Thomsen, A. R. B. *et al.* GPCR-G Protein-β-Arrestin Super-Complex Mediates Sustained G Protein Signaling. *Cell* **166**, 907–919 (2016).

120. He, G. *et al.* A GPCR-G protein-β-arrestin megacomplex enabled by a versatile allosteric modulator. *Cell* **189**, 1434-1450.e22 (2026).

121. Nobles, K. N. *et al.* Distinct Phosphorylation Sites on the β2-Adrenergic Receptor Establish a Barcode That Encodes Differential Functions of β-Arrestin. *Sci. Signal.* **4**, ra51 (2011).

122. Jewell-Motz, E. A., Small, K. M., Theiss, C. T. & Liggett, S. B. α2A/α2C-Adrenergic Receptor Third Loop Chimera Show That Agonist Interaction with Receptor Subtype Backbone Establishes G Protein-coupled Receptor Kinase Phosphorylation*. *J. Biol. Chem.* **275**, 28989–28993 (2000).

123. Butcher, A. J. *et al.* Differential G-protein-coupled Receptor Phosphorylation Provides Evidence for a Signaling Bar Code*. *J. Biol. Chem.* **286**, 11506–11518 (2011).

124. Liggett, S. B. Phosphorylation Barcoding as a Mechanism of Directing GPCR Signaling. *Sci. Signal.* **4**, pe36 (2011).

125. Azzi, M. *et al.* β-Arrestin-mediated activation of MAPK by inverse agonists reveals distinct active conformations for G protein-coupled receptors. *Proc. Natl. Acad. Sci.* **100**, 11406–11411 (2003).

126. Wei, H. *et al.* Independent β-arrestin 2 and G protein-mediated pathways for angiotensin II activation of extracellular signal-regulated kinases 1 and 2. *Proc. Natl. Acad. Sci.* **100**, 10782–10787 (2003).

127. Wingler, L. M. & Lefkowitz, R. J. Conformational Basis of G Protein-Coupled Receptor Signaling Versatility. *Trends Cell Biol.* **30**, 736–747 (2020).

128. Seyedabadi, M., Gharghabi, M., Gurevich, E. V. & Gurevich, V. V. Structural basis of GPCR coupling to distinct signal transducers: implications for biased signaling. *Trends Biochem. Sci.* **47**, 570–581 (2022).

129. Ma, Y., Patterson, B. & Zhu, L. Biased signaling in GPCRs: Structural insights and implications for drug development. *Pharmacol. Ther.* **266**, 108786 (2025).

130. Whistler, J. L., Chuang, H., Chu, P., Jan, L. Y. & Zastrow, M. von. Functional Dissociation of μ Opioid Receptor Signaling and Endocytosis Implications for the Biology of Opiate Tolerance and Addiction. *Neuron* **23**, 737–746 (1999).

131. Zhang, J. *et al.* Role for G protein-coupled receptor kinase in agonist-specific regulation of μ-opioid receptor responsiveness. *Proc. Natl. Acad. Sci.* **95**, 7157–7162 (1998).

132. Bohn, L. M., Gainetdinov, R. R., Lin, F.-T., Lefkowitz, R. J. & Caron, M. G. μ-Opioid receptor desensitization by β-arrestin-2 determines morphine tolerance but not dependence. *Nature* **408**, 720–723 (2000).

133. Bohn, L. M. *et al.* Enhanced Morphine Analgesia in Mice Lacking β-Arrestin 2. *Science* **286**, 2495–2498 (1999).

134. Soergel, D. G. *et al.* Biased agonism of the μ-opioid receptor by TRV130 increases analgesia and reduces on-target adverse effects versus morphine: A randomized, double-blind, placebo-controlled, crossover study in healthy volunteers. *PAIN*® **155**, 1829–1835 (2014).

135. Viscusi, E. R. *et al.* A randomized, phase 2 study investigating TRV130, a biased ligand of the μ-opioid receptor, for the intravenous treatment of acute pain. *Pain* **157**, 264–272 (2015).

136. Sorkin, A. & Zastrow, M. von. Endocytosis and signalling: intertwining molecular networks. *Nat. Rev. Mol. Cell Biol.* **10**, 609–622 (2009).

137. Calebiro, D. *et al.* Persistent cAMP-Signals Triggered by Internalized G-Protein–Coupled Receptors. *PLoS Biol.* **7**, e1000172 (2009).

138. Ferrandon, S. *et al.* Sustained cyclic AMP production by parathyroid hormone receptor endocytosis. *Nat. Chem. Biol.* **5**, 734–742 (2009).

139. Calebiro, D., Miljus, T. & O'Brien, S. Endomembrane GPCR signaling: 15 years on, the quest continues. *Trends Biochem. Sci.* **50**, 46–60 (2025).

140. Irannejad, R. *et al.* Conformational biosensors reveal GPCR signalling from endosomes. *Nature* **495**, 534–538 (2013).

141. Irannejad, R. *et al.* Functional selectivity of GPCR-directed drug action through location bias. *Nat. Chem. Biol.* **13**, 799–806 (2017).

142. Wright, S. C. *et al.* BRET-based effector membrane translocation assay monitors GPCR-promoted and endocytosis-mediated G q activation at early endosomes. *Proc. Natl. Acad. Sci.* **118**, (2021).

143. Nash, C. A., Wei, W., Irannejad, R. & Smrcka, A. V. Golgi localized β1-adrenergic receptors stimulate Golgi PI4P hydrolysis by PLCε to regulate cardiac hypertrophy. *eLife* **8**, e48167 (2019).

144. Liccardo, F. *et al.* Subcellular activation of β-adrenergic receptors using a spatially restricted antagonist. *Proc. Natl. Acad. Sci.* **121**, e2404243121 (2024).

145. Lin, T.-Y. *et al.* Cardiac contraction and relaxation are regulated by distinct subcellular cAMP pools. *Nat. Chem. Biol.* **20**, 62–73 (2024).

146. Abadir, P. M., Walston, J. D. & Carey, R. M. Subcellular characteristics of functional intracellular renin–angiotensin systems. *Peptides* **38**, 437–445 (2012).

147. Wang, Q. *et al.* 5-HTR3 and 5-HTR4 located on the mitochondrial membrane and functionally regulated mitochondrial functions. *Sci. Rep.* **6**, 37336 (2016).

148. Boivin, B. *et al.* Functional β-adrenergic receptor signalling on nuclear membranes in adult rat and mouse ventricular cardiomyocytes. *Cardiovasc. Res.* **71**, 69–78 (2006).

149. Kumar, V., Jong, Y.-J. I. & O'Malley, K. L. Activated Nuclear Metabotropic Glutamate Receptor mGlu5 Couples to Nuclear Gq/11 Proteins to Generate Inositol 1,4,5-Trisphosphate-mediated Nuclear Ca2+ Release*. *J. Biol. Chem.* **283**, 14072–14083 (2008).

150. Jong, Y.-J. I., Kumar, V. & O'Malley, K. L. Intracellular Metabotropic Glutamate Receptor 5 (mGluR5) Activates Signaling Cascades Distinct from Cell Surface Counterparts*. *J. Biol. Chem.* **284**, 35827–35838 (2009).

151. Wang, Y. *et al.* Intracellular β1-Adrenergic Receptors and Organic Cation Transporter 3 Mediate Phospholamban Phosphorylation to Enhance Cardiac Contractility. *Circ. Res.* **128**, 246–261 (2021).

152. Schiaffino, M. V. & Tacchetti, C. The ocular albinism type 1 (OA1) protein and the evidence for an intracellular signal transduction system involved in melanosome biogenesis. *Pigment Cell Res.* **18**, 227–233 (2005).

153. Rozenfeld, R. & Devi, L. A. Regulation of CB1 cannabinoid receptor trafficking by the adaptor protein AP-3. *FASEB J.* **22**, 2311–2322 (2008).

154. O'Brien, S. L. *et al.* Intracrine FFA4 signaling controls lipolysis at lipid droplets. *Nat. Chem. Biol.* **22**, 109–119 (2026).

155. Eiger, D. S., Hicks, C., Gardner, J., Pham, U. & Rajagopal, S. Location bias: A "Hidden Variable" in GPCR pharmacology. *BioEssays* **45**, e2300123 (2023).

156. Lohse, M. J., Bock, A. & Zaccolo, M. G Protein–Coupled Receptor Signaling: New Insights Define Cellular Nanodomains. *Annu. Rev. Pharmacol. Toxicol.* **64**, 387–415 (2023).

157. Klauer, M. J., Willette, B. K. A. & Tsvetanova, N. G. Functional diversification of cell signaling by GPCR localization. *J. Biol. Chem.* **300**, 105668 (2024).

158. Sutherland, E. W. Studies on the Mechanism of Hormone Action. *Science* **177**, 401–408 (1972).

159. BERTHET, J., RALL, T. W. & SUTHERLAND, E. W. The relationship of epinephrine and glucagon to liver phosphorylase. IV. Effect of epinephrine and glucagon on the reactivation of phosphorylase in liver homogenates. *J. Biol. Chem.* **224**, 463–75 (1957).

160. Sutherland, E. W. & Rall, T. W. THE PROPERTIES OF AN ADENINE RIBONUCLEOTIDE PRODUCED WITH CELLULAR PARTICLES, ATP, Mg ++ , AND EPINEPHRINE OR GLUCAGON. *J. Am. Chem. Soc.* **79**, 3608–3608 (1957).

161. Taussig, R., Iñiguez-Lluhi, J. A. & Gilman, A. G. Inhibition of adenylyl cyclase by Gi alpha. *Sci. (N. York, NY)* **261**, 218–21 (1993).

162. Sprang, S. R., Chen, Z. & Du, X. Structural basis of effector regulation and signal termination in heterotrimeric Galpha proteins. *Adv. protein Chem.* **74**, 1–65 (2007).

163. Kleinboelting, S. *et al.* Crystal structures of human soluble adenylyl cyclase reveal mechanisms of catalysis and of its activation through bicarbonate. *Proc. Natl. Acad. Sci.* **111**, 3727–3732 (2014).

164. Raaijmakers, J. H. & Bos, J. L. Specificity in Ras and Rap Signaling*. *J. Biol. Chem.* **284**, 10995–10999 (2009).

165. Rooij, J. de *et al.* Mechanism of Regulation of the Epac Family of cAMP-dependent RapGEFs*. *J. Biol. Chem.* **275**, 20829–20836 (2000).

166. Fesenko, E. E., Kolesnikov, S. S. & Lyubarsky, A. L. Induction by cyclic GMP of cationic conductance in plasma membrane of retinal rod outer segment. *Nature* **313**, 310–313 (1985).

167. DiFrancesco, D. & Tortora, P. Direct activation of cardiac pacemaker channels by intracellular cyclic AMP. *Nature* **351**, 145–147 (1991).

168. DiFrancesco, D. The Role of the Funny Current in Pacemaker Activity. *Circ Res* **106**, 434–446 (2010).

169. Brand, T. The Popeye domain-containing gene family. *Cell Biochem. Biophys.* **43**, 95–103 (2005).

170. Brand, T. & Schindler, R. New kids on the block: The Popeye domain containing (POPDC) protein family acting as a novel class of cAMP effector proteins in striated muscle. *Cell. Signal.* **40**, 156–165 (2017).

171. Taylor, S. S., Buechler, J. A. & Yonemoto, W. Camp-Dependent Protein Kinase: Framework for a Diverse Family of Regulatory Enzymes. *Annu. Rev. Biochem.* **59**, 971–1005 (1990).

172. Skålhegg, B. S. & Taskén, K. Specificity in the cAMP PKA signaling pathway differential expression regulation and subcellular localization of subunits oF PKA. *Front. Biosci.* **2**, d331-342 (1997).

173. TASKÉN, K. & AANDAHL, E. M. Localized Effects of cAMP Mediated by Distinct Routes of Protein Kinase A. *Physiol. Rev.* **84**, 137–167 (2004).

174. Kelly, M. P. *et al.* Cyclic nucleotide phosphodiesterases as drug targets. *Pharmacol. Rev.* **77**, 100042 (2025).

175. Conti, M. & Beavo, J. Biochemistry and Physiology of Cyclic Nucleotide Phosphodiesterases: Essential Components in Cyclic Nucleotide Signaling. *Annu. Rev. Biochem.* **76**, 481–511 (2007).

176. Heijman, J., Dewenter, M., El-Armouche, A. & Dobrev, D. Function and regulation of serine/threonine phosphatases in the healthy and diseased heart. *J. Mol. Cell. Cardiol.* **64**, 90–98 (2013).

177. Virshup, D. M. & Shenolikar, S. From Promiscuity to Precision: Protein Phosphatases Get a Makeover. *Mol. Cell* **33**, 537–545 (2009).

178. Avet, C. *et al.* Effector membrane translocation biosensors reveal G protein and βarrestin coupling profiles of 100 therapeutically relevant GPCRs. *eLife* **11**, e74101 (2022).

179. BRUNTON, L. L., HAYES, J. S. & MAYER, S. E. Hormonally specific phosphorylation of cardiac troponin I and activation of glycogen phosphorylase. *Nature* **280**, 78–80 (1979).

180. Hayes, J. S., Brunton, L. L., Brown, J. H., Reese, J. B. & Mayer, S. E. Hormonally specific expression of cardiac protein kinase activity. *Proc National Acad Sci* **76**, 1570–1574 (1979).

181. Hayes, J. S., Brunton, L. L. & Mayer, S. E. Selective activation of particulate cAMP-dependent protein kinase by isoproterenol and prostaglandin E1. *J. Biol. Chem.* **255**, 5113–5119 (1980).

182. Corbin, J. D., Keely, S. L., Soderling, T. R. & Park, C. R. Hormonal regulation of adenosine 3',5'-monophosphate-dependent protein kinase. *Adv. Cycl. nucleotide Res.* **5**, 265–79 (1975).

183. Corbin, J. D. & Keely, S. L. Characterization and regulation of heart adenosine 3':5'-monophosphate-dependent protein kinase isozymes. *J. Biol. Chem.* **252**, 910–918 (1977).

184. Buxton, I. L. & Brunton, L. L. Compartments of cyclic AMP and protein kinase in mammalian cardiomyocytes. *J. Biol. Chem.* **258**, 10233–10239 (1983).

185. Jurevicius, J. & Fischmeister, R. cAMP compartmentation is responsible for a local activation of cardiac Ca2+ channels by beta-adrenergic agonists. *Proc. Natl. Acad. Sci.* **93**, 295–299 (1996).

186. Zaccolo, M. *et al.* Genetically encoded FRET reporter for cAMP. *Nat Cell Biol* **2**, 25–29 (2000).

187. Zaccolo, M. & Pozzan, T. Discrete Microdomains with High Concentration of cAMP in Stimulated Rat Neonatal Cardiac Myocytes. *Science* **295**, 1711–1715 (2002).

188. Zaccolo, M., Zerio, A. & Lobo, M. J. Subcellular Organization of the cAMP Signaling Pathway. *Pharmacol Rev* **73**, 278–309 (2021).

189. Bock, A., Irannejad, R. & Scott, J. D. cAMP signaling: a remarkably regional affair. *Trends Biochem. Sci.* **49**, 305–317 (2024).

190. Terrin, A. *et al.* PGE1 stimulation of HEK293 cells generates multiple contiguous domains with different [cAMP]: role of compartmentalized phosphodiesterases. *J Cell Biology* **175**, 441–451 (2006).

191. Chen, W., Levine, H. & Rappel, W.-J. A mathematical analysis of second messenger compartmentalization. *Phys. Biol.* **5**, 046006 (2008).

192. Mika, D., Leroy, J., Vandecasteele, G. & Fischmeister, R. PDEs create local domains of cAMP signaling. *J. Mol. Cell. Cardiol.* **52**, 323–329 (2012).

193. Conti, M., Mika, D. & Richter, W. Cyclic AMP compartments and signaling specificity: Role of cyclic nucleotide phosphodiesterases. *J. Gen. Physiol.* **143**, 29–38 (2014).

194. Brescia, M. & Zaccolo, M. Modulation of Compartmentalised Cyclic Nucleotide Signalling via Local Inhibition of Phosphodiesterase Activity. *Int. J. Mol. Sci.* **17**, 1672 (2016).

195. Surdo, N. C. *et al.* FRET biosensor uncovers cAMP nano-domains at β-adrenergic targets that dictate precise tuning of cardiac contractility. *Nat Commun* **8**, 15031 (2017).

196. Anton, S. E. *et al.* Receptor-associated independent cAMP nanodomains mediate spatiotemporal specificity of GPCR signaling. *Cell* **185**, 1130-1142.e11 (2022).

197. Herget, S., Lohse, M. J. & Nikolaev, V. O. Real-time monitoring of phosphodiesterase inhibition in intact cells. *Cell. Signal.* **20**, 1423–1431 (2008).

198. Bock, A. *et al.* Optical Mapping of cAMP Signaling at the Nanometer Scale. *Cell* **184**, 2793 (2021).

199. Barnes, A. P. *et al.* Phosphodiesterase 4D Forms a cAMP Diffusion Barrier at the Apical Membrane of the Airway Epithelium*. *J. Biol. Chem.* **280**, 7997–8003 (2005).

200. Koschinski, A. & Zaccolo, M. Activation of PKA in cell requires higher concentration of cAMP than in vitro: implications for compartmentalization of cAMP signalling. *Sci Rep-uk* **7**, 14090 (2017).

201. Chao, Y.-C., Surdo, N. C., Pantano, S. & Zaccolo, M. Imaging cAMP nanodomains in the heart. *Biochem. Soc. Trans.* **47**, 1383–1392 (2019).

202. Yadav, R. & Zaccolo, M. GPCR signaling via cAMP nanodomains. *Biochem. J.* **482**, 519–533 (2025).

203. Greenwald, E. C. & Saucerman, J. J. Bigger, Better, Faster: Principles and Models of AKAP Anchoring Protein Signaling. *J. Cardiovasc. Pharmacol.* **58**, 462–469 (2011).

204. Omar, M. H. & Scott, J. D. AKAP Signaling Islands: Venues for Precision Pharmacology. *Trends Pharmacol. Sci.* **41**, 933–946 (2020).

205. Carr, D. W. *et al.* Interaction of the regulatory subunit (RII) of cAMP-dependent protein kinase with RII-anchoring proteins occurs through an amphipathic helix binding motif. *J. Biol. Chem.* **266**, 14188–14192 (1991).

206. Peng, M. *et al.* Spatial Organization in Protein Kinase A Signaling Emerged at the Base of Animal Evolution. *J. Proteome Res.* **14**, 2976–2987 (2015).

207. Wong, W. & Scott, J. D. AKAP signalling complexes: focal points in space and time. *Nat. Rev. Mol. Cell Biol.* **5**, 959–970 (2004).

208. Lin, F., Wang, H. & Malbon, C. C. Gravin-mediated Formation of Signaling Complexes in β2-Adrenergic Receptor Desensitization and Resensitization*. *J. Biol. Chem.* **275**, 19025–19034 (2000).

209. Piggott, L. A., Bauman, A. L., Scott, J. D. & Dessauer, C. W. The A-kinase anchoring protein Yotiao binds and regulates adenylyl cyclase in brain. *Proc. Natl. Acad. Sci.* **105**, 13835–13840 (2008).

210. Dessauer, C. W. Adenylyl Cyclase–A-kinase Anchoring Protein Complexes: The Next Dimension in cAMP Signaling. *Mol. Pharmacol.* **76**, 935–941 (2009).

211. Taskén, K. A. *et al.* Phosphodiesterase 4D and Protein Kinase A Type II Constitute a Signaling Unit in the Centrosomal Area*. *J. Biol. Chem.* **276**, 21999–22002 (2001).

212. Dodge, K. L. *et al.* mAKAP assembles a protein kinase A/PDE4 phosphodiesterase cAMP signaling module. *EMBO J.* **20**, 1921–1930 (2001).

213. Klauck, T. M. *et al.* Coordination of Three Signaling Enzymes by AKAP79, a Mammalian Scaffold Protein. *Science* **271**, 1589–1592 (1996).

214. Schillace, R. V. & Scott, J. D. Association of the type 1 protein phosphatase PP1 with the A-kinase anchoring protein AKAP220. *Curr. Biol.* **9**, 321–324 (1999).

215. Steen, R. L., Martins, S. B., Taskén, K. & Collas, P. Recruitment of Protein Phosphatase 1 to the Nuclear Envelope by a-Kinase Anchoring Protein Akap149 Is a Prerequisite for Nuclear Lamina Assembly. *J. Cell Biol.* **150**, 1251–1262 (2000).

216. Gao, T. *et al.* cAMP-Dependent Regulation of Cardiac L-Type Ca2+ Channels Requires Membrane Targeting of PKA and Phosphorylation of Channel Subunits. *Neuron* **19**, 185–196 (1997).

217. Hoshi, N. *et al.* AKAP150 signaling complex promotes suppression of the M-current by muscarinic agonists. *Nat. Neurosci.* **6**, 564–571 (2003).

218. Nauert, J. B., Klauck, T. M., Langeberg, L. K. & Scott, J. D. Gravin, an autoantigen recognized by serum from myasthenia gravis patients, is a kinase scaffold protein. *Curr. Biol.* **7**, 52–62 (1997).

219. Carnegie, G. K., Smith, F. D., McConnachie, G., Langeberg, L. K. & Scott, J. D. AKAP-Lbc Nucleates a Protein Kinase D Activation Scaffold. *Mol. Cell* **15**, 889–899 (2004).

220. Agarwal, S. R., Sherpa, R. T., Moshal, K. S. & Harvey, R. D. Compartmentalized cAMP signaling in cardiac ventricular myocytes. *Cell. Signal.* **89**, 110172 (2022).

221. Folkmanaite, M. & Zaccolo, M. Regulation of cardiac function by cAMP nanodomains. *Biosci. Rep.* **43**, BSR20220953 (2023).

222. Lefkowitz, R. J., Stadel, J. M. & Caron, M. G. Adenylate Cyclase-Coupled Beta-Adrenergic Receptors: Structure and Mechanisms of Activation and Desensitization. *Annu. Rev. Biochem.* **52**, 159–186 (1983).

223. Bers, D. M. Cardiac excitation–contraction coupling. *Nature* **415**, 198–205 (2002).

224. Hartzell, H. C. Regulation of cardiac ion channels by catecholamines, acetylcholine and second messenger systems. *Prog. Biophys. Mol. Biol.* **52**, 165–247 (1988).

225. Nathanson, N. M. A multiplicity of muscarinic mechanisms: Enough signaling pathways to take your breath away. *Proc. Natl. Acad. Sci.* **97**, 6245–6247 (2000).

226. Papa, A. *et al.* Rad regulation of CaV1.2 channels controls cardiac fight-or-flight response. *Nat. Cardiovasc. Res.* **1**, 1022–1038 (2022).

227. Brittsan, A. G. & Kranias, E. G. Phospholamban and Cardiac Contractile Function. *J. Mol. Cell. Cardiol.* **32**, 2131–2139 (2000).

228. Valdivia, H. H., Kaplan, J. H., Ellis-Davies, G. C. R. & Lederer, W. J. Rapid Adaptation of Cardiac Ryanodine Receptors: Modulation by Mg2+ and Phosphorylation. *Science* **267**, 1997–2000 (1995).

229. Marx, S. O. *et al.* PKA Phosphorylation Dissociates FKBP12.6 from the Calcium Release Channel (Ryanodine Receptor) Defective Regulation in Failing Hearts. *Cell* **101**, 365–376 (2000).

230. SOLARO, R. J., MOIR, A. J. G. & PERRY, S. V. Phosphorylation of troponin I and the inotropic effect of adrenaline in the perfused rabbit heart. *Nature* **262**, 615–617 (1976).

231. Barefield, D. & Sadayappan, S. Phosphorylation and function of cardiac myosin binding protein-C in health and disease. *J. Mol. Cell. Cardiol.* **48**, 866–875 (2010).

232. DiPilato, L. M., Cheng, X. & Zhang, J. Fluorescent indicators of cAMP and Epac activation reveal differential dynamics of cAMP signaling within discrete subcellular compartments. *Proc. Natl. Acad. Sci.* **101**, 16513–16518 (2004).

233. Allen, M. D. & Zhang, J. Subcellular dynamics of protein kinase A activity visualized by FRET-based reporters. *Biochem. Biophys. Res. Commun.* **348**, 716–721 (2006).

234. Liu, S., Zhang, J. & Xiang, Y. K. FRET-based direct detection of dynamic protein kinase A activity on the sarcoplasmic reticulum in cardiomyocytes. *Biochem. Biophys. Res. Commun.* **404**, 581–586 (2011).

235. Lefkimmiatis, K., Leronni, D. & Hofer, A. M. The inner and outer compartments of mitochondria are sites of distinct cAMP/PKA signaling dynamics. *J. Cell Biol.* **202**, 453–462 (2013).

236. Sprenger, J. U. *et al.* In vivo model with targeted cAMP biosensor reveals changes in receptor–microdomain communication in cardiac disease. *Nat. Commun.* **6**, 6965 (2015).

237. Oliveria, S. F., Dell'Acqua, M. L. & Sather, W. A. AKAP79/150 Anchoring of Calcineurin Controls Neuronal L-Type Ca2+ Channel Activity and Nuclear Signaling. *Neuron* **55**, 261–275 (2007).

238. Nichols, C. B. *et al.* Sympathetic Stimulation of Adult Cardiomyocytes Requires Association of AKAP5 With a Subpopulation of L-Type Calcium Channels. *Circ. Res.* **107**, 747–756 (2010).

239. Oliveria, S. F., Dittmer, P. J., Youn, D., Dell'Acqua, M. L. & Sather, W. A. Localized Calcineurin Confers Ca2+-Dependent Inactivation on Neuronal L-Type Ca2+ Channels. *J. Neurosci.* **32**, 15328–15337 (2012).

240. Navedo, M. F. & Santana, L. F. CaV1.2 sparklets in heart and vascular smooth muscle. *J. Mol. Cell. Cardiol.* **58**, 67–76 (2013).

241. Leroy, J. *et al.* Spatiotemporal Dynamics of β-Adrenergic cAMP Signals and L-Type Ca2+ Channel Regulation in Adult Rat Ventricular Myocytes. *Circ. Res.* **102**, 1091–1100 (2008).

242. Muller, G. K. *et al.* PDE1 Inhibition Modulates Cav1.2 Channel to Stimulate Cardiomyocyte Contraction. *Circ. Res.* **129**, 872–886 (2021).

243. Lygren, B. *et al.* AKAP complex regulates Ca2+ re-uptake into heart sarcoplasmic reticulum. *Embo Rep* **8**, 1061–1067 (2007).

244. Carlson, C. R. *et al.* AKAP18δ Anchors and Regulates CaMKII Activity at Phospholamban-SERCA2 and RYR. *Circ. Res.* **130**, 27–44 (2022).

245. Beca, S. *et al.* Phosphodiesterase 4D Regulates Baseline Sarcoplasmic Reticulum Ca2+ Release and Cardiac Contractility, Independently of L-Type Ca2+ Current. *Circ. Res.* **109**, 1024–1030 (2011).

246. Beca, S. *et al.* Phosphodiesterase Type 3A Regulates Basal Myocardial Contractility Through Interacting With Sarcoplasmic Reticulum Calcium ATPase Type 2a Signaling Complexes in Mouse Heart. *Circ. Res.* **112**, 289–297 (2013).

247. Bergan-Dahl, A. *et al.* Activated CaMKIIδ translocates to the RyR nanodomain in cardiomyocytes. *Cardiovasc. Res.* **121**, 2177–2188 (2025).

248. Chao, Y.-C. *et al.* Targeting Troponin I Phosphorylation for Precision Treatment of Diastolic Dysfunction. *bioRxiv* 2025.11.18.689162 (2025) doi:10.1101/2025.11.18.689162.

249. Sumandea, C. A. *et al.* Cardiac Troponin T, a Sarcomeric AKAP, Tethers Protein Kinase A at the Myofilaments*. *J. Biol. Chem.* **286**, 530–541 (2011).

250. Subramaniam, G. *et al.* Integrated Proteomics Unveils Nuclear PDE3A2 as a Regulator of Cardiac Myocyte Hypertrophy. *Circ. Res.* **132**, 828–848 (2023).

251. Zaccolo, M. & Kovanich, D. Nanodomain cAMP signaling in cardiac pathophysiology: potential for developing targeted therapeutic interventions. *Physiol. Rev.* **105**, 541–591 (2025).

252. Liu, S., Anderson, P. J., Rajagopal, S., Lefkowitz, R. J. & Rockman, H. A. G Protein-Coupled Receptors: A Century of Research and Discovery. *Circ. Res.* **135**, 174–197 (2024).

253. Demby, A. & Zaccolo, M. Investigating G-protein coupled receptor signalling with light-emitting biosensors. *Front. Physiol.* **14**, 1310197 (2024).

254. Demby, A. & Zaccolo, M. GPCR signalling: Yet another variant route in a highly complex road map. *Cell Calcium* **124**, 102965 (2024).

255. Klarenbeek, J., Goedhart, J., Batenburg, A. van, Groenewald, D. & Jalink, K. Fourth-Generation Epac-Based FRET Sensors for cAMP Feature Exceptional Brightness, Photostability and Dynamic Range: Characterization of Dedicated Sensors for FLIM, for Ratiometry and with High Affinity. *PLoS ONE* **10**, e0122513 (2015).

256. Depry, C., Allen, M. D. & Zhang, J. Visualization of PKA activity in plasma membrane microdomains. *Mol. Biosyst.* **7**, 52–58 (2010).

257. Nikolaev, V. O., Bünemann, M., Hein, L., Hannawacker, A. & Lohse, M. J. Novel Single Chain cAMP Sensors for Receptor-induced Signal Propagation. *J. Biol. Chem.* **279**, 37215–37218 (2004).

258. Zhang, J., Ma, Y., Taylor, S. S. & Tsien, R. Y. Genetically encoded reporters of protein kinase A activity reveal impact of substrate tethering. *Proc National Acad Sci* **98**, 14997–15002 (2001).

259. Nikolaev, V. O., Bünemann, M., Schmitteckert, E., Lohse, M. J. & Engelhardt, S. Cyclic AMP imaging in adult cardiac myocytes reveals far-reaching beta1-adrenergic but locally confined beta2-adrenergic receptor-mediated signaling. *Circ. Res.* **99**, 1084–91 (2006).

260. Grisan, F. *et al.* Studying β1 and β2 adrenergic receptor signals in cardiac cells using FRET-based sensors. *Prog. Biophys. Mol. Biol.* **154**, 30–38 (2019).

261. Hein, L. & Kobilka, B. K. Adrenergic receptor signal transduction and regulation. *Neuropharmacology* **34**, 357–366 (1995).

262. Yang, Y. *et al.* Adrenergic G protein-coupled receptors in liver physiology and pathology: research advances and clinical implications. *npj Gut Liver* **2**, 27 (2025).

263. Cero, C. *et al.* β3-Adrenergic receptors regulate human brown/beige adipocyte lipolysis and thermogenesis. *JCI Insight* **6**, e139160 (2021).

264. Guimarães, S. & Moura, D. Vascular Adrenoceptors: An Update. *Pharmacol. Rev.* **53**, 319–356 (2001).

265. Manti, S., Gambadauro, A., Galletta, F., Ruggeri, P. & Piedimonte, G. Update on the Role of β2AR and TRPV1 in Respiratory Diseases. *Int. J. Mol. Sci.* **25**, 10234 (2024).

266. Hein, L., Altman, J. D. & Kobilka, B. K. Two functionally distinct α2-adrenergic receptors regulate sympathetic neurotransmission. *Nature* **402**, 181–184 (1999).

267. Perez, D. M. α1-Adrenergic Receptors in Neurotransmission, Synaptic Plasticity, and Cognition. *Front. Pharmacol.* **11**, 581098 (2020).

268. Woo, A. Y. H. & Xiao, R. β-Adrenergic receptor subtype signaling in heart: From bench to bedside. *Acta Pharmacol. Sin.* **33**, 335–341 (2012).

269. García-Sáinz, J. A., Vázquez-Prado, J. & Medina, L. del C. α1-Adrenoceptors: function and phosphorylation. *Eur. J. Pharmacol.* **389**, 1–12 (2000).

270. Piascik, M. T. & Perez, D. M. α1-Adrenergic Receptors: New Insights and Directions. *J. Pharmacol. Exp. Ther.* **298**, 403–410 (2001).

271. Hein, L. Adrenoceptors and signal transduction in neurons. *Cell Tissue Res.* **326**, 541–551 (2006).

272. Cherezov, V. *et al.* High-resolution crystal structure of an engineered human beta2-adrenergic G protein-coupled receptor. *Sci. (N. York, NY)* **318**, 1258–65 (2007).

273. Palczewski, K. *et al.* Crystal Structure of Rhodopsin: A G Protein-Coupled Receptor. *Science* **289**, 739–745 (2000).

274. Rasmussen, S. G. F. *et al.* Structure of a nanobody-stabilized active state of the β(2) adrenoceptor. *Nature* **469**, 175–80 (2011).

275. Warne, T. *et al.* Structure of a β1-adrenergic G-protein-coupled receptor. *Nature* **454**, 486–491 (2008).

276. Warne, T. *et al.* The structural basis for agonist and partial agonist action on a β1-adrenergic receptor. *Nature* **469**, 241–244 (2011).

277. Su, M. *et al.* Structural Basis of the Activation of Heterotrimeric Gs-Protein by Isoproterenol-Bound β1-Adrenergic Receptor. *Mol. Cell* **80**, 59-71.e4 (2020).

278. Hilger, D., Masureel, M. & Kobilka, B. K. Structure and dynamics of GPCR signaling complexes. *Nat. Struct. Mol. Biol.* **25**, 4–12 (2018).

279. Green, S. A., Rathz, D. A., Schuster, A. J. & Liggett, S. B. The Ile164 β2-adrenoceptor polymorphism alters salmeterol exosite binding and conventional agonist coupling to Gs. *Eur. J. Pharmacol.* **421**, 141–147 (2001).

280. Xu, X. *et al.* Constrained catecholamines gain β2AR selectivity through allosteric effects on pocket dynamics. *Nat. Commun.* **14**, 2138 (2023).

281. Xu, X. *et al.* Binding pathway determines norepinephrine selectivity for the human β1AR over β2AR. *Cell Res.* **31**, 569–579 (2021).

282. Xiao, R.-P. β-Adrenergic Signaling in the Heart: Dual Coupling of the β2-Adrenergic Receptor to Gs and Gi Proteins. *Sci.'s STKE* **2001**, re15 (2001).

283. Shiina, T., Kawasaki, A., Nagao, T. & Kurose, H. Interaction with beta-arrestin determines the difference in internalization behavor between beta1- and beta2-adrenergic receptors. *J. Biol. Chem.* **275**, 29082–90 (2000).

284. Freedman, N. J. *et al.* Phosphorylation and Desensitization of the Human β1-Adrenergic Receptor. *J. Biol. Chem.* **270**, 17953–17961 (1995).

285. Green, S. A. & Liggett, S. B. A proline-rich region of the third intracellular loop imparts phenotypic beta 1-versus beta 2-adrenergic receptor coupling and sequestration. *J. Biol. Chem.* **269**, 26215–26219 (1994).

286. Liang, W., Austin, S., Hoang, Q. & Fishman, P. H. Resistance of the human beta 1-adrenergic receptor to agonist-mediated down-regulation. Role of the C terminus in determining beta-subtype degradation. *J. Biol. Chem.* **278**, 39773–81 (2003).

287. Bristow, M. R. *et al.* Beta 1- and beta 2-adrenergic-receptor subpopulations in nonfailing and failing human ventricular myocardium: coupling of both receptor subtypes to muscle contraction and selective beta 1-receptor down-regulation in heart failure. *Circ. Res.* **59**, 297–309 (2018).

288. Nikolaev, V. O. *et al.* β_2-Adrenergic Receptor Redistribution in Heart Failure Changes cAMP Compartmentation. *Science* **327**, 1653–1657 (2010).

289. Bathe-Peters, M. *et al.* Visualization of β-adrenergic receptor dynamics and differential localization in cardiomyocytes. *Proc. Natl. Acad. Sci.* **118**, e2101119118 (2021).

290. Xiao, R.-P. *et al.* Coupling of β2-Adrenoceptor to Gi Proteins and Its Physiological Relevance in Murine Cardiac Myocytes. *Circ. Res.* **84**, 43–52 (1999).

291. Communal, C., Singh, K., Sawyer, D. B. & Colucci, W. S. Opposing Effects of β1- and β2-Adrenergic Receptors on Cardiac Myocyte Apoptosis. *Circulation* **100**, 2210–2212 (1999).

292. Zhu, W.-Z. *et al.* Dual modulation of cell survival and cell death by β2-adrenergic signaling in adult mouse cardiac myocytes. *Proc. Natl. Acad. Sci.* **98**, 1607–1612 (2001).

293. Engelhardt, S., Hein, L., Wiesmann, F. & Lohse, M. J. Progressive hypertrophy and heart failure in beta1-adrenergic receptor transgenic mice. *Proc. Natl. Acad. Sci. United States Am.* **96**, 7059–64 (1999).

294. Bisognano, J. D. *et al.* Myocardial-directed overexpression of the human beta(1)-adrenergic receptor in transgenic mice. *J. Mol. Cell. Cardiol.* **32**, 817–30 (2000).

295. Milano, C. A. *et al.* Enhanced Myocardial Function in Transgenic Mice Overexpressing the β2-Adrenergic Receptor. *Science* **264**, 582–586 (1994).

296. Dorn, G. W., Tepe, N. M., Lorenz, J. N., Koch, W. J. & Liggett, S. B. Low- and high-level transgenic expression of β2-adrenergic receptors differentially affect cardiac hypertrophy and function in Gαq-overexpressing mice. *Proc. Natl. Acad. Sci.* **96**, 6400–6405 (1999).

297. Liggett, S. B. *et al.* Early and Delayed Consequences of β2-Adrenergic Receptor Overexpression in Mouse Hearts. *Circulation* **101**, 1707–1714 (2000).

298. Xiao, R. P. *et al.* Beta 2-adrenergic receptor-stimulated increase in cAMP in rat heart cells is not coupled to changes in Ca2+ dynamics, contractility, or phospholamban phosphorylation. *J. Biol. Chem.* **269**, 19151–19156 (1994).

299. Zhou, Y. Y. *et al.* Localized cAMP-dependent signaling mediates beta 2-adrenergic modulation of cardiac excitation-contraction coupling. *Am. J. Physiol.-Hear. Circ. Physiol.* **273**, H1611–H1618 (1997).

300. Kuschel, M. *et al.* β2-Adrenergic cAMP Signaling Is Uncoupled From Phosphorylation of Cytoplasmic Proteins in Canine Heart. *Circulation* **99**, 2458–2465 (1999).

301. Kuznetsov, V., Pak, E., Robinson, R. B. & Steinberg, S. F. β2-Adrenergic Receptor Actions in Neonatal and Adult Rat Ventricular Myocytes. *Circ. Res.* **76**, 40–52 (1995).

302. Berisha, F. *et al.* cAMP Imaging at Ryanodine Receptors Reveals β2-Adrenoceptor Driven Arrhythmias. *Circ. Res.* **129**, 81–94 (2021).

303. Germack, R. & Dickenson, J. M. Induction of beta3-adrenergic receptor functional expression following chronic stimulation with noradrenaline in neonatal rat cardiomyocytes. *J. Pharmacol. Exp. Ther.* **316**, 392–402 (2005).

304. Baker, J. G. The selectivity of β-adrenoceptor agonists at human β1-, β2- and β3-adrenoceptors. *Br. J. Pharmacol.* **160**, 1048–1061 (2010).

305. Baker, J. G. The selectivity of beta-adrenoceptor antagonists at the human beta1, beta2 and beta3 adrenoceptors. *Br. J. Pharmacol.* **144**, 317–22 (2005).

306. Jong, K. A. D., Ehret, S., Heeren, J. & Nikolaev, V. O. Live-cell imaging identifies cAMP microdomains regulating β-adrenoceptor-subtype-specific lipolytic responses in human white adipocytes. *Cell Rep.* **42**, 112433 (2023).

307. Schobesberger, S. *et al.* β3-Adrenoceptor redistribution impairs NO/cGMP/PDE2 signalling in failing cardiomyocytes. *eLife* **9**, e52221 (2020).

308. Gorelik, J., Wright, P. T., Lyon, A. R. & Harding, S. E. Spatial control of the βAR system in heart failure: the transverse tubule and beyond. *Cardiovasc. Res.* **98**, 216–224 (2013).

309. Kuschel, M. *et al.* Gi Protein-mediated Functional Compartmentalization of Cardiac β2-Adrenergic Signaling*. *J. Biol. Chem.* **274**, 22048–22052 (1999).

310. Altschuld, R. A. *et al.* Response of Failing Canine and Human Heart Cells to β 2 -Adrenergic Stimulation. *Circulation* **92**, 1612–1618 (1995).

311. Bartel, S., Krause, E.-G., Wallukat, G. & Karczewski, P. New insights into β2-adrenoceptor signaling in the adult rat heart. *Cardiovasc. Res.* **57**, 694–703 (2003).

312. Yang, H.-Q. *et al.* β2-Adrenergic Stimulation Compartmentalizes β1 Signaling Into Nanoscale Local Domains by Targeting the C-Terminus of β1-Adrenoceptors. *Circ. Res.* **124**, 1350–1359 (2019).

313. Xiao, R. P. & Lakatta, E. G. Beta 1-adrenoceptor stimulation and beta 2-adrenoceptor stimulation differ in their effects on contraction, cytosolic Ca2+, and Ca2+ current in single rat ventricular cells. *Circ. Res.* **73**, 286–300 (1993).

314. Chen-Izu, Y. *et al.* Gi-Dependent Localization of β2-Adrenergic Receptor Signaling to L-Type Ca2+ Channels. *Biophys. J.* **79**, 2547–2556 (2000).

315. Bhargava, A. *et al.* Super-resolution Scanning Patch Clamp Reveals Clustering of Functional Ion Channels in Adult Ventricular Myocyte. *Circ. Res.* **112**, 1112–1120 (2013).

316. Parton, R. G., Way, M., Zorzi, N. & Stang, E. Caveolin-3 Associates with Developing T-tubules during Muscle Differentiation. *J. Cell Biol.* **136**, 137–154 (1997).

317. Rybin, V. O., Xu, X., Lisanti, M. P. & Steinberg, S. F. Differential Targeting of β-Adrenergic Receptor Subtypes and Adenylyl Cyclase to Cardiomyocyte Caveolae. *J. Biol. Chem.* **275**, 41447–41457 (2000).

318. Nieves-Cintrón, M. *et al.* AKAP150 participates in calcineurin/NFAT activation during the down-regulation of voltage-gated K+ currents in ventricular myocytes following myocardial infarction. *Cell. Signal.* **28**, 733–740 (2016).

319. Fraser, I. D. C. *et al.* Assembly of an A kinase-anchoring protein–β2-adrenergic receptor complex facilitates receptor phosphorylation and signaling. *Curr. Biol.* **10**, 409–412 (2000).

320. Cong, M. *et al.* Regulation of Membrane Targeting of the G Protein-coupled Receptor Kinase 2 by Protein Kinase A and Its Anchoring Protein AKAP79*. *J. Biol. Chem.* **276**, 15192–15199 (2001).

321. Gardner, L. A., Tavalin, S. J., Goehring, A. S., Scott, J. D. & Bahouth, S. W. AKAP79-mediated targeting of the cyclic AMP-dependent protein kinase to the beta1-adrenergic receptor promotes recycling and functional resensitization of the receptor. *J. Biol. Chem.* **281**, 33537–53 (2006).

322. Crespo, P., Xu, N., Simonds, W. F. & Gutkind, J. S. Ras-dependent activation of MAP kinase pathway mediated by G-protein βγ subunits. *Nature* **369**, 418–420 (1994).

323. Chesley, A. *et al.* The β2-Adrenergic Receptor Delivers an Antiapoptotic Signal to Cardiac Myocytes Through Gi-Dependent Coupling to Phosphatidylinositol 3′-Kinase. *Circ. Res.* **87**, 1172–1179 (2000).

324. Zhang, W. *et al.* β-Adrenergic Receptor-PI3K Signaling Crosstalk in Mouse Heart: Elucidation of Immediate Downstream Signaling Cascades. *PLoS ONE* **6**, e26581 (2011).

325. Daaka, Y., Luttrell, L. M. & Lefkowitz, R. J. Switching of the coupling of the β2-adrenergic receptor to different G proteins by protein kinase A. *Nature* **390**, 88–91 (1997).

326. Shenoy, S. K. *et al.* β-Arrestin-dependent, G Protein-independent ERK1/2 Activation by the β2 Adrenergic Receptor*. *J Biol Chem* **281**, 1261–1273 (2006).

327. Jo, S.-H., Leblais, V., Wang, P. H., Crow, M. T. & Xiao, R.-P. Phosphatidylinositol 3-Kinase Functionally Compartmentalizes the Concurrent Gs Signaling During β2-Adrenergic Stimulation. *Circ. Res.* **91**, 46–53 (2002).

328. Kerfant, B.-G. *et al.* PI3Kγ Is Required for PDE4, not PDE3, Activity in Subcellular Microdomains Containing the Sarcoplasmic Reticular Calcium ATPase in Cardiomyocytes. *Circ. Res.* **101**, 400–408 (2007).

329. Crackower, M. A. *et al.* Regulation of Myocardial Contractility and Cell Size by Distinct PI3K-PTEN Signaling Pathways. *Cell* **110**, 737–749 (2002).

330. Alloatti, G. *et al.* Phosphoinositide 3-kinase γ controls autonomic regulation of the mouse heart through Gi-independent downregulation of cAMP level. *FEBS Lett.* **579**, 133–140 (2005).

331. Audi, S. *et al.* The 'top 100' drugs and classes in England: an updated 'starter formulary' for trainee prescribers. *Br. J. Clin. Pharmacol.* **84**, 2562–2571 (2018).

332. Diaconu, C. *et al.* Beta-blockers in Cardiovascular Therapy: A Review. *J. Mind Méd. Sci.* **6**, 216–223 (2019).

333. Oliver, E., Jr, F. M. & D'Ocon, P. Beta-blockers: Historical Perspective and Mechanisms of Action. *Rev. Española Cardiol. (Engl. Ed.)* **72**, 853–862 (2019).

334. Fumagalli, C., Maurizi, N., Marchionni, N. & Fornasari, D. β-blockers: Their new life from hypertension to cancer and migraine. *Pharmacol. Res.* **151**, 104587 (2020).

335. Quirke, V. Putting Theory into Practice: James Black, Receptor Theory and the Development of the Beta-Blockers at ICI, 1958–1978. *Méd. Hist.* **50**, 69–92 (2006).

336. Frishman, W. & Halprin, S. Clinical pharmacology of the new beta-adrenergic blocking drugs. Part 7. New horizons in beta-adrenoceptor blockade therapy: Labetalol. *Am. Hear. J.* **98**, 660–665 (1979).

337. Giannattasio, C. *et al.* α1-Blocking Properties of Carvedilol During Acute and Chronic Administration. *J. Cardiovasc. Pharmacol.* **19**, S18–S22 (1992).

338. Maffei, A. & Lembo, G. Nitric oxide mechanisms of nebivolol. *Ther. Adv. Cardiovasc. Dis.* **3**, 317–327 (2009).

339. Bristow, M. R., Nelson, P., Minobe, W. & Johnson, C. P-121: Characterization of β1-adrenergic receptor selectivity of nebivolol and various other beta-blockers in human myocardium. *Am. J. Hypertens.* **18**, 51A-52A (2005).

340. Taylor, S. H. Intrinsic sympathomimetic activity: Clinical fact or fiction? *Am. J. Cardiol.* **52**, D16–D26 (1983).

341. Willette, R. N. *et al.* In Vitro and In Vivo Characterization of Intrinsic Sympathomimetic Activity in Normal and Heart Failure Rats. *J. Pharmacol. Exp. Ther.* **289**, 48–53 (1999).

342. Maack, C. *et al.* Different intrinsic activities of bucindolol, carvedilol and metoprolol in human failing myocardium. *Brit J Pharmacol* **130**, 1131–1139 (2000).

343. Brixius, K., Bundkirchen, A., Bölck, B., Mehlhorn, U. & Schwinger, R. H. G. Nebivolol, bucindolol, metoprolol and carvedilol are devoid of intrinsic sympathomimetic activity in human myocardium. *Br. J. Pharmacol.* **133**, 1330–1338 (2001).

344. Committees, C.-I. I. and. The Cardiac Insufficiency Bisoprolol Study II (CIBIS-II): a randomised trial. *Lancet* **353**, 9–13 (1999).

345. Packer, M. *et al.* Effect of carvedilol on the morbidity of patients with severe chronic heart failure: results of the carvedilol prospective randomized cumulative survival (COPERNICUS) study. *Circulation* **106**, 2194–9 (2002).

346. Group, M.-H. S. Effect of metoprolol CR/XL in chronic heart failure: Metoprolol CR/XL Randomised Intervention Trial in-Congestive Heart Failure (MERIT-HF). *Lancet* **353**, 2001–2007 (1999).

347. Flather, M. D. *et al.* Randomized trial to determine the effect of nebivolol on mortality and cardiovascular hospital admission in elderly patients with heart failure (SENIORS). *Eur. Hear. J.* **26**, 215–225 (2005).

348. Investigators, B.-B. E. of S. T. *et al.* A Trial of the Beta-Blocker Bucindolol in Patients with Advanced Chronic Heart Failure. *N. Engl. J. Med.* **344**, 1659–1667 (2001).

349. GROUP, T. X. I. S. H. F. S. Xamoterol in severe heart failure. *Lancet* **336**, 1–6 (1990).

350. Maack, C. *et al.* Characterization of β1-selectivity, adrenoceptor-Gs-protein interaction and inverse agonism of nebivolol in human myocardium. *Br. J. Pharmacol.* **132**, 1817–1826 (2001).

351. Kiuchi, K. *et al.* Myocardial beta-adrenergic receptor function during the development of pacing-induced heart failure. *J. Clin. Investig.* **91**, 907–914 (1993).

352. Mann, D. L., Kent, R. L., Parsons, B. & 4th, G. C. Adrenergic effects on the biology of the adult mammalian cardiocyte. *Circulation* **85**, 790–804 (2018).

353. Members:, A. F. *et al.* 2023 Focused Update of the 2021 ESC Guidelines for the diagnosis and treatment of acute and chronic heart failure. *Eur. J. Hear. Fail.* **26**, 5–17 (2024).

354. Poole-Wilson, P. A. *et al.* Comparison of carvedilol and metoprolol on clinical outcomes in patients with chronic heart failure in the Carvedilol Or Metoprolol European Trial (COMET): randomised controlled trial. *Lancet* **362**, 7–13 (2003).

355. Yue, T. L. *et al.* Carvedilol, a new vasodilator and beta adrenoceptor antagonist, is an antioxidant and free radical scavenger. *J. Pharmacol. Exp. Ther.* **263**, 92–98 (1992).

356. Dulin, B. & Abraham, W. T. Pharmacology of carvedilol. *Am. J. Cardiol.* **93**, 3–6 (2004).

357. Naccarelli, G. V. & Lukas, M. A. Carvedilol's antiarrhythmic properties: Therapeutic implications in patients with left ventricular dysfunction. *Clin. Cardiol.* **28**, 165–173 (2005).

358. Wisler, J. W. *et al.* A unique mechanism of β-blocker action: Carvedilol stimulates β-arrestin signaling. *Proc National Acad Sci* **104**, 16657–16662 (2007).

359. Benkel, T. *et al.* How Carvedilol activates β2-adrenoceptors. *Nat Commun* **13**, 7109 (2022).

360. Lefkowitz, R. J. *et al.* How carvedilol does not activate β2-adrenoceptors. *Nat. Commun.* **14**, 7866 (2023).

361. Kostenis, E. *et al.* Reply to: How carvedilol does not activate β2-adrenoceptors. *Nat. Commun.* **14**, 7867 (2023).

362. Willette, R. N., Mitchell, M. P., Ohlstein, E. H., Lukas, M. A. & Jr., R. R. R. Evaluation of Intrinsic Sympathomimetic Activity of Bucindolol and Carvedilol in Rat Heart. *Pharmacology* **56**, 30–36 (1998).

363. Zhou, Q. *et al.* Carvedilol and its new analogs suppress arrhythmogenic store overload–induced Ca2+ release. *Nat. Med.* **17**, 1003–1009 (2011).

364. Ozgen, N. *et al.* Protein Kinase D Links Gq-coupled Receptors to cAMP Response Element-binding Protein (CREB)-Ser133 Phosphorylation in the Heart*. *J. Biol. Chem.* **283**, 17009–17019 (2008).

365. Bristow, M. R. *et al.* Receptor Pharmacology of Carvedilol in the Human Heart. *J. Cardiovasc. Pharmacol.* **19**, S68–S80 (1992).

366. Böhm, M. *et al.* β-Adrenergic signal transduction following carvedilol treatment in hypertensive cardiac hypertrophy. *Cardiovasc. Res.* **40**, 146–155 (1998).

367. Shen, A. *et al.* β-blockers augment L-type Ca2+ channel activity by targeting spatially restricted β2AR signaling in neurons. *eLife* **8**, e49464 (2019).

368. Lattion, A.-L., Abuin, L., Nenniger-Tosato, M. & Cotecchia, S. Constitutively active mutants of the β1-adrenergic receptor. *FEBS Lett.* **457**, 302–306 (1999).

369. Andreka, P. *et al.* Bucindolol Displays Intrinsic Sympathomimetic Activity in Human Myocardium. *Circulation* **105**, 2429–2434 (2002).

370. Yao, A. *et al.* Characteristic Effects of α1-β1,2-Adrenergic Blocking Agent, Carvedilol, on [Ca2+]i in Ventricular Myocytes Compared With Those of Timolol and Atenolol. *Circ. J.* **67**, 83 (2002).

371. Baker, J. G., Hall, I. P. & Hill, S. J. Agonist Actions of "β-Blockers" Provide Evidence for Two Agonist Activation Sites or Conformations of the Human β1-Adrenoceptor. *Mol. Pharmacol.* **63**, 1312–1321 (2003).

372. Baker, J. G., Hall, I. P. & Hill, S. J. Agonist and Inverse Agonist Actions of β-Blockers at the Human β2-Adrenoceptor Provide Evidence for Agonist-Directed Signaling. *Mol. Pharmacol.* **64**, 1357–1369 (2003).

373. Galandrin, S. & Bouvier, M. Distinct signaling profiles of beta1 and beta2 adrenergic receptor ligands toward adenylyl cyclase and mitogen-activated protein kinase reveals the pluridimensionality of efficacy. *Mol. Pharmacol.* **70**, 1575–84 (2006).

374. Triposkiadis, F. *et al.* The Sympathetic Nervous System in Heart Failure. *J. Am. Coll. Cardiol.* **54**, 1747–1762 (2009).

375. McDonagh, T. A. *et al.* 2021 ESC Guidelines for the diagnosis and treatment of acute and chronic heart failure. *Eur. Hear. J.* **42**, 3599–3726 (2021).

376. Heidenreich, P. A. *et al.* 2022 AHA/ACC/HFSA Guideline for the Management of Heart Failure: Executive Summary: A Report of the American College of Cardiology/American Heart Association Joint Committee on Clinical Practice Guidelines. *Circulation* **145**, e876–e894 (2022).

377. Smith, I. C., Bombardier, E., Vigna, C. & Tupling, A. R. ATP Consumption by Sarcoplasmic Reticulum Ca2+ Pumps Accounts for 40-50% of Resting Metabolic Rate in Mouse Fast and Slow Twitch Skeletal Muscle. *PLoS ONE* **8**, e68924 (2013).

378. Tuomainen, T. & Tavi, P. The role of cardiac energy metabolism in cardiac hypertrophy and failure. *Exp. Cell Res.* **360**, 12–18 (2017).

379. Wei, W. & Smrcka, A. V. Internalized β2-Adrenergic Receptors Oppose PLC-Dependent Hypertrophic Signaling. *Circ. Res.* **135**, e24–e38 (2024).

380. Butler, S., Wang, R., Wunder, S. L., Cheng, H.-Y. & Randall, C. S. Perturbing effects of carvedilol on a model membrane system: Role of lipophilicity and chemical structure. *Biophys. Chem.* **119**, 307–315 (2006).

381. Guo, D. *et al.* Selective Inhibition on Organic Cation Transporters by Carvedilol Protects Mice from Cisplatin-Induced Nephrotoxicity. *Pharm. Res.* **35**, 204 (2018).

382. Ross, E. M. Coordinating Speed and Amplitude in G-Protein Signaling. *Curr. Biol.* **18**, 1896 (2008).

383. Ross, E. M. & Wilkie, T. M. GTPASE-ACTIVATING PROTEINS FOR HETEROTRIMERIC G PROTEINS: Regulators of G Protein Signaling (RGS) and RGS-Like Proteins. *Biochemistry* **69**, 795–827 (2000).

384. Cassel, D., Eckstein, F., Lowe, M. & Selinger, Z. Determination of the turn-off reaction for the hormone-activated adenylate cyclase. *J. Biol. Chem.* **254**, 9835–9838 (1979).

385. Brandt, D. R. & Ross, E. M. GTPase activity of the stimulatory GTP-binding regulatory protein of adenylate cyclase, Gs. Accumulation and turnover of enzyme-nucleotide intermediates. *J. Biol. Chem.* **260**, 266–272 (1985).

386. Berman, D. M., Wilkie, T. M. & Gilman, A. G. GAIP and RGS4 Are GTPase-Activating Proteins for the Gi Subfamily of G Protein α Subunits. *Cell* **86**, 445–452 (1996).

387. Berman, D. M., Kozasa, T. & Gilman, A. G. The GTPase-activating Protein RGS4 Stabilizes the Transition State for Nucleotide Hydrolysis*. *J. Biol. Chem.* **271**, 27209–27212 (1996).

388. Siderovski, D. P., Hessel, A., Chung, S., Mak, T. W. & Tyers, M. A new family of regulators of G-protein-coupled receptors? *Curr. Biol.* **6**, 211–212 (1996).

389. Masuho, I. *et al.* A Global Map of G Protein Signaling Regulation by RGS Proteins. *Cell* **183**, 503-521.e19 (2020).

390. Sjögren, B. The evolution of regulators of G protein signalling proteins as drug targets – 20 years in the making: IUPHAR Review 21. *Br. J. Pharmacol.* **174**, 427–437 (2017).

391. Hollinger, S. & Hepler, J. R. Cellular Regulation of RGS Proteins: Modulators and Integrators of G Protein Signaling. *Pharmacol. Rev.* **54**, 527–559 (2002).

392. Doupnik, C. A., Davidson, N., Lester, H. A. & Kofuji, P. RGS proteins reconstitute the rapid gating kinetics of Gβγ-activated inwardly rectifying K+ channels. *Proc. Natl. Acad. Sci.* **94**, 10461–10466 (1997).

393. Saitoh, O., Kubo, Y., Miyatani, Y., Asano, T. & Nakata, H. RGS8 accelerates G-protein-mediated modulation of K+currents. *Nature* **390**, 525–529 (1997).

394. Jeong, S.-W. & Ikeda, S. R. G Protein α Subunit Gαz Couples Neurotransmitter Receptors to Ion Channels in Sympathetic Neurons. *Neuron* **21**, 1201–1212 (1998).

395. Melliti, K., Meza, U., Fisher, R. & Adams, B. Regulators of G Protein Signaling Attenuate the G Protein–mediated Inhibition of N-Type Ca Channels. *J. Gen. Physiol.* **113**, 97–110 (1999).

396. Posokhova, E. *et al.* Essential Role of the m2R-RGS6-IKACh Pathway in Controlling Intrinsic Heart Rate Variability. *PLoS ONE* **8**, e76973 (2013).

397. Yang, J. *et al.* RGS6, a Modulator of Parasympathetic Activation in Heart. *Circ. Res.* **107**, 1345–1349 (2010).

398. Jones, S. V., Heilman, C. J. & Brann, M. R. Functional responses of cloned muscarinic receptors expressed in CHO-K1 cells. *Mol. Pharmacol.* **40**, 242–247 (1991).

399. Alea, M. P., Borroto-Escuela, D. O., Romero-Fernandez, W., Fuxe, K. & Garriga, P. Differential expression of muscarinic acetylcholine receptor subtypes in Jurkat cells and their signaling. *J. Neuroimmunol.* **237**, 13–22 (2011).

400. Brown, D. A. Muscarinic Acetylcholine Receptors (mAChRs) in the Nervous System: Some Functions and Mechanisms. *J. Mol. Neurosci.* **41**, 340–346 (2010).

401. Eglen, R. M., Reddy, H., Watson, N. & Challiss, R. A. J. Muscarinic acetylcholine receptor subtypes in smooth muscle. *Trends Pharmacol. Sci.* **15**, 114–119 (1994).

402. Ehlert, F. J. Pharmacological analysis of the contractile role of M2 and M3 muscarinic receptors in smooth muscle. *Recept. channels* **9**, 261–77 (2003).

403. Eglen, R. M. Muscarinic Receptor Subtype Pharmacology and Physiology. *Prog. Med. Chem.* **43**, 105–136 (2005).

404. Proctor, G. B. Muscarinic receptors and salivary secretion. *J. Appl. Physiol.* **100**, 1103–1104 (2006).

405. Hulme, E. C., Birdsall, N. J. M. & Buckley, N. J. Muscarinic Receptor Subtypes. *Annu. Rev. Pharmacol. Toxicol.* **30**, 633–673 (1990).

406. Haga, K. *et al.* Structure of the human M2 muscarinic acetylcholine receptor bound to an antagonist. *Nature* **482**, 547–551 (2012).

407. Kruse, A. C. *et al.* Structure and Dynamics of the M3 Muscarinic Acetylcholine Receptor. *Nature* **482**, 552–556 (2012).

408. Thal, D. M. *et al.* Crystal structures of the M1 and M4 muscarinic acetylcholine receptors. *Nature* **531**, 335–340 (2016).

409. Burger, W. A. C., Sexton, P. M., Christopoulos, A. & Thal, D. M. Toward an understanding of the structural basis of allostery in muscarinic acetylcholine receptors. *J. Gen. Physiol.* **150**, 1360–1372 (2018).

410. Maeda, S., Qu, Q., Robertson, M. J., Skiniotis, G. & Kobilka, B. K. Structures of the M1 and M2 muscarinic acetylcholine receptor/G-protein complexes. *Science* **364**, 552–557 (2019).

411. Standish, A., Enquist, L. W. & Schwaber, J. S. Innervation of the Heart and Its Central Medullary Origin Defined by Viral Tracing. *Science* **263**, 232–234 (1994).

412. Petraitiene, V., Pauza, D. H. & Benetis, R. Distribution of adrenergic and cholinergic nerve fibres within intrinsic nerves at the level of the human heart hilum†. *Eur. J. Cardio-Thorac. Surg.* **45**, 1097–1105 (2014).

413. Salamon, R. J. *et al.* Parasympathetic and sympathetic axons are bundled in the cardiac ventricles and undergo physiological reinnervation during heart regeneration. *iScience* **26**, 107709 (2023).

414. Hafez, O. A. & Chang, R. B. Regulation of Cardiac Function by the Autonomic Nervous System. *Physiology* **40**, 258–270 (2025).

415. Herring, N. Autonomic control of the heart: going beyond the classical neurotransmitters. *Exp. Physiol.* **100**, 354–358 (2015).

416. Wickman, K., Nemec, J., Gendler, S. J. & Clapham, D. E. Abnormal Heart Rate Regulation in GIRK4 Knockout Mice. *Neuron* **20**, 103–114 (1998).

417. Mark, M. D. & Herlitze, S. G-protein mediated gating of inward-rectifier K+ channels. *Eur. J. Biochem.* **267**, 5830–5836 (2000).

418. Jakobs, K. H., Aktories, K. & Schultz, G. GTP-dependent inhibition of cardiac adenylate cyclase by muscarinic cholinergic agonists. *Naunyn-Schmiedeberg's Arch. Pharmacol.* **310**, 113–119 (1979).

419. Hazeki, O. & Ui, M. Modification by islet-activating protein of receptor-mediated regulation of cyclic AMP accumulation in isolated rat heart cells. *J. Biol. Chem.* **256**, 2856–2862 (1981).

420. Harvey, R. D. & Belevych, A. E. Muscarinic regulation of cardiac ion channels. *Br. J. Pharmacol.* **139**, 1074–1084 (2003).

421. Watanabe, A. M. & Jr, H. R. B. Interaction between cyclic adenosine monophosphate and cyclic gunaosine monophosphate in guinea pig ventricular myocardium. *Circ. Res.* **37**, 309–317 (2018).

422. Keely, S. L., Lincoln, T. M. & Corbin, J. D. Interaction of acetylcholine and epinephrine on heart cyclic AMP-dependent protein kinase. *Am. J. Physiol.-Hear. Circ. Physiol.* **234**, H432–H438 (1978).

423. Schmied, R. & Korth, M. Muscarinic receptor stimulation and cyclic AMP-dependent effects in guinea-pig ventricular myocardium. *Br. J. Pharmacol.* **99**, 401–407 (1990).

424. Gupta, R. C., Neumann, J., Boknik, P. & Watanabe, A. M. M2-specific muscarinic cholinergic receptor-mediated inhibition of cardiac regulatory protein phosphorylation. *Am. J. Physiol.-Hear. Circ. Physiol.* **266**, H1138–H1144 (1994).

425. Zhang, J. Z. & MacLeod, K. M. Dissociation of negative inotropic effect of carbachol from changes in cAMP and PKA in perfused rat hearts. *Am. J. Physiol.-Hear. Circ. Physiol.* **271**, H404–H409 (1996).

426. Biegon, R. L. & Pappano, A. J. Dual mechanism for inhibition of calcium-dependent action potentials by acetylcholine in avian ventricular muscle. Relationship to cyclic AMP. *Circ. Res.* **46**, 353–362 (1980).

427. Pappano, A. J., Hartigan, P. M. & Coutu, M. D. Acetylcholine inhibits positive inotropic effect of cholera toxin in ventricular muscle. *Am. J. Physiol.-Hear. Circ. Physiol.* **243**, H434–H441 (1982).

428. Hartzell, H. C. & Titus, L. Effects of cholinergic and adrenergic agonists on phosphorylation of a 165,000-dalton myofibrillar protein in intact cardiac muscle. *J. Biol. Chem.* **257**, 2111–2120 (1982).

429. Jurevicius, J. & Fischmeister, R. Acetylcholine inhibits Ca2+ current by acting exclusively at a site proximal to adenylyl cyclase in frog cardiac myocytes. *J. Physiol.* **491**, 669–675 (1996).

430. Levy, M. N. Sympathetic-parasympathetic interactions in the heart. *Circ. Res.* **29**, 437–45 (1971).

431. Levy, M. N. Neural control of the heart: the importance of being ignorant. *J. Cardiovasc. Electrophysiol.* **6**, 283–93 (1995).

432. Iancu, R. V., Jones, S. W. & Harvey, R. D. Compartmentation of cAMP Signaling in Cardiac Myocytes: A Computational Study. *Biophys. J.* **92**, 3317–3331 (2007).

433. Baldwin, T. A. & Dessauer, C. W. Function of Adenylyl Cyclase in Heart: the AKAP Connection. *J. Cardiovasc. Dev. Dis.* **5**, 2 (2018).

434. Tomek, J. & Zaccolo, M. Compartmentalized cAMP signalling and control of cardiac rhythm. *Philos. Trans. R. Soc. B* **378**, 20220172 (2023).

435. Figueroa, K. W., Griffin, M. T. & Ehlert, F. J. Selectivity of Agonists for the Active State of M1 to M4 Muscarinic Receptor Subtypes. *J. Pharmacol. Exp. Ther.* **328**, 331–342 (2009).

436. Korth, M. & Kühlkamp, V. Muscarinic receptors mediate negative and positive inotropic effects in mammalian ventricular myocardium: differentiation by agonists. *Br. J. Pharmacol.* **90**, 81–90 (1987).

437. Mohan, R. M. *et al.* Neuronal Nitric Oxide Synthase Gene Transfer Promotes Cardiac Vagal Gain of Function. *Circ. Res.* **91**, 1089–1091 (2002).

438. Cheng, E. P. *et al.* Restoration of Normal L-Type Ca2+ Channel Function During Timothy Syndrome by Ablation of an Anchoring Protein. *Circ. Res.* **109**, 255–261 (2011).

439. Belevych, A. E., Sims, C. & Harvey, R. D. ACh-induced rebound stimulation of L-type Ca(2+) current in guinea-pig ventricular myocytes, mediated by Gbetagamma-dependent activation of adenylyl cyclase. *J. Physiol.* **536**, 677–92 (2001).

440. Marionneau, C. *et al.* Specific pattern of ionic channel gene expression associated with pacemaker activity in the mouse heart. *J. Physiol.* **562**, 223–234 (2005).

441. Mesirca, P. *et al.* Selective blockade of Cav1.2 (α1C) versus Cav1.3 (α1D) L-type calcium channels by the black mamba toxin calciseptine. *Nat. Commun.* **15**, 54 (2024).

442. Weiss, S., Oz, S., Benmocha, A. & Dascal, N. Regulation of cardiac L-type Ca^{2+} channel CaV1.2 via the β-adrenergic-cAMP-protein kinase A pathway: old dogmas, advances, and new uncertainties. *Circ. Res.* **113**, 617–31 (2013).

443. Murphy, J. G. *et al.* AKAP-Anchored PKA Maintains Neuronal L-type Calcium Channel Activity and NFAT Transcriptional Signaling. *Cell Rep.* **7**, 1577–1588 (2014).

444. Lemke, T. *et al.* Unchanged β-Adrenergic Stimulation of Cardiac L-type Calcium Channels in Cav1.2 Phosphorylation Site S1928A Mutant Mice*. *J. Biol. Chem.* **283**, 34738–34744 (2008).

445. Brandmayr, J. *et al.* Deletion of the C-terminal Phosphorylation Sites in the Cardiac β-Subunit Does Not Affect the Basic β-Adrenergic Response of the Heart and the Cav1.2 Channel*. *J. Biol. Chem.* **287**, 22584–22592 (2012).

446. Murad, F., Chi, Y.-M., Rall, T. W. & Sutherland, E. W. Adenyl Cyclase III. THE EFFECT OF CATECHOLAMINES AND CHOLINE ESTERS ON THE FORMATION OF ADENOSINE 3‘,5‘-PHOSPHATE BY PREPARATIONS FROM CARDIAC MUSCLE AND LIVER. *J. Biol. Chem.* **237**, 1233–1238 (1962).

447. LARAIA, P. J. & SONNENBLICK, E. H. Autonomic Control of Cardiac C-AMP. *Circ. Res.* **28**, 377–384 (1971).

448. Flitney, F. W. & Singh, J. Evidence that cyclic GMP may regulate cyclic AMP metabolism in the isolated frog ventricle. *J. Mol. Cell. Cardiol.* **13**, 963–979 (1981).

449. Warrier, S. *et al.* β-Adrenergic- and muscarinic receptor-induced changes in cAMP activity in adult cardiac myocytes detected with FRET-based biosensor. *Am. J. Physiol.-Cell Physiol.* **289**, C455–C461 (2005).

450. Fischmeister, R. & Hartzell, H. C. Mechanism of action of acetylcholine on calcium current in single cells from frog ventricle. *J. Physiol.* **376**, 183–202 (1986).

451. Skeberdis, V. A., Jurevičius, J. & Fischmeister, R. Beta-2 Adrenergic Activation of L-Type Ca++ Current in Cardiac Myocytes 1. *J. Pharmacol. Exp. Ther.* **283**, 452–461 (1997).

452. Dobrzynski, H. *et al.* Distribution of the Muscarinic K+ Channel Proteins Kir3.1 and Kir3.4 in the Ventricle, Atrium, and Sinoatrial Node of Heart. *J. Histochem. Cytochem.* **49**, 1221–1234 (2001).

453. Dobrzynski, H., Janvier, N. C., Leach, R., Findlay, J. B. C. & Boyett, M. R. Effects of ACh and adenosine mediated by Kir3.1 and Kir3.4 on ferret ventricular cells. *Am. J. Physiol.-Hear. Circ. Physiol.* **283**, H615–H630 (2002).

454. Anderson, A. *et al.* Expression and relevance of the G protein-gated K+ channel in the mouse ventricle. *Sci. Rep.* **8**, 1192 (2018).

455. Campos-Ríos, A., Rueda-Ruzafa, L. & Lamas, J. A. The Relevance of GIRK Channels in Heart Function. *Membranes* **12**, 1119 (2022).

456. Ahmad, Z., Green, F. J., Subuhi, H. S. & Watanabe, A. M. Autonomic regulation of type 1 protein phosphatase in cardiac muscle*. *J. Biol. Chem.* **264**, 3859–3863 (1989).

457. Herzig, S., Meier, A., Pfeiffer, M. & Neumann, J. Stimulation of protein phosphatases as a mechanism of the muscarinic-receptor-mediated inhibition of cardiac L-type Ca2+ channels. *Pflügers Arch.* **429**, 531–538 (1995).

458. Stemmer, P. M., Ledyard, T. H. & Watanabe, A. M. Protein dephosphorylation rates in myocytes after isoproterenol withdrawal. *Biochem. Pharmacol.* **59**, 1513–1519 (2000).

459. Tedford, H. W. & Zamponi, G. W. Direct G Protein Modulation of Cav2 Calcium Channels. *Pharmacol. Rev.* **58**, 837–862 (2006).

460. Kamp, T. J., Hu, H. & Marban, E. Voltage-dependent facilitation of cardiac L-type Ca channels expressed in HEK-293 cells requires β-subunit. *Am. J. Physiol.-Hear. Circ. Physiol.* **278**, H126–H136 (2000).

461. Dolphin, A. C. G Protein Modulation of Voltage-Gated Calcium Channels. *Pharmacol. Rev.* **55**, 607–627 (2003).

462. Zamponi, G. W. & Currie, K. P. M. Regulation of CaV2 calcium channels by G protein coupled receptors. *Biochim. Biophys. Acta (BBA) - Biomembr.* **1828**, 1629–1643 (2013).

463. McHugh, D., Sharp, E. M., Scheuer, T. & Catterall, W. A. Inhibition of cardiac L-type calcium channels by protein kinase C phosphorylation of two sites in the N-terminal domain. *Proc. Natl. Acad. Sci.* **97**, 12334–12338 (2000).

464. George, W. J., Polson, J. B., O'Toole, A. G. & Goldberg, N. D. Elevation of Guanosine 3′,5′-Cyclic Phosphate in Rat Heart after Perfusion with Acetylcholine*. *Proc. Natl. Acad. Sci.* **66**, 398–403 (1970).

465. Fischmeister, R. & Hartzell, H. C. Cyclic guanosine 3',5'-monophosphate regulates the calcium current in single cells from frog ventricle. *J. Physiol.* **387**, 453–472 (1987).

466. Han, X., Kobzik, L., Balligand, J.-L., Kelly, R. A. & Smith, T. W. Nitric Oxide Synthase (NOS3)–Mediated Cholinergic Modulation of Ca2+ Current in Adult Rabbit Atrioventricular Nodal Cells. *Circ. Res.* **78**, 998–1008 (1996).

467. Balligand, J. L., Kelly, R. A., Marsden, P. A., Smith, T. W. & Michel, T. Control of cardiac muscle cell function by an endogenous nitric oxide signaling system. *Proc. Natl. Acad. Sci.* **90**, 347–351 (1993).

468. Han, X. *et al.* Muscarinic cholinergic regulation of cardiac myocyte ICa-L is absent in mice with targeted disruption of endothelial nitric oxide synthase. *Proc. Natl. Acad. Sci.* **95**, 6510–6515 (1998).

469. KLATT, P., CACHO, J., CRESPO, M. D., HERRERA, E. & RAMOS, P. Nitric oxide inhibits isoproterenol-stimulated adipocyte lipolysis through oxidative inactivation of the β-agonist. *Biochem. J.* **351**, 485 (2000).

470. Buxton, I. L. *et al.* NG-nitro L-arginine methyl ester and other alkyl esters of arginine are muscarinic receptor antagonists. *Circ. Res.* **72**, 387–395 (1993).

471. Zhang, Y. *et al.* Higher-order transient membrane protein structures. *Proc. Natl. Acad. Sci.* **122**, e2421275121 (2025).

472. Ostrom, K. F. *et al.* Physiological roles of mammalian transmembrane adenylyl cyclase isoforms. *Physiol. Rev.* **102**, 815–857 (2022).

473. Bauman, A. L. *et al.* Dynamic Regulation of cAMP Synthesis through Anchored PKA-Adenylyl Cyclase V/VI Complexes. *Mol. Cell* **23**, 925–931 (2006).

474. Carbajal, A. G., Bavencoffe, A., Walters, E. T. & Dessauer, C. W. Depolarization-Dependent C-Raf Signaling Promotes Hyperexcitability and Reduces Opioid Sensitivity of Isolated Nociceptors after Spinal Cord Injury. *J. Neurosci.* **40**, 6522–6535 (2020).

475. Garza-Carbajal, A. *et al.* Mechanism of gabapentinoid potentiation of opioid effects on cyclic AMP signaling in neuropathic pain. *Proc. Natl. Acad. Sci.* **121**, e2405465121 (2024).

476. Kritzer, M. D., Li, J., Dodge-Kafka, K. & Kapiloff, M. S. AKAPs: The architectural underpinnings of local cAMP signaling. *J. Mol. Cell. Cardiol.* **52**, 351–358 (2012).

477. Zaccolo, M. & Pozzan, T. Discrete Microdomains with High Concentration of cAMP in Stimulated Rat Neonatal Cardiac Myocytes. *Science* **295**, 1711–1715 (2002).

478. Lobingier, B. T. *et al.* An Approach to Spatiotemporally Resolve Protein Interaction Networks in Living Cells. *Cell* **169**, 350-360.e12 (2017).

479. Paek, J. *et al.* Multidimensional Tracking of GPCR Signaling via Peroxidase-Catalyzed Proximity Labeling. *Cell* **169**, 338-349.e11 (2017).

480. Polacco, B. J. *et al.* Profiling the proximal proteome of the activated μ-opioid receptor. *Nat. Chem. Biol.* 1–11 (2024) doi:10.1038/s41589-024-01588-3.

481. Shchepinova, M. M. *et al.* Spatiotemporally resolved GPCR interactome uncovers unique mediators of receptor agonism. *Cell Chem. Biol.* **32**, 722-735.e7 (2025).

482. Maziarz, M. *et al.* Revealing the Activity of Trimeric G-proteins in Live Cells with a Versatile Biosensor Design. *Cell* **182**, 770-785.e16 (2020).

483. Korhonen, T., Hänninen, S. L. & Tavi, P. Model of Excitation-Contraction Coupling of Rat Neonatal Ventricular Myocytes. *Biophys. J.* **96**, 1189–1209 (2009).

484. Lobo, M. J. *et al.* Phosphodiesterase 2A2 regulates mitochondria clearance through Parkin-dependent mitophagy. *Commun Biology* **3**, 596 (2020).

485. Brescia, M., Chao, Y.-C., Koschinski, A., Tomek, J. & Zaccolo, M. Multi-Compartment, Early Disruption of cGMP and cAMP Signalling in Cardiac Myocytes from the. *Int J Mol Sci* **21**, 7056 (2020).